RADIATION RISKS FROM HIGH-LET ALPHA PARTICLE EMITTERS USING RADIUM-223 AS A MODEL

A thesis submitted for the degree of Doctor of Philosophy

by

Isabella Maria Bastiani

Department of Life Sciences, Brunel University London

October 2021

Abstract

[^{223}Ra]$RaCl_2$ was recently approved for the treatment of bone metastatic disease in prostate cancer patients. Once intravenously administered ^{223}Ra localises to areas of increased calcium turnover. During its decay, ^{223}Ra will emit high linear energy transfer (LET) α-particles that are effective in targeting metastatic sites. α-particles have a range of ≤ 100 μm suggesting normal tissue sparing; however, there is uncertainty regarding the heterogeneous distribution of dose at the cellular/tissue levels. It remains unclear if ^{223}Ra may also result in unwanted exposure of neighbouring bone marrow (BM) cells. To date, the potential risk of BM exposure as a consequence of this treatment remains unquantified.

The aim of this project was to resolve these uncertainties by assessing changes in the genomic structure of peripheral blood lymphocyte (PBLs) potentially in contact with ^{223}Ra. To do so, blood samples from patients enrolled on to the ADRRAD clinical trial were collected. The treatment included 6 intravenous injections of [^{223}Ra]$RaCl_2$ each administered 4 weeks apart (55 kbq/kg) and 2 Gy fractionated IMRT (daily for 5 days a week over 7.5 weeks). Blood samples were collected prior to each ^{223}Ra administration and PBL cultured to 1st i*n vitro* division. The PBLs were assayed by Multiplex-fluorescent-in-situ-hybridization (M-FISH) and Giemsa solid stain for cytogenetic analysis.

In this study we demonstrated that chromosomal aberration complexity reflects the treatment regime. This indicates PBLs were exposed to α-particle by ^{223}Ra. The change in chromosomal spectrum was used to create a novel method for absorbed blood dose estimation and this was compared to existing physical models. The persistence and transmissibility of aberrations was evaluated with chromatid aberrations consistent with delayed effects observed in follow up samples. A lower administered activity of ^{223}Ra was suggested to be as effective as larger administer activities, this indicates that the dosing strategy may need re-evaluating.

Table of Contents

Table of figures

Abbreviations

ADT: Androgen deprivation therapy

BF: Blood Flow

CML: Chronic myeloid leukaemia

CRPC: Castration resistant prostate cancer

CT: computerized tomography

CTPV: computerized tomography plan volume

DAPI: 4’,6-diamidino-2-phenylindole

DEAC: 7-Diethylaminocoumarin-3-carboxylic acid

DMSO: Dimethyl sulfoxide

DNA: Deoxyribonucleic acid

DSB: Double strand break

EBRT: External beam radiotherapy

FISH: Fluorescence in situ hybridization

FITC: Fluorescein isothiocyanate

GP: General practitioner

HR: Homologous recombination

HSC: Haematopoietic stem cell

IAEA: International Atomic Energy Agency

ICRP: International Commission on Radiological Protection

IMRT: Intensity-modulated radiation therapy

LET: Linear energy transfer

LN: Lymph nodes

LOH: Loss of heterozygosity

M-FISH: Multiplex fluorescence in situ hybridization

MRI: Magnetic resonance imaging

NHEJ: Non homologous end joining

NHS: National health service

PBL: Peripheral blood lymphocytes

PC: Prostate cancer

PCC: Premature chromosome condensation

PSA: Prostate specific antigen

RBE: Relative biological effect

ROS: Reactive oxygen species

S.S.: Solid stain

SEM: Standard error of the mean

SSA: Single strand annealing

SSB: Single strand break

SSC: Saline-sodium citrate

SSCT: Saline-sodium citrate with tween

TNM: Tumour Node Metastasis

^{103}Pb: Lead-103

^{125}I: Iodine-123

^{192}Ir: Iridium-192

^{207}Pb: Lead-207

^{207}Ti: Thallium-207

^{208}Pb: Lead-208

^{211}Bi: Bismuth-211

^{211}Pb: Lead-211

^{212}Bi: Bismuth-212

^{212}Pb: Lead-212

^{212}Po: Polonium-212

^{215}Po: Polonium-215

^{216}Po: Polonium-216

^{219}Rn: Radon-219

^{220}Rn: Radon-220

^{223}Ra: Radium-223

^{224}Ra: Radium-224

^{226}Ra: Radium-226

^{228}Ra Radium-228

^{239}Pu: Plutonium-239

^{241}Am: Americium-241

3D: Three Dimensional

3DCRT: 3D Image Guided Radiotherapy

^{60}Co: Cobalt-60

^{99m}Tc-MDP: ^{99m}Tc-Methyl diphosphonate

Chapter 1: Literature Review

1.1 Prostate cancer

1.1.1 Incidence and mortality

Prostate cancer (PC) is the most common cancer affecting men in the UK, contributing to 26% of cancer cases in 2017 with 1 in 8 men being diagnosed with PC in their lifetime (1). Indeed, PC is the most frequently diagnosed cancer in 112 countries followed by lung cancer and worldwide it was recognised as the second most common cancer with 1.3 million cases diagnosed in 2018 (2, 3). In the UK, over 47,000 men are diagnosed with PC every year and in turn 11,000 deaths are associated to the disease annually (4). The death rate is highly dependent on the stage of disease and age at diagnosis with the highest incidence in men over the age of 65 (5). Family history, genetics and ethnicity have all been identified as factors contributing towards the increase in PC incidence (6-11). This being said, the most common factor remains age with the majority of cases being diagnosed in men over the age of 65 and with 80% of men in their 80s showing early signs of PC, Figure 1.11 (12, 13).

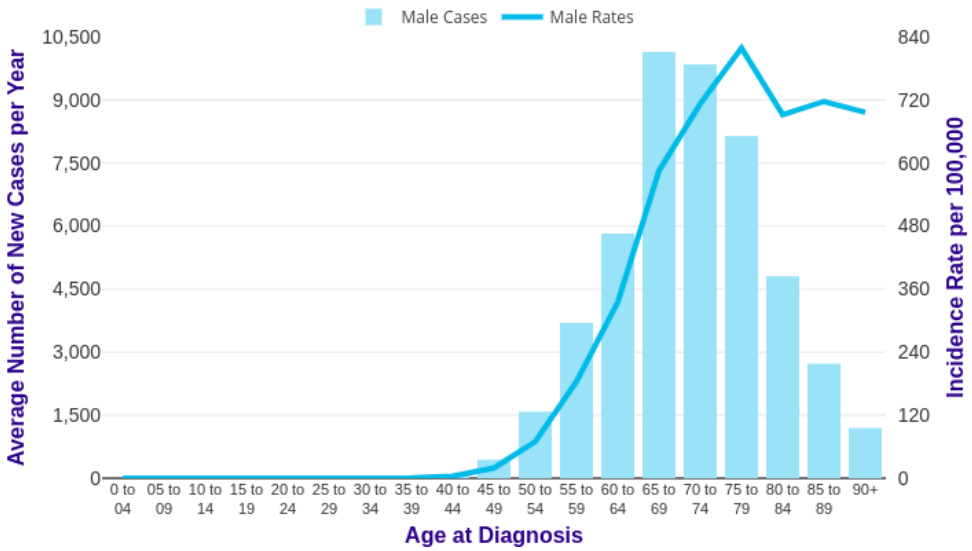

Figure 1.11 Age and the incidence of PC.

Prostate cancer rates and new cases per year are associated with older population groups with incidence increasing as early as 45 years. Note that a drop or plateau in incidence in the

oldest age groups often indicates reduced diagnostic activity. Image and data available for reuse by Cancer Research UK (1).

Due to the late average age of onset, mortality from PC itself is low, indeed deaths from patients diagnosed in early stages of disease are more likely to be attributed to other age-related illnesses (14). For these reasons, early screening programs for PC remains controversial (15-17), and it is also hard to clinically evaluate whether early-stage prostate tumours may potentially become malignant within the lifetime of the patient. In the UK there is no early screening programme for PC. Routine screening via Prostate-Specific Antigens (PSA) test remains controversial with over diagnosis and treatment of early stage PC in elderly patients remaining problematic (18-21). An informed choice programme is, however, available via the NHS, where men over the age of 50 can arrange for PSA levels to be tested after consulting their GP if they present primary PC symptoms or have a family history of PC.

1.1.2 Prostate cancer formation and progression

Cancer itself is a collection of diseases/malignancies where cells of a tissue become abnormal, gaining the ability to divide uncontrollably and invade nearby tissue. Abnormalities in cells may accumulate and eventually result in the formation of a tumour, and this may be benign or malignant. A malignant tumour has the ability to invade nearby tissues and possibly metastasise (spreading and growth at distant sites), while benign tumours are easily removed as they remain confined within the original location (22). Malignant cells are able to uncontrollably grow via their own means with no external signalling required. To do so they acquire resistance to anti-growth signals and are no longer limited by replication, resulting in indefinite growth and division (23, 24). Cancer cells are able to evade apoptosis and cell mediated death by eluding the immune system by continuously mutating, which also results in the acquired invasive properties which promote inflammation and angiogenesis (new blood vessel formation providing oxygen and nutrients to the growing tumour) (25-27). The underpinning drive for this is genomic instability, which prompts the genetic diversity of cancer cells throughout disease progression (25, 28-30).

PC originates in the prostate which is an exocrine gland found in men and is involved in the production of seminal fluid. 90-95% of PC cases are characterised as acinar adenocarcinoma, because they form within the acinar gland cells (31). Other rare forms of PC account for the remaining proportion, and this includes ductal adenocarcinoma originating within prostate ducts, squamous cell cancer originating in flat cells lining the outer prostate, small cell PC within small round cells, neuroendocrine tumours within neuroendocrine cells and sarcomas developing in supporting gland tissues (32, 33). PC symptoms occurs usually once the tumour is large enough to put pressure on the urethra, and this results in urogenital symptoms such as increased urination, urgency and blood in the urine.

Primary disease diagnosis is carried out by examination by a physician and by PSA testing, which assesses whether elevated levels (above 4.0 ng/ml) are present in the blood (34). PSA is a protease part of the normal process regulating seminal fluid viscosity, which is released by epithelial cells of the prostate and also by PC cells. Elevated levels of PSA will leak into the blood stream where they can be detected, and the quantification of blood PSA levels has been approved for disease diagnosis (35). PSA testing alone is controversial however, as PC has been diagnosed also in patients with low PSA levels as well as high PSA levels not being solely attributable to PC incidence (36). The PSA test is, however, a good indicator when physical examination is also carried out to assess where the prostate presents an abnormal surface and with prostate biopsy (37, 38).

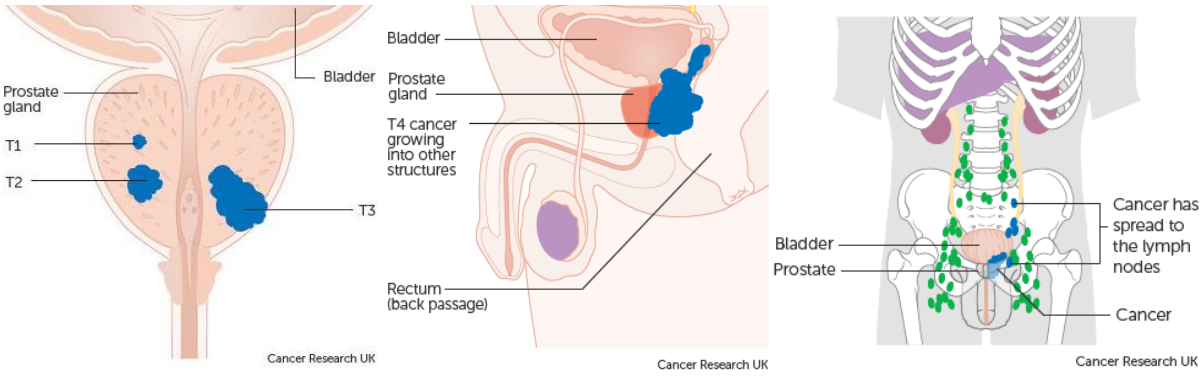

Figure 1.22 Overview of PC disease spread.

Left panel indicating tumour (T) 1-3 stages of disease localized to the prostate gland. Middle panel highlighting T4 where the cancer has breached the prostate and spread to surrounding regions. Right panel depicting adavanced prostate cancer with metastatic sites

spread to neighbouring organs (blue) and distant metastatic sites (green) including spread to bone. Images available for reuse by Cancer Research UK (1).

1.1.3 Cancer scoring system

Once primary diagnosis has been made, a prostate biopsy is taken for confirmatory tests for an assessment of disease stage. To assess the prostate cells sampled, the Gleason score system is used to quantify on a scale from 1-5 how abnormal the prostate biopsies are compared to normal healthy prostate tissue. 1-2 scores being close to normal prostate cells and 3-5 being cells presenting increasing abnormalities. This is carried out on the largest area of the tumour and then on the second largest area with scores being added together. High scores are associated with a higher likelihood of tumour growth and spread (39).

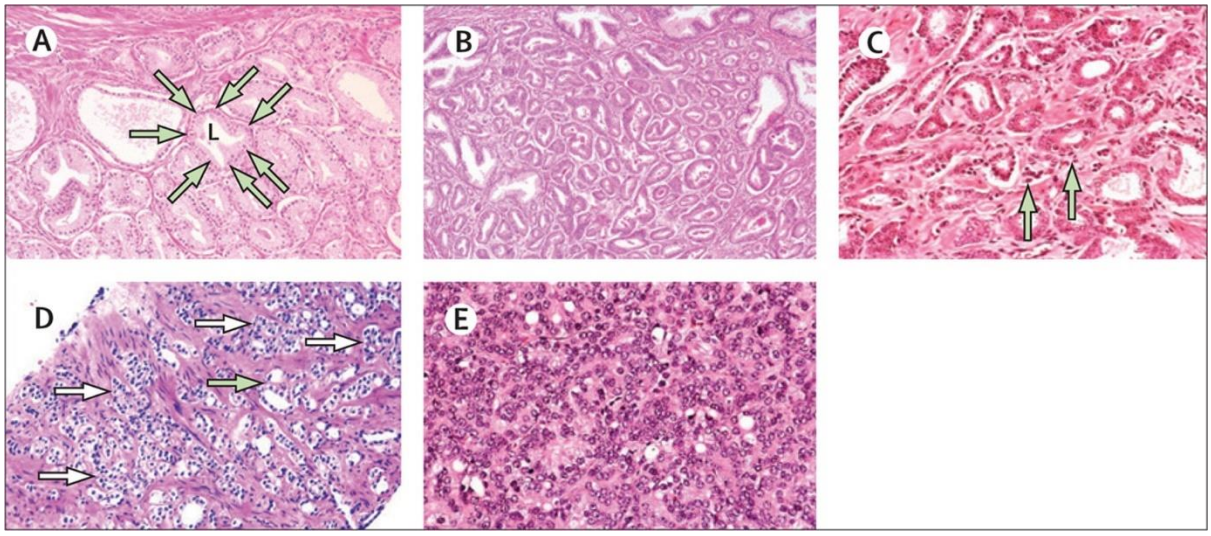

Figure 1.33 Gleason scoring of prostate biopsies.

A. Grade 1 highlighting the lumen (L) of an acinus duct presenting abnormal morphology. B. Grade 2 indicating multiple abnormal acinus ducts. C. Grade 3. Small infiltration of cells into the surrounding stroma. D. Grade 4. Multiple sites of cell infiltration with abnormal morphology of lumen. E. Grade 5 presenting poor morphology of glandular structures and poorly differentiated cells. X40 magnification for A,B and D, x100 magnification for C and E. Image available for unrestricted use by The Lancet Oncology under Creative Commons CC-BY license (40).

The TNM (tumour, node and metastases) stage assessment is carried out when abnormal cells are identified by Gleason scoring system along with PSA results. The TNM stage includes assessment of tumour, nodes and metastases for an overall assessment of disease progression. The tumour is evaluated for its size with a scoring of 1-4 with further subdivisions for each score as illustrated in Figure 1.22. Scores 1 and 2 are restricted to the prostate gland while scoring of 3 indicates breaking through and spreading to seminal vesicles, and the most severe score of 4 being where the tumour has spread into organs nearby. The nodes are scored as 0: having no cancer cells or 1: having cancer cells, similarly to this metastasis having a score of 0 if not present and a score of 1 if present with further subcategories of metastatic burden (41).

1.1.4 Advanced prostate cancer

Advanced prostate cancer is characterized by the spread of disease to distant sites such as organs or lymph nodes, termed metastases. The metastases may be observed in areas other than the pelvis including the spinal cord and long bones. Examples of these may be seen in Figure 1.44., where bone scintigraphy shows the spread of metastases to bone (42). Clinically, bone metastases are associated with poor prognosis and mortality of the patient (43, 44). The effects of bone metastases are accompanied by severe pain, spinal fracture and spinal cord compression potentially resulting in paralysis. The quality of life of the patient is greatly affected by these skeletal events rendering daily tasks challenging (45). To monitor disease progression, bone scans and CT scans can identify metastases in both lymph nodes and bone tissue. PSA levels are a good indicator of progression; rising PSA levels after prostatectomy is a clear indicator of increased metastatic burden.

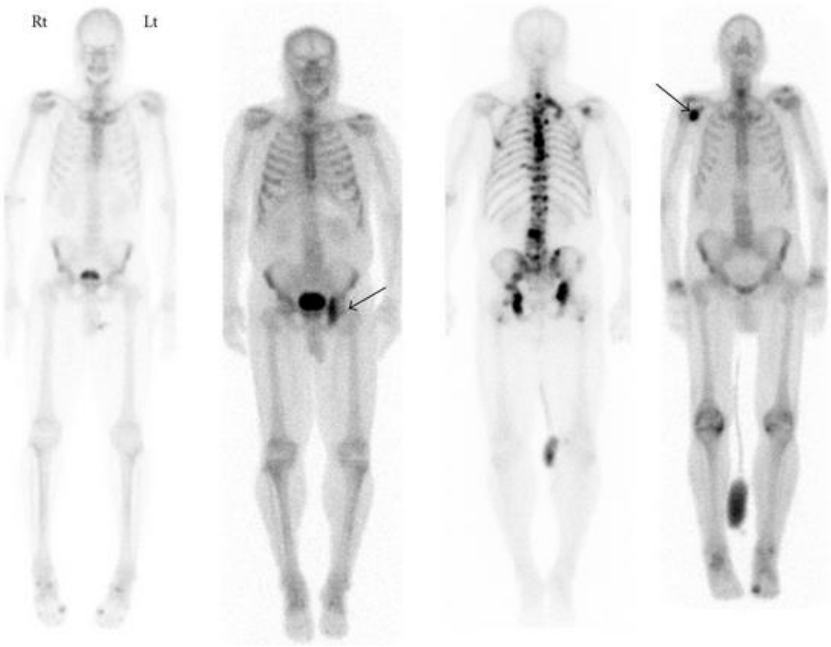

Figure 1.44 Scintigraphy of bone metastases.

Bone scintigraphy of patients displaying varying degrees of bone metastases. To the left an individual with a normal bone scan, second image is a prostate cancer patient with metastases in pelvis and lumbar spine. Third image of patient displaying widespread metastasis including pelvis and spine. Image to the right is of a distant metastasis without pelvic or lumbar spine abnormalities (46). Image available for use and modification under the Creative Commons Attribution License.

1.2 Bone metastases and effects on bone niche

1.2.1 Prostate cancer spread to bone

As discussed above, early stage prostate cancer is localised to the prostate gland. With disease advancement, malignant cells will gain the ability to metastasise to surrounding tissue and invade blood vessels. Once mobile, circulating tumour cells may disperse and invade distant tissues/organs of the body. The bone is often the target for distant metastatic sites, most notably those of advanced prostate and breast cancer disease (47). Prostate cancer cells have a preferential localization to bone tissue as the bone microenvironment contains optimal factors to promote growth (as reviewed by (48, 49)). In prostate cancer, bone metastasis are predominantly of osteoblastic nature, characterized by the formation of new bone, although the process is still poorly understood (50). The most widely accepted theory of bone disease formation is the “seed and soil” hypothesis whereby the metastatic cells “seed” target a favourable growth environment “soil” (51). These tumour metastatic cells are able to exploit the bone niche by hijacking the BM growth microenvironment, which facilitates the growth and expansion of disease. While metastatic sites expand, a feedback loop is created with secretion of growth factors from tumour cells that further stimulate bone growth and resorption as summarized in Figure 1.55 (48, 52, 53). Preferential bone sites for metastatic growth include bones rich in red marrow such as the ribs, pelvis and spine (54).

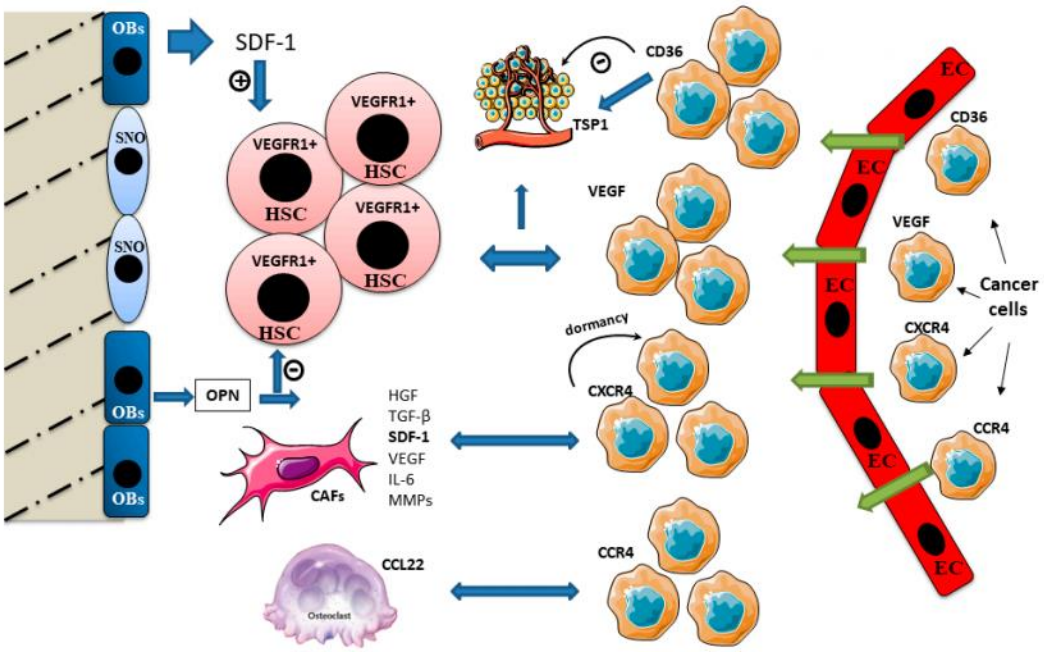

Figure 1.55 Bone niche crosstalk during metastatic growth.

Bone niche to the left and vascular niche to the right**.** HSC niche is localized in the centre of the BM marrow in proximity to the vascular niche. Endothelial cells (EC) residing here are actively involved in the HSC mobilization and homing. Circulating metastasis will utilize the tightly regulated signalling between niche bone and BM niche to infiltrate and home within bone tissue. Immature osteoblasts (OBs) secreting stromal derived factor 1 (SDF-1) and Osteopontin (OPN) positively and negatively regulating HSC maintenance. Cancer associated fibroblasts (CAFs) releasing factors promoting metastatic formation and growth including VEGF. Cancer cells presenting CD36 ligand are attracted from thrombospondin (TSP1) expression and cells presenting CXCR4 chemokine receptors are homed to bone sites. Mature osteoclasts express chemokine ligand CCL22 promoting metastatic growth of metastatic cells containing CCR4 chemokine (52)**.** Image available for re-use under the Creative Commons Attribution License.

1.2.2 Disruption of normal bone maintenance

The bone endosteum is vascularised connective tissue containing bone growth/maintenance cells osteoblasts and osteoclasts, located between the compact and

spongy bone layers and the BM. The endosteal and vascular niches together (bone niche) are actively involved in the retention and release of stem cells residing here, along with osteoblast and osteoclast cellular differentiation (55). The bone niche is also tightly involved with the regulation of the BM microenvironment which includes haematopoietic stem cells (HSC) and their progenitor cells (55). In normal bone formation, solid and avascular mesenchymal tissues are replaced by mineralized cartilage and fibrocartilage. Minerals such as calcium are actively transported by osteoblasts and deposited. Once deposited the minerals undergo maturation from amorphous calcium phosphate to hydroxyapatite with important changes to mineral orientation and organization (56). This process is tightly regulated by both mineral concentration, cellular signals, and pH gradients (as reviewed by (57)).

Although the majority of bone metastases in PC patients are osteoblastic in nature (58), PC patients may present metastases of osteoblastic, osteolytic or a mixture of both types (as reviewed by (48, 59)). The type of metastases will affect the bone remodelling and resorption processes. 3D evaluations of bone section from advance prostate cancer patients have shown increases in bone trabeculae along with bone volume increase and bone surface irregularities (60, 61). The process is associated with synchronised increase in bone resorption and formation (62). The adherence, proliferation and overall tumour growth is accompanied by severe discomfort for the patient due to the formation of bone lesions. These lesions include but are not limited to bone fracture, spinal cord compression and bone marrow aplasia, all of which are associated with poor quality of life for the patient (47). Further complications may arise from spinal cord injury including chronic BM failure and paralysis (63, 64). The occurrence of bone metastases remains the major cause of morbidity in in PC patients (47, 65, 66).

1.2.3 Bone marrow haematopoiesis

The BM is involved in the replenishment of blood components and the process by which these components are formed is termed haematopoiesis. The BM is separated into the vascular and non-vascular components. The vascular part includes blood vessels that supply nutrients to the bone and transport newly produced blood components away from the

bone, the non-vascular BM is where haematopoiesis occurs, and haematopoietic stem cells reside (HSCs). In adult life, haematopoietic marrow is concentrated to the central skeleton and proximal ends of femurs and humeral bones. In adults, cellular replenishment of blood components occurs rapidly with a turnaround of 1 trillion cells per day (average 70 kg male) (67, 68). This rapid replenishment is thanks to the ability of HSCs to self-renew and also divide/differentiate into multiple blood cell types. During cell division, a HSC will divide in to two daughter cells, one retaining stem cell qualities enabling it to further replicate into more HSCs and the second daughter cell instead being a committed stem cell which will undergo cellular differentiation in to an early lymphoid or myeloid lineage progenitor cell. These progenitor cells will in turn divide and differentiate into many different cells ranging in functions.

HSCs are not continuously dividing and instead spend most time in cellular quiescence to prevent exhaustion (69). In a healthy adult, HSCs may replicate on average every 40 weeks with a range of between 25 and 50 weeks depending on general health and age (70). HSCs respond to specific signals released in their microenvironment from neighbouring cells in the bone niche. These signals will stimulate HSCs to either exit or remain in cellular quiescence (71, 72). The micro environmental conditions are crucial for the correct maintenance of HSCs and a myriad of factors are required to keep this balance; effects on the microenvironment will have detrimental impacts on the replenishing of blood cells and may contribute towards leukemogenesis (73).

Progenitor cells migrate towards the central cavity of the BM where blood vessels are present and only mature cells will be able to enter the blood stream by the presence of membrane proteins which enable the attachment and passage through the blood vessels endothelium. Multipotent lymphoid progenitors (MLP) will either enter the blood stream or remain in the BM to mature. MLP that remain in the BM for maturation are later termed B-Lymphocytes while MLP that enter the blood stream will migrate to the thymus for maturation and are thus termed T-Lymphocytes. MLP in the thymus cortex will undergo self-tolerance selection and 2-4% of T cells will successfully succeed and mature into several forms of thymocytes (74). Activation is the next step and once activated resting T lymphocytes may undergo blastogenic transformation. These newly formed large T cells will divide and produce medium and small lymphocytes with the same antigen specificity.

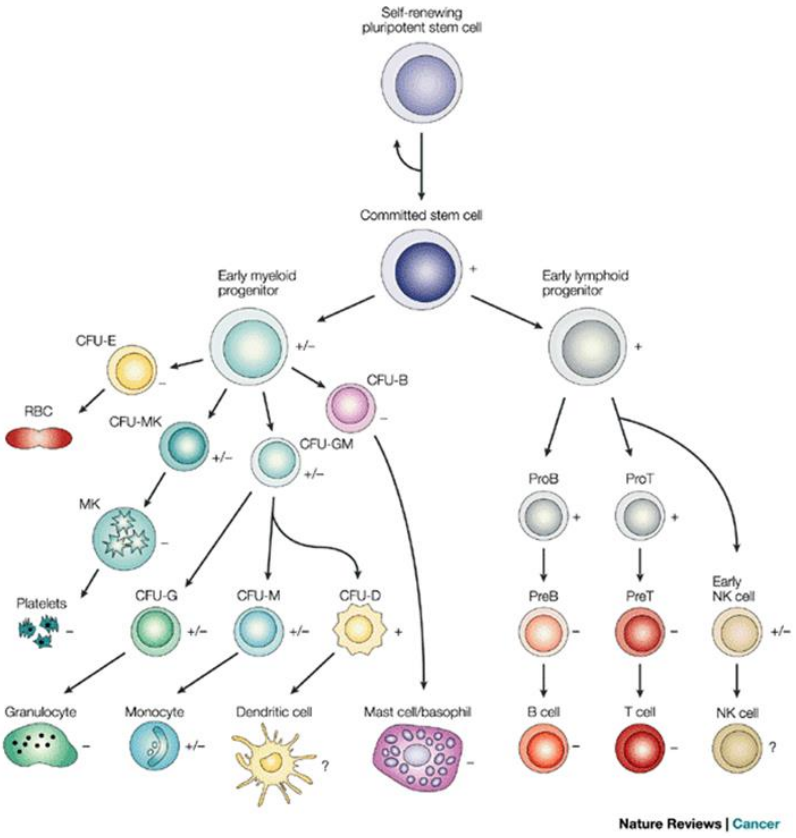

Figure 1.66. Normal haematopoiesis.

HSCs giving rise to myeloid and lymphoid progenitor cells carrying on differentiation in to mature circulating blood components (75). Image Licenses agreement granted for re-use under Springer Nature Licence for publication of image in Thesis/Dissertation as defined by the Sherpa guideline.

Once matured, T cells may migrate from the thymus once again to the blood stream, thymic output varies with age with younger individuals having a higher thymic output than older individuals and women having a higher thymic output than men throughout their life (76). Peripheral blood lymphocytes (PBL) mainly consist of naïve cells or memory T cells, naïve cells being those which are yet to be exposed to an antigen and are thus non-specific. T cells will cycle periodically from blood to lymphoid tissue, migrating through the body, awaiting activation by a specific antigen. If the T cell does not encounter an antigen it may circulate in the blood for weeks or months and long-lived memory T cells may circulate the system for years. If an antigen is encountered, lymphocytes will proliferate within the lymphoid tissue and once antigen activated, they will migrate from the lymphoid tissue to target sites via blood stream (77).

1.3 Traditional treatments and disease management

The treatment of PC varies depending on the stage of disease and whether the cancer has spread only to neighbouring tissues or to distant metastatic sites. In cases of localized disease, treatment may include prostatectomy surgery and/or brachytherapy. Once the cancer has breached the prostate and moved to neighbouring tissues such as lymph nodes, external beam radiotherapy (EBRT) and hormonal therapy may be recommended to prevent further spread. Further advancement and metastasis to distant sites such as bone are then further managed by chemotherapy and bone targeted therapies to alleviate symptoms. Recently, the use of ^{223}Ra has been approved for the treatment of bone metastasis, this being the first treatment showing reduction of skeletal related events associated with bone metastasis and increased survival for the patients (78-80).

1.3.1 Surgery

A radical prostatectomy is a treatment option for men with localized disease, which involves the surgical removal of the prostate gland and surrounding tissue. Surgical removal is the most effective treatment resulting in both high survival rates and low incidence of relapse. Although side effects may include pain, urinary incontinence and erectile dysfunction, many studies support radical prostatectomy even for younger patient cohorts as many side effects are limited and are often overcome with time (81-83). Active surveillance has been suggested as an alternative to prostatectomy for higher risk patients presenting localized disease. This includes regular GP visits to monitor any changes, however, this remains controversial. A 15-year retrospective clinical analysis of 3170 prostate cancer patients (mean age 65.3 ± 6.4 years) found 86% of patients to still be alive at time of study with a follow up range of up to 25.3 years. The overall survival rate of study participants was found to be consistent with the expected survival rates for male of similar ages in the local area (84). This supporting prostatectomy as an effective treatment for localised diseased in older men. A recent study with both older and a younger cohort ($\leq$ 55 and $>$ 55 years of age respectively) also found similar results with the younger cohort showing 72.4% disease progression free survival in their 8 year follow up (85).

1.3.2 Radiotherapy

Radiotherapy treatments utilizing ionising radiation (IR) are common for PC management and treatment even with localized disease. As IR traverses the body it interacts with tissue and associated cells depositing energy through a series of ionisation and excitation events along the radiation tracks. Exposure is often described in terms of dose which, independent on radiation quality, defines the amount of energy deposited per unit mass and has the unit of gray (Gy), where 1 Gy equals 1 joule per kilograms (J/kg). Brachytherapy treatment consists of radioisotope implantation in the tumour site, via interstitial brachytherapy with permanent implantation of a radioisotope or temporary implantation. Permanent implantation will be with low dose rate radionucleotides implanted as "seeds" (86), these will slowly decay targeting the prostate area. Temporary implantation instead uses high dose rate radionucleotides, these use catheters to circulate the radioisotopes within the targeted area for as little as 10-20 minutes before being removed. Low-dose rate brachytherapy is usually recommended for early stage prostate cancer patients while high dose rate brachytherapy is usually offered for locally advanced disease (87). A higher dose rate radioisotope commonly used in temporary brachytherapy is iridium-192 (^{192}Ir) with a half-life of 75.2 days. This isotope is a gamma and beta emitter with an average energy of 400 keV. ^{192}Ir has a high penetrance into the tissue, therefore the exposure times with ^{192}Ir are kept low to prevent non-target tissue exposure. Iodine-125 (^{125}I) is a gamma emitter with a half-life of 59.5 days and a low average energy release of 27 keV. ^{125}I is used as a permanent implant similarly to Palladium-103 (^{103}Pd) also with a low energy release (average beta particle release of 21 keV) and with a half-life of 17 days (88). No significant differences in patient outcomes have been observed between these different isotopes and all remain widely used (89). The side effects of brachytherapy are similar to those following prostatectomy. When compared through a French multicentre patient questionnaire with 435 patients, urinary incontinence was found to be more common following prostatectomy, whilst urinary frequency, urgency and pain was associated with brachytherapy (90). A US study with retrospective comparison of 1305 PC patients also found no significant difference in treatment outcome with a suggestion that brachytherapy may be more effective in higher risk groups (91). With the French study highlighting similar cost effectiveness for both

treatments, the choice between brachytherapy and prostatectomy is considered on patients' individual needs.

For patients with a higher risk of metastases in the surrounding tissue, EBRT may be administered either in conjunction with brachytherapy or after prostatectomy. EBRT provides a wider uniform dose to the pelvic region targeting seminal vesicles and lymph nodes (92), which prevents disease progression. Different forms of EBRT exist and the most commonly used methods for PC treatment include three-dimensional conformal radiation therapy (3DCRT), Intensity-modulated radiation therapy (IMRT) and Image-guided radiation therapy (IGRT). All three EBRT types utilize CT scans to map the target zone of the tumour and surrounding tissues, the beam then maps these areas. Differences between accuracies in zone targeting exist between treatments and in recent years IMRT has become the most common technique used with recent studies suggesting IMRT has the highest accuracy in dose delivery to target tissue, minimizing normal tissue exposure over 3DCRT (93). The main side effects following EBRTs include those from genitourinary toxicity previously associated with brachytherapy, and additionally, due to the wider field of exposure gastrointestinal toxicity symptoms, such as diarrhoea and changes in bowel movement. Overall, both IMRT and IGRT have been shown to have low rates of acute toxicity, and a combination of the two treatments have also been shown to result in low rate of late toxicity (94, 95).

1.3.3 Hormone therapy

In cases of disease advancement, androgen deprivation therapy (ADT) and combined androgen blockade are often prescribed by GPs with the aim of rapidly controlling disease progression (96). The treatment may also be used in cases where the patient is at higher risk from EBRT and/or to aid radiotherapy outcome by shrinking the tumour area. Tumour volume shrinkage by ADT is well documented with median reduction up to 50% within months of prescription and it has been shown to be an effective treatment paired with EBRT to minimize the exposure area during treatment (97-100). ADT therapy targets the testosterone pathway utilized by prostate cancer cells for growth. By blocking androgen receptors present on the cell surface or reducing the production of testosterone itself, it is possible to inhibit the PC cell growth. These effects are usually limited to a short period of time (101, 102) as PC cells will eventually be able to bypass the receptor block and initiate

testosterone production themselves (103). Patients who are no longer responding to hormone therapy are deemed castrate resistant. Current treatments for advanced castrate resistant PC focus on the palliative care attempting to control the disease and manage the associated symptoms.

1.3.4 Chemotherapy

As part of general standard of care in the UK, Castration resistant prostate cancer (CRPC) patients are offered chemotherapy for ongoing palliative care. Two chemotherapy agents are usually used: docetaxel and cabazitaxel, docetaxel being the most commonly administered in the UK (104). Both drugs target the microtubular network by binding to microtubules during mitosis, as this action stabilizes the microtubules preventing depolymerization. This block is recognised by the cell resulting in mitotic arrest and eventually apoptosis is initiated resulting in cell death. Clinical trials have demonstrated improved survival for CRPC alone and in combination with ADT, for those patients in the hormone sensitive stage (105-110). As with ADT, resistance to these treatments is often achieved by PC cells. Although the mechanisms are not fully understood they are believed to be associated with the acquired ability to reduce intracellular drug concentrations, circumventing the drug action by antagonizing the agent and/or apoptotic escape (as reviewed in (111-113)). In cases where the above treatments have been exhausted, some patients may also be recommended for clinical trials involving immunotherapy or radiotherapy. Recent advances in targeted radiotherapy aim to not only improve the reduction in metastasis size/number and primary tumour size but also to alleviate the symptoms which affect the quality of life of the patient.

1.4 The re-emergence of particle therapies

In the last decade, radiopharmaceuticals have gained popularity for novel clinical applications, and many been investigated for the targeted treatment of numerous cancers (114-117). The advantage of radiopharmaceuticals over traditional radiotherapies is the increased ability to target only malignant cells whist sparing surrounding tissues. This is achieved by the radiopharmaceutical being engineered to preferentially bind to cancer cells or via pharmacokinetic properties of the radiopharmaceutical itself. Many clinical trials are underway for both beta (Lutetium-177 (118-120) and Yttrium-90 (121-123)) and alpha particle therapies (Thorium-227 (124, 125), ^{223}Ra (126-128) and Astatine-211 (129)). The approved radiopharmaceuticals are either aimed to be combined with existing therapies or are being produced as new labelled radiopharmaceuticals. There is a drive towards replacing many existing beta-particle therapy with alpha particle radiopharmaceuticals to reduce non-targeted tissue exposure (130). An example of this is radiopharmaceuticals currently labelled with ^{90}Y and ^{177}Lu for neuroendocrine tumours which may be replaced soon with new alpha-particle emitter ^{212}Pb label (131). This recently showing promising results in AlphaMedix phase I clinical trial for both reduction of metastatic load and improving quality of life (132).

1.4.1 Beta particle therapy

Many clinical trials have evaluated the use of β-particle emitters for the management of bone metastases in CRPC patients (133-136). These treatments remain the last resort, with a focus on palliative care to alleviate symptoms of disease progression. Current β- emitters include strontium-89(^{89}Sr), samarium-153 (^{153}Sm), rhenium-186 (^{186}Re) and rhenium-188 (^{188}Re). The main concern with the use of β-particles in bone treatment is the potential toxicity due to the deeper penetrance within non-targeted BM regions, particularly for patients of high metastatic burden (137). This toxicity is mainly reported as temporary drops in the blood cells however, a few leukaemia cases have also been associated with past treatment with ^{89}Sr (138, 139) and with ^{153}Sm, ^{186}Re, ^{188}Re also showing low haematological toxicity (140-145). Due to the localised energy deposition of β-particles, higher doses are

needed to achieve the same killing effect as α-particles and with the increased dose, higher toxicity to the haematopoietic system may occur. Ultimately β-emitters remain widely used for palliative care for many cancers which have spread to bone regions.

1.4.2 Alpha particle therapy

Interest in α-particle therapies have grown in recent years as they offer more targeted cell killing, meaning this treatment has applications for patients with a high metastatic burden and, for patients earlier in their disease who may have a better prognosis. Many α-particle emitters are currently in clinical trial for a variety of cancers, disease stages and as combination therapies. Actinium-225 (^{225}Ac) is being investigated as a treatment for CRPC patients and is currently under Phase I clinical trial for dose escalation with initial findings showing good tolerability in patients who had also previously received other forms of chemotherapy and treatment with both α and β emitting radionuclides (146). Further clinical trials are also being carried out with Thorium-227 (^{227}Th) conjugated to monoclonal antibodies targeting cancer cells known to express mesothelin within their cell membrane, this having shown promising results with *in vitro* and *in vivo* animal testing (147). ^{223}Ra has been approved for the treatment of bone metastases in CRPC patients having generated a great deal of interest for treatment of bone metastases from other cancers, combination therapies and potential paring with nanoparticle therapy for theragnostic applications (148-151). All initial trials listed suggest good haematological tolerability of α-particle emitters, however many of the studies still in early phase.

1.4.3 Pharmacokinetics of ^{223}Ra

Newly targeted forms of radiotherapy such as ^{223}Ra aim to control metastatic formation and growth by targeting areas of high bone remodelling, while minimising exposure to non-target regions of the BM. Radium is often found as a by-product of uranium mining and to date it is currently mostly used in nuclear medicine. ^{223}Ra is manmade by bombarding naturally occurring Radium-226 (^{226}Ra) with neutrons resulting in unstable Radium-227 (^{227}Ra) which will eventually decay to ^{223}Ra. Radium is a chemical element that is highly reactive and is known as one of the alkaline earth metals along with beryllium, magnesium,

calcium, strontium and barium. Alkaline earth metals are known for their bone seeking properties as they target hydroxyapatite which makes up 50% of the bone matrix. Radium, being an alkaline earth metal, acts as a calcium mimic and ^{223}Ra has been shown to be a useful, targeted form of internal radiotherapy which localises to areas of high bone turnover.

^{223}Ra is administered intravenously as ^{223}Ra dichloride under the trade name of Xofigo. It rapidly localises to areas of freshly mineralized bone areas, within 24 hours of administration (152-155). Clearance from blood is also rapid with the majority of the radioisotope cleared through the gastrointestinal tract and the remaining through the kidneys (154). The clearance of ^{223}Ra from the blood has been found to be linear, and independent of the injected activity. Previous studies on rodents found minimal uptake of ^{223}Ra in non-targeted areas such as the kidneys and spleen (156).

^{223}Ra has a half-life of 11.4 days and during its decay pathway it will emit 4 α and 2-β particles (Figure 1.1212). 94% of its decay energy will be released as α-particles. α-particles have the shortest range compared to β and ϒ-rays, this results in highly targeted treatment. Although the range may be short, the distribution of energy along the track is dense, localized pockets of energy will result in severe damage to matter increasing the cell killing effect (155, 157). Studies have shown ^{223}Ra to be effective in delivering localised cell death in target areas, and this makes it an ideal treatment for bone disease in advance prostate cancer patients (157-161). The cytotoxic effects are mainly attributed to the high frequency of lethal double strand breaks (DSB) directly induced as well as reactive oxygen species formed. The use of α-particle has limited dependence upon radioresistance across tissue, cell cycle and changes in oxygen levels within tumours.

As ^{223}Ra is rapidly cleared from the blood, the highest absorbed doses are observed in neighbouring sites of target bone metastases, including osteogenic cells and the red BM. ^{223}Ra clearance from the blood is followed by excretion via the gastrointestinal tract, with the intestinal wall being the 3rd site of high absorbed dose. As α-particles have a short range the majority of dose will be delivered to the surrounding gut and while β-particle may reach the intestinal lining, these consist of only 4% of ^{223}Ra emitted energy. Although it does result in high absorbed doses in bone areas, ^{223}Ra is associated with low numbers of

haematological events and myelosuppression, with these being only temporary effects chiefly observed during treatment (162, 163).

1.4.4 Clinical outcomes with ^{223}Ra

The ALSYMPCA (ALpharadin in SYMPtomatic Prostate Cancer) study resulted in the approval of ^{223}Ra for CRPC treatment. ALSYMPCA was an international clinical study which begun in June 2008 with termination in February 2013. ALSYMPCA evaluated the efficacy and safety of ^{223}Ra dichloride in patients with hormone refractory PC and skeletal metastases. The study consisted of a randomised administration of placebo or ^{223}Ra administered intravenously every 4 weeks for 6 cycles. A total of 921 patients were recruited, 307 being administered a placebo and 614 being administered ^{223}Ra. The results found ^{223}Ra to increase patient survival. The overall survival for the placebo group was estimated at 11.3 months with a median of 10.1-12.8 months survival. The overall survival for the ^{223}Ra was 14.9 months with a median of 13.9-16.1 months showing a clear increase in overall survival for patients receiving the treatment (79).

A secondary outcome of the study was the time of occurrence for the first skeletal related event (SRE) (164). In the ALSYMPCA trial these were recorded as the first date where EBRT was used to relieve skeletal symptoms such as bone fractures of both vertebrate and non-vertebrate and spinal cord compression. The placebo group time of first SRE was 8.1 (range 6.7-11.9) months whilst in the ^{223}Ra group the first SRE occurred at 16.4 (range 14.3-18.3) months, showing ^{223}Ra subjects having delayed first SREs. The SRE were also found to have a delayed onset along with overall reduction in events and low myelosuppression incidence (79). Later studies also confirmed the delay in SRE including patients having received chemotherapy treatment prior to ALSYMPCA enrolment (165, 166). Although no long term follow up is available, a recent 3 year follow up confirmed there to be no delayed safety concerns indicating that ^{223}Ra was well tolerated, coupled with meaningful quality of life improvements along with overall slower decline over time (78-80, 162). Ultimately the ALSYMPCA clinical trial resulted in the FDA approval of ^{223}Ra in 2013 for the treatment CRPC patients presenting bone metastases.

1.5 Principles of ionizing radiation

Radiation is the transmission of energy through space and material mediums. Radiation may be non-ionizing (below 10 eV), transmitted in longer waves and lower frequency, or of ionizing kind transmitted in shorter waves and higher frequency (generally above 10 eV). Ionizing radiation possesses sufficient energy to ionize electrons during its interaction with matter, which results in the atom or molecule being electrically charged forming an ion. Radiation may travel in the form of electromagnetic waves or sub-atomic particles. Ionizing electromagnetic waves include Gamma and X-rays which are highly penetrating as they do not have mass or an electrical charge. Particulate radiation includes alpha, beta and neutron particles all of which have various characteristics due to their mass and charge; this affects the penetrance with denser particles travelling shorter distances.

α-particle are large particles composed of two protons and two neutrons identical to a helium-4 nucleus with a positive charge of +2 (167). Due to their size and charge they interact heavily with matter having a large energy release, often described as clusters of ionizing radiation, which slows their speed. β-particle are described as having a negative charge of -1 or positrons with a positive charge of +1 (167). Due to their small size (~8000 times smaller than an α-particle), they can travel a larger distance within matter and therefore have a slower energy release. Protons are larger than a β-particles (~1838 times), have no electrical charge and are able to travel further than β-particles. Protons carry a positive charge and long range proton exposure usually only occurs as a result of artificial acceleration. Therefore, long range proton exposure will not typically occur from nuclear decay. In terms of tissue penetrance, external exposure to α-particles is not deemed dangerous as the energy is absorbed by the skin as the penetrance is usually less than a few cells in thickness. β-particles have a higher penetrance and can pass through the skin layers to deeper tissues by a few centimetres. Instead, gamma and X-ray exposure is typically more penetrating traversing a human body and requires a thick layer of lead or concrete of the order of 1m (depending on energy) to provide significant shielding (167). Due to their neutral charge, neutrons will readily pass through most materials, with the most effective shielding materials being water or hydrocarbons such as polyethylene of paraffin wax. However, in terms of internalised exposure, α and β particle exposure is more dangerous as

they are more ionizing per unit dose, therefore if internalised they will have a higher relative biological effectiveness (RBE). The RBE describes the ratio of dose required for the same biological effect across differing radiation types. Typically, x-rays or gamma rays are described as low-LET and α-particles as high-LET.

1.5.1 Measuring ionizing radiation

Radioactive decay occurs when an unstable nucleus loses energy to achieve a stable state and may be achieved through particle decay (α,β or neutron) or through ϒ decay, electron capture. Briefly, α-particle decay is characterized by the ejection of two protons and two neutrons, equivalent to a helium atom to stabilize the nucleus. β-particle decay involves the transformation of a neutron into a proton with the emission of an electron or vice versa with the emission of a positron instead. Neutrons are uncharged and relatively stable therefore neutron release usually results from nuclear fission, fusion, from cosmic particle interaction or from particle accelerators. Rather than interacting with the electrons of an atom they interact with the nucleus, resulting in recoil protons, or in the case of higher energy neutrons "spallation products", for example a fast neuron interacting with a carbon atom or oxygen atoms may result in the nucleus breaking up in to 3 or 4 α-particles respectively. It is through these secondary charged particles that energy is deposited to the tissue resulting in biological damage. The international (SI) unit for measuring radioactivity is the Becquerel (Bq). A Bq is equal to the quantity of radioactive material in which one nucleus decays per second. The decay of a radioactive material may be described by its half-life, this being the time required for half of the unstable nuclei within the material to decay. Radiation exposure is described as the energy released or produced within a material medium and may be defined in different ways to account for the level of harm induced. The absorbed dose describes the effect radiation has on a medium irrespective of radiation quality and it is measured in SI units called gray (Gy). α-particles are significantly more biologically effective than low-LET radiation for a wide range of biological end-points, requiring significantly less dose to produce an equivalent biological effect. With the specific RBE depending on a number of factors such as the energy/LET of the particle, dose, biological end-point studied and cell type. When considering the long-term cancer risk the

concept of equivalent dose is commonly used (units of a sievert, Sv), which is calculated by multiplying the absorbed dose (Gy) to a given tissue by a weighting factor, w_R, chosen by the ICRP committee to reflect the higher biological effectiveness of high-LET radiation compared with low-LET radiations. High-LET α-particle have chosen a w_R value of 20 (168).

Linear energy transfer (LET) refers to the action of radiation upon matter and describes how much energy an ionizing particle transfers to the material traversed per unit distance. LET varies depending on type of particle, and the unit used to measure LET is keV/µm (169). The most common way of measuring LET is the track average method, obtained by dividing the track into equal lengths and calculating the respective energy per unit of length, this being expressed as the mean energy of the whole track. The energy average is also used and yields similar results for monoenergetic particles. This method divides the energy deposits evenly and calculates the mean distance over which they are deposited (167). In the case of X-ray exposure, these photons interact within the tissue producing energetic electrons (and in the case of a pair-production event an electron-positron pair). These electrons subsequently deposit energy (through ionisation and excitation events) as they slow down and can produced secondary and territory etc electrons which themselves can produced addition ionisation events along their track. It is via these electron tracks and their interactions that photons deposit energy within the cells and tissues of the body. Particle exposure instead deposits energy as it travels through matter causing the particle to decelerate releasing constant amounts of energy generally increasing to a Bragg peak, just before achieving thermal equilibrium with the absorbing material (170, 171). The LET value for particle exposure will vary based on the method used, the track average and energy average will be significantly different when considering heavy particles as these will decelerate faster releasing more energy per track length. The RBE enables the comparison between the effects of different LET radiation and is dependent on: the type of radiation, dose, dose rate, dose administration (i.e. fractionation), and the biological effect being assayed (172). Figure 1.7 shows the increased RBE following fractionated treatment by neutron and X-rays compared to single dose. With respect to radiation protection, RBE for relevant biological endpoints have been used to guide the choice of radiation weighting factors for stochastic effects such as cancer, or specific RBE for a given deterministic effect (173). Deterministic effects are tissue reactions with severity increasing with radiation dose above a threshold,

below which there are no clinically observable effects. These effects are predominately a result of significant cell death within the tissue. In contrast, the probability of genetic mutations and cancer increases with dose with no strong evidence for a threshold (174).

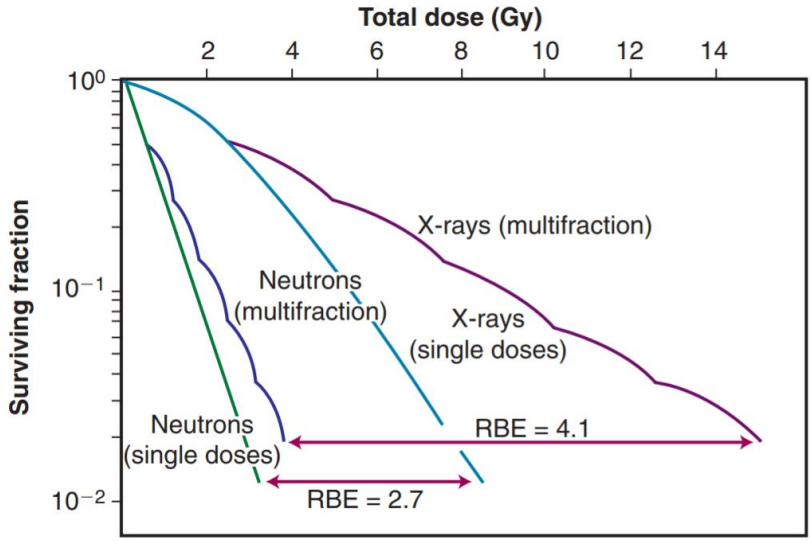

Figure 1.77. Increased RBE with multiple fractions.

The survival fraction following neutron and X-ray exposure was plotted as an RBE endpoint. The RBE of neutrons is higher than X-rays. A single fraction for each radiation type is seen as inducing lower RBE than multiple fractions. Image from Zeman (2016 (172)).

1.5.2 Increasing LET and DNA damage

The use of ionizing radiation in medicine includes diagnostic X-rays, to capture images for medical procedures and dental evaluation, nuclear medicine with internally administered radioisotopes for both diagnostics and treatment, and standard external radiotherapy for disease treatment and management such as cancer. Cells exposed to ionizing radiation may result in changes to the DNA through both direct and indirect mechanisms. Irreparable damage to the DNA will result in the cell being unable to normally function and divide eventually inducing cellular senescence and ultimately cell death pathways. The direct interaction of radiation with DNA may result in molecular disruptions causing different lesions such as base damage, including pyrimidine dimers (thymine and cytosine bases) and purine lesions (adenine and guanine bases), and breaks of single (SSBs) or double strand (DSBs).

As reviewed by Hill 2020 (175), ionising radiation is very effective in the induction of DNA clustered damage and a wide spectrum of damage being induced both directly and indirectly. Most notably the highly harmful DSB which is often mis-repaired leading to cell changes and/or cell death. DSBs produced by increasing LET result in multiple lesions, including strand breaks and base damage, spatially close to one another. These clustered lesions termed complex DSBs. 70% of cell damage is attributed to indirect effects by free radical formation from the interactions of the radiation with water in the cells (176). If the energy deposition is within the surrounding water molecules rather than the DNA itself, this can cause H_2O molecules to undergo radiolysis resulting in the formation of unstable reactive oxygen species (ROS). These ROS molecules are highly unstable as they contain an unpaired electron and as such these molecules are likely to interact with the neighbouring DNA. ROS induces hydroxylation of nucleic acid bases, potentially resulting in the formation of SSBs and DSBs (177, 178). Of the induced damage, DSBs are considered the most lethal to the cell as if left unrepaired they may lead to cell death while SSBs are instead readily repaired. However frequent these lesions by ROS may be, the damage induced by free radicals is mainly of simple kind. With any DSBs produced presenting a low number of lesions namely less than two lesions within one or two helical turns of DNA. Direct damage to the DNA will result in the highest number of complex strand lesions this posing a greater risk to the cell as complex DSBs are more challenging to repair.

Low LET radiation results in random distribution of energy from many tracks, the resulting damage is sparsely distributed with small clusters of 1-2 lesions. By contrast, high LET radiation mainly results in clustered damage (within 10 base pairs) along a single track with clusters containing an average of 4-5 lesions with some being found exceeding 25 lesions (179-181).

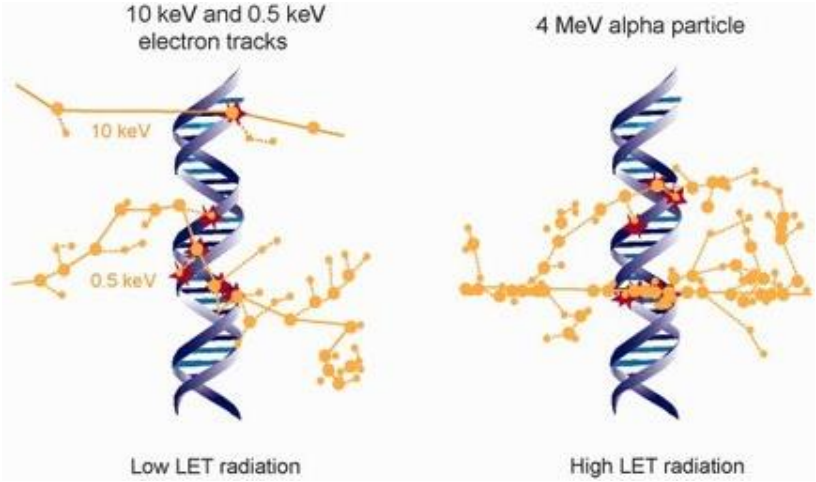

Figure 1.88. DNA damage induced by ionizing radiation.

Distribution of DNA damage inducing events after direct exposure low and high LET IR. Ionization events localize along the particle tracks. Large dots represent ionizations and small dots represent excitations along the radiation track. Energy deposition clusters in high LET exposure results in complex damage within a small unit distance (182). Monte Carlo simulated tracks are drawn for the 0.5 keV e− and the α particle on the same scale as the DNA redrawn from Goodhead et al. 1995 (183). The track for the 10 keV e− are by free drawing and shown only for illustration purposes. Image available for re-use under the Creative Commons Attribution CC BY license.

Figure 1.99. illustrates the spatial density of low LET and high LET tracks within a PBL cell nucleus. Depending on the LET, the lesions will have a different frequency and distribution within the cell nucleus. *In vitro* studies have shown the ratio of SSB to DSB to decrease with increasing LET (184-187), whilst the amount of base pair damage is found to remain consistently two-fold higher than that of strand breaks irrespective of LET (188). In terms of DSBs, more complexity is induced after exposure to high LET radiation. Following low LET exposure 30% of DSBs are complex, with ≥3 strand breaks within 10 base pairs, this increasing to 70% following high LET exposure (189, 190). This is reflected in the RBE of particulate radiation being higher than X-ray and ϒ-gamma exposure, resulting in a higher amount of damage within a cell nucleus. Therefore, the killing effect from particulate radiation is higher and whilst the penetrance is lower than X-ray and ϒ-gamma exposure,

there is a potential for particle radiotherapy to be highly targeted to tumour cells only with high tissue sparing for surrounding normal cells.

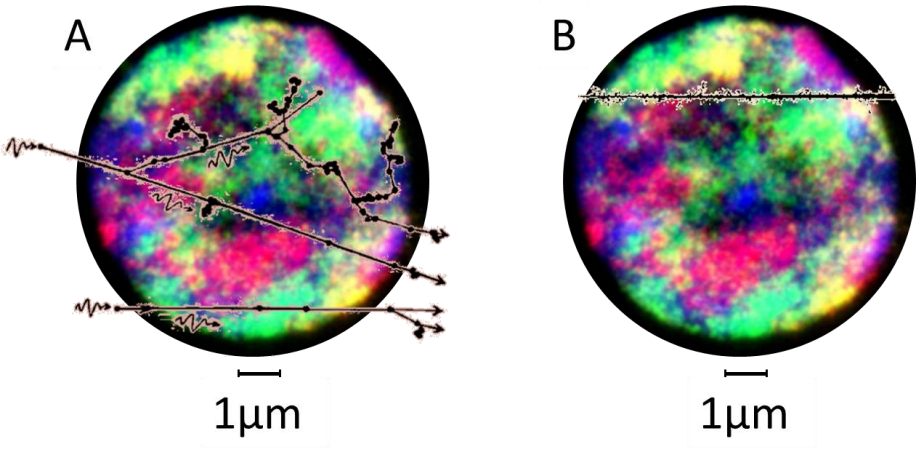

Figure 1.99 Distribution of energy deposition by different LET in PBL nucleus.

PBL interphase cell nuclei captured via multiplex-fluorescent-in-situ-hybridization painting with highlighted chromosome territories by 5 colour probe set. A) Low LET tracks have small event spurs of energy randomly distributed across the nucleus resulting in similar number of lesions per spur. B) High LET tracks having clustered blobs of energy release resulting in varying size of energy deposition and thus varied number of lesions per blob. 1Gy exposure of x-ray or gamma ray corresponds to ~ 1000 electron tracks traversing a PBL nucleus compared to an average of approximately ~ 2 alpha particle tracks of corresponding 1Gy exposure. Track and energy deposits were overlaid from previous publications for illustration only (191). Image available for re-use under the original image copyright 2021 National Academy of Sciences for non-commercial reuse.

The biological effectiveness of α-particles varies significantly based on the particle energy. As an α-particle traverses a tissue, it will decelerate increasing energy deposition towards the end of the track (As seen in Figure). With a same given dose, decreasing the α-particle energy (hence increasing the LET) has been shown to increase clonogenic survival of cells

traversed by a single track (192). By exposing varying cell types *in vitro* to 120 keVμm^{-1} α-particle Goodhead et al. 1999 (193) found the cell survival of some epithelial cell lines to be as high 90% whilst some heamatopoietic cells as low as 0%. This highlighting that cell survival to α-particles is also based on more complex factors including the cell geometry, cell type and stage of maturation.

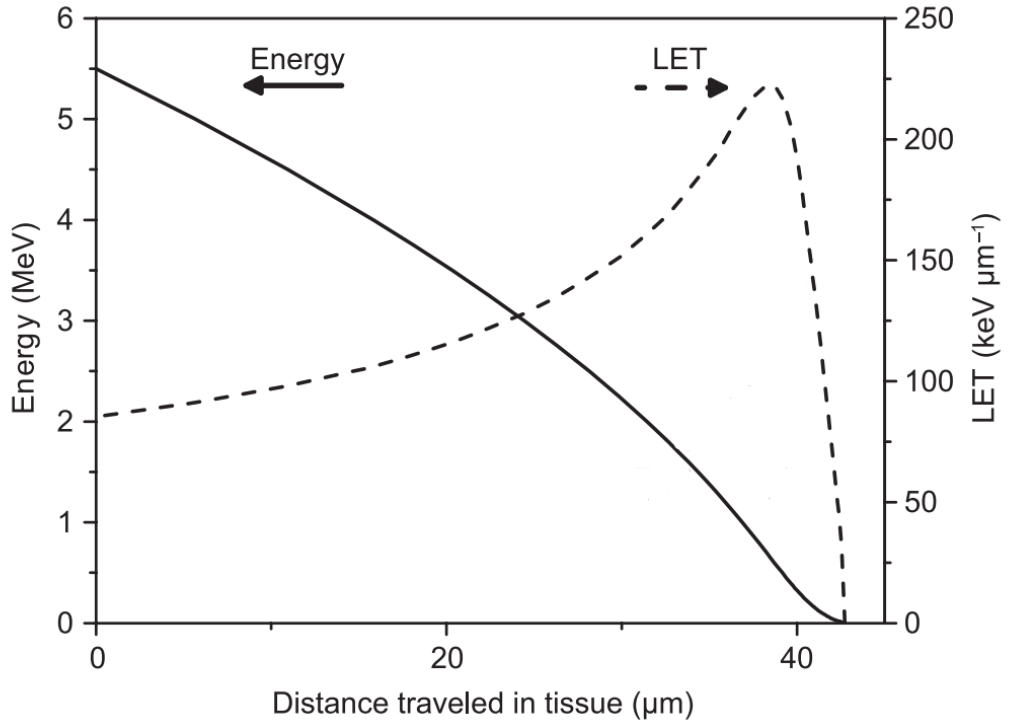

Figure 1.1010 Changes in α-particle energy traversing tissue.

The distance travelled by a 5.5 MeV α-particle corresponds to 222Rn decay can be seen assuming the trave to be through water. The figure was adapted by Bliss et al. 2015 (192). Image available for re-use under the original image copyright 2021 National Academy of Sciences for non-commercial reuse.

1.5.3 Repairing of radiation induced damage

Cells are equipped with repair processes for all kind of DNA lesions, this thought to be a direct result of evolutionary adaptation to environmental hazards (chemical, radiation and UV exposure) and or spontaneous DNA damage. The repair process is also essential for the

selection process for T cell antigen specific protein selection, which requires shuffling of DNA to create new combinations of cell surface proteins (170). The variety of lesions described above means multiple repair systems must be available for the cell to survive and adapt. Depending on the damage, a cell may undergo programmed cell death, cell cycle delay, repair and/or cellular senescence. The cellular responses are not mutually exclusive, and most cells will undergo cell cycle delay as an immediate response (194). For ionizing radiation exposure, the repair of DSBs is most relevant since unrepaired DSBs may lead to rapid cell death. This is exploited in radiotherapy treatments whereby high DSB induction is more likely to result in cell death as the cell will be unable to correctly repair all DSBs.

With induction of DSBs, the survival of the cell therefore depends on the rapid repair of these lesions. To do so, the principle repair pathways in human cells are homologous recombination (HR) and non-homologous end joining (NHEJ). The pathways for DSB detection, strand invasion, litigation and end processing have been well characterized as reviewed by Bradbury and Jackson (2003 (195)) and Pandita and Richardson (2009 (196)) detailing all the proteins and cascade responses. The point of the cell cycle at the time of exposure will often (but not exclusively) dictate what pathway is activated. HR pathway effectively utilizes a sister chromatid as a template for its repair. DNA end resection is activated in the presence of a DSB and through nucleolytic degradation, a 3' single-stranded DNA is formed ready for homologous strand invasion (197). HR has the highest strand fidelity as the template used is identical, however, to do this the cell must actively be replicating (73-77). Single strand alignment (SSA) may also be regarded as a variant of HR as it utilizes repeat sequences within the opposing strand, however, this is error prone as the intervening sequences between repeats may be prone to deletions and it is thus associated with the formation of chromosomal translocation (198).

Most cells sit in interphase unless actively stimulated to divide, therefore the most common pathway for repair is instead NHEJ. NHEJ does not contain a template for the repair of the damaged strands and instead the two broken strands are joined back together. This process is driven by the presence of microhomologies on single strands of the break sites. If these microhomologies are perfectly intact the repair is likely to be successful and the strands will be accurately re-joined (78-82). Often, though, the microhomologies are not intact and the litigation process results in mis-repair. The strand repair outcomes can be seen in Figure

1.10, which highlights the potential for loss of heterozygosity (LOH) and exchange such as a translocation. Further variants of NHEJ also exist including alternative end joining (Alt-NHEJ), which also relies on microhomologies for repair, however, these are limited to those within DNA-end resections. This process is also highly error prone often resulting in deletions, sequence alterations and translocations.

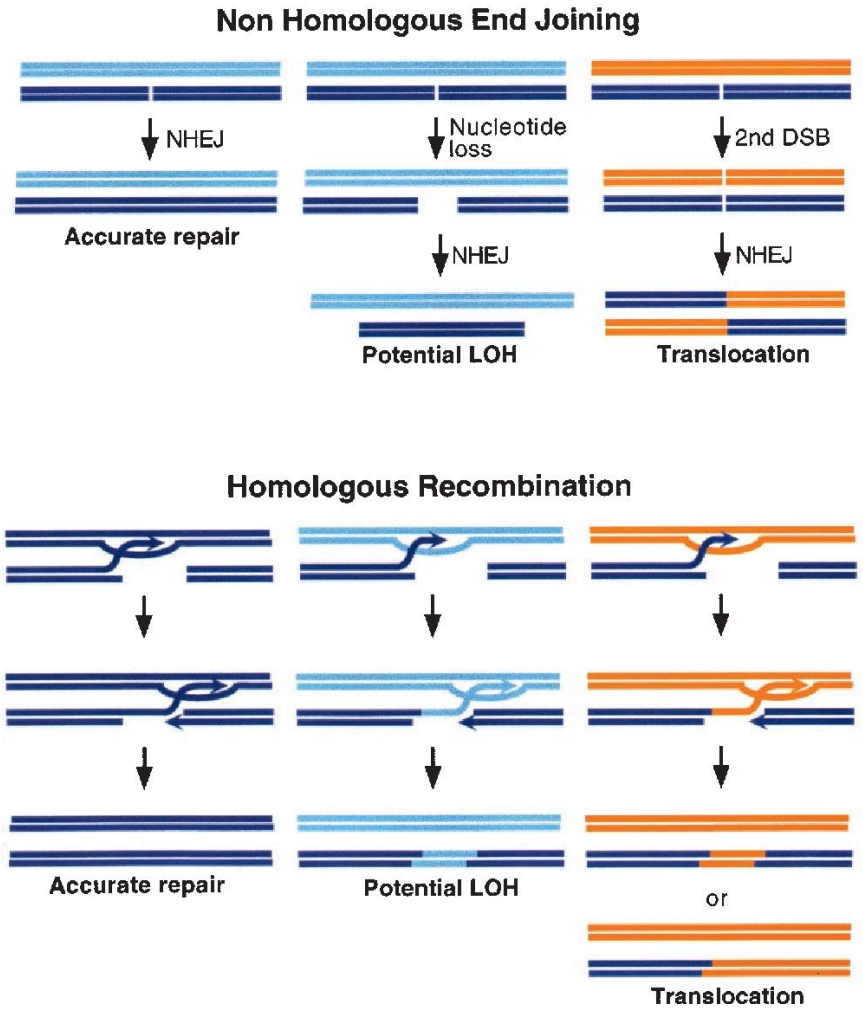

Figure 1.1111 DSB repair outcomes following homologous recombination and non-homologous end joining.

Parallel line pairs indicate the chromatids of each chromosome, with homologous chromosomes in light and dark blue colour. Orange lines indicates a non-homologous chromosome. First column describes the correct repair following NHEJ and HR. The middle column the incorrect repair resulting in LOH (loss of heterozygosity) with use of homologous chromosome and final column resulting in a reciprocal translocation from non-homologous

chromosome template guide (199). Image Licenses agreement granted for re-use under Springer Nature Licence for publication of image in Thesis/Dissertation as defined by the Sherpa guideline.

1.5.4 Cell death pathways

In the event that DNA damage cannot be repaired, the cell may initiate apoptosis. The apoptotic pathway will be depended on the type of damage induced and also the cell type. This may result in the intrinsic apoptotic pathway usually following incorrect repair of SSBs and DSBs and the initiation involves mitochondrial release of cytochrome c with apoptosome formation (200, 201). Activation of the extrinsic pathway instead occurs following detection of extrinsic signalling by death receptor which will in turn result in caspase activation for cell death. The membrane stress pathway is activated following ROS oxidative damage in the plasma membrane or directly from heavy damage from high doses of radiation resulting in many DSBs; both will result ceramide production and messenger signalling cascade initiated (202, 203).

Most cells will undergo cell death by mitotic catastrophe which results in the premature mitotic phase being initiated prior to correct completion of S and G2 phase. Cell death may then occur in the mitotic phase or during interphase. Alternatively, a cell may be forced into cellular senescence with permanent arrest in G1, whereby the cell remains viable and metabolically active but unable to undergo further mitosis (204). Ionizing radiation is also thought to be able to directly induce programmed necrosis (205, 206). Some cells may undergo delayed mitotic death which may be triggered by G2 arrest or after a number of cell divisions(207). The G2/M checkpoint halts the cell cycle progression preventing the segregation of unstable chromosomes (such as dicentric chromosomes), this follows prolonged activation of the spindle assembly checkpoint. If the aberrant cell is able to evade the G2/M checkpoint lagging chromosomes and their fragments will be form micronuclei external to the cell nucleus (208).

1.6 Chromosomal aberration induction

1.6.1 DNA organization

Chromosomal structures have long been observed as the structures involved in cell replication. It was only until Watson and Crick (1953 (209)) published their description of the double helical structure of DNA with X-ray crystallography by Rosalind Franklin (as reviewed by Thompson 2018 (210)) and Maurice Wikins (as reviewed by Arnott 2006 (211)) that the chromosomal genetic content was truly appreciated. The helix is formed by two polynucleotide chains composed of four nucleotide subunits. Nucleotides are composed of a five-carbon sugar (deoxyribose) to which phosphate groups and nitrogen composed bases are attached. The nucleotide bases are pyrimidine (cytosine and thymine) and purine (adenine and guanine). The base pairs of each stand are linked together by hydrogen bonds that will break during strand replication and re-join following completion. The nucleotides of each strand are linked through covalent bonds to sugar and phosphate forming the backbone of the DNA strand. The 3D structure formed achieves a helix structure from the complementary nucleotide rearrangement within the paired strands from bulkier two ring purine to single ring pyrimidine. The base pairs are held at similar widths through the DNA strand and so are the sugar-phosphate 'backbones' which in turn wind around each other forming a double helix. Each helix turn comprises 10 base pairs (154).

Human cells contain approximately 2 m of DNA that is tightly packed in the cell nucleus which is on average 6 µm in diameter. The packaging is achieved by complex processes not fully understood but that involve specialized proteins which fold, loop and coil the DNA into a high level of organization (212). Proteins are recruited to the DNA strand and together these form the DNA-protein complex termed chromatin. The proteins involved are called histones and these are small positively charged proteins (H1, H2A, H2B, H3 and H4) which interact with the negatively charged DNA sugar-phosphate backbone (213). This occurs in repeated fashion along the entire DNA strand. The nucleosome is the basic repeating structure along the length and is formed from 8 histone proteins interacting with a DNA length of approximately 146 base pairs. The first turn is termed a histone octamer as it comprises of 8 histones (2 of each H2A, H2B, H3 and H4) the turn is then completed from H1 recruitment of a further 20 base pairs forming the chromatosome. The nucleosome is

further compacted into a 30 nm fibre, although not fully understood, it appears H1 thought to be involved in the stabilization of the fibre. The 30 nm fibre continues to compact and coil. forming loops of 300 nm length and eventually folding to achieve a fibre of 200 nm axial extent (214) that is further tightly coiled into the chromatid of a chromosome.

1.6.2 Chromosomal aberration induction

Incorrect repair following ionizing radiation is associated with the occurrence of chromosomal aberrations. The mechanisms involved in the formation of chromosomal aberrations are still not fully understood but to date three main theories are considered. The 1st theory, breakage and reunion, proposed by Sax in 1938-1941 based on the formation of primary breaks along chromosomes and three possible outcomes (215-217). Breaks may in the first instance re-join or 'restitute' correctly to reform the original structure. The second outcome forms a new structure via an exchange mechanism through incorrect re-joining or repair, and lastly no repair, which appears as open ends with acentric fragments of chromatid or chromosomal kind. This theory is also known as the classical theory and it is the most widely accepted (218, 219). The 2nd theory is the exchange theory by Revell which assumes the most likely outcome is the formation of unstable lesions, rather than a primary break (220, 221). If the lesions are distant to one another these will eventually be repaired and therefore not be detected. However, if two lesions are in close proximity the exchange will begin and this can result in a complete exchange or an incomplete exchange. Complete exchanges will give rise to rearrangements visible as chromosomal aberrations at metaphase stage, in the case of an incomplete exchange a discontinuity will arise within the chromosome. As the chromosome containing discontinuities undergoes condensation as part of mitosis, these disruptions will appear along the chromosome as simple breaks. This theory suggests therefore that the occurrence of breaks within the chromosome are not the primary event however instead arise from failed exchanges (222, 223). Work by Savage in 1998 characterized the exchange theory further as "no exchange- no break", highlighting how some exchanges were better characterized by 1st theorem and some by 2nd (223). In terms of complex exchanges, random movement of broken ends with eventual reunion is hard to explain and that one DSB interacting via reciprocal recombination may be a feasible model (224).

The 3rd theory, the most modern, being the molecular theory proposed in 1978-1981 by Chadwick and Leenhouts (225, 226). Their work indicates that exchange type aberrations may occur from one DSBs and that these DSBs have a linear quadratic dose response. This coined the term “one DSB-one exchange”. Today it is generally accepted that the formation of chromosomal aberrations is a direct result of incorrect repair of DSBs, this supported by a number of studies of human chromosome instability syndromes all pointing towards disruption of DSB repair pathways as reviewed by Pfeiffer et al (222). HR pathways are activated by the presence of one DSB which will result in two cleaved ends along the DNA strand HEJ will initiate invasion within the homologous strand at sites where sequence homology is found. If the invasion does not occur at the appropriate site of homology but instead at sites of repeat sequences, chromosomal aberrations can be created. This supporting how one DSB can result in exchange aberrations such as translocation, inversions and deletions. NHEJ repair instead do not require a sister chromatid present for repair, as two open ends must interact it means two DSBs resulting in four open ends must be initiated to induce exchange type aberrations. Later studies utilizing premature chromosomal condensation (PCC) confirmed that breaks induced after ionizing radiation are precursors to chromosomal aberrations (227). PCC permits the detection of chromosomal damage rapidly after exposure in cells that are not actively cycling compared to standard techniques where exposed cells are stimulated to divide and arrested in metaphase stage. In the time taken for the cell to reach metaphase stage a series of events related to repair and restitution of the DNA strands will occur leading to the formation of chromosomal aberrations. The premature condensation avoids these events as it is induced rapidly after exposure by the fusion (Or drug-induced cytochalasin B) of the exposed interphase cell in G_0 to a mitotic cell usually a Chinese hamster ovary or HeLa cells. The technique has proven itself useful when assessing post irradiation repair processes and kinetics of chromosomal break restitution. PCC studies have found that open chromosomal fragments restitute with time, that exchanges occur very rapidly and whilst the chromosomal fragments found to decrease in frequency with time, the dicentric/translocation/ring frequency remained similar (228, 229). This evidence supports the idea that most exchanges are formed by the mis repair of breaks.

Ionizing radiation exposure has been shown to result in an increased yield of DSBs with an increase of absorbed dose. DSB mis repair by both HR and NHEJ can result in the formation of chromosomal and chromatid aberrations, depending on cell cycle point of exposure. As such, the higher the number of DSBs therefore the higher the chance of mis repair and formation of chromosomal aberrations whether it be as per the 1st theorem, with random recombination of opened ends and/or with the 2nd / 3rd theory based on mis repair of unstable lesions. Ultimately, further advances in molecular detection of induced damage sites, repair pathway characterization and improved detection limits for chromosomal aberration characterization have shown validity in all the above theories.

1.6.3 Chromosomal aberration classification

A normal human karyotype consists of 46 chromosomes in each diploid cell, 22 homologous autosome chromosomes and one pair of sex chromosomes (X and Y). Chromosomes are classified based on their size and subdivided in to 8 categories (A. Chromosomes 1-3, B. 4-5, C.6-12, D.13-15 E.16-18, F. 19-20 G.21-22 and sex chromosomes X-Y). At metaphase, the chromosomes are structured with the two sister chromatids joined together by the centromere. The two chromosome arms are classified as p (equal or shorter upper arm) or q (equal or longer lower arm).

The most widely accepted classification for chromosomal aberrations is by Savage (1976 (230)), here summarized. Structural chromosomal aberrations can be subdivided in to asymmetrical and symmetrical exchanges. Chromosomal aberrations may be intrachanges, involving only one chromosome, and interchanges, involving more than one chromosome. Asymmetrical exchanges are when the lesion gives rise to one or more acentric fragments. The acentric fragments consists of a chromosomal section not containing a centromere. Symmetrical exchanges instead do not result in the formation of an acentric fragment. Symmetrical exchanges, for example reciprocal translocations, are stable as they retain the ability to divide successfully as no genetic material is lost and each chromosome retains the centromeric structure for segregation during division. Unstable aberrations instead include dicentric chromosomes, rings and acentric fragments. In the case of dicentric chromosomes, these are also classed as unstable due to the presence of two centromeres. During mitosis a

dicentric chromosome is likely to be attracted to opposing poles this stemming from kinetochore structures being available within both centromeric regions. The fusion of this to microtubule structures will pull the centromeres in opposing directions, this either resulting in breakage of the chromosome or mitotic arrest with the formation of a bridge between the two cell nuclei. Centric rings are rarely able to undergo cellular division as it is likely for crossover of the two chromatids resulting in bridge formation with similar outcomes to the dicentric chromosomes. However, in the case of no crossover it is possible for centric rings to correctly duplicate and segregate as found in autosomal ring syndromes (231). The larger the chromosome the more likely for there to be cross over, therefore correct segregation is more likely in smaller chromosomes. The correct segregation of rings ultimately, like dicentric chromosomes, results in loss of genetic material via acentric fragment mis segregation. Complex chromosomal aberrations defined by Savage and Simpson (1994(232)) involve three or more breaks in two or more chromosomes. These may be of stable or unstable kind depending on whether fragments, dicentrics or rings are also formed.

Gain of genetic material can include duplication of genes. This is particularly found in cancer evolution studies and has also been shown to be induced *in vitro* from low dose ionizing radiation although the mechanisms are still questioned (233). Chromosome loss and gain may also be of whole chromosomes, usually induced by chromosome segregation errors during mitosis. This can be caused by acentric chromosome mis segregation induced errors and/or directly by ionizing radiation of cells undergoing mitosis leading to the formation of a lagging chromosome (234, 235).

1.6.4 LET and chromosomal aberration spectrum

The progression through cell cycles is tightly monitored by cell checkpoints whereby cycle progression can be blocked in the event of DNA damage. PBLs *in vivo* reside mainly in G_0 therefore the resulting sampled PBL will containing primarily chromosomal rather than chromatid aberrations. While exposure of cells in G_2/S will result primarily in chromatid aberrations (236). The frequency and spectrum of chromosomal aberration induced after ionizing radiation exposure is associated with radiation dose and also the energy or quality of radiation (237-239). At doses up to 2 Gy, low LET exposure has been associated with the

induction of simple chromosomal aberrations. This is partly due to energy deposition being more homogenous and more 'spread out' along the radiation track. The aberration induction of simple chromosomal aberration has been shown to follow a linear quadratic curve and this is applied in biodosimetry for dose estimation (236). The linear component is often associated with the damaged produced by a single track. The quadratic component is instead related to the miss-repair between DNA damage produced by two independent tracks, this being more significant at higher dose. Most notably the dicentric chromosome assay has been used for decades in biodosimetry for accidental exposure scenarios to estimate the dose received by the individual (240). High LET radiation is instead associated with complex chromosomal aberrations, due to clustered damage from heavy energy deposition along the particle track. The aberrations induced from high LET instead follow a linear relationship (236) however, complex aberrations may also occur at high doses following low LET exposure. The formation of multiple lesions in close proximity to one another are more likely to result in complex chromosomal aberration formation (241). Clustered damage resulting in DSB spatially distributed within a small area has been found to result in small deletion within a gene, termed intragenic deletions, and these can have phenotypic effects on the cell (242-244). Due to the clustered damage induced by high LET, the probably of a complex rearrangement formed will be increased and this has been demonstrated by the passage of a single α-particle track (241). Instead, the formation of complex aberrations by low LET is dose dependent as multiple radiation tracks may be needed for a similar level of lesions in close proximity for a similar level of interaction (245). The DSBs induced by high LET repair slower compared to those of low LET radiation Jenner 1993 and in general the DSBs induced by high LET are more complex (246).

Differences in numbers of chromosomes involved in complex aberrations have also been observed, with aberrations induced by low LET mainly involving three-four chromosomes whilst high LET exposure involve up to seven chromosomes 6). *In vitro* study by Anderson *et al.* (2000 (237)) identified chromosomal aberrations in PBL exposed to 0.5 Gy α-particles (121 keV/μm) to mainly involves four or more chromosomes in each exchange. Insertions, (chromosomal fragment exchanges and insertions into different chromosomal regions), are characteristic features of high-LET induced complex exchanges. Ultimately, the proximity of breaks will also have an important role in their aberration outcome (247).

1.7 Delayed effects of ionizing radiation exposure

1.7.1 Delayed chromosomal instability

Genomic instability is a main driver for tumorigenesis and is the increased tendency of genome changes in a cell (25, 27). IR induces DNA damage that may result in mutations and chromosome aberrations (insertions, deletions or major rearrangements). The molecular, biochemical and cellular events involved in the prolonged genomic instability within exposed cells and daughter progeny are not well understood. One of the best characterized models is the *de novo* occurrence of chromosomal aberrations in progeny of cells exposed to ionizing radiation of clonal and non-clonal descent. These have been extensively studied in the context of carcinogenesis and the formation of heterogenous tumours via acquired sequential genomic modifications (as reviewed by Botchler 2015 (248)). In the case of non-clonal delayed effects, aberrations appear in the progeny of cells exposed to ionizing radiation but not presenting initial aberrations themselves; in the progeny a subset of cells appears normal whilst others contain *de novo* aberrations. Early *in vitro* studies demonstrated delayed effects appearing in the cell populations up to six generation later (249-251). This scenario cannot be attributed solely to a repair defect within the original cell as if that was the case, all the resulting progenies should be equally affected and appear phenotypically identical to one another. Non-clonal delayed effects have been shown to result mainly in lethal rearrangements that once present in the daughter cell will lead to cell death (252, 253). Lethal rearrangements are thought to have little correlation to carcinogenesis itself but have been linked to delayed apoptotic mechanisms (254). As reviewed by Kadhim *et al.* (1995 (255)), *in vitro* studies have demonstrated from early on that cell progeny my display *de novo* chromosomal aberration which in turn may be transmissible to further progeny (256-261). Indirect damage from ROS/RNS have been linked with increased genomic instability, and this is supported by hypoxia studies which demonstrated significantly less damage after exposure of cells in 2% oxygen environments (262). Hypoxia studies also suggest oxidative stress has a role in delayed damage after exposure (as reviewed by (263-265)).

Delayed effects have also been observed in cell populations not directly exposed to ionizing radiation, including cells exposed to particle radiation known to have not been traversed

(266-271). These effects are termed as bystander effects and although the mechanisms are not fully understood, as reviewed by Butterworth (2013 (272)) studies have suggested gap junction communication or signalling via extracellular environment. Indeed, a number of studies have found increased chromosomal aberrations in neighbouring non exposed cells *in vitro* (273, 274) and *in vivo* (275, 276) which may be explained by bystander effects.

1.7.2 Chromosomal instability and disease phenotypes

Ionizing radiation has been long utilized as part of medical treatment for various cancers and diseases, it has itself also been recognised as an inductor of primary cancers in unwanted exposures. Epidemiological data has provided evidence supporting an increased cancer risks from radiation doses > 100 mSv, with a linear no threshold response generally assumed to assess risks at lower dose. However, the benefit associated with low dose exposure from medical diagnostic imaging (<100 mSv) is likely to outweigh the risk (277). The risk following higher dose exposure from radiotherapy instead poses a greater risk of cancer, the incidence is approximately 40% reflecting long life expectancy but will be dependent on cancer site and associated treatment plan (277). However, the risk for delayed effects is often outweighed by the risk of not using radiation for disease treatment/management. Ionizing radiation has been associated with an increased risk of secondary cancers in patients with better prognosis (for whom delayed effects are an important consideration) when utilized as part of primary cancer treatment (138, 278-282). Secondary cancers are likely to arise from the exposure of non-target tissues surrounding the tumour site and this is one of the key driving forces towards finding newly targeted treatments that spare surrounding normal tissues in an attempt to minimize this risk. For a radiotherapy treatment to be effective it must have the ability to inflict irreparable damage to the target cell genome. The principle is based on induction of highly lethal DSBs which results in effective cell death. When the damage inflicted is great, the cell will undergo programmed or interphase cell death. If the damage to the cell is potentially reparable, the cell will arrest at a cell cycle checkpoint and repair will be attempted. Incorrect repair may yield balanced rearrangements that do not affect cell survival and a cell containing these may successfully undergo division with daughter cells presenting these rearrangements (283).

For an aberration to be persistent through multiple cell divisions the chromosomal aberration must yield structural rearrangements that are physically able to segregate during mitosis. In the case of acentric fragments, these are able to replicate but unlikely to undergo correct segregation as they are lacking the essential centromere structure needed for this. On occasion dicentric chromosomes may successfully segregated to one cell nucleus, however, this is unlikely to occur for multiple cell divisions, therefore the half-life of a dicentric is approximately two replications (or 1.5 years) (168). It should be noted that inactivation of one centromere has been thought possible with dicentric chromosomes successfully going through cell divisions. This process is not fully understood but thought to be associated with the proximity of the two centromeres to one another (as reviewed by Stimpson *et al.* 2012 (284)). Ultimately genetic material is still lost with the acentric fragment likely to incorrectly segregated through cell division rendering the cell unstable. The occurrence of centric rings is a rare event and therefore the persistence of a ring even more so.

The most likely aberration to persist for many cell divisions is the reciprocal translocation, as each rearranged chromosome contains a single centromere. Expansion of cells containing stable transmissible aberrations has been linked to the development of certain cancers, most notably the example of the Philadelphia chromosome linked to chronic myeloid leukaemia (CML). It was 1st observed in the 1960s by Nowell and Hungerford (285) and later characterized as a reciprocal translocation between chromosome 9 and 22 by Rowley in 1973 (286). The rearrangement is found in 95% of CML cases with the incidence found to increase with age and associated with poor prognosis (287). The rearrangement results in the movement of proto-oncogene ABL to chromosome 22 location adjacent within that of BCR gene, the fusion of these two genes result in hybrid BCR/ABL onco-gene. Depending on the break location the transcription of this gene results in the production of an aberrant mRNA later translated in to a chimeric p210 or p190 protein. The rearrangement therefore causing physiological signalling impairment and disrupting the cell stability (288). The link between ionizing exposure during treatment and CML is well established with radiotherapy patients monitored via haematological counts throughout treatment (as reviewed (278, 289, 290)). Delayed cases of CML have been recognised 10 years following treatment for thyroid carcinoma (291) and 25 years after breast and uterine cancer radiotherapy (292). This

prolonged delayed highlighting the need for long term patient monitor after therapy completion with young patients being at particular risk (293, 294).

Study of occupationally exposed individuals have identified increased chromosomal aberration to be associated with increased carcer risk. Nordic population study followed up 3182 individuals following mainly occupational exposure between 1970 and 1988 (295). Chromosomal aberrations, chromatid aberrations and micronuclei were scored. By the last follow up 85 cancer cases were identified. The mean time from cytogenetic analysis to first cancer appearance was between 2.2 and 7.9 years depending on county. A statistically significant trend was observed for chromosomal aberrations and increased cancer risk. A further study by Bonassi *et al.* (1995 (296)) suggested increased frequencies of chromosomal aberrations to be associated with increased risk of haematological malignancies. Observing cases of respiratory track, digestive and lymphatic/haematopoietic cancers. A nested case control study by Bonassi *et al.* (2000 (297)) of previous published studies supported chromosomal aberrations as precursors to cancer pathways. There are still uncertainties in studies due to confounding factors and the delayed effects following increased frequency of chromosomal aberrations are still uncertain. With study by Smerhovsky *et al.* (2001 (298)) of radon exposed miners also observing increased frequencies of chromosomal aberrations frequency in PBLs and cancer incidence providing evidence of this in late follow ups (over 4 years).

1.7.3 Malignancies following Radium exposure

Malignancies from other Radium isotopes have also been reported following accidental exposures. During world war I thousands of women were hired in factories around the world to paint luminous dye on clock dials. Unbeknown to them the dye contained radium and women were exposed to varying doses of radium through ingestion of the radioisotope via licking the brush tip into a fine point for painting and by inhalation. A string of bone related diseases and sarcomas were attributed to the radium exposure from Radium-226 (^{226}Ra) and Radium-228 (^{228}Ra) isotopes. Increased mortality due to the occurrence of acute toxicity resulting in severe anaemia and later bone necrosis was observed by the workers (299-302). Late biological effects of radium bone deposition resulted in excess cases of

leukaemia (303), multiple myeloma (301), osteogenic sarcomas (304), carcinomas of mastoid air cells, paranasal sinuses carcinoma (299) and breast cancer (305). External exposure to Radium isotopes does not pose a great health risk as the released α-particles lack the energy to penetrate the outer areas of the skin unlike gamma ray that pose a serious health risk hazard. Therefore, few studies have been reported regarding external exposure. Only two cases linked to delayed cataract formation after low dose exposure to isotopes have been published (306, 307). The first from accidental exposure over the period of 11 years to an imperfectly shielded Radium source (unknown details) (307) and the second during medical treatment of haemangioma in childhood patients with ^{226}Ra external skin applications (face and head regions) resulting in early cataract occurrence in adulthood (306).

Radium-224 (^{224}Ra) is another Radium isotope that was widely used for the treatment of ankylosing spondylitis between 1952-1980. Ankylosing spondylitis causes inflammation in ligaments causing joint stiffness and pain, and the ^{224}Ra was used to target abnormal osseous material formed during increased calcium turnover in inflamed regions (the target area of treatment being the calcifying ligaments). This aimed to reduce joint stiffness that in its severest form was due to fusion of areas such as vertebrae with new osseous material, greatly affecting the quality of life of patients. Similarly, to ^{223}Ra, ^{224}Ra localises to high bone turnover areas where calcium uptake is increased. Although an effective treatment, ^{224}Ra it was later discontinued after findings of increased CML and malignant bone tumours (308-310). It has since resurfaced in Germany for the treatment of severe cases were alternative non-radiotherapy-based treatments are not considered successful, reinforcing the effectiveness of the treatment in certain circumstances (311). ^{224}Ra is currently being re-evaluated for treatment and remains commercially available for management of ankylosing spondylitis (312, 313).

The use of ^{223}Ra in the clinic is novel and therefore the use of ^{223}Ra as routine treatment is restricted to CRPC patients with no other reported uses. ^{223}Ra and ^{224}Ra remain the only radioisotopes utilized for clinical treatment with the main differences being the decay pathways, these differing in half-life, energy and kind of particle emitted and the resulting products. Both treatments are administered intravenously and following injection ^{224}Ra has been shown to localized on the bone surface resulting in higher exposure to soft tissue (314)

while ^{223}Ra instead localises to the bone matrix and decays over a longer period suggesting lower toxicity to neighbouring tissue (156, 157). ^{223}Ra will instead release all 4 α-particles over the course of minutes at a much steadier pace (Figure 1.1212). This is likely associated with the low haematological adverse events. Suggested models indicate that ^{223}Ra exposure of the neighbouring BM cavity may result in pockets of tissues being spared rendering any adverse effect temporary and recoverable (315). To date, only two cases of leukaemia have been associated with ^{223}Ra treatment for prostate cancer with no causal link being established between ^{223}Ra administration and secondary malignancies as in both cases the patients received varying forms of chemotherapy and radiotherapy (316, 317). Retention of ^{224}Ra by soft tissue has been studied further for long term malignancies. Patients who received treatment between 1945-1955 have been followed up and a significant number of non-skeletal solid malignancies were observed with an increase of breast cancer incidences, thyroid carcinomas, liver, kidney and bladder cancer in both males and females (318). Follow up of patients 26 years post treatment also showed an enhanced incidence of leukaemia. Of 1006 exposed patients, 19 developed leukaemia and of those 11 were myeloid leukaemia (7 cases observed vs 1.8 cases expected, P = 0.003) (319).

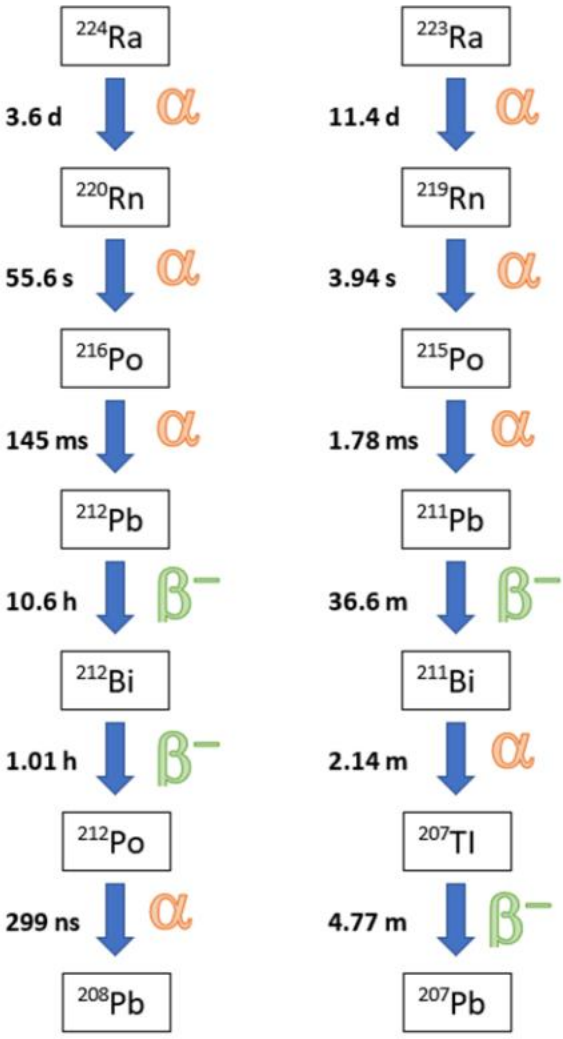

Figure 1.1212. Decay chain of ^{224}Ra and ^{223}Ra.

The most likely decay chains are here described with the number of α and β particles released for each radioisotope. The time taken for each daughter product to decay is included. ^{224}Ra decay results in the emission a 5.7 MeV α-particle during decay to Radon-220 (^{220}Rn), 6.3 MeV α-particle in the decay to Polonium-216 (^{216}Po), 6.8 MeV α-particle in the decay to Lead-212 (^{212}Pb) and 8.8 MeV α-particle decay from Polonium-212 (^{212}Po) to Lead-208 (^{208}Pb). β-particles released from the decay of ^{212}Pb to Bismuth-212 (^{212}Bi) and to ^{212}Po. During decay of ^{223}Ra 4 α-particles are released with energies of 5.78 MeV to Radon-219 (^{219}Rn), 6.88 MeV to Polonium-215 (^{215}Po), 7.53 MeV to Lead-211 (^{211}Pb) and 6.62 MeV to Thallium-207 (^{207}Ti). Two β-particles were also released during the decay of ^{211}Pb to Bismuth-211 (^{211}Bi) and from ^{207}Ti to Lead-207 (^{207}Pb).

1.8 Introducing aims of the research

1.8.1 ADRRAD clinical trial aims

The ADRRAD (Neo-adjuvant Androgen Deprivation Therapy, Pelvic Radiotherapy and RADium-223 for new presentation T1-4 N0-1 M1B adenocarcinoma of prostate) clinical trial aims to test the safety and efficacy of combining ADT, IMRT and ^{223}Ra. This is a novel treatment combination aimed to treat men with hormone sensitive PC presenting a limited number of metastasis (<4). Emerging evidence has suggested early combination treatment carried out during ADT administration, when the patient remains hormone sensitive, improves survival. This includes the use of docetaxel earlier than standard and IMRT to primary tumour site following metastasizing. Recent approval of ^{223}Ra for the treatment of distant bone metastatic sites has resulted in overall improvement in both quality of life and survival, however combinations of ^{223}Ra with other treatments has yet to be done. The combination of ADT to control disease progression, primary tumour site radiation exposure via IMRT and metastatic targeting by ^{223}Ra may prove to be an effective new treatment regime. This trial represents a pilot study to explore the above hypothesis, with an initial small patient cohort to test the feasibility and safety.

1.8.2 Project specific aims

The successful use of ^{223}Ra earlier in disease progression stage may also result in improved survival. In the future the use of ^{223}Ra for patients with a better prognosis for a variety of cancer types may also lead to improved outcomes. Radiotherapies with α-particle emitters have generated a great deal of interest as they have the potential to be highly targeted treatments with high normal tissue sparing and therefore minimal toxicity following treatment completion. However, uncertainties remain regarding the dose deposition at metastatic site and the risks associated with combination of ^{223}Ra to other treatments. As haematopoietic stem cells reside in close proximity to target sites, there is a risk of direct expose to α-particles. The ^{223}Ra treatment in the ADRRAD clinical trial follows a total of six intravenous administration which may also result in circulatory system exposure including mature circulating PBLs. The long term risks following haematopoietic cell exposure is

unknown including whether the risk of secondary treatment related leukaemia may be increased. The research reported in this thesis aimed to measure changes in the PBL population that may be a direct result of ^{223}Ra exposure. Specifically, this is a cytogenetic project which seeks to characterise the chromosomal damage observed in circulating PBLs to make estimates of dose to the blood compartment and, to assess any long-term potential for toxicity in these patients. To do so, the frequency and spectra of chromosomal aberration was sampled before, during and following treatment. The hypotheses for the study were as follows:

1) The frequency of chromosomal aberrations will significantly increase over treatment schedule (from control samples, during IMRT+^{223}Ra treatment cycles and in the following ^{223}Ra only cycles).
2) A significant dose is deposited in the bone marrow from ^{223}Ra during treatment.
3) The spectrum of chromosomal aberrations will be significantly different during treatment and in follow up samples, reflecting PBL expansion from BM.
4) There will be evidence of *de novo* genomic instability in follow up samples, which may suggest increased delayed radiation risks as a result of the treatment.

Chapter 2: Methods

2.1 Treatment scheduling and sample collection

Blood samples from patients receiving IMRT and ^{223}Ra were sampled every 4 weeks and shipped to Brunel University London. As per treatment schedule, Figure 2.11, each blood sample was collected just before the next cycle of ^{223}Ra administration. A control sample (C1) was collected prior to the treatment starting and following this a total of 6 ^{223}Ra cycles were administered. Follow-up samples were also collected either 8 weeks (F1) or 4 months (F2) after the end of treatment. A 1 year follow-up (F3) was collected for all patients, corresponding to one year after the first administration of ^{223}Ra. EBRT in the form of IMRT was scheduled as 37 fractions administered daily from C1, the last fraction being delivered between C2 and C3 timepoints.

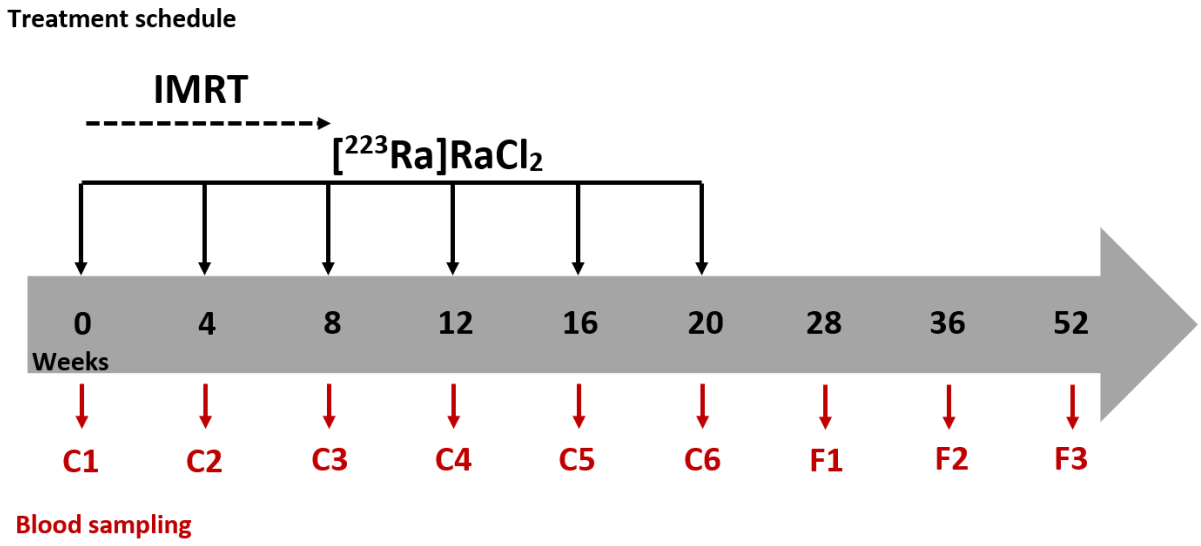

Figure 2.11 Treatment timeline.

IMRT daily fractions (5 days a week) of 2 Gy for 7.5 weeks. [^{223}Ra]$RaCl_2$ is administered every 4 weeks for a total of 6 injections. Blood samples were collected prior to each injection, with a control sample collected at week 0 prior to treatment starting (C1). Accordingly, blood samples C2 and C3 are representative of mixed field exposure, while C4-C6 are ^{223}Ra only. Follow up samples were collected 8 weeks (F1) and 4 months (F2) after the end of treatment and 1 year (F3).

Fresh whole blood samples were collected by collaborators at Northern Ireland Cancer Trial Centre in lithium heparinised tubes and shipped to Brunel University London (BUL) within 24 hours. Samples were packaged in a Royal Mail SafeboxTM with insulating material to avoid tubes touching in a waterproof container to absorb sample liquid with Special DeliveryTM Next Day postage. The packages included clear labels highlighting biological category A, "DO NOT X-RAY" and maintain temperature between 4-30°C. Upon arrival, the samples were processed and whole blood stimulated to divide as *in vitro* cultures to enable the collection of 1st cell division for cytogenetic assessment.

2.2 Ethical review of sampling

Ethical approval was sought by chief investigator Prof Joe O'Sullivan and co-workers from the Northern Ireland Cancer Centre, Belfast for the clinical trial, "Neo-adjuvant Androgen Deprivation Therapy, Pelvic Radiotherapy and RADium-223 for new presentation T1- 4 N0/1 M1B adenocarcinoma of prostate (ADRRAD Trial)". Favourable ethical opinion was received from the Office for Research Ethics Committees Northern Ireland on the 4th June 2015 Rec reference 15/NI/0074. An amendment for collaborative translational studies for the purpose of carrying out a Multiplex-Fluorescence-In-Situ-Hybridization (M-FISH) chromosomal analysis of blood samples from participants in the ADRRAD clinical trial was accepted on 15th June 2015 by Belfast Health and Social Care Trust. Brunel Ethical Research approval was sought and obtained by Dr Rhona Anderson for the analysis of blood samples from thirty patients on 7th September 2016. Further ethical approval by Brunel University London (BUL) was approved on 8th November 2017 (7327-TISS-Nov/2017- 8684-2) for investigation of "Radiation risks from high-LET α–emitters using Radium-223 as a model", the approval consents to patient samples being delivered to BUL on cyclical basis for a total of 6 patients for chromosome analysis.

2.2.1 Exclusion and inclusion criteria

30 patients in total were recruited for the ADRRAD clinical trial, the inclusion and exclusion criteria were set by the Chief Investigator of ADRRAD as described in clinical trial publications (320-322). Written informed consent was obtained prior to any study-related procedures. Histologically confirmed prostate cancer stage T1-4 N0-1, M1b with >3 bone metastases showing uptake at bone scintigraphy. WHO performance status 0 or 1 with a life expectancy of at least 12 months. The patients were of age ≥ 18 years prior to consent. Absence of any psychological, familial, sociological or geographical condition potentially hampering compliance with the study protocol and follow-up schedule; those conditions were discussed with the patient before registration in the trial. The patient was willing and able to comply with the protocol, including follow-up visits and examinations. Haematological counts were collected at each visit, the acceptable levels outlined as follows in

Table 2.11.

The patients were excluded if they had a history of allografts requiring immunosuppressive therapy, malignancy within the last 5 years or if they had an active uncontrolled bacterial/viral/fungal infection during the clinical trial period. They were also excluded on the basis of having a serious illness or medical condition, such as but not limited to:

i) Any infection ≥ National Cancer Institute Common Terminology Criteria for Adverse Events (NCI-CTCAE) version 4.03 Grade 2.
ii) Cardiac failure New York Heart Association (NYHA) III or IV.
iii) Crohn's disease or ulcerative colitis.
iv) Bone marrow dysplasia.
v) Faecal incontinence.
vi) History of diverticulitis.

Patients were excluded if they had received treatment with an investigational drug within the previous 4 weeks or such treatment was planned during the treatment period or follow-up. If they had received previous radiotherapy to > 25% of bone marrow, including hemibody radiation and/or received systemic therapy with radionuclides (e.g., Strontium-

89, Samarium-153, Rhenium-186, or Rhenium-188, or Radium-223 chloride) for the treatment of bony metastases.

Blood components	Acceptable levels
Absolute neutrophil count (ANC)	≥ 1.5 x10^9/L
Platelet count	≥ 100 x10^9/L
Haemoglobin	≥ 10.0g/dL (100 g/L)
Total bilirubin level	≤ 1.5 x ULN
Aspartate aminotransferase (AST) and alanine aminotransferase (ALT)	≤ 2.5 x ULN
Creatinine	≤ 1.5 x ULN
Albumin	> 25g/L

Table 2.11. Haematological parameters for inclusion criteria.

Blood components were monitored throughout the trial with treatment administration only if the patient is within the acceptable ranges. ULN: institutional upper limit of normal.

Patients with visceral metastases, history of spinal cord compression, autologous bone marrow transplant or stem cell rescue within 4 months of study entry were also excluded. While patients who received cytotoxic chemotherapy >6 weeks prior of starting cycle 1 ^{223}Ra were accepted, biologic response modifiers such as G-CSF taken within 3 week of study entry resulted in exclusion.

2.3 Cell culturing and harvesting of PBL

2.3.1 Whole blood processing and culturing

The original sample volume and conditions were logged prior to commencing with all details of the sample being updated into the Human Tissue list to ensure HTA compliance. All work was performed in a Class II microbiological cabinet using aseptic techniques.

Culture media was prepared fresh under sterile conditions, for this, PBMAX Karyotyping Medium (ThermoFisher, Cat. Number 12557021) was defrosted overnight and supplemented with phytohaemagglutinin (PHA) purified (ThermoFisher, Cat. Number R30852801) 0.5 µg/ml of media, BrdU 10µM per culture and heparin 10 µl/ml of media (Sigma-Aldrich Cat. Number 9041-08-1), the media was mixed well and warmed to 21°C.

The whole blood sample was mixed well by inverting of tube and a volume of 0.4 ml was used to inoculate with 2.6 ml of freshly prepared media within a pre-labelled 15 ml falcon tubes with sample description, patient ID number, cycle of treatment and date. The falcon tube was placed in a humidified incubator at 37°C (95% air/5% CO_2) with the cap left slightly open to allow gaseous exchange at a 45° angle. Cells were cultured to achieve 1st division metaphases for staggered times of 50-60 hours.

2.3.2 PBL lymphocyte isolation and culturing

The remaining whole blood sample was emptied into a 50 ml falcon tube and diluted 1:1 with room temperature RPMI 1640 (Fisher Scientific, Cat. Number 11875093). The exact total volume was then replicated with room temperature Histopaque 1077 (Sigma Diagnostics, Cat. Number SD10771) in another 50 ml tube. The blood was gently overlaid via pipette onto the Histopaque at a 45° angle. The tube was centrifuged at 420 g for 20 minutes with no break. The centrifugation enabled the separation of blood components based on density as described in Figure 2.22.

The mononuclear cell layer “buffy coat” was collected in a 15 ml tube via Pasteur pipette, washed by adding up to 10 ml of RPMI and centrifuged at 420 g for 10 minutes. After removal of the supernatant the pellet was re-suspended in a known volume of medium dependent on cell number. A manual count of PBL was performed via haemocytometer and the PBL seeded at a density of $4x10^5$ per ml of media as described in section 2.3.4. The culture was incubated at a 45° angle at 37°C with a humidified atmosphere of 95% air/5% CO_2. Cells were cultured to achieve 1st division metaphases for times of 50-60 hours.

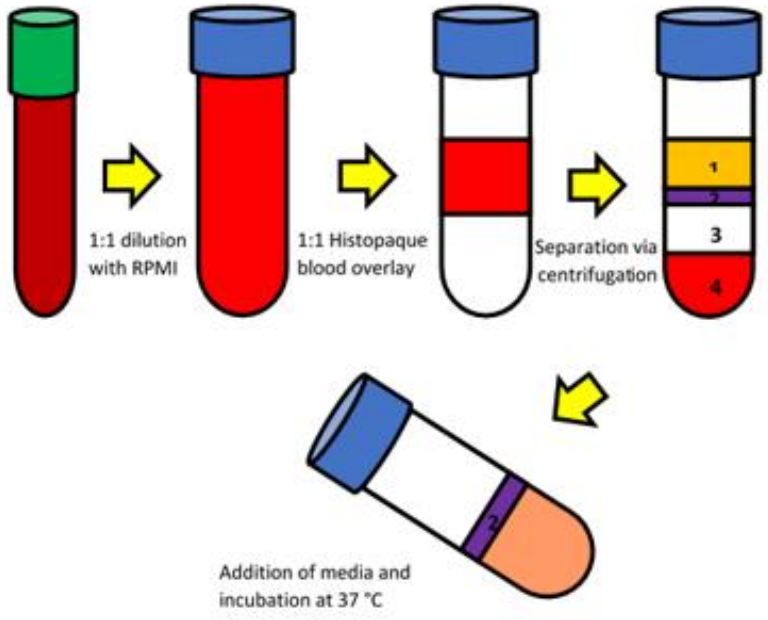

Figure 2.22 Isolation of PBL from whole blood.

Whole blood samples were firstly diluted and then overlaid on Histopaque. Separation by density resulted in four layers being formed: 1. Plasma layer, 2. Buffy coat, 3. Histopaque layer 4. Erythrocyte layer.

2.3.3 Freezing of isolated PBL

Excess PBL were frozen in liquid nitrogen for culture backup. 1 ml of freeze medium was prepared per culture with 90% of incomplete culture medium without stimulants and 10% DMSO. Incomplete culture medium was prepared under sterile conditions and frozen at –

20°C for long term storage, medium composed of 90% RPMI 1640, 10% Foetal Bovine serum and 0.01% Penicillin Streptomycin (manufacturer info).

Counted cells were centrifuged at 200 g for 10 minutes, supernatant was then removed, and freeze medium added. Cells were transferred to pre labelled cryovials with sample description, patient ID number, cycle of treatment, cell count and date. Cryovials were placed into freezer boxes for storage at –80°C for 24 hours, these were then moved to liquid nitrogen tank for long term storage.

2.3.4 Haemocytometer counts

A 20 µl sample was collected from a known volume of isolated PBL cell suspension and added to 20 µl of Trypan blue (Fisher Scientific Cat Number 11538886) viability dye in an Eppendorf tube. The haemocytometer was prepared by firstly wiping with Industrial methylated spirit (IMS) and allowing to dry fully, with one's breath the haemocytometer was moistened, and a coverslip overlaid. The presence of Newton's refraction rings on the edges of the coverslip indicated proper adhesion.

A 10 µl aliquot of cell suspension was placed on a haemocytometer to allow being drawn under the coverslip via capillary motion. Dead cells were visible as blue/violet under bright field microscope (microscope details) as seen in figure 10.

The total viable cell count was then averaged per square counted and corrected dependent on dilution factor to achieve the number of cells per ml of suspension as follows:

$$Total\ live\ cell\ count \times \frac{Dilution\ factor}{Squares\ counted} \times 10^{-4} = Cells\ per\ ml\ of\ suspension$$

The total cells per ml are then expressed as total cells per sample dependent on the known volume of PBL from which the aliquoted 10 µ suspension was taken, this was then used to attain the desired seeding concentration by splitting accordingly.

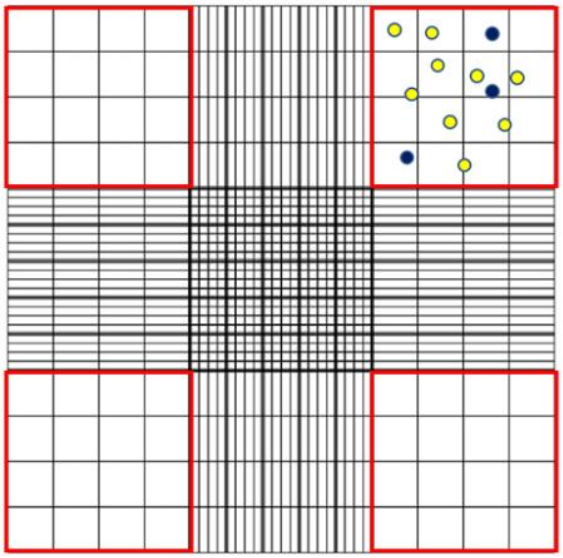

Figure 2.33 Cell count using haemocytometer.

Live cells not stained by Trypan blue (vitality exclusion dye) were scored in outer four chambers (highlighted in red) the total live cell count was then used to estimate the total number of cells in isolated PBL suspension.

2.3.5 Sample harvesting

Cells were collected in 1st division metaphase from PBL and whole blood cultures described in section 2.3.1 and 2.3.2. To arrest the cell cycle at the metaphase stage, 50 µl/ml of Colcemid KaryoMAX (ThermoFisher, Cat. Number 1521012), a tubulin inhibitor, was added to each culture under sterile conditions 4 hours prior to harvest and mixed gently, the cultures were returned to incubator to complete incubation.

Cell suspensions ready for harvest were centrifuged at 200 g for 10 minutes. The supernatant was removed, and the cell pellet re-suspended before addition of 0.075 M KCl hypotonic solution (Fisher Scientific Cat Number10575090) was added to the cell pellet to enable the swelling of cells. For whole blood cultures a volume of up to 6 ml of hypotonic was used, for isolated PBL cultures 8 ml was instead used. Samples were incubated for 8 minutes in a water bath at 37°C in upright position, the samples were then centrifuged at 200 g for 10 minutes and supernatant was removed before being transferred on ice to a fume hood for fixation.

Fixation was carried out with methanol acetic acid at ratio 3:1 methanol (Thermo Fisher Catalogue Number 15654570) and acetic acid (Thermo Fisher Catalogue Number 1743468) and kept on ice. The total volume of fixative added to the cell pellet was dependent on the type of culture, for whole blood cultures a volume of 6ml was used and isolated lymphocytes instead received a volume of 5 ml. The fixation was carried out dropwise with the help of vortex mixer, with the aim of preserving PBL in their swollen state. The fixation process was carried out until the fixative appeared clear when in suspension. The fixed PBL and whole blood were stored in the freezer at -20°C in labelled racks ready for slide preparation.

2.4 Sample preparation for cytogenetic outputs

2.4.1 Slide preparation for metaphase spreads

Fixed chromosome preparations were centrifuged at 200 g for 10 minutes, the old fixative was removed, and the resulting pellet was re-suspended in approximately 200 µl of fresh fixative and kept on ice. The cell suspension was then dropped on clean slides. Depending on lab temperature and humidity two methods were used when dropping slides:

a) 12 µl of the chromosome preparation was dropped directly on to frozen clean slides four consecutive times and dried on a heated block at 50°C until methanol-acetic acid has evaporated.

b) Clean slides were flooded with distilled water and wiped dry. 12 µl of the chromosome preparation was dropped on to slide four consecutive times and dried on damp heated block at 50°C until methanol acetic acid evaporated.

The slides were left to air dry fully before phase microscopy analysis for both quality and number of metaphase cells.

2.4.2 Assessing metaphase slides for quality and numbers

The slides were selected based on quality and number of metaphases; the selection was carried out under phase microscopy. Slides with >200 usable metaphases were processed for M-FISH analysis whilst slides with <200 metaphases were processed for solid stain analysis. The quality of the slides was assessed according to spread, length of chromatid arms, and completeness of metaphases. The usable metaphase cell selection included those which were not overspread or encapsulated/tight.

2.5 Staining techniques for cytogenetic analysis

2.5.1 Harlequin preparation for solid stain analysis

Fresh slides were aged on a hot plate for 45 minutes at 90°C and immersed in Hoescht (Thermo Fisher Scientific Cat Number 62249) for 10 minutes, then transferred to a flat tray and covered in 2x Saline-Sodium Citrate (SSC) (Thermo Fisher Cat Number 15557036), before being exposed in UV box to 999990 μJ/cm^2 for 60 minutes. After exposure, slides were washed with distilled water two times and air dried.

Giemsa (VWR Cat Number 350864) was diluted (final ~3-5%) with distilled water in a coplin jar. Fresh slides were placed in the Giemsa solution for up to 5 minutes, removed and rinsed with distilled water. After being allowed to air dry, coverslip slides were mounted with 4 drops of DPX (Fisher Scientific Cat Number 15538321) mounting medium. Slides were then ready for scoring via brightfield microscopy with oil immersion at x100 magnification.

2.5.2 2nd division analysis for M-FISH sample selection

To assess the number of in vitro PBL divisions, metaphase cells were harlequin stained as described 2.5.1 and cells analysed by bright field microscopy. BrdU is a thymine analogue and was incorporated by the cell during division. Metaphase spreads containing even staining of both chromatids were scored as 1st division with those containing counterstain of 1 chromatid scored as 2nd division cells (Figure 2.4). For this analysis 100 cells were scored per slide with the aim of identifying samples with ≤5% 2nd division metaphase cells. All samples with ≤5% 2nd division cells were selected for M-FISH painting.

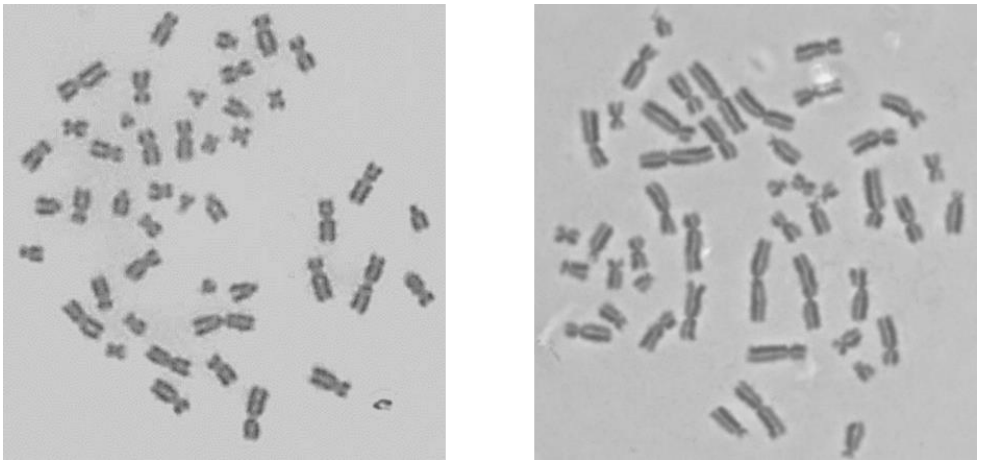

Figure 2.44. Differential staining for identification of 2nd cell division PBL methapse spreads.

Left panel 1st division cell with uniform staining, right panel differential staining between chromatids whereby BrdU has been incorporated in one chromatid preventing Giemsa staining.

2.5.3 M-FISH paining

Slides were selected based on quality and metaphase count as outlined in sections 2.4.2 and 2.5.2. Multiplex fluorescence *in situ* hybridisation (M-FISH) enables the staining of each homologous chromosome pair using 24 painting probes labelled with 5 different fluorochromes combinations. These probes being made from micro-dissected chromosomes, with fragments amplified by PCR and bound to 1 or more fluorochromes. These probe sets also containing a human repetitive (Cot-1) DNA to reduce hybridisation of the probe to non-target repetitive sequences on other chromosomes. The commercially available probe set 24XCyte (MetaSystems D-0125-600-DI) was used. Of this set, four of the fluorochromes bind directly to the DNA, namely Diethylamino-coumarin (DEAC), FITC, Spectrum Orange ™ and Texas Red®. The 5th fluorochrome binds indirectly to the DNA molecule by Biotin reporter molecule which is detected by the Streptavidin-Cy™5.

2.5.4 Chromosome hardening and denaturing

All steps were carried out at room temperature unless stated otherwise. The slides were firstly rehydrated in an ethanol series of 100%, 70%, 50% 30% for 1 minute each. The slides were then transferred to 0.1xSSC at room temperature for 1min. The denaturation of the slide was then initiated by placing slides into pre warmed coplin jar containing 2xSSC at 70°C and incubated for 30 minutes. The coplin jar was then removed from the water bath and cooled for 20 minutes prior to transferring slides to 0.1xSSC at room temperature for 1 minute. Slides were then placed in 0.07N NaOH (stocks) at room temperature for 1min. Slides were then placed into pre-cooled 0.1xSSC at 4°C for 1min and then 2xSSC at 4°C for 1 min. The slides were then dehydrated in ethanol series 30%, 50%, 70%, 100% for 1 min each.

2.5.5 Probe denaturation and hybridisation

10 µl of 24XCyte probe cocktail (Metasystems Cat Number D-0125-600-DI) was prepared for a 22x22 mm^2 area. The probe was denatured with incubation at 75°C for 5 minutes. The probe was then placed on ice and then incubated at 37°C for 30 minutes. The probe cocktail was then spun via vortex mixer. The denatured pre-hybridised cocktail was pipetted onto the denatured chromosome preparation. The mixture was then overlaid with a 22x22 cover slip and sealed with rubber cement allowing the sealant to fully dry before incubating 1-2 days in a humidified chamber at 37°C.

2.5.6 Post-hybridization wash and counterstaining

The rubber cement and coverslips was removed. The slide was then placed immediately in pre-warmed coplin jar 0.4xSSC at 72°C for 2 minutes and then placed in 2xSSCT for 1-2 minutes.

To counterstain, the slide was washed in double distilled water and left to air dry before placing 20µl of DAPI/antifade (Metasystems Cat Number D-0902-500-DA) on the 22x22 probe covered area and overlaid with a 24 x 60 mm^2 cover slip and sealed with varnish. Slides were stored at -20°C for microscopy analysis via Metafer and ISIS system (software details).

2.5.7 Chromosome image acquisition and data storage

The slide was set up on Zeiss (Zeiss Axioplan 2 microscope) microscope, paired to Metafer4 software. Firstly, the scanning location was set manually to the precise area painted. The selected area was firstly scanned (x10 magnification) under DAPI channel to locate the exact location of the metaphases cells utilizing automatic recognition based on pre-set classifier. Once all DAPI images were captured, cells were selected based on whether the metaphase cell appeared complete or not. Images containing obviously incomplete metaphase cells and those having incorrectly captured interphase cells were excluded from further imaging.

The selected image locations were rescanned individually with classifier set to capture images under x63 oil magnification. Once the metaphase cell was identified, the selected classifier rotated between fluorophore specific excitation wavelengths capturing images positive for each probe set. Each hybridized fluorochrome will undergo photochemical process by exposure to light, shifting into an excitation state. Part of the absorbed energy is lost by internal structural changes and interactions with other molecules, before returning to its ground state during which the fluorochrome emits light. The wavelength emitted will be longer compared to that of the absorbed light (Stoke Shift), this resulting from the loss of energy during the excitation state. This emitted light is captured to image FITC, Spectrum Orange, Texas red, Cy5, DEAC and DAPI signals. The classifier automatically switched to the next cell until all previously identified cell locations are imaged. Upon completion, a case file was generated containing all individual and superimposed images for each cell.

Case files created on Metafer4 were stored on the university secure network, the secure network was backed up daily and enabled remote image processing from all analysis stations.

2.5.8 ISIS cytogenetic analysis

The files were imported into ISIS software for chromosomal analysis where individual metaphases were selected for analysis based on staining quality and metaphase completeness. Only metaphase cells with even fluorochromes staining were selected along with metaphases with ≥43 chromosomes. The images were firstly processed to remove any background not part of the metaphase, the object threshold was altered to select individual DAPI stained material only. The individual colour channels were then manually checked and adjusted automatically to ensure the lowest background to noise ratio for each fluorophore. This enabled differentiation of chromosomes which were negative and those positive for the fluorophore in question.

The software is programmed to recognise the superimposed images captured for each fluorophore and assigned a pseudo colour to each homologous chromosome as per Figure 2.66. Using the individual labelling scheme all chromosomes and DNA material stained were karyotyped. Once this was carried out, DAPI was used to correctly orientate each chromosome and then the karyogram was assessed for abnormalities. The resulting chromosomes were then classified according to Savage classification.

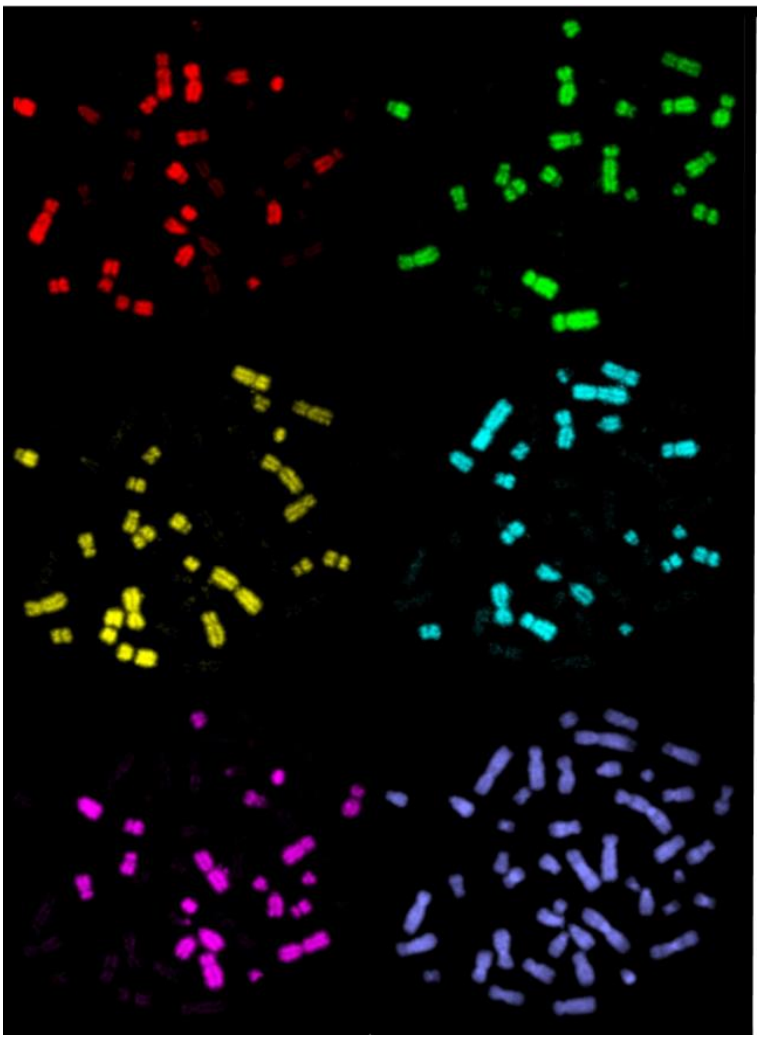

Figure 2.55. Individual fluorescence channels for metaphase cell.

A single metaphase cell is shown visualised in each fluorescence channel. Upper left panel Red fluorescence from positive Spectrum Orange probe signal. Upper right green fluorescence from positive for FITC. Middle left gold fluorescence from positive Cy5 probe signa. Middle left aqua fluorescence from positive DEAC signal. Lower left Pink fluorescence from positive Texas red probe signal. Lower right DAPI positive signal staining all chromosomal material.

Chromosome pair	Labelling scheme				
	Aqua	Green	Orange	RED	NIR
1					
2					
3					
4					
5					
6					
7					
8					
9					
10					
11					
12					
13					
14					
15					
16					
17					
18					
19					
20					
21					
22					
X					
Y					

Figure 2.66 M-FISH probe labelling scheme.

Metasystems 24XCyte probe labelling scheme for homologous pairs. Sex chromosome staining differs between X and Y. Probe colour combination results in computer-generated pseudo colours.

2.6 Scoring criteria of aberrations

2.6.1 M-FISH classification

M-FISH paints each chromosome with a combination of fluorochromes. For a cell to be classed as normal, the whole chromosome length must be evenly stained by individual/multiple fluorochromes. This results in evenly stained homologues with their respective pseudo colours being then assigned as per Figure 2.66. A structurally abnormal chromosome will have an abnormal appearance of DAPI and/or fluorochromes through the length of the chromosomes. The abnormal distribution may comprise extra fluorophores in a specific region or absence of fluorophores. In the case of absence of fluorophores, the DAPI should also be absent in that region to be a true aberration. Pseudo colours alone were not utilized for the assessment of colour junctions and were instead used to assist with the initial analysis pointing towards the main chromosomes involved.

Normal metaphase cells were scored as cells containing 46 chromosomes all containing one centromere with no acentric fragments present within the spread. Cells presenting missing chromosomes but no chromosomal aberration were classed as structurally normal. Only cells containing at least 43 chromosomes were classed as scorable, with the number of missing chromosomes recorded.

Aberrations identified by M-FISH were classified according to their structural appearance following Savage 1976 (230) classification. As M-FISH analysis enables the identification of each chromosome pair involved, the aberrations were scored based on the number of chromosomal interactions and exchange type as per Speicher *et al.* (1996 (323)). Chromosomal intrachanges, involving only one chromosome, could not be scored by M-FISH technique unless obvious under DAPI, instead chromosomal interchange involving more than one chromosome were scored. The chromosomal interchanges were classified as asymmetrical when the lesion gave rise to one or more acentric fragments. The acentric fragments were identified by the lack of centromeric structure identified under DAPI staining in the chromosomal section. Symmetrical exchanges were instead scored when the exchanges resulted in no acentric fragments.

Simple asymmetrical exchanges scored, as seen in Figure 2.77, include dicentric chromosomes and rings, while symmetrical exchanges including reciprocal translocation. In the occurrence of a break occurring without restitution this was scored as a break only event. In the rare case of chromosomes presenting multiple breaks and fragments this was termed chromosomal fragmentation. The term event was used when describing a chromosomal aberration. In the case of a cell containing two reciprocal translocations this was scored as two events.

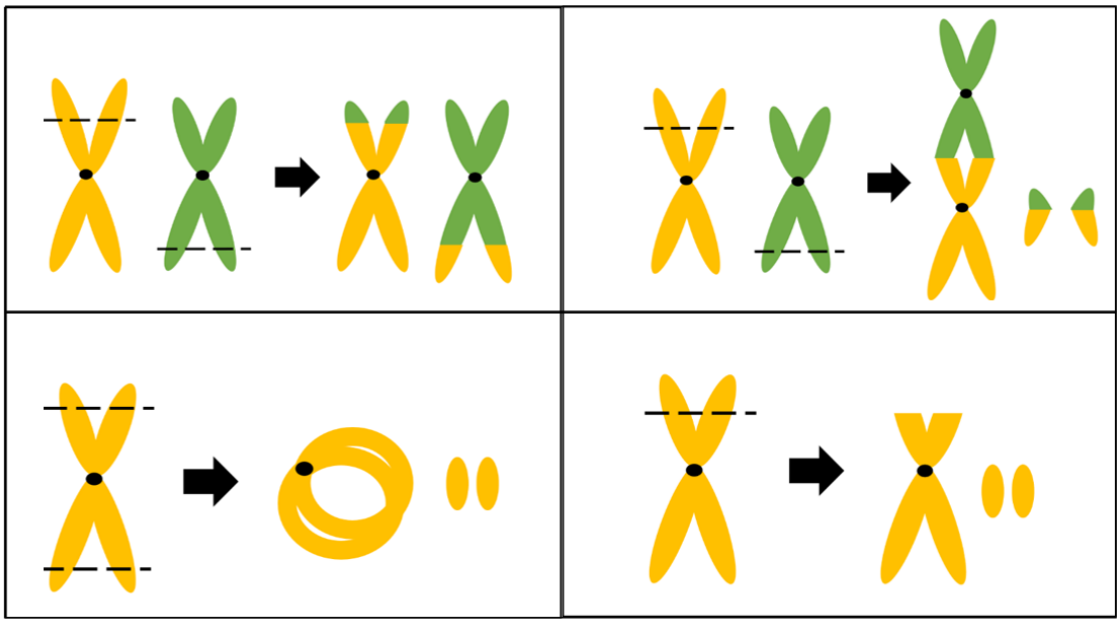

Figure 2.77. Symmetrical and asymmetrical chromosomal aberrations.

Top left panel reciprocal translocation (symmetrical aberration), top right dicentric chromosome, bottom left centric ring and bottom right break only (asymmetrical aberrations).

Complex chromosomal aberrations are defined as rearrangements that involve ≥3 breaks and involve ≥2 chromosomes resulting in complex patterns potentially involving multiple symmetrical and asymmetrical exchanges as defined by Savage (1994 (232)). The CAB system of classification was used to describe the minimum number of chromosomes, chromosome arms and breaks involved in the exchange. Complex exchanges may include multiple rearrangements as seen in Figure 2.88, depending on the re-joining, this may result in symmetrical or asymmetrical complex exchanges. In the event of a chromosomal fragment containing two open ends, this may insert itself between other segments forming an insertion.

The exchanges illustrated in Figures 2.7-2.9 are of complete kind, meaning all fragments in the event are present and where possible re-joined. As M-FISH enables the staining of each homologous chromosome a comparison of an abnormal chromosome to its homologue could be made. Therefore, missing elements in the exchange result in the aberration being scored as either a true or an unresolved incomplete event. A true incomplete event when the missing element was large enough for detection and the cell appears to not be overspread. An unresolved incomplete being based on the expected size of the fragment being very small and thus below system resolution and/or alternatively overcast by a nearby cell/debri.

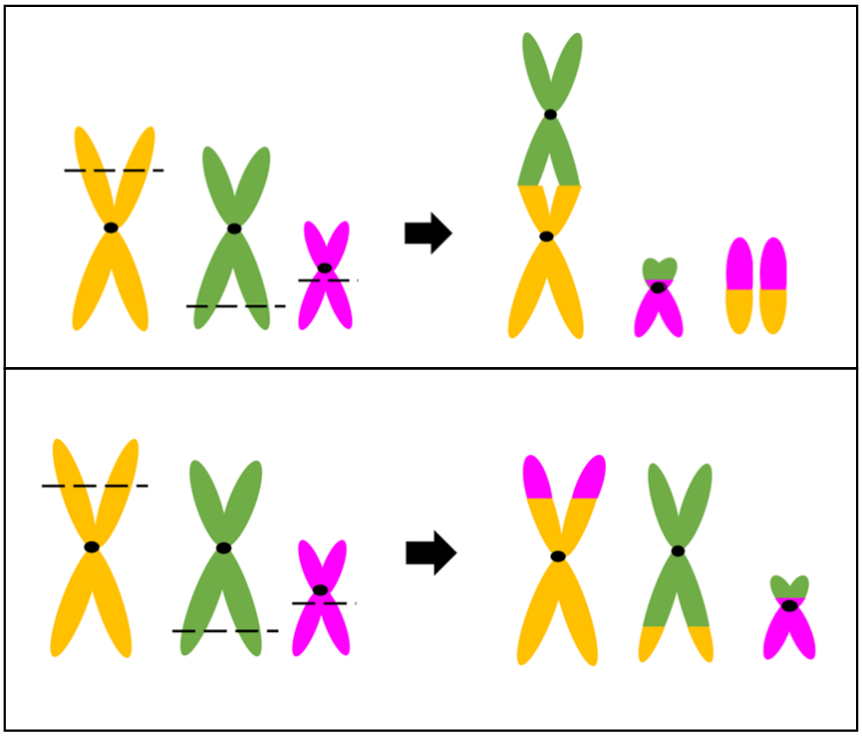

Figure 2.88. Complex chromosomal aberrations.

The illustrated events involve three chromosomes, three arms and there are three breaks. These described as CAB 3/3/3. The complex aberration in the top panel is classed as non-transmissible due to the presence of a dicentric chromosome and fragment. The lower panel depicts a stable transmissible complex aberration.

Chromatid aberrations may also be scored in M-FISH analysis, this based on the DAPI channel. Chromatid aberration scored include sister unions whereby the sister chromatids fuse as seen in Figure 2.99. Similarly to break only events, a chromatid may also result in an

acentric chromatid fragment. Depending on the size of the chromatid fragment this may be a single minute or larger chromatid fragment. The discontinuity may be a true break if the fragment is detached from the chromosomal structure more than the width of the chromatid, if this is not the case, it is scored as a chromatid gap. Due to the processing of chromosomes presence of bloating and fluorophore flare, chromatid aberrations were not readily scored, albeit obvious chromatid aberrations were still recorded.

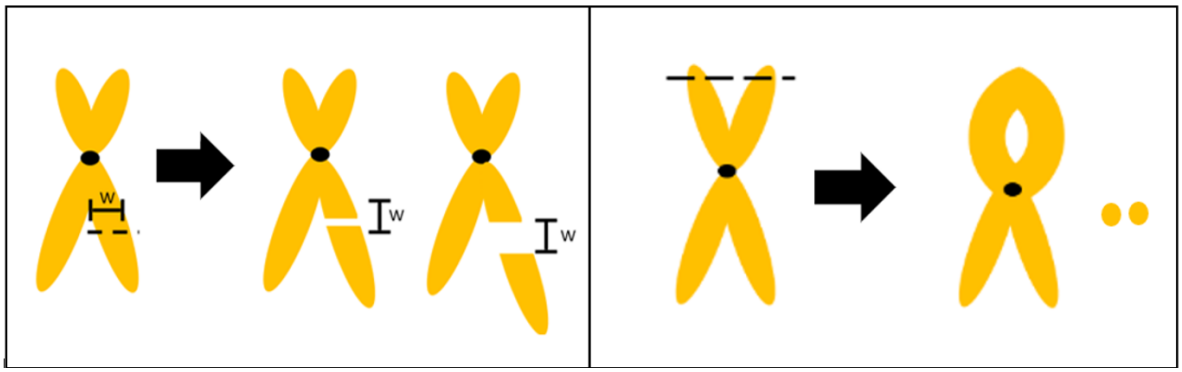

Figure 2.99. Chromatid aberrations.

Left panel chromatid discontinuities including gap and break. To the right sister union.

2.6.2 Solid stain classification

Individual metaphases were selected for analysis based on staining quality and metaphase completeness (described in Methods section 2.4.2). Only slides with uniformly stained metaphases with ≥43 chromosomes were analysed. Analysis was carried out under bright field (Zeiss Axio Lab A_1 microscope) with the aid of phase contrast and/or green filter. The slides were analysed by rastering to avoid scoring the same metaphase multiple times. 200 1^{st} division metaphase cells were scored per slide noting location of each metaphase cell scored.

Metaphases with abnormalities were then scored based on chromosomal, chromatid or aneuploidy. Unlike M-FISH where homologous pairs can be identified and the pattern of rearrangements scored, solid stain enables identification of abnormalities based on chromosomal morphology. Therefore, only aberrations of the unstable kind were easily

detectable. This included centromeric aberrations such as the presence of excess centromeres (polycentric chromosomes including dicentric and tricentric structures), loss of centromeric structures (acentric fragments) and ring structures including centric rings (containing a centromere) and acentric rings (no centromere present). Acentric fragments were further assigned based on their size, larger fragments and small fragments called double minutes. A chromosome discontinuity was scored based on the presence of an acentric fragment near the chromosome, if the discontinuity was larger than the width of the chromatid, this was scored as a break. If the width was approximated to be smaller it was instead scored as a gap. Examples of these can be seen in Figure 2.1010. As per M-FISH classification, chromatid aberrations involving only one chromatid, include gaps, breaks, acentric fragments and sister unions. Acentric chromatid fragments were identified by the presence of a single chromatid fragment. A sister union was classified by the interaction of sister chromatids being fused together resulting in a loop like structure in either the p or q arm. Unlike M-FISH analysis it cannot be deduced whether an exchange is of simple or complex kind (except polycentric chromosomes with >2 centromeres) and therefore whether these interactions are complete.

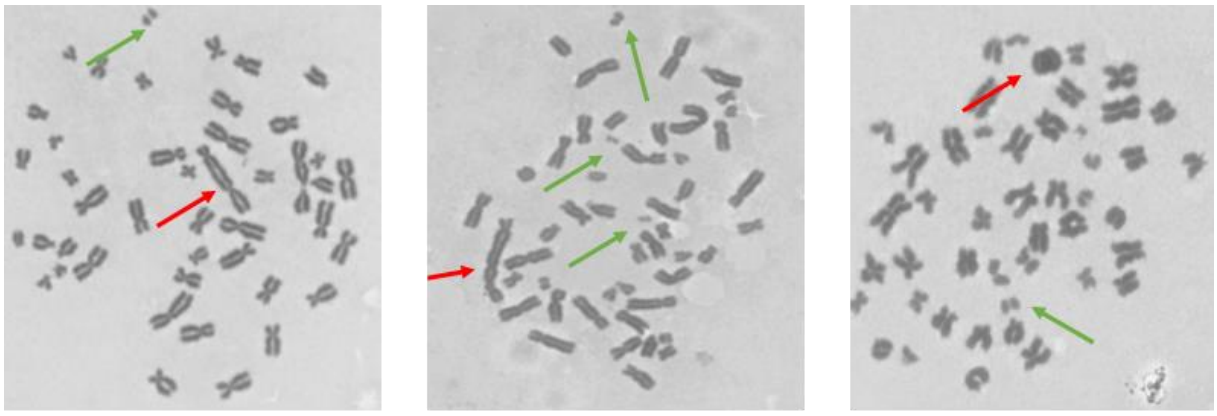

Figure 2.1010. Solid stain unstable chromosomal exchanges.

Left panel includes dicentric chromosome (red) and resulting acentric fragment (green). Middle panel includes a polycentric chromosome (red) with associated acentric fragments (green). Right panel includes ring (red) and associated acentric fragment (green). Images captured under brightfield x100 magnification with oil immersion.

2.7 Bio dosimetry models for dose estimation

Blood dose was calculated by employing three methods as summarized in Figure 2.1111. Physically derived blood doses were estimated from the injected ^{223}Ra activity by applying existing pharmacokinetic clearance models and IMRT blood dose estimate from the dose deliver schedule with planned area from the computed tomography scans (CT). The blood dose ratio (^{223}Ra:IMRT) was used with standard biodosimetric methods by employing the dicentric assay to estimate an absorbed blood dose for radiation quality. A novel cytogenetic derived model was proposed (which may be applicable in cases of unknown exposure) utilizing a *de novo* method based on the observed aberrations sampled from the PBL pool. The ^{223}Ra:IMRT dose ratio was estimated from the proportion of cells containing markers of high LET and those containing only markers of low LET. This inputted also with standard biodosimetric methods employing the dicentric assay, resulting in a third set of blood dose estimates for each radiation quality.

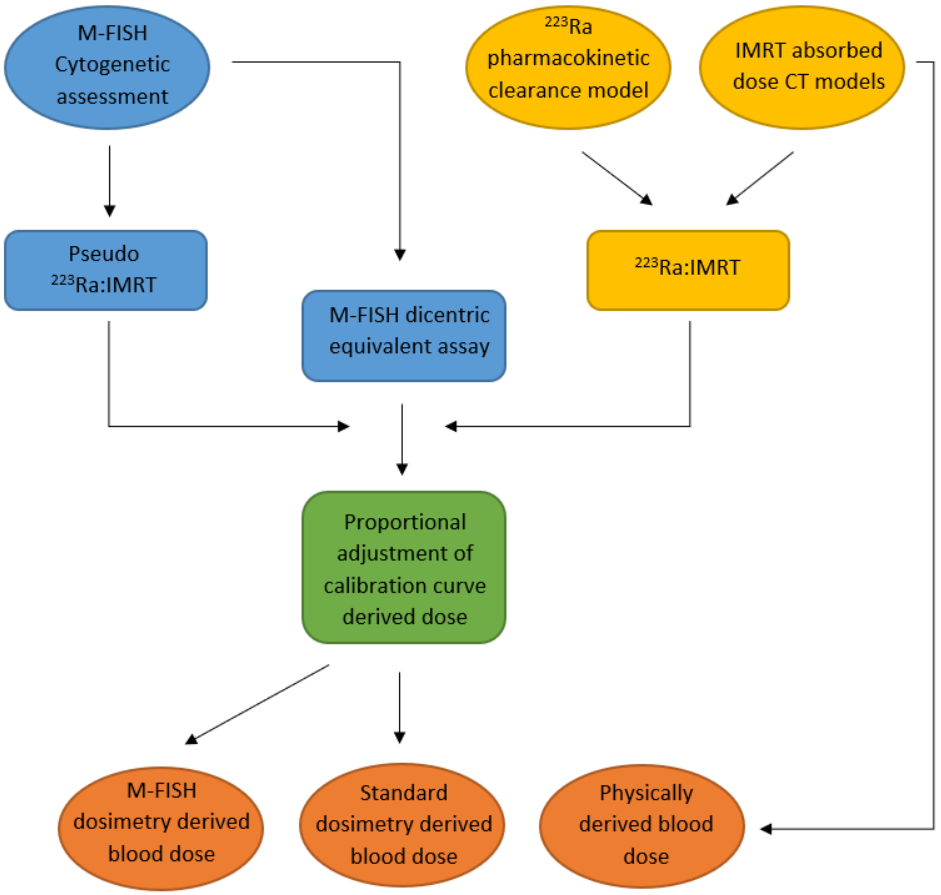

Figure 2.1111. Blood dose methods summary.

In blue cytogenetic methods used for dose assessment. In yellow physically derived models for ^{223}Ra and IMRT absorbed blood dose. Green criticality model application. Orange absorbed blood dose outputs.

2.7.1 ^{223}Ra blood dose

Clinical data was collected for each cycle point, including the weight of the patient (kg) and the total injected activity of ^{223}Ra (kBq). Patient-specific injected activities were modelled against existing pharmacokinetic clearance models to establish the circulatory dose. As ^{223}Ra clears rapidly following intravenous administration, with <1% activity following 24 h, it was assumed that the additional dose deposited from 24 h to t= ∞ was negligible. To estimate the blood dose, three studies were selected as they shared common sampling timepoints (152-154). The median values, with upper and lower ranges, for 15 min, 4 h and 24 h were averaged to estimate the percentage of circulating ^{223}Ra at each timepoint. These were estimated as 22% circulating ^{223}Ra after 15 min (9-28%), 3% (1.3- 4.95%) after 4 h and 0.8 % (0.37-1%) at 24 h.

The physical decay constant was calculated from the half-life of ^{223}Ra as seen in Equation 2.11. Where $\mathrm{T}_{\frac{1}{2}}$ represents the half-life of ^{223}Ra (s) and λ the decay constant.

$$\mathrm{T}_{\frac{1}{2}} = \frac{\mathrm{Ln}2}{\lambda} \qquad \textbf{Equation 2.11.}$$

To estimate the physical dose deposited by circulating ^{223}Ra, the total activity was estimated at each timepoint as per Equation 2.22. Where t= time (s), A_0 the average initial activity (Bq/kg/s) at injection time, A_t the average activity at desired time point (Bq/Kg/s) and the mass of the blood calculated assuming 75ml pf blood per kg of body weight.

^{23}Ra decays in three short lived daughter products (^{219}Rn, ^{215}Po and ^{211}Bi), the energy release of these was also considered, with the total α-particle energy release estimated to be 4.30 × 10^{-12} J (Equation 2.22). The number of disintegrations were estimated for each time point and multiplied by the total α-particle energy release as per Equation 2.33 where E

represents the total α-particle energy release (J) and D the absorbed dose rate. These steps were repeated for each time point.

$$A_t = A_0 \times e^{-\lambda t} \qquad \textbf{Equation 2.22}$$

Finally, the dose rate to blood was calculated by dividing this rate of energy deposition by the mass of blood of the patient (estimated as 75 mL of blood per kg body weight). The absorbed doses per timepoint were then plotted per treatment cycle with time, and the area under the curve was calculated (GraphPad Prism 9 (GraphPad Software) computed using trapezoid rule function) to estimate the total blood dose per cycle within 24 h of administration.

$$D = (A_t \times t) \text{ x } E \qquad \textbf{Equation 2.33}$$

2.7.2 ^{223}Ra whole body and organ dose

To calculate the absorbed radiation doses to the whole body, osteogenic cells and red marrow, the reported absorbed radiation doses to organs (Gy/MBq) published by in the European Medicines Agency Xofigo Safety report (324) were multiplied by the known injected activity per patient (MBq). The estimates include the effect from the α-particle component only.

2.7.3 IMRT blood dose

The following blood dose models were derived by Moquet *et al.* (2018 (325)) as part of the RTGene study where two different methods were employed to estimate the blood dose of varying cancer types having received radiotherapy treatment via IMRT. The blood dose

models enable the quantification of blood dose per fraction and as cumulative dose by end of treatment.

2.7.3.1 Blood flow model

The blood flow model (BF) enabled estimation of dose within the high dose organ area. The blood dose per fraction (D_B) was estimated from the supplied dose per fraction data with the high dose volume per organ (both supplied from the patient treatment planning fields supplied by the clinical team). Two variates of the model were used: $BF_{1,}$ which was applied as per Moquet *et al.* (2018 (325)) as seen in Equation 2.44 which estimates blood volume (V_B) by assuming 75 ml of blood per kg and, BF_2 which uses the static volume of blood in each organ for V_B, estimated by calculating a scaling factor between the whole-body volume and the area irradiated (prostate and/or lymph nodes), based on treatment plan information. This scaling factor was then applied to the whole-body blood volume estimates to achieve a static blood volume for prostate and lymph nodes.

$$D_B = D_f (V_{95} \div V_B) \qquad \textbf{Equation 2.44}$$

2.7.3.2 CT planned volume blood dose

The CT planned volume blood dose model (CTPV) enabled dose estimation of both high and low dose areas. The CT volume mapped for each patient was utilized to calculate a scaling factor for each patient in reference to whole body volume. With whole body volume being calculated based on the average patient weight (Kg) over the course of treatment (326). The equation supplied by Moquet *et al.* (2018 (325)) was then implemented with the supplied dose (Gy) to the body volume covered by the CT scan as per Equation 2.55 to estimate the absorbed blood dose. N_F represents the number of fractions of radiotherapy and S is the patient specific scaling factor.

$$\mathrm{D_B} = (\mathrm{D_{PB}} \div \mathrm{N_F}) \div \mathrm{S} \qquad \textbf{Equation 2.55}$$

The model proposed by Moquet *et al.* (2018 (325)) considers the total CT volume area consisting of both high and low dose regions (this model named CTPV1), to calculate the high dose region only ($CTPV_2$), high dose volume information only was used. $CTPV_2$ was estimated also by Equation 2.55 but the average dose for prostate and lymph nodes was used and as a result the scaling factor was also adapted to reflect organ volume to whole body volume scaling.

2.7.4 Blood dose ratio

The ^{223}Ra:IMRT ratio was estimated in two-ways. By physical dose estimation from the ^{223}Ra clearance model (Methods 2.7.1) and IMRT CTPV model (Methods 2.7.3) and, also by M-FISH cytogenetic assessment. The M-FISH ratio (here termed M-$FISH_{LET}$) was derived from the assumption that cells containing at least one complex exchange were exposed to ^{223}Ra, whilst cells containing only simple exchanges were classed as IMRT exposed. The ratio of cells containing complex rearrangements to cells containing simple arrangements was utilized as a pseudo ratio of ^{223}Ra:IMRT.

2.7.4.1 Selecting the appropriate calibration curves

The calibration curve selected for IMRT was that described by Lloyd 1986 where whole blood was irradiated *in vitro* with ^{60}Co (0-5 Gy). To plot the calibration curve, the yield of dicentrics and corresponding dose was inputted in Dose Estimate V5.2 Yield Curve Fitting function. The standard error of the mean calculated and modelled to a Linear quadratic fit. The resulting yield curve including upper and lower 95% confidence intervals along with coefficient r.

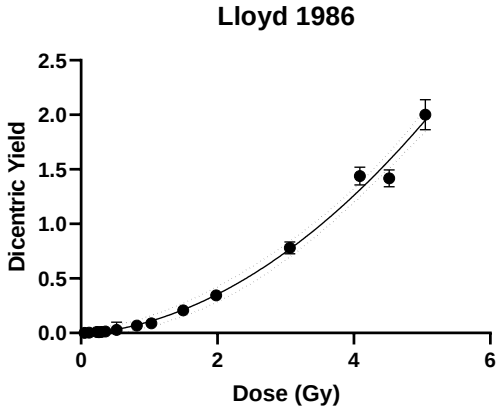

Figure 2.1212 γ calibration curve Lloyd 1986.

X ray *in vitro* calibration curve by Lloyd 1986 (327). Whole blood was irradiated using a ^{60}Co source with dose range of 0-5 Gy.The dicentric yield was plotted per dose and 95% CI calculated through Dose estimate V 5.2. Yield = 0.0004 (+/- 0.0009) + 0.0149 (+/- 0.0060) * D + 0.0756 (+/- 0.0031) * D2, Correlation coefficient r = 0.9960.

As there is currently no ^{223}Ra calibration data for *in vitro* exposures, α-particle emitting radionucleotides of similar energy were selected. Two calibration curves were selected, firstly Purrott *et al.* 1980 where whole blood was irradiated in the range of 0-1.6 Gy with ^{239}Pu and, Curwen *et al.* 2012 where PBL were irradiated on mylar layer with monoenergic alpha-particles of energies 3.26 MeV (LET of 121 keV/µm) over a dose range of 0-1 Gy. Through Dose Estimate V5.2 the dicentric yield was plotted within the Yield Curve Fitting function and modelled for linear fit along with upper/lower 95% CI.

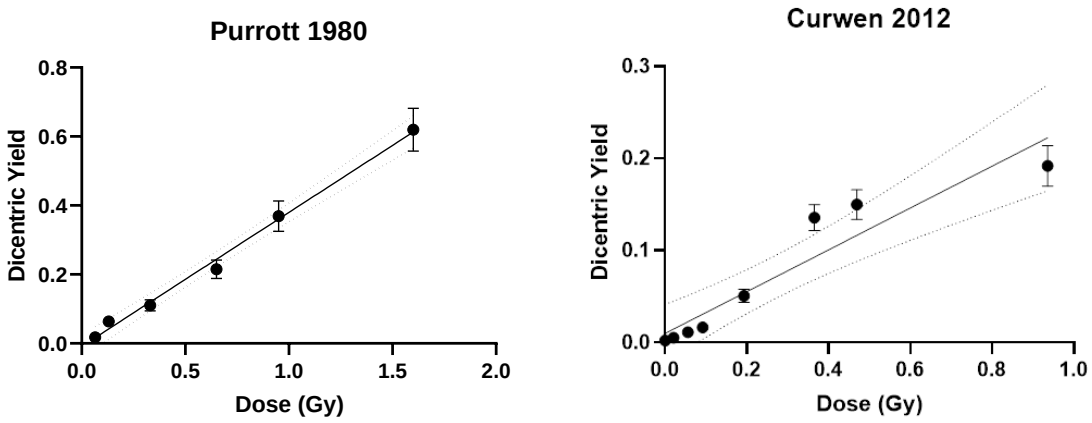

Figure 2.1313 α calibration curves Purrott 1980 and Curwen 2012.

a) ^{239}Pu *in vitro* calibration curve by Purrott 1980 (328). Whole blood was irradiated in the dose range of 0-1.6 Gy (doses converted from rad to Gy). Yield = 0.0019 (+/- 0.0126) + 0.3696 (+/- 0.0322) * D, Correlation coefficient r = 0.9970. b) ^{238}Pu *in vitro* calibration curve by Curwen 2012 (239). Isolated PBL monolayer was irradiated in dose range 0-1 Gy Yield = 0.0009 (+/- 0.0038) + 0.2632 (+/- 0.0310) * D, Correlation coefficient r = 0.9450. 95% CI calculated through Dose estimate V 5.2

2.7.4.2 Biodosimetric blood dose estimation

Dose estimation was first carried out utilizing the dicentric equivalent frequency as determined by M-FISH. For the IMRT, the ^{60}Co calibration curve of Lloyd and colleagues, 1986, (Figure 2.1212) was used. For ^{223}Ra, the ^{239}Pu calibration curve of Purrott *et al.* 1980 (Figure 2.1313) was used, together with the Dose Estimate software V5.2 (329). To calculate the absorbed blood dose in this mixed exposure scenario, the "criticality" model was used (330). All aberrations were firstly assumed to be attributed to ^{223}Ra and from the dicentric equivalent yield the dose was estimated. The absorbed blood dose ratio (^{223}Ra:IMRT) calculated according to section 2.7.4. was then used to estimate the IMRT dose and then the gamma calibration curve used to estimate the dicentric equivalent yield. This IMRT yield was then subtracted from the total yield to give a 'new' ^{223}Ra dicentric equivalent yield. This iterative process was repeated until self-consistent estimates were obtained.

2.7.4.3 Partial body exposure

To test whether the dicentric equivalent frequencies conformed to partial body the variance from Poisson distribution was assessed for each pooled cycle/patient measuring the dispersion index (σ^2/y). Values conforming to the Poisson distribution were expected to be around 1, those exceeding this were indicative of overdispersion characteristic of partial body exposure.

2.8 Statistical analysis

Statistical analysis was carried out on GraphPad Prism 9 (GraphPad Software). The data was tested for normality by Kolmogorov–Smirnov test and the Shapiro–Wilk test. Unless stated otherwise, the mean of two or more groups was tested by ANOVA for assessment of significant difference. Statistical significance was confirmed by P values ≤ 0.05.

Chapter 3: Are treatment-induced chromosome aberrations consistent with mixed radiation exposure?

3.1 Introduction

ADRRAD clinical trial patients were enrolled on to a 6 month radiotherapy schedule comprising of mixed radiotherapy treatment with low LET IMRT targeting primary tumour sites and, high LET ^{223}Ra targeting distant metastatic sites. To date, the number of studies which seek to understand the biological action of ^{223}Ra *in vivo* in humans is limited (331) indeed, a great deal of uncertainty about the heterogeneous distribution of dose at the cellular and tissue levels remains. Due to the pharmacokinetic properties of ^{223}Ra, the radionuclide will rapidly localise to areas of high bone remodelling following intravenous administration. During this period, it is possible for circulating PBL cells to be directly exposed to ^{223}Ra, albeit briefly, and once localised, progenitor hematopoietic cells may also be exposed. To assess whether PBL were exposed to ^{223}Ra during the 6 month targeted treatment period, cytogenetic analysis was carried out to enable the identification of chromosomal aberrations consistent with high LET α-particle exposure.

The frequency of chromosomal aberrations, predominantly those of simple kind, increase with increasing dose. This true for low LET exposures, such as IMRT, whereby the frequency of simple chromosomal rearrangements increases linearly with dose up to 2 Gy (332). However, the spectrum of chromosomal aberrations has been associated not only with increased dose but also to the LET quality. High LET exposure results in greater damage per unit of dose and in turn results in mainly of complex chromosomal aberrations, even at low doses (191, 237, 239, 328). This association of LET and spectrum of aberrations has been demonstrated in both *in vitro* and *in vivo* studies (as reviewed (333-335)). Chromosomal aberrations are useful biomarkers in assessing the risks associated following an unexpected exposure and following radiotherapy (236). Therefore, a cytogenetic assessment identifying the frequency and chromosomal spectra during ^{223}Ra treatment may elucidate the extent of non-targeted exposure of circulating PBL during the localization period.

In order to assess whether PBL were exposed to ^{223}Ra during treatment, cytogenetic analysis was carried out to firstly ascertain whether a significant increase of chromosomal

aberrations was evident from the treatment. To do so, blood samples were collected from five patients prior to radiotherapy treatment C1 (acting as control samples) and in 4 week cycles prior to each ^{223}Ra administration (C2-C5), circulating PBL were cultured to 1st *in vitro* division and arrested in metaphase stage. Metaphase cells were painted by M-FISH for the identification of each homologous pair of chromosomes and differential staining for X and Y sex chromosome pair. Each cell was karyotyped to identify chromosomal rearrangements and/or deletions (Methods 2.6.1). This enabled the identification of complex patterns of chromosomal aberration between chromosomes consistent with α-particle exposure.

The aim of this chapter was to identify whether the spectrum of chromosomal aberrations was consistent with mixed field exposure. A change in the spectrum and frequency chromosomal aberrations was identified between combination therapy cycles (C2-C3) and ^{223}Ra only cycles (C4-C5). The presence of complex chromosomal aberrations was considered a marker of ^{223}Ra exposure *in vivo*, enabling the discrimination from the PBL population exposed to IMRT containing aberrations of simple kind only. A high frequency of complex chromosomal events was observed during treatment. The presence of complex chromosomal aberrations may be indicative of significant blood exposure during the localisation period of ^{223}Ra. Indeed, an increasing trend of the complex chromosomal aberration frequency was also evident following IMRT completion. This suggesting ^{223}Ra as an inductor of complex chromosomal in PBL potentially during the localization to the bone.

3.2 Results

3.2.1 M-FISH assessment of pre-treatment control samples

A control sample for each patient, C1, was collected before IMRT and ^{223}Ra exposure. To be scored, all metaphase cells were required to have a minimum of 43 centromeres, any cell presenting less than 43 centromeres were classed as “no score” and omitted from analysis. For the purpose of this analysis, examining treatment induced structural aberrations, a cell was considered abnormal only if a structural change was present. Cells presenting only numerical imbalances were noted as structurally normal cells. No detailed patient history was collected for the study, but as per inclusion criteria (methods 2.1) for the study, the patients had not previously received radiotherapy or exposure to radionucleotides for investigative purposes. Therefore, any background frequency of chromosomal aberrations is not attributable to recent ionizing radiation exposure and are expected to be relatively low. The frequency of chromosomal aberrations can be seen detailed in Table 3.1 as aberration types, including simple aberrations (dicentric chromosomes, translocation and rings), break only events and, complex rearrangements.

The frequency of exchanges visualised was low with a mean frequency of 0.024 ± 0.011 for reciprocal translocations, 0.020 ± 0.009 frequency of break only events and 0.004 ± 0.004 for complex exchanges. A total of 10 abnormal cells were detected from 252 cells analysed (0.0395 ± 0.012) across all patients (Patient-1-5) with no aberrations identified for Patient-5. No simple dicentric chromosomes or rings were identified, consistent with the reported lack of recent exposure to ionizing radiation. Lloyd *et al.* (1980 (336)) suggests that the frequency of dicentrics in the general population is in the region of 0.0008; approximately 1 in 1000 cells scored. As a total of 50 cells were scored per patient, the likelihood of identifying a simple dicentric chromosome was therefore expected the be small and indeed none were identified. The frequency of break-only events was also found to be consistent with the control group studied by Heath *et al.* (1984 (337)) of 0.21 ± 48 and, lower than the general population frequency reported by Bender (1988 (338)) (0.421 ± 0.032).

Of the exchanges recorded, the highest pooled frequency was attributed to translocations (0.024 ± 0.011) and break-only events (0.020 ± 0.009) with one cell from Patient-2

containing a complex exchange. Increased age is associated with an elevation of chromosomal aberrations particularly reciprocal translocations as these are balanced arrangements (339-341). The median age for the ADRRAD clinical trial was reported as 63 (322) therefore, an elevated frequency compared to younger patient cohorts may be expected. Of the two patients presenting simple translocations, Patient-2 had a frequency of 0.098 ± 0.051 and Patient-3 a frequency of 0.020 ± 0.020. The pooled frequency from all patients was found to be in a similar range to Bender *et al.* (1988 (338)) who reported frequencies of 0.050 ± 0.009 in normal individuals, with an increased frequency skewed towards the over 40s age bracket. Tucker *et al.* (1994 (341)) observed a range of 0.822-2 stable aberrations/100 cells in the 50+ age brackets. Ramsey *et al.* (1995 (342)) who also report similar age ranges, reported 2.5 stable aberrations (including insertions) in 100 cells for individuals above 50 years of age. Both Tucket *et al.* (1994) and Ramsey *et al.* (1995) observed large interindividual variation in age range of 60-80. Although differences were also observed in our study, these were found to be in line with both reported studies above.

One cell containing a complex exchange was found in PBL sampled from Patient-2. Within the aberrant cell, 5 distinct chromosome aberration events were observed. Specifically, the complex chromosomal exchange, classified as CAB 5/6/9, along with two incomplete reciprocal translocations (one with missing fragment and the other translocation a true-incomplete) and two break-only events also with missing fragments. The cell was identified as unstable and therefore unlikely to be capable of long-term transmission. Cells containing a high degree of damage such as the cell here discussed, are unusual in individuals that have not previously been exposed to IR. General population studies have previously reported such cells as “one off” or “rogue cells” highlighting their presence but excluding them from further analysis as the origin is unknown (343-347). This cell was included in our analysis as emerging studies are now identifying many previously analysed cell samples as containing “hidden complex aberrations” (348). For our study, the number of exchanges per cell, along with complex aberration induction, will be explored further in the context of the type of radiation exposure. Accordingly, this rogue cell was included for statistical analysis.

Cycle	Patient ID	Cells scored	Abnormal cells	Simple Aberrations			Complex	Break only
				Dicentric	Translocation	Ring		
1	1	51	2 (0.039 ± 0.027)	-	-	-	-	0.020 ± 0.020
	2	51	5 (0.098 ± 0.042)	-	0.098 ± 0.051	-	0.020 ± 0.020	0.039 ± 0.027
	3	50	1 (0.020 ± 0.020)	-	0.020 ± 0.020	-	-	-
	4	50	2 (0.039 ± 0.027)	-	-	-	-	0.039 ± 0.027
	5	50	-	-	-	-	-	-
	Total	252	10 (0.040 ± 0.012)	-	0.024 ± 0.011	-	0.004 ± 0.004	0.020 ± 0.009
2	1	55	15 (0.273 ± 0.061)	0.146 ± 0.066	0.236 ± 0.082	-	0.036 ± 0.025	0.018 ± 0.018
	3	101	29 (0.287 ± 0.045)	0.099 ± 0.033	0.178 ± 0.041	-	0.030 ± 0.022	0.099 ± 0.039
	4	104	36 (0.346 ± 0.047)	0.125 ± 0.035	0.192 ± 0.049	0.010 ± 0.010	0.096 ± 0.032	0.115 ± 0.031
	Total	260	80 (0.308 ± 0.029)	0.119 ± 0.024	0.196 ± 0.031	0.004 ± 0.004	0.058 ± 0.016	0.088 ± 0.020
3	1	100	39 (0.390 ± 0.049)	0.150 ± 0.044	0.160 ± 0.039	0.010 ± 0.010	0.180 ± 0.041	0.080 ± 0.031
	2	101	46 (0.455 ± 0.050)	0.149 ± 0.038	0.277 ± 0.068	0.020 ± 0.014	0.188 ± 0.048	0.188 ± 0.054
	4	101	45 (0.446 ± 0.050)	0.228 ± 0.052	0.257 ± 0.059	0.020 ± 0.014	0.198 ± 0.051	0.198 ± 0.051
	5	105	48 (0.457 ± 0.049)	0.314 ± 0.056	0.314 ± 0.061	0.029 ± 0.016	0.133 ± 0.038	0.210 ± 0.059
	Total	407	178 (0.437 ± 0.025)	0.211 ± 0.024	0.253 ± 0.029	0.020 ± 0.007	0.174 ± 0.022	0.170 ± 0.025
4	1	48	20 (0.417 ± 0.072)	0.104 ± 0.045	0.250 ± 0.082	-	0.375 ± 0.102	0.083 ± 0.050
	2	102	52 (0.510 ± 0.050)	0.265 ± 0.059	0.255 ± 0.052	-	0.294 ± 0.065	0.147 ± 0.040
	3	103	52 (0.505 ± 0.050)	0.165 ± 0.044	0.252 ± 0.051	-	0.185 ± 0.045	0.291 ± 0.061
	Total	253	124 (0.490 ± 0.032)	0.194 ± 0.031	0.253 ± 0.033	-	0.265 ± 0.037	0.194 ± 0.032
5	1	106	49 (0.462 ± 0.049)	0.208 ± 0.051	0.208 ± 0.042	0.019 ± 0.013	0.349 ± 0.064	0.113 ± 0.034
	4	101	46 (0.455 ± 0.050)	0.168 ± 0.042	0.307 ± 0.067	0.040 ± 0.020	0.218 ± 0.054	0.188 ± 0.044
	5	102	35 (0.343 ± 0.047)	0.158 ± 0.042	0.158 ± 0.039	0.010 ± 0.010	0.059 ± 0.028	0.099 ± 0.030
	Total	309	124 (0.421 ± 0.028)	0.179 ± 0.026	0.224 ± 0.029	0.023 ± 0.009	0.211 ± 0.030	0.133 ± 0.021

Table 3.11. Chromosomal aberration types identified by M-FISH. The number of chromosomal aberrations was expressed as a frequency out of total cells scored per sample. The frequency of Standard error of the mean included per sample and for total cycle collation.

3.2.2 Treatment induced aberrations

The ADDRAD treatment schedule follows mixed exposure by IMRT+^{223}Ra for a period of 7.5 weeks followed by three further stand-alone administrations of ^{223}Ra, each administered cyclically every 4 weeks. Figure 2.11 details the first 8 weeks of treatment, where C1-C3 are reflective of daily IMRT fractions (37 planned fractions of 2 Gy each) with two ^{223}Ra intravenous injections (4 weeks apart). Aberrant cells may be induced between sampling times and later observed, with an increasing frequency expected over the treatment schedule. The frequency of aberrant cells was found to significantly increase from 0.0395 ± 0.012 at C1 background level, to 0.307 ± 0.029 ($P<0.001$) at C2 and, 0.437 ± 0.025 ($P= 0.003$) by C3. A small increase in frequency was noted from C3 to C4 (0.490 ± 0.031) but this was found to not be statistically significant ($P= 0.593$). The frequency of abnormal cells was expected to continue rising with treatment progression, instead it was found to level after completion of mixed therapy with a C5 aberrant cell frequency of 0.421 ± 0.028. There was no statistical difference between C4 and C5 ($P= 0.371$), or between C3 and C5 ($P= 0.989$), but C5 remained at a significantly higher frequency than C2 ($P=0.026$).

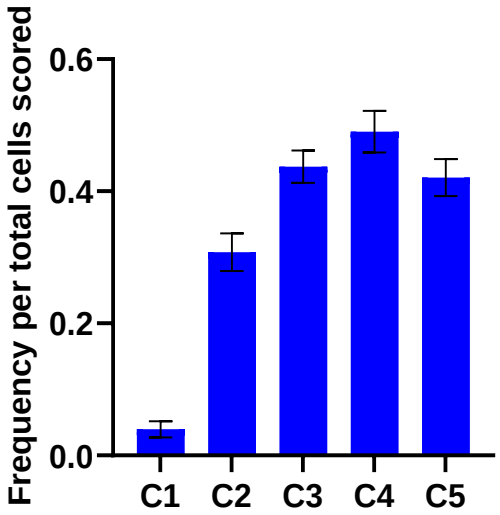

Figure 3.11. Structurally abnormal cells identified by M-FISH.

Data from 5 patients was collected prior to treatment (C1), 3 patients were analysed per treatment cycle with the exeption of C3 where 4 patients were evaluated. Patient ID and number of cells scored for each as per Table 3.11. The standard error of the mean was included for collated data per cycles.

Similarly, to the frequency of structurally aberrant cells, the frequency of total chromosomal events was found to initially increase with treatment progression. The number of chromosomal events statistically increased between C1 (0.047 ± 0.019) and C2 (0.480 ± 0.071 (P<0.0002)) and, further to 0.918 ± 0.093 at C3 (P <0.0001). The frequency of chromosomal events (0.966 ± 0.094) at C4 was not statistically different from C3 (P= 0.991) and neither with C5 (0.7086 ± 0.091 (P= 0.1608)). Overall, there was no difference in frequency of chromosomal events between C2-C5 (P= 0.266), suggesting a clearance of heavily damaged cells (containing multiple chromosomal events) from the peripheral pool.

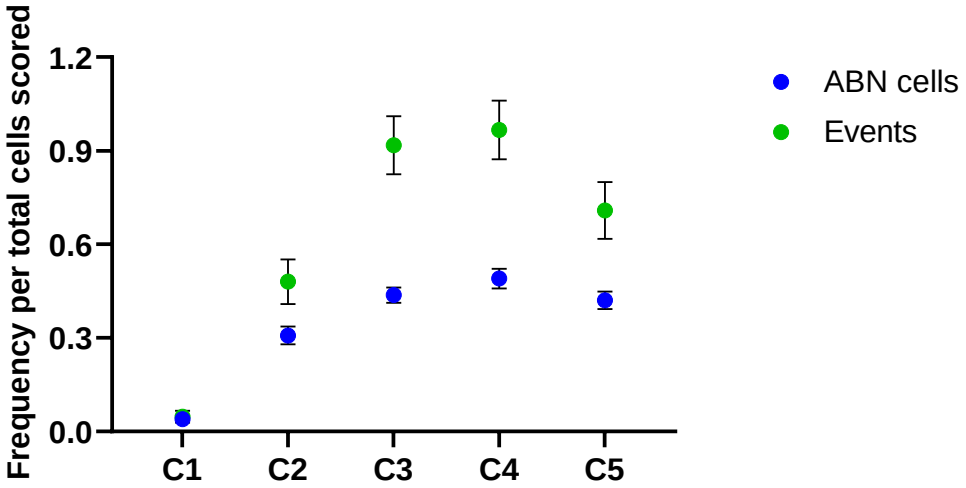

Figure 3.22. Structural chromsomal events observed during treatment.

Structual chromsomal events (Simple, complex and/or break only) and abnormal cells (ABN) were collated for five patients over C1-C5 of treatment. Patient ID and number of cells scored for each as per Table 3.11. The standard error of the mean included for collated cycles.

All together this suggested a peak in both the frequency of abnormal cells and, the number of chromosomal events/damage cell around C4 with differences in aberration burden being seen between treatment cycles. This is highlighted by the samples at C2 having a similar yield of chromosomal events to abnormal cells indicating a distribution of events/cell just above 1, whilst, by C3-C4 sample times, damaged cells are potentially carrying 2-3 events/cell. This is consistent with either a dose escalation, suggesting multiple exposures of a cell to IMRT fractions, or where a fraction of cells is exposed to ^{223}Ra resulting in a higher damage burden.

3.2.3 Aberration spectrum varies with treatment schedule

In vivo and i*n vitro* studies have suggested chromosomal aberration spectrum to be dependent on LET with high LET exposure (>100 keV/mm) increasing the frequency of complex exchanges, even at low doses (as reviewed by (349)). Simple chromosomal aberrations have been associated primarily with low LET exposure from X-rays or y-rays up to 2 Gy, as per IMRT fractionated treatment (332). Therefore, it was hypothesised that as earlier treatment cycles are mainly associated with low LET exposure, this would result in a high frequency of simple chromosomal aberrations. Upon completion of this IMRT schedule, the frequency of complex aberrations would increase in later cycles due to the ongoing ^{223}Ra only exposure.

Table 3.11 summarises the findings between C1-C5 sampled for five patients. Simple chromosomal events were grouped based on two breaks involved in the event, break only events were scored with the involvement of one break, fragmentation of one chromosome was scored when more than two breaks were identified. Complex chromosomal events were defined as two or more chromosomes with more than two breaks as per classification in methods 2.6.1. By assessing each exchange per cell, it was possible to question whether a particular subset of chromosomal aberrations was prevalent during mixed therapy and ^{223}Ra alone as seen in pooled cycle data in Figure 3.3. Simple chromosomal events were observed to increase in frequency once treatment commenced between C1 (0.024 ± 0.011) and C2 (0.319 ± 0.042) (one-way ANOVA P< 0.001). An increasing trend was observed until C3 (0.484 ± 0.042) (C2-C3 P= 0.031) followed by a plateau in later cycles. No other statistical difference was noted between treatment cycles, suggesting the majority of simple events were formed in the early stages of treatment and retained through C4 and C5. The frequency of complex events was also found to follow an increasing trend with treatment time from 0.004 ± 0.004 at C1 to 0.265 ± 0.037 at C4. Statistical increases were observed between C1-C2 (P<0.001), C2-C3 (P=0.007) and C2-C4 (P<0.001). No significant difference was observed between C3-C4 (0.174 ± 0.022 and 0.265 ± 0.037, P=0.07) or, between C4-C5 (0.265 ± 0.037 and 0.210 ± 0.030, P=0.576), suggesting slower induction of complex aberrations between C3-C5.

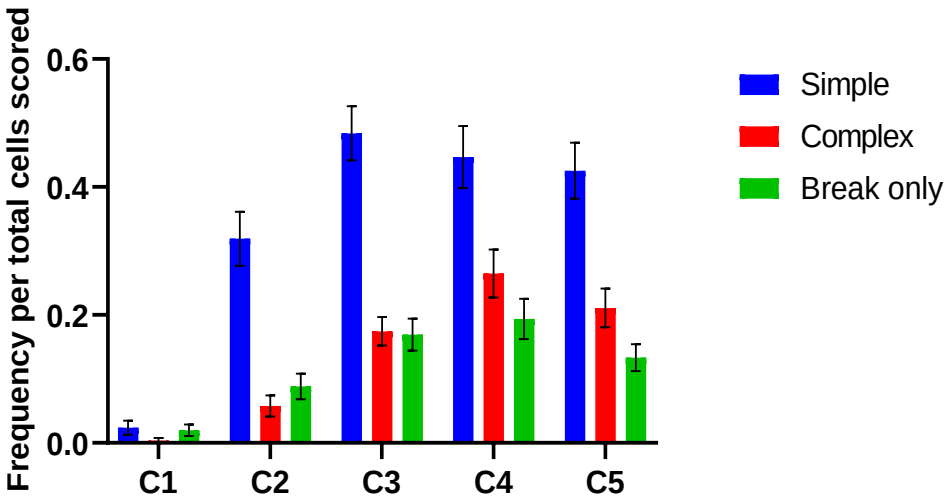

Figure 3.33. Structural chromsomal aberrations observable during treatment.

Simple chromosomal aberrations including dicentrics, translocations and rings. Complex chromosomal aberrations defined as rearrangements that involve ≥3 breaks and involve ≥2 chromosomes, Break only involving one chromsome with a chromsomal break. Patient ID and number of cells scored for each as per Table 3.11. Standard error of the mean inluded per cycle.

The frequency of break-only events followed a similar increasing trend between C1 and C4 with statistical significance (0.020 ± 0.009 and 0.194 ± 0.032, P< 0.001). A statistical difference was also observed between C2 and C4 (0.088 ± 0.020 and 0.170 ± 0.025, P=0.027). Like the frequency of complex aberrations, that of break-only events levelled by C5 with no statistical difference from C4 (0.194 ± 0.032 and 0.133 ± 0.021, P= 0.392) Chromosomal fragmentation events included in break-only category, were found to be rare however emerging after C3, all patients displayed at least one fragmentation event in C5.

Overall, both simple and complex exchange events were observed during treatment, consistent with a mixed exposure scenario. As IMRT treatment is completed by C3 sample collection, the following C4, reflective of further ^{223}Ra-only, was expected to result in a lower induction of further simple chromosomal events. Indeed, there is no increase from C3 sample to C4 or in the later C5 sample. The simple aberration category comprises of stable reciprocal translocations and unstable exchanges including dicentric chromosomes and rings (Table 3.11). To assess whether the plateau was associated with aberrant cell clearance,

simple exchanges were plotted (Figure 3.4). Dicentric and translocations have a similar rate of induction as it is after a random chance whether a chromosome rearranges itself to form a dicentric or translocation exchange. In cases where translocation exchange frequencies are considerably higher than dicentrics frequencies, this may indicate *in vivo* preferential clearance of cells containing unstable chromosomal events or dilution from haematopoietic repopulation containing stable aberrations.

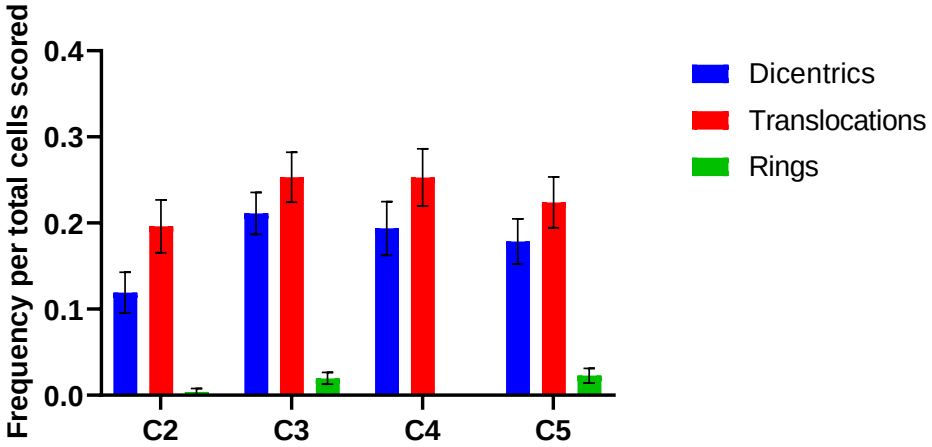

Figure 3.44. Simple chromosomal aberrations across treatment.

Total frequencies of simple exchnages including dicentric, tranlsocation and rings. Patient ID and number of cells scored for each as per Table 3.11. Standard error of the mean included per cycle collation.

The frequency of rings was found to be small throughout treatment cycles with no rings found in C4. The frequency of rings in C5 (0.023 ± 0.009) was similar to C3 (0.020 ± 0.007), suggesting no clearance in the patients that did display rings in earlier cycles. No statistical differences were found between translocations and dicentrics at C3 (0.253 ± 0.029 and 0.211 ± 0.024, P=935), C4 (0.253 ± 0.033 and 0.194 ± 0.031, P= 0.887) and C5 (0.224 ± 0.029 and 0.179 ± 0.026, P= 0.951). A small difference was noted in C2 where a higher frequency of translocations over dicentrics, however this was not statistically significant (0.196 ± 0.030 and 0.119 ± 0.024, P=0.654). The near 1:1 ratio for translocations : dicentrics suggests that cells containing unstable chromosomal events are not being cleared more rapidly than those containing stable events.

As stated previously, low LET exposures of 2 Gy fractions result mainly in simple exchanges per cell whilst, high LET exposure results in mostly complex exchanges. Therefore, a higher proportion of cells containing simple only aberrations was expected during IMRT administration. The frequency of cells containing at least one complex exchange was expected to be largest by the end of treatment where ^{223}Ra only was administered alone. To assess this, PBL were categorised based on the chromosomal exchanges observed per cell. Complex cells were classified as cells containing at least one complex event and deemed to be a result of ^{223}Ra exposure, while simple cells were scored as cells containing only simple exchange events, likely induced from IMRT exposure. Cells containing solely break-only events were excluded from this analysis.

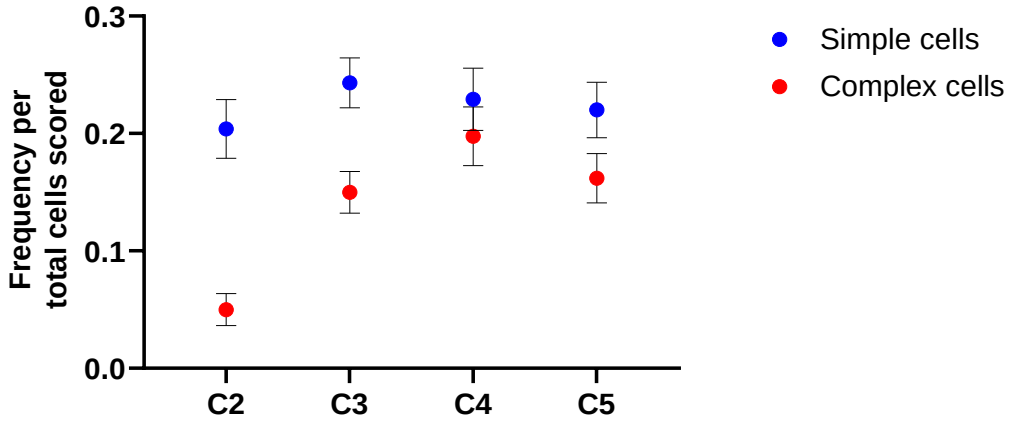

Figure 3.55. Nominal simple and complex cells observed through treatment.

IMRT exposed cells categorised as those containing simple exchange events only and ^{223}Ra cells categorised as those containing at least one complex exchange. Patient ID and number of cells scored for each as per Table 3.11**.** Standard error of the mean included per cycle collation.

As per Figure 3.5, the majority of aberrant cells sampled during mixed radiotherapy (C2-C3) contained only simple type exchanges (IMRT). In C2, the frequency of IMRT exposed cells being 4 times higher than the frequency of cells contain at least one complex exchange (^{223}Ra exposed group). Similarly, in C3 the frequency of IMRT exposed cells was 1.6 times higher than the frequency of ^{223}Ra exposed cells. The frequency of IMRT exposed cells remains higher than ^{223}Ra exposed cells in C4 (0.229 ± 0.026 and 0.198 ± 0.025 respectively) and C5 (0.220 ± 0.024 and 0.162 ± 0.021) however, after completion of mixed therapy, this

does not increase further, whilst the frequency of ^{223}Ra exposed cells increases. When comparing the frequency of cells arising from IMRT following completion in C3, there appears to be a plateau (C3-C5) whereby no new simple chromosomal aberrations are induced. Instead, the frequency of cells containing complex aberrations rises from 0.150 ± 0.018 in C3 to 0.198 ± 0.025 in C4, suggesting ^{223}Ra as the inductor of new complex aberrations. The sampled cells in C4 present a near 1:1 ratio (simple : complex cells) with IMRT exposed cell frequency being only 1.16 times higher. In C5, the IMRT exposed cells persist at a frequency of 0.220 ± 0.024, which is 1.36 times more than cells containing complex exchanges of frequency 0.161 ± 0.021. Overall, a higher proportion of cells containing simple only exchanges was found in earlier cycles, with the frequency of cells containing complex exchanges increasing in ^{223}Ra only samples.

3.2.4 PBLs shown no evidence of dose escalation

^{223}Ra is cleared from the circulatory pool over a 24 h period, it was questioned whether cells could be exposed to multiple α-particle tracks. If so, this may suggest an increased frequency of chromosomal events in cells exposed to multiple by α-particles “hits”. It has been proposed that one α-particle cell traversal will result primarily in one complex event (191). A deviation from this expected number of complex events may indicate multiple exposure of a PBL during the cycle sampled. The same principle was also applied to cells likely exposed to IMRT. Cells containing a high number of simple events may be indicative of a cell exposed to a higher dose during fractionation.

As per Figure 3.6, >72% of cells with a complex exchange were found to contain one discrete complex exchange. This suggesting most cells to be exposed to a single α-particle track. An increasing trend for cells containing multiple independent complex exchanges was observed in ^{223}Ra only cycles (C3-C5), however, no statistical significance was observed. C2 was found to not contain any cells with ≥3 complex events, this likely due to the low frequency of complex events for this cycle (as per Table 3.1). No statistical differences were identified for IMRT exposed cells with the number of independent single exchanges remaining consistent across all cycles.

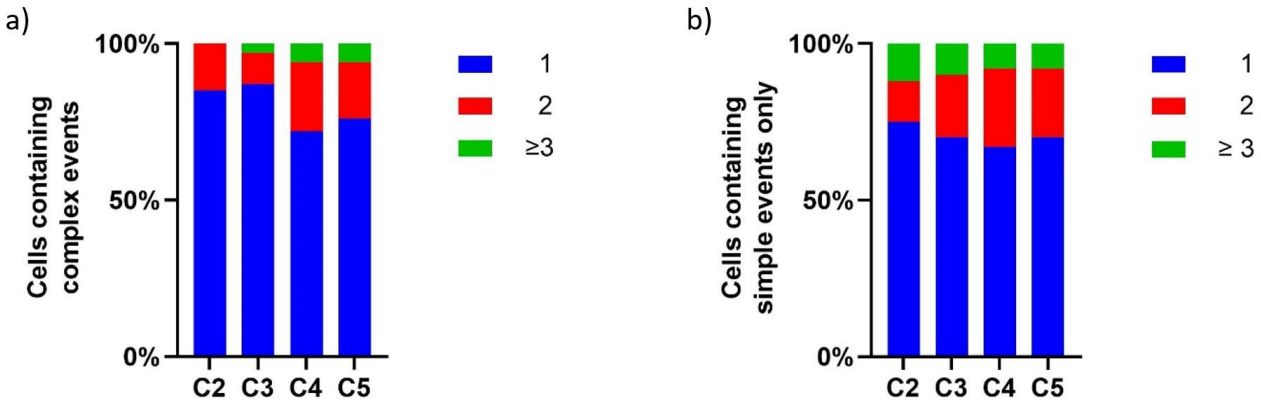

Figure 3.66. The likelihood of multiple "hit" exposure for high and low LET.

a) cells containing at least one complex exchange consistent with ^{223}Ra exposure. b) includes cells containing simple exchanges consistent with IMRT exposure. These are expressed as a percentage of the total abnormal cells. Each abnormal cell was categorised as having 1, 2 or ≥ 3 events of respective exchange per cell.

3.2.5 Chromosomal ratios as LET signatures

The term C-ratio, defined as the ratio between complex exchanges and simple exchanges, has previously been proposed as a cytogenetic signature of LET (334, 350). Previous studies have found high LET radiation to be more effective in the induction of clustered DNA damage (185, 351, 352), the mis-repair rate was also found to be higher (as reviewed in (170, 353)) and, thus, a more complex pattern of chromosomal aberrations are observed when compared to low LET exposures of similar dose, or, lower. As the treatment schedule follows exposure from ^{223}Ra only in the later C4 and C5 samples, we questioned whether a change in C-ratio may be observed in these high-LET exposure only cycles. The first two treatment cycles, C2 and C3 were hypothesised to have similar C-ratios with a higher proportion of simple exchanges consistent with primarily low LET exposures.

The C-ratio for ^{223}Ra only cycles was found to be higher than mixed exposure cycles as predicted, ranging from 0.593 ± 0.106 in C4 and 0.496 ± 0.088 for C5 as seen in Figure 3.13. The C-ratio for C2 was found to be low at 0.181 ± 0.057. The C3 C-ratio was found to be

higher than that of C2 at 0.360 ± 0.056. Comparing this to other studies, such as Lee *et al.* the expected C-ratio for *in vitro* exposure to 2 Gy of X rays was expected to be in the region of 0.23 (calculated from 37 complex exchanges : 163 simple exchanges) (354). Here, the C2 value was found to be consistent with the published data, but the C3 ratio of 0.360 ± 0.056 was larger. An *in vivo* study by Hartel *et al.* (2009 (355)) of prostate cancer patients treated with a similar IMRT treatment plan to that examined here, found a C-ratio of approximately 0.29 (calculated from frequency of 0.2 and 0.7, complex and simple exchanges respectively), once again consistent with C2 sample analysed here. This suggests an incremental increase in complex aberration induction with each subsequent dose of ^{223}Ra.

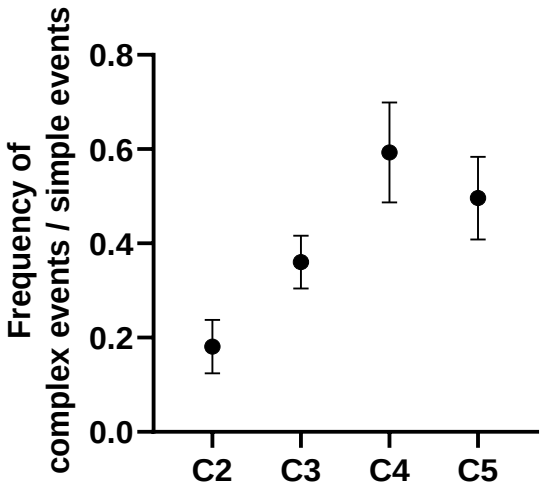

Figure 3.77 C-ratio across treatment.

The C-ratio was calculated utilazing the combined number of simple events and complex events per cycle. Frequencies of events from five patients as per Table 3.1. Error propagation was estimated from the deviation of SEM per cycle.

Another ratio suggested to be interchangeable with the C-ratio is the I-ratio, this being a ratio of simple translocations to insertions. The frequency of cells containing insertions was found to increase with treatment progression, not surprising as insertions are by definition a complex event, and complex cells were seen to increase in frequency as per Figure 3.9. Unlike the C-ratio where simple events frequency is compared to complex event frequency, the number of INS is compared relative to reciprocal translocation exchanges, irrespective of how many INS occur in each complex event.

In the study four very complex cells were identified at different sampled cycles. For Patient-3, two cells were found to contain between 7 and 10 INS in the C2 sample, in Patient-1 C3 sample, one complex cell involving 21 chromosomes was visualised and lastly, in Patient-2 C4, an estimated 4 INS categorised as part of 3 different complex rearrangements was seen within one cell. These cells containing unusually complex rearrangements resulted in the C2 I-ratio being particularly small (Figure 3.88). The I-ratio was calculated with the inclusion of the discussed cells (data set A) and without (data set B). This resulted in small non-significant variations between C3 and C4 data sets but a large variation in C2.

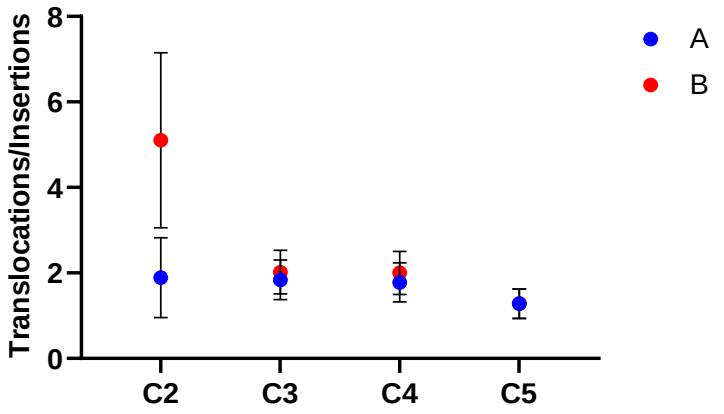

Figure 3.88. High frequency of insertions consistent with α-particle exposure.

A) including all insertions B) excluding very complex cells where insertions were approximated. These include two cells with 7 and 10 insertions in C2, one cell with 5 insertions in C3 and, one cell in C4 with 4 INS. Error propagation was utilized to estimate a deviation of SEM per cycle.

The I ratio has previously been used to highlight differences in LET and for this patient cohort it highlights that samples C3-C5 are consistent with exposure to a high LET source. The C2 samples had a lower frequency of insertions but the error is much higher and still consistent with a high LET exposure scenario.

3.3 Discussion

The aim of this chapter was to assess PBLs for markers of ionizing radiation exposure and to examine whether these could reflect the mixed radiotherapy treatment regime. PBLs were sampled as they represent a cell population that circulates the entirety of the body and infiltrates in most tissues. Therefore, PBLs may be exposed during IMRT pelvic treatment and, following ^{223}Ra intravenous administration. PBLs were sampled cyclically every 4 weeks, during each visit prior to the next ^{223}Ra administration. Due to the sampling schedule, cytogenetics was deemed the most appropriate technique as PBLs exposed to ionizing radiation may conserve chromosomal aberrations of both unstable and stable kind for months following exposure (356-359). As per treatment schedule, following the collection of the pre-treatment control sample, both IMRT and ^{223}Ra were administered on the same day. Following this, 2 Gy daily fractions were delivered for a total of 7.5 weeks with the next ^{223}Ra administration after 4 weeks (and every 4 weeks following). The exposure was therefore of mixed quality including both Low and High LET over the 6 months of treatment.

The number of published studies quantifying transmissible reciprocal translocations and unstable dicentric chromosomes following IMRT radiotherapy in patients is limited, (354, 355, 360-362). With this, it was possible to compare the collected frequencies and patterns of rearrangements to those identified here. The number of studies following *in vivo* ^{223}Ra exposure is even fewer, with only one recent publication by Schumann *et al.* (2021 (363)) identifying γ-H2AX foci in PBLs following intravenous ^{223}Ra treatment. A previous *in vitro* study also by Schumann *et al.* (2018 (364)), identified a linear relationship between the α-particle induced γ-H2AX damage tracks following exposure of healthy donor blood. Generally, studies following α-particle exposure *in vivo* are limited as α-particles only pose a risk when internalized. The majority of cytogenetic studies have been *in vitro* (191, 237, 328) and identified high frequencies of complex chromosomal rearrangement patterns compared to simple chromosomal aberrations. This suggests complex chromosomal aberrations to be a potential marker for high LET exposure, including following exposures where the radiation type is not known as reviewed by Anderson (2019 (349)).

In our study, PBLs were found to contain markers of High LET α-particle exposure from the first treatment sample C2 with an average frequency of 0.058 ± 0.016. The majority of published papers following ^{223}Ra treatment report low haematological toxicity from the isotope as the majority of dose is assumed to be delivered at the target site (78, 80, 365, 366). Delving further into the treatment schedule a cycle dependency was observed, with mixed exposure cycles presenting high frequencies of simple chromosomal aberrations (C2=0.319 ± 0.042 and C3=0.484 ± 0.042) consistent with IMRT exposure, but also an increasing trend in complex rearrangements (C2=0.058 ± 0.016 and C3=0.174 ± 0.022). After the completion of IMRT, the frequency of simple events was found to plateau (C3= 0.253 ± 0.029 and C4= 0.253 ± 0.033), suggesting, as per published *in vitro* and *in vivo* studies ((332, 367, 368)), that low LET exposure up to 2 Gy results mainly in simple chromosomal rearrangements. The frequency of complex events was instead found to increase further in C4 (C3= 0.174 ± 0.022 and C4= 0.265 ± 0.037) which was representative of a ^{223}Ra further administration, this suggesting ^{223}Ra to be a direct inductor of complex rearrangements.

As the mode of administration of IMRT and ^{223}Ra differ, it was important to assess whether PBL circulating cells may be exposed more than once during treatment. In the case of multiple α-particle tracks traversing a cell, a higher chance of multiple complex rearrangements in each damaged cell may be plausible. Whilst for multiple exposure of a PBL to IMRT, multiple simple chromosomal exchanges may instead occur. It was found that neither IMRT or ^{223}Ra was likely to have "re-irradiated" a cell. Therefore, no dose escalation was expected for each cell exposed, therefore IMRT exposure to blood would only be reflective of a maximum dose of 2 Gy and ^{223}Ra 55 kbq/Kg of injected activity. In terms of the distribution of chromosomal events, a distinction between cells containing at least one complex event and cells containing simple exchanges only, was observed. This could potentially be exploited to enable distinct dose estimations to be made for each of the component radiation types of these patients, as explored in Chapter 4.

The number of studies sampling chromosomal aberrations following IMRT by M-FISH analysis is limited. One study by Hartel *et al.* (2018 (369)) examined the frequency of chromosomal events before, during and by the end of treatment as part of a study comparing the effects of IMRT with IMRT combined with carbon boost. This study examined eight prostate cancer patients receiving IMRT only treatment, five of which had a small

irradiation field comprising prostate and seminal vesicles. The other group comprised of three patients who received exposure to a much wider area including the prostate and pelvic nodes. Both groups received 76 Gy tumour dose over daily fractions ranging between 2-2.24 Gy. The three patients having a larger target volume are likely to be more comparable to the ADRRAD patient cohort in this study, also received prostate and lymph node irradiation with planned doses of 74 Gy administered as 2 Gy daily fractions. The study by Hartel *et al.* (2018 (369)) identified the frequency of simple aberrations during treatment of 0.1 and 0.3 for the smaller and larger areas, respectively. This may be comparable to this studies C2 samples, where the frequency was found to be 0.340 ± 0.058. As the study also measured simple aberrations after treatment (0.15 and 0.70, corresponding for smaller and larger irradiated field) these were also compared with the C3 sample in this study which corresponded to the end of IMRT treatment of 0.534 ± 0.065, and were within similar range.

The frequencies of complex events were also quantified in the study by Hartel *et al.* (2018 (369)) both during and after radiotherapy. The frequency was found to increase from 0.01-0.05, in the smaller and larger target volume group, to 0.02-0.20. These were consistent with our study at C2 (0.058 ± 0.016) and C3 (0.174 ± 0.022). Given this, this could suggest that the majority of chromosomal aberrations detected during C2 and C3 are consistent with that of IMRT exposure only. It is widely accepted that complex chromosomal aberrations induced by low LET are dependent on dose (355, 370, 371), however, it is ultimately not possible to confine all complex events as being attributed to ^{223}Ra. The same being said with ^{223}Ra, although studies have suggested most aberrations from high LET exposure to be of complex kind it cannot be excluded that some events may be of simple kind.

Another point to consider is the lethal effect of α-particles on cells, with *in vitro* studies suggesting 2-6 α-particles transversion to be sufficient for cell death, while surviving cells arising from fewer track traversals may result in cell chromosomal aberrations (372, 373). It could be considered that ^{223}Ra is more likely to induce a high level of damage and these heavily damaged cells may be cleared more rapidly from the peripheral blood pool by sampling time. Therefore, the sampled population may be representative of cells traversed by fewer α-particles, and as suggested by our data the likelihood of multiple track exposure was low for our sampled PBLs. This being said, the cell survival to α-particles is also based on

more complex factors including the cell geometry, cell type and stage of maturation stage (193) which could not be quantified with our *in vivo* model. Due to the sampling being 4 weeks after the ^{223}Ra administration it is not possible to carry out an assay to quantify the apoptotic response *in vivo* to test whether a difference was observed between mixed exposure cycles and ^{223}Ra only. In our study it was found that the frequency of complex aberrations increased in C4, ^{223}Ra only cycle, to 0.265 ± 0.037 this frequency is larger than C3 and of that of the previously described study by Hartel *et al.* (2018 (369)). As the ^{223}Ra administered dose varies between patients, unlike IMRT, interindividual variation was observed. Patient-1 and 2 had a statistical increase in complex aberrations from C3 to C4, increasing from 0.180 ± 0.041 and 0.188 ± 0.048 to 0.375 ± 0.102 and 0.294 ± 0.065 respectively P= 0.0234 (unpaired t test of pooled cycles). This indicates that ^{223}Ra to be an inductor of complex chromosomal aberrations *in vivo*, although further analysis should be undertaken with a larger patient cohort to identify differences between patient responses and/or potentially the clearance of aberrations.

The C-ratio has been suggested as an indicator of high or low LET exposure in unknown exposure scenarios as it compares the frequency of complex : simple exchanges. The dynamics of cell exposure are different *in vivo* to *in vitro* studies, it is therefore hard to make a comparison with what the expected C-ratio range should be. Hartel *et al.* (2009 (355)) found a low C-ratio for IMRT exposed patients, estimated here as 0.29 from a frequency of 0.2 complex exchanges and 0.7 frequency of simple exchanges. In the same publication, an *in vitro* calibration curve of lymphocytes to exposed varying doses of X-rays, identified a C-Ratio of 0.06 ± 0.04 at 1 Gy following a dose dependent increase to 1.1 ± 0.2 at 6 Gy. In our study, the C-ratio during mixed field exposure was of 0.181 ± 0.057 for C2 and 0.360 ± 0.056 for C3. These values are in a similar range to the *in vivo* and *in vitro* data from Hartel *et al.* (2009 (355)). The estimated C-ratio for our study was also comparable to *in vitro* data by Lee *et al.* (354). This suggests C2-C3 to be consistent with mainly low LET exposure with the increased C-ratio in C3 likely attributed to a further dose administration of ^{223}Ra. In the ^{223}Ra only cycle the C-ratio was found to increase further with 0.593 ± 0.106 and 0.496 ± 0.088 the increase reflective of high LET exposure resulting in a higher induction of complex aberrations. All together these findings suggest that for the ADRRAD patient cohort a significant proportion of complex aberrations are likely to have been induced by ^{223}Ra

during the treatment. To our knowledge, this is the first-time that cytogenetic markers consistent with exposure of non-target cells by ^{223}Ra as part of radiotherapy treatment has been found *in vivo*.

In our study, the I-ratio which compares simple translocations to insertion was not as informative. Although the number of complex exchanges was high, the number of insertions was relatively low. Technically there were difficulties as the number of insertions was not successfully quantified for all complex events as some heavily damaged cells count not successfully be resolved. Excluding unresolved cells where the insertion number was approximated, the I-ratio did suggest a large effect from low LET exposure for C2 and a dominant effect from high LET exposure for C3-C5. Further work will be needed to assess whether the I-ratio is a feasible measure for unknown exposure scenarios.

Cytogenetic assessment was carried out on all patients prior to radiotherapy to draw a baseline frequency of chromosomal aberrations. The frequency of aberrant cells was found to be lower than expected in the control samples, considering previous treatments and age of the patients. Ramsey *et al.* (1995 (342)) found stable aberrations to be elevated in healthy adults over the age of 50, particularly stable transmissible aberrations including translocations and insertions, at a frequency of 0.251 (2.506 aberrations per 100 cells). In the case of our control group, no stable insertions were identified, and the frequencies of translocations were found to be <0.100. This being said, although the frequency of translocations was found to be low, the same study found patients of this age group to have greater variation in their frequency of stable translocations. Three individuals in this study had a statistically higher proportion of translocations ranging from 3.9-4.9 per 100 cells. This interindividual variation was also observed in this study whereby Patient-1, 4 and 5 reported no reciprocal translocations whilst Patient-2 had a frequency of 0.098 ± 0.051 and Patient-3 of 0.020 ± 0.020. Although differences were observed, the frequency of aberrations for each patient were still found to be within the expected normal range for individuals in the 50+ age bracket. The rogue cell identified in Patient-2 was found to be unstable therefore unlikely to be originating from clonal expansion of previously exposed stem cells and unlikely to further result in clonal daughter cells in following treatment cycles. No increased frequency in simple unstable events such as dicentrics or rings was observed, this suggesting no recent exposure to ionizing radiation as confirmed by eligibility criteria of the study

(appendix). A normal population study by Wojda *et al.* (2006 (326)) also found the frequency of structural chromosomal aberrations to vary per age group, the over 60s category frequency ranging from 0.38-0.7. The reported frequencies were accompanied by larges deviations in standard error which were attributed to interindividual variation. When observing the frequency of total chromosomal events in our study group, the frequency for C1 was found to be 0.047 ± 0.020 this sitting well between the reported range by Wojda *et al.* (2006 (326)).

The results discussed suggest ^{223}Ra to induce primarily complex chromosomal aberrations, and IMRT being mostly responsible for the simple chromosomal aberrations detected. Although it cannot be excluded that a fraction of complex aberrations may be induced from IMRT, the frequency of complex aberrations appears to potentially increase in later ^{223}Ra only cycle. Instead, the frequency of simple chromosomal aberrations plateaus following IMRT completion suggesting ^{223}Ra to not induce a significant fraction of simple chromosomal exchanges. The control samples of all patients do not indicate previous recent exposure to an ionizing agent therefore the sampled aberrations were attributed to the treatment schedule.

Chapter 4: Dose estimates from a mixed exposure scenario

4.1 Introduction

The novel radiotherapy treatment regime implemented in the ADRRAD clinical trial, raises questions as to whether a significant dose is delivered to non-target tissues. Non-target exposure may be a result of the IMRT treatment to the pelvic region and/or following the use of novel $RaCl_2$ for distant metastatic site targeting. The risk associated with IMRT non-target exposure is well recognised and continuous improvements are made to enhance target dose delivery while minimising surrounding tissue exposure (93, 94, 107, 374-379). Instead, the risk associated by ^{223}Ra non-target exposure has yet to be studied, primarily due to the novel application for bone metastatic disease management only approved in the last 10 years. Therefore, quantifying the absorbed blood dose to non-target tissues is one of the first steps towards evaluating short and long term effects from the proposed treatment schedule (168). The aim of this chapter was to estimate the absorbed blood dose for each radiation quality whilst testing the feasibility of a novel approach for mixed field exposure dose quantification. In doing so, the application of each model was compared and limitations discussed.

The calcium mimetic properties, induction of complex lethal damage and non-target tissue sparing have rendered ^{223}Ra an optimum treatment for CRPC and potentially has clinical applications for treatment of other cancers also tending to metastasise to the bone. Once intravenously administered, the structure of $RaCl_2$ enables immediate solubility into the blood, this results in free ^{223}Ra carrying a positive charge during circulation. The calcium mimetic properties enable ^{223}Ra to rapidly localise to metastatic regions of the bone within 24 h (152-155). The decay of ^{223}Ra is characterised by the release of α-particles, these particles deposit densely ionizing radiation clusters along their tract. The clustered damage from the energy deposits may cause complex irreparable damage in metastatic cells and ultimately result in cell death. α-particles have been found to have a low penetrance of ≤100 μm (380), this potentially meaning little to no exposure of neighbouring non-target tissues. Although the range of emitted α-particles is short, ^{223}Ra is not directly delivered to bone

metastatic sites, instead a 24 h period of transit (following intravenous administration) may result in unwanted blood exposure (154, 363). This is of particular concern for not only acute toxicity following exposure of circulating blood cells resulting in temporary conditions such as anaemia (which are monitored during the trial), but also long term toxicity. Accumulating evidence suggests vascular endothelia damage to have potential long term effects such as increasing the risk of cardiovascular diseases (as reviewed in (381, 382)) even at low dose exposure (as reviewed in (383)). We therefore question whether ^{223}Ra treatment may result in a significant dose delivered to the blood over the 6 month treatment period.

It is known that IMRT treatment results in a significant exposure to the blood (325, 369) and as the treatment schedule is reflective of a mixed exposure scenario, the expected dose delivered to the blood will be estimated for both ^{223}Ra and IMRT. Existing blood dose models for IMRT are mostly based on physical methods which employ complex parameters of exposure fields mapped by MRI or CT beam plans for target volume of exposure, along with complex blood flow simulations within the field itself (384, 385). Recently, blood dose estimation by Moquet *et al.* (2018 (325)) has enabled the quantification of blood dose by IMRT utilizing two simplified models with fewer parameters, these models found to be comparable to that of cytogenetic dicentric assay. Utilising the ADRRAD patient data paired with the models described by Moquet *et al.* (2018 (325)), the IMRT absorbed blood dose may be estimated. Estimation of internalized radionucleotide dose is instead more complex, mainly due to the unique pharmacokinetics of each radionucleotide. The quantification of dose delivered by ^{223}Ra to target sites has been previously characterized using scintigraphy and modelling software packages which enable reasonable estimations to be made at the target sites (386-389). However, due to the low range of α-particles, scintigraphy is based on the daughter products of ^{223}Ra, therefore this system is useful for quantification of ^{223}Ra deposits within bone and tissue but not during circulation following intravenous administration. For the quantification of dose in circulation, previous data of the pharmacokinetics and clearance of the ^{223}Ra was instead implemented (152-155).

An existing biodosimetric model proposed for mixed has successfully been implemented to estimate the dose following neutron and gamma exposure (236). This model was designed for criticality exposure scenarios whereby an individual is exposed to both high LET neutron

and low LET gamma external radiation. This model relies on physically derived estimates of exposure to model a dose ratio, therefore optimal in cases where the emissions by causative agents are known. This model, paired with the traditional dicentric assay, enables the estimation of absorbed dose for each radiation quality. Applying this model to our physical blood dose estimates (from IMRT and ^{223}Ra) followed by the dicentric assay, the estimation of absorbed blood dose may be possible during treatment for each sampled cycle.

In the previous chapter, M-FISH analysis was implemented to assess whether markers of high LET exposure consistent with α-particle damage were present in the sampled PBLs. M-FISH analysis enables not only the quantification of aberrations but also detailed analysis of the aberration complexity, enabling the assessment of each chromosome involved in the exchange and whether this is consistent with a spectrum of low LET or high LET exposure. We therefore question whether cytogenetic markers of high and low LET exposure observed in PBL could be utilised for a direct dose estimation in a situation where the ^{223}Ra and IMRT ratio was unknown. This potentially leading to a novel approach for dose estimation after an unknown exposure by mixed ionizing agents. To do so, the frequency of cells consistent with ^{223}Ra exposure and those of IMRT exposure identified in the previous chapter were employed as a pseudo ratio of ^{223}Ra:IMRT dose estimated by physical parameters. Implementing the traditional dicentric chromosome assay, the dose for ^{223}Ra and IMRT may be estimated and compared to that derived by physical parameters.

4.2 Results

4.2.1 Physical dose estimations

4.2.1.1 ^{223}Ra blood dose estimation

To assess absorbed blood dose during this localization period, the injected activity of all patients was firstly collected for each treatment cycle. The injected activities can be seen in Figure 4.11 including the mean injected activity across the 6 months of treatment and the upper/lower limits. The differences in the injected activity were a direct result of variations between patient weights. Patients of higher body weight were administered a larger activity of ^{223}Ra compared to patients of lower body weight. This following ^{223}Ra being administered as 55 kbq/kg of body weight. However, when comparing the mean activity of each patient across treatment cycles, there was little effect between patients (two-way ANOVA P= 0.011). Multiple comparisons of patient mean highlighted only Patient-8 and 13 as having a statistically different injected mean dose (two-way ANOVA mean patient comparison, P= 0.043). Some intra-patient differences were also observed following large weight fluctuations during the 6 month treatment period and hence differences in the administered activity. However, the fluctuations did not result in a significant difference (2 way ANOVA P= 0.135).

To calculate the absorbed blood dose during the localisation period, the pharmacokinetic properties of the ^{223}Ra were taken into consideration. The majority of the ^{223}Ra is thought to localised to metastatic regions or excreted within 24 h of intravenous administration with ≤1% activity remaining in the blood. Consequently, it was assumed that the additional dose deposited to the blood outside of the 24 h window may be negligible. As per method section 2.7.1, three clearance models were combined from 3 different study groups (152, 154, 155). The median amount of ^{223}Ra free in circulation across each study was averaged for three timepoints as well as the upper and lower limits. As a degree of uncertainty was associated between individuals of each study and between studies, the error following ^{223}Ra absorbed blood dose for this model was estimated to be as high as 50%.

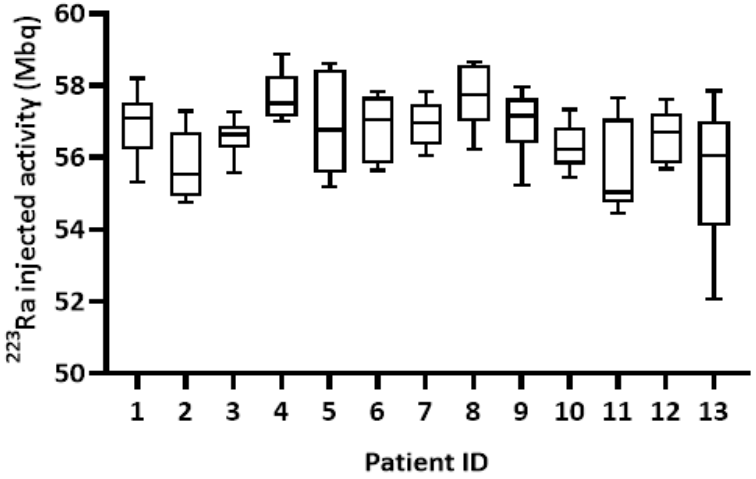

Figure 4.11 ^{223}Ra average administered activity.

The injected activity at each cycle point was collected for 6 cycles, with the exception of Patient-4 where five cycles were available. A total of 13 patients were analysed. Upper and lower limits estimated for each patient treatment administration.

The reported mean absorbed blood dose for each patient can be seen in Table 4.11, with the average dose per cycle estimated as 0.012 ± 0.002 Gy. As per injected activity, the corresponding mean blood dose was found to vary between patients, however this was not found to be significant ($P \geq 0.057$). No statistical difference was observed between patients absorbed blood dose ($P = 0.097$). The absorbed blood dose values presented here are representative of one cycle of ^{223}Ra, as the treatment regime includes a total of 6 cycles, the cumulative blood dose by the end of treatment may be in the region 0.072 Gy.

	Absorbed blood dose (Gy)		
Patient ID	Mean	Upper Limit	lower limit
1	0.012	0.016	0.006
2	0.011	0.016	0.006
3	0.012	0.016	0.006
4	0.012	0.016	0.006
5	0.012	0.016	0.006
6	0.012	0.016	0.006
7	0.012	0.016	0.006
8	0.012	0.016	0.006
9	0.012	0.016	0.006
10	0.012	0.016	0.006
11	0.011	0.016	0.006
12	0.012	0.016	0.006
13	0.011	0.016	0.006

Table 4.11. Total ^{223}Ra expected blood dose.

The mean dose represents the average absorbed dose delivered to the blood per cycle for 13 patients. The error bars shown are upper and lower ranges included from published studies as per method section 2.7.1. The estimated error for the mean dose was in the region of 50%.

4.2.1.2 IMRT blood dose estimation

As IMRT exposure is not internalised like ^{223}Ra, the exposure of the patient was instead during beam on times only. IMRT employs conformal beams to accurately target a designated area minimising exposure to non-target organs/tissues. Unlike ^{223}Ra, this treatment is tailored to the disease burden of each patient with the number of fractions, dose and area covered dependent on patient specific information. The IMRT absorbed blood dose was estimated using two existing models previously implemented by Moquet *et al.* (2018 (325)) in the RTGene study as summarised in methods 2.7.3. The study by Moquet *et al.* (2018 (325)) included patients with a variety of different cancers and radiotherapy treatment regimes including three PC patients. The treatment to PC patients included the primary tumour site only (prostate) with a total of 60 Gy administered in 2 Gy fractions. The model did not include PC patients also receiving concomitant boost to the lymph nodes. The blood dosimetry models presented were found to be consistent with the traditional dicentric assay and therefore provide a suitable model to apply to our study (325). To assess the exposure of the circulatory system, it was necessary to consider patient specific differences in both the anatomical sense and disease progression wise. The individual patient data can be seen summarised in Table 4.22, including the planned doses, target volume size and estimated body volume (derived as per methods 2.7.3).

The two models reported by Moquet *et al.* (2018) were implemented for IMRT absorbed dose estimation. The first model was based on the time taken for blood to flow through the planned treatment area as seen in Figure 4.22. The model was here termed blood flow model (BF). The BF model proposed originally by Moquet *et al.* (2018) assumed that whole blood volume was constant between patients and was approximated to 6 L and that the exposure of the whole blood volume was of 1-minute. As individual patient weights were available for our study, it is possible to estimate the blood volume more accurately. The blood volume was estimated assuming each kg of body weight contained 75 ml of blood (390), this model variant here termed BF_1. The BF_1 model included the absorbed blood dose estimation of the high dose regions of the CT plan, including the prostate and lymph node area. Applying the method described in section 2.7.3.1, the cumulative dose per patient was calculated and reported here in Table 4.2.

			Prostate			Lymph nodes		
ID	Body Volume (cm^3)	N Fractions	Target volume (cm^3)	Total dose (Gy)	Dose/fraction (Gy)	Target volume (cm^3)	Total dose (Gy)	Dose/fraction (Gy)
1	119208	37	169.9	74.3	2.009	719.9	61.5	1.662
2	100525	37	155.1	74.1	2.004	750.1	61.5	1.662
3	83000	37	125.5	74.5	2.014	649.5	61.4	1.660
4	85426	30	158.7	74.1	2.469	745.0	61.0	2.032
5	85297	35	182.1	69.6	1.989	844.1	55.9	1.597
6	92208	37	142.7	74.4	2.009	777.1	61.3	1.658
7	100990	37	124.0	74.2	2.006	686.9	61.2	1.654
8	75258	37	92.5	73.9	1.998	427.3	61.3	1.657
9	86604	37	157.7	74.3	2.008	676.1	53.0	1.431
10	87505	37	185.1	74.2	2.007	689.9	60.9	1.646
11	73386	37	119.5	74.0	2.001	639.3	60.5	1.635
12	104059	37	93.5	74.2	2.006	649.1	60.6	1.638
13	85624	35	134.2	70.6	2.018	723.9	50.6	1.446

Table 4.22. Individual patient IMRT treatment plan. The target volumes, dose delivered and N of fractions were supplied from ADRRAD clinical trial team for 13 patients. The body volume estimated as per method 2.7.3 and the dose per fraction calculated utilizing the Total dose/ N fractions.

The cumulative prostate only dose (30-37 fractions) was found to be in the range of 0.880-1.962 Gy, this comparable to the dose published by the Moquet *et al.* (2018 (325)) study of 0.38-1.92 Gy. However, the current model attributed a dose of 6.27 – 8.09 Gy to lymph node exposure. The original model proposed by Moquet *et al.* 2018, did not consider the dose to lymph nodes. To account for the differences in dynamic flow, a second model variant was proposed estimating the static fluid exposed within the lymph nodes (BF_2).

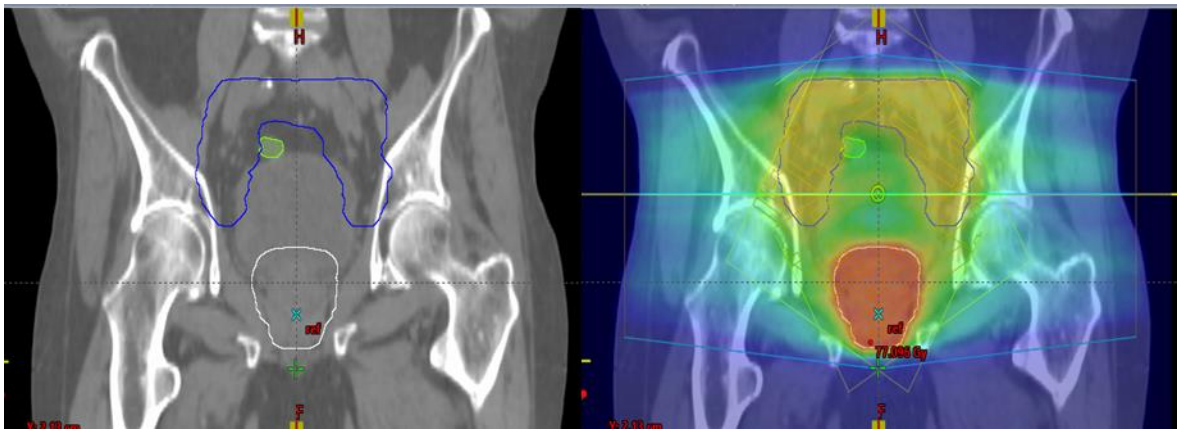

Figure 4.22. CT plan of pelvic region for IMRT targeting.

Left panel includes high dose volume to organs including prostate in white outline and lymph nodes outlined in blue. Right panel including CT plan with high dose volumes prostate in red and lymph nodes in yellow along with low dose volumes in green surrounding.

The blood flow within the prostate has previously been estimated by Inaba (1992(391)) ranging from 7.8-39.7 ml per 100 g with a lower blood flow estimated for healthy individuals compared to PC patients. The size of the prostate has been found to increase with age in both healthy individuals and more so in those with PC (392), the prostate enlargement will in turn be associated with an increased blood flow within the organ. The average prostate weight ranges from 7-16 g for healthy individuals and for PC patients 46.2-60.2 g depending on disease burden (393, 394). Using 23.75 ml/100 g as median value, the prostate blood flow per minute was estimated to range between 1.7-3.8 ml for a healthy individual and 11-14.3 ml for PC patients. In our study, the prostate weight was not available, therefore the blood volume was instead estimated from the known planned area for prostate targeting. A scaling factor between whole body volume and prostate volume, both identified via CT scan

for dose planning, was used as per method section 2.7.3.1. The resulting scaling factor was then applied to scale the whole-body blood volume in respect to prostate. The prostate blood volume was found to be between 7-14 ml depending on patient, this sitting comfortably within the expected ranges described by Inaba (1992 (391)). The same approach was carried out for lymph nodes with the estimated blood volume ranging 32.4-52.3 ml. The total blood dose by high dose volume was estimated for all patients by the end of the IMRT schedule and found to range between 0.004-0.015 Gy per fraction as seen in Table 4.3.

The studies on prostatic blood flow presented here, suggest the blood flow to the prostate to be less than the whole blood volume circulating the prostate per minute and as suggested by Moquet *et al.* 2018, this presents a large uncertainty in the model. The second model, BF_2, was estimated by similar principle as 75 ml are estimated per kg of body weight. This was used to calculate the whole body blood volume and scaled down to prostate size. However, the dose estimated for the prostate in BF_2 was representative of a static volume of blood being exposed to IMRT and would not represent an accurate flow model for dose estimation. With more detailed information regarding beam on times, it may be possible to improve this model.

Published literature suggests the beam on times to be ≥3 minutes for prostate treatment depending on high dose volume (375, 376), therefore the prostate dose for BF_2 may exceed 0.900-2.340 Gy. In the first model, BF_1, lymph nodes were treated similarly to the prostate and this itself is unlikely to be a good model for the organ. Lymph nodes do not circulate blood and instead circulate lymph fluid and due to the dynamics of fluid shift, 4 L are usually redistributed through the day (395). A mechanical shifting also plays an essential part in the movement of lymph; during IMRT administration, the patient was maintained in a still position, therefore the movement of lymph was likely to be minimal. With this being considered, the BF_2 model may be a more accurate representation of static PBL irradiation in this tissue that may then be filtered to the circulatory system. Combining the two models, cumulative absorbed blood dose by 95% high dose volume sits between 1.131 – 2.717 Gy. This included the prostate volume calculated as per BF_1 and the static volume of fluid within lymph nodes at time of exposure as per BF_2. However, these models do not consider the low

dose regions that are also exposed during treatment; therefore, both will be underestimating the total blood dose.

				BF_1			BF_2	$BF_{1P} + BF_{2LN}$
Patient ID	V_B body (ml)	V_B prostate (ml)	V_B LN (ml)	Prostate D_B (Gy)	LN D_B (Gy)	Total dose D_B (Gy)	LN D_B (Gy)	Total dose D_B (Gy)
1	9030	12.9	54.5	0.038	0.132	0.170	0.007	0.045
2	7615	11.7	56.8	0.041	0.164	0.205	0.010	0.050
3	6288	9.5	49.2	0.040	0.171	0.212	0.009	0.049
4	6560	12.2	57.2	0.060	0.231	0.291	0.014	0.073
5	6461	13.8	63.9	0.056	0.209	0.265	0.015	0.071
6	6985	10.8	58.9	0.041	0.184	0.225	0.011	0.052
7	7650	9.4	52.0	0.033	0.149	0.181	0.008	0.040
8	5700	7.0	32.4	0.032	0.124	0.157	0.004	0.037
9	6290	11.5	49.1	0.050	0.154	0.204	0.007	0.058
10	6629	14.0	52.3	0.056	0.171	0.227	0.009	0.065
11	5559	9.1	48.4	0.043	0.188	0.231	0.009	0.052
12	7883	7.1	49.2	0.024	0.135	0.159	0.007	0.031
13	6486	10.2	54.8	0.042	0.161	0.203	0.009	0.051

Table 4.33. BF_1 absorbed blood dose estimate.

The data was collected for 13 patients. V_B blood volume, D_B blood dose per fraction. BF_1 model considering prostate only (BF_{1p}), BF_2 model considering lymph nodes (LN) dose (BF_{2LN}). Reported estimated uncertainty of 25% for all BF model variants.

The second model for blood dose estimation described by Moquet *et al.* (2018 (325)) was carried out applying the CT plan volume along with the planned doses. The model was here termed CTPV to reflect the use of the CT plan volume. With this approach, it was possible to estimate the total absorbed blood dose including that from low dose volumes. For the IMRT

administration, a CT plan was made by the clinical team with the prostate and lymph nodes areas denoted for irradiation. Due to organ shift, an extra area around these was added to account for the movement, this resulting in larger area comprised of 95% high dose regions and low dose regions as depicted in Figure 4.2.

Two variants of the CTPV model were made, the first, $CTPV_1$, applies a scaling factor between whole CT scan volume and body volume. In the original publication, Moquet *et al.* (2018 (325)) suggested this value to be 2.5 as patient specific measures were not available. In our study, patient specific data was available, therefore the scaling factor was calculated for each patient. The scaling factor was found to be between 2.08-2.64 depending on patient weight, with the largest deviation from the scaling factor for Patient-10 being of 16% smaller than the published 2.5 scaling factor by Moquet *et al.* (2018 (325)). The total dose delivered during IMRT treatment can be seen in Table 4.4. The dose was found to be considerably larger than that published by Moquet *et al.* (325). The increase in dose was likely a reflection on large lymph node volume being irradiated. The second variant of the model, $CTPV_2$, was devised to take in to account the high dose regions of prostate and lymph nodes rending a comparison between the BF and CTPV models possible. To do so, a scaling factor for each component as per BF_2 was employed as outlined in methods 2.7.4.2. The resulting dose for $CTPV_2$ was found to be comparable to that of BF_2 within the uncertainty estimates. BF_1 and $CTPV_1$ cannot be directly compared as they employ different irradiation volumes, BF_1 appears to significantly overestimate the lymph node dose and as highlighted by the author, the method also has the largest uncertainty associated. For the dose estimations to follow, $CTPV_1$ and $CTPV_2$ were therefore utilized.

ID	CT scan volume (cm_3)	Scaling factor	Total blood dose (Gy)	
			$CTPV_1$	$CTPV_2$
1	29098	2.52	3.877	0.477
2	49399	2.11	3.834	0.573
3	34749	2.46	3.723	0.593
4	52081	2.29	3.397	0.669
5	40312	2.29	3.484	0.702
6	46235	2.17	4.152	0.632
7	48652	2.08	3.418	0.507
8	35113	2.36	3.513	0.439
9	31041	2.42	3.307	0.549
10	40980	2.08	4.195	0.637
11	37932	2.25	3.981	0.648
12	32753	2.64	3.464	0.445
13	39694	2.20	3.088	0.538

Table 4.44. IMRT absorbed blood dose estimates.

Whole CT plan area CTPV1 and high dose regions only $CTPV_2$. Scaling factor estimated from patient body volume derived from average weight during treatment. Patient numbers n=13 patients for whom treatment plan and patient specific data were available. Uncertainties estimated up to 6% for both CTPV models.

4.2.2 Utilizing cytogenetic markers of IR exposure for dose estimation

4.2.2.1 Evaluating the accuracy of dicentric chromosomes scored by M-FISH

The dicentric assay has long been the gold standard for biodosimetric estimations after exposure to a known source. The assay traditionally uses Giemsa staining where chromosomes are evenly stained in one colour, as per Figure 4.3. Solid stain (S.S.) Giemsa analysis enables the detection of structural rearrangements altering the normal

chromosome morphology. This enables the identification of chromosomes containing more than one centromere along with any associated acentric fragment.

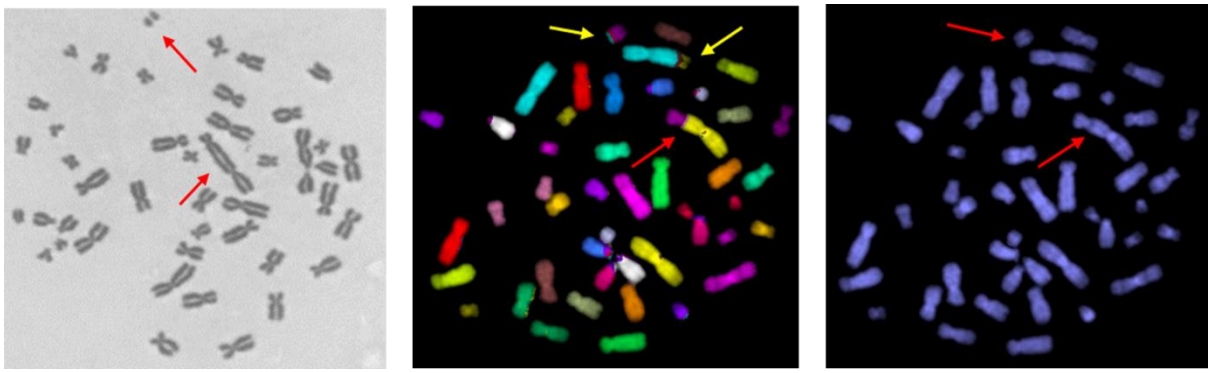

Figure 4.33. Dicentric chromosome identification.

In the right panel, a 1st division PBL imaged under bright field microscopy x100 magnification under oil. The middle panel shows a complex chromosomal rearrangement between 3 chromosomes as per yellow and red arrows. As highlighted by red arrow a chromosome within this rearrangement contains 2 centromeres. To the right a DAPI stained view of the same middle cell, highlighted by red arrows are the dicentric chromosome with acentric fragment. Images collected at x63 magnification under oil, pseudo-colours assigned utilizing MetaSystems ISIS software imaging system.

For dose assessment, dicentric chromosome frequencies were collected as outlined in Methods 2.6. from M-FISH painted metaphase cells instead of the traditional Giemsa staining. During M-FISH, the chromosomes are hybridized with a probe set specific for 22 homologue chromosomes and 2 sex chromosomes, each labelled with 5 spectrally distinct fluorophores, Figure 2.66. The combination of fluorophores results in computer generated unique pseudo colours for each homologue pair, along with whole chromosome staining with fluorescent DAPI. M-FISH provides further detail on the complexity of the rearrangement, dicentric chromosomes may be detected as part of a larger complex event. Cells containing unstable complex chromosomal events with chromosomes found to contain more than 1 centromere were further broken down in to their dicentric component events. The collation of the two dicentric populations (derived from simple and complex exchanges)

was termed as “dicentric equivalents” for the purpose of this analysis and this is comparable to the dicentric frequencies collected in other studies.

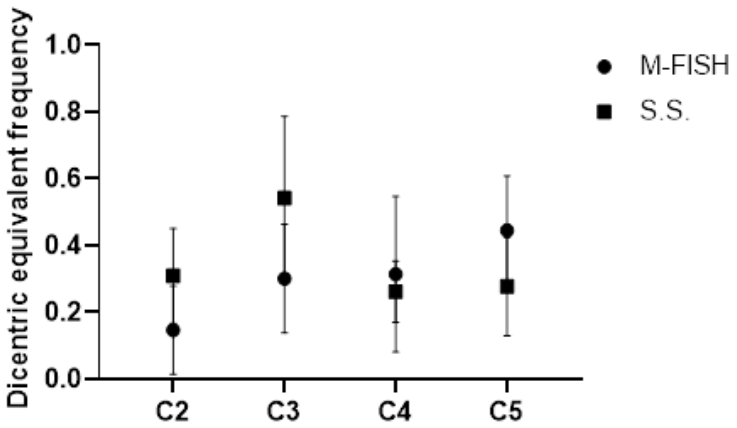

Figure 4.44. Validating the yields of dicentric equivalents scored via M-FISH.

The total dicentric frequency was plotted for Patient-1. Filled squares S.S. with n = 78 C2, n = 50 C3, N = 188 C4, N = 87 C6. M-FISH data for Patient-1 also plotted with the number of cells scored reported in Table 4.4. 95% confidence intervals included as error bars.

As M-FISH staining does not have specific centromeric staining, it has been suggested that the M-FISH technique is less accurate than traditional S.S. Giemsa staining. This due to the lack of pancentromeric probe resulting in misclassification of some dicentric chromosomes as translocations and *vice versa* (396, 397). To compare whether the two techniques yielded similar dicentric equivalent frequencies between C1 and C5, Patient-1 treatment cycles were stained for both S.S. and M-FISH, the total number of cells scored via M-FISH technique can be seen in Figure 4.44. All samples displayed some differences with C4 being the most consistent between techniques. These variations were attributed to different slides being used from the same preparations and differences in sample size. Overall, there were no statistical differences between cycle sampled and respective technique (P = 0.0878 one-way ANOVA , Tuckey’s multiple comparisons test), Table 4.55. As no statistical difference was found between techniques, the frequency of dicentric equivalents was collected via M-FISH technique for further patients.

As per Table 4.5 the frequency of dicentric equivalents was found to increase with cycle with a peak at C4 of 0.395 ± 0.052. Simple dicentric frequency was found increasing between C2 and C3 with a plateau after mixed radiotherapy completion. The frequency of dicentrics from complex is instead found to increase further in C4 ^{223}Ra only cycle. The increase in frequency potentially reflecting a dose response relationship between mixed radiotherapy treatments and ^{223}Ra only cycle.

			Simple dicentric events		Dicentric from complex events		Total Dicentric Equivalents	
Cycle	ID	Cells scored	N	Frequency ± SEM	N	Frequency ± SEM	N	Frequency ± SEM
2	1	55	8	0.146 ± 0.066	0	-	8	0.145 ± 0.066
	3	101	10	0.099 ± 0.033	6	0.059 ± 0.059	16	0.158 ± 0.067
	3	104	13	0.125 ± 0.035	8	0.077 ± 0.026	21	0.202 ± 0.048
	Total	260	31	0.119 ± 0.024	14	0.054 ± 0.025	45	0.173 ± 0.035
3	1	100	15	0.150 ± 0.0440	15	0.150 ± 0.069	30	0.30 ± 0.0820
	2	101	15	0.149 ± 0.038	23	0.228 ± 0.064	38	0.376 ± 0.076
	4	101	23	0.228 ± 0.052	22	0.218 ± 0.099	45	0.446 ± 0.111
	5	105	33	0.314 ± 0.056	12	0.114 ± 0.037	45	0.429 ± 0.065
	Total	407	86	0.211 ± 0.024	72	0.177 ± 0.035	158	0.388 ± 0.042
4	1	48	5	0.104 ± 0.045	10	0.208 ± 0.084	15	0.313 ± 0.099
	2	102	27	0.265 ± 0.059	26	0.255 ± 0.072	53	0.520 ± 0.062
	3	103	17	0.165 ± 0.044	15	0.146 ± 0.047	32	0.311 ± 0.116
	Total	253	49	0.194 ± 0.031	51	0.202 ± 0.038	100	0.395 ± 0.052
5	1	106	22	0.208 ± 0.051	25	0.236 ± 0.061	47	0.443 ± 0.083
	4	101	17	0.168 ± 0.042	18	0.178 ± 0.067	35	0.347 ± 0.084
	5	102	16	0.157 ± 0.041	2	0.020 ± 0.0140	18	0.176 ± 0.043
	Total	309	55	0.179 ± 0.026	45	0.146 ± 0.031	100	0.324 ± 0.042

Table 4.55. Dicentric equivalents frequencies per treatment cycle by M-FISH.

The number (N) and frequency of simple dicentrics, dicentric from deconstructed complex exchanges and total dicentric equivalents is shown. A total of five patients were analysed. Standard error of the mean (SEM) included per cycle collation.

4.2.3 Absorbed blood dose estimation by biodosimetry approach

Calibration curves for ^{223}Ra were chosen based on the energy of the α-particle of Plutonium isotopes as no previous calibration curve has been designed or published for ^{223}Ra. Two calibration curves were selected, the first being by Purrott 1980 of ^{239}Pu with an energy of 5.16 MeV per α-particle (328, 398). The exposure conditions of ^{239}Pu used by Purrott mimics that of ^{223}Ra as the radioisotope was mixed with whole blood with PBLs being cultured after. The second calibration curve by Curwen *et al.* 2012 instead uniformly exposes isolated PBLs plated on mylar layer with 3.26 MeV α-particles (LET 121 keV/µm) originating from a ^{238}Pu source with an initial energy of 5.50 MeV (239, 399). For comparison, the dicentric equivalent frequencies were used to estimate a ^{223}Ra absorbed dose assuming all dose was attributed solely to ^{223}Ra.

As the dicentric equivalent frequency increases with cycle time, so do the dose estimates for ^{223}Ra as seen in Table 4.66. The highest estimated dose for ^{223}Ra was 1.498 ± 0.150 Gy with the Curwen *et al.* 2012 calibration curve at C4, while a dose of 1.064 ± 0.109 Gy was estimated when the Purrott 1980 curve was applied. Although both calibration curves by Purrott and Curwen *et al.* yielded similar result at dose estimates up to 1 Gy, it was considered appropriate to utilize Purrott calibration curve for following dose estimates. The reasoning being that ^{223}Ra is administered intravenously to the blood coming in to contact randomly with all blood component cells, the calibration curve by Curwen *et al.* utilizes a monolayer of isolated PBLs essentially delivering a homogenous dose to the cells. As the dose delivered in *vivo* is likely to not be homogeneous, calibration curve by Purrott who added the radionucleotide to a blood sample containing PBL, it is also likely to reflect a more non-homogeneous exposure. The error for Curwen calibration curve was also found to be larger at doses >1 Gy, this being a result of the calibration curve maximum dose being 1 Gy while Purrott calibration curve having a maximum dose of 1.6 Gy. For IMRT exposure, the calibration curve by Lloyd 1986 was applied, this being a well-established curve, it has been utilized in many exposure scenarios for γ-ray and X-ray dose estimation by Public Heath England (327). The highest dose estimated using the Lloyds 1986 calibration curve was for C4 and estimated as 2.189 ± 0.119 Gy.

Cycle	ID	Cells	Total Dicentrics	^{223}Ra dose (Gy) Purrott	^{223}Ra dose (Gy) Curwen	IMRT dose (Gy) Lloyd
2	1	55	8	0.782 ± 0.198	0.549 ± 0.195	1.290 ± 0.246
	3	101	16	0.423 ± 0.109	0.598 ± 0.151	1.351 ± 0.182
	4	104	21	0.515 ± 0.118	0.764 ± 0.168	1.537 ± 0.180
	Total	260	45	0.463 ± 0.073	0.654 ± 0.098	1.416 ± 0.115
3	1	100	30	0.807 ± 0.150	1.125 ± 0.206	1.895 ± 0.184
	2	101	38	1.013 ± 0.167	1.426 ± 0.232	2.133 ± 0.184
	4	101	45	1.200 ± 0.181	1.689 ± 0.252	2.330 ± 0.185
	5	105	45	1.154 ± 0.174	1.625 ± 0.243	2.283 ± 0.181
	Total	407	158	1.045 ± 0.086	1.472 ± 0.118	2.168 ± 0.097
4	1	48	15	0.840 ± 0.219	1.184 ± 0.307	1.936 ± 0.264
	2	102	53	1.401 ± 0.194	1.971 ± 0.271	2.524 ± 0.184
	3	103	32	0.835 ± 0.150	1.177 ± 0.209	1.930 ± 0.182
	Total	253	100	1.064 ± 0.109	1.498 ± 0.150	2.189 ± 0.119
5	1	106	47	1.195 ± 0.176	1.681 ± 0.246	2.324 ± 0.180
	4	101	35	0.932 ± 0.160	1.313 ± 0.223	2.043 ± 0.184
	5	102	18	0.472 ± 0.115	0.667 ± 0.158	1.431 ± 0.182
	Total	309	100	0.870 ± 0.090	1.226 ± 0.123	1.972 ± 0.108

Table 4.66. Equivalent dose estimation for ^{223}Ra and IMRT.

Equivalent dose utilizing α-particle calibration curves from Purrott and Curwen *et al.* γ-ray dose utilizing calibration curve by Lloyd. Estimated dose for 5 patients between C2-C5. Dose calculated with Dose Estimate Version 5.2 and reported with standard error.

To estimate the absorbed blood dose for each component radiation, a model usually reserved for criticality scenario was used (236), this described in methods 2.7.4.2. To calculate the absorbed blood dose, the ratio between component radiation was needed. For this, the usual model requires physical dose measures as calculated in section 0, in addition to this, we propose a novel model based on the spectrum of chromosomal aberrations

sampled *in vivo*. The model was termed M-FISH$_{LET}$ as this was based on the ratio of cells presenting complex chromosomal aberrations consistent with ^{223}Ra α-particle exposure and cells presenting simple aberrations only consistent with IMRT x-ray exposure, this acting as a pseudo for the ^{223}Ra:IMRT dose ratio (Table 4.77).

Cellular classification			D_B per cycle			^{223}Ra : IMRT		
Cycle	^{223}Ra cells (f)	IMRT cells (f)	^{223}Ra (Gy)	IMRT $CTPV_1$ (Gy)	IMRT $CTPV_2$ (Gy)	$CTPV_1$	$CTPV_2$	M-$FISH_{LET}$
C2	0.050 ± 0.014	0.204 ± 0.025	0.012 ± 0.002	2.021 ± 0.050	0.318 ± 0.017	1:174	1:27	1:4
C3	0.150 ± 0.018	0.243 ± 0.021	0.023 ± 0.003	3.739 ± 0.092	0.587 ± 0.031	1:161	1:25	2:3
C4	0.198 ± 0.025	0.229 ± 0.026	0.035 ± 0.003	3.739 ± 0.092	0.587 ± 0.031	1:108	1:17	1:1
C5	0.162 ± 0.021	0.220 ± 0.024	0.046 ± 0.004	3.739 ± 0.092	0.587 ± 0.031	1:81	1:13	3:4

Table 4.77. Absorbed blood dose ratio per cycle.

The ratio was calculated utilizing the cumulative dose per cycle respective to the previously received IMRT blood dose per fractions and ^{223}Ra blood dose per injection. M-$FISH_{LET}$ (^{223}Ra cells : IMRT cells), $CTPV_1$ (^{223}Ra (Gy) : IMRT $CTPV_1$ (Gy)) and $CTPV_2$ (^{223}Ra (Gy) : IMRT $CTPV_2$ (Gy)). Physical dose estimates were based on data available for N = 10 patients, M-FISH cellular frequencies for N = 5 patients. Standard error of the mean included for frequencies and physical dose estimates.

The absorbed blood dose ratios were estimated for C2-C5, this was equivalent to four intravenous injections of ^{223}Ra and completed IMRT schedule of 37 fractions by C5. For the physical dose ratio, this was based on the average absorbed blood dose per fraction across all thirteen patients for both the IMRT and ^{223}Ra dose. The M-FISH$_{LET}$ ratios described in section 2.3.1, was obtained from blood samples received from five patients with a minimum of three patient samples analysed per cycle. The absorbed blood dose ratios for all models can be seen in Table 4.7.

Applying these blood dose ratios to the dicentric assay, the absorbed blood dose was estimated in three ways (Table 4.8). The CTPV methods were derived from the physical absorbed blood dose estimates as per method section 2.1. CTPV$_1$ estimated the absorbed blood dose across the planned volume including both high and low dose volumes whilst CTPV$_2$ including the high dose regions only. The M-FISH$_{LET}$ absorbed blood dose was instead estimated from the ratio of cells consistent with high LET exposure (^{223}Ra) and low LET exposure (IMRT). The CTPV derived ratios assume all IMRT induced aberrations at C3 are conserved in following C4 and C5. While for the ^{223}Ra, the aberrations follow an increasing pattern through treatment. This resulting in a plateau in dose for CTPV$_1$ as the resulting ratio is based on a large IMRT dose with a small ^{223}Ra dose. For CTPV$_2$, as the model is based on high dose regions areas the IMRT, the estimated dose was lower than CTPV$_1$, therefore when expressed as a ratio with ^{223}Ra this assumed a significant proportion of dose to be ^{223}Ra attributed, this resulting in a decrease in measured dose for C4 and C5. The M-FISH model is instead based off *in vivo* observations and the ratio was directly affected by cellular activities.

The absorbed blood dose estimates from the CTPV models suggest the dose after 20 IMRT fractions, measured at C2 (Table 4.8), was between 1.327 ± 0.115 Gy and 1.395 ± 0.115 Gy. The M-FISH$_{LET}$ method was found to be in similar range at 0.956 ± 0.114 Gy at C2. The IMRT absorbed blood dose after the end of fractionation (C3 assuming 37 completed fractions) was estimated for CTPV$_1$ as 2.148 ± 0.096 Gy and 2.073 ± 0.096 Gy for CTPV$_2$, with M-FISH$_{LET}$ blood dose estimates of 1.167 ± 0.092 Gy.

Cycle	Patient ID	Cells scored	Dicentric equivalents (yield ± SE)		$CTPV_1$		$CTPV_2$		$M\text{-}FISH_{LET}$	
					^{223}Ra	IMRT	^{223}Ra	IMRT	^{223}Ra	IMRT
2	1	55	8	(0.145 ± 0.066)	0.007 ± 0.033	1.268 ± 0.246	0.044 ± 0.054	1.201 ± 0.246	0.207 ± 0.105	0.845 ± 0.245
	3	101	16	(0.158 ± 0.067)	0.008 ± 0.029	1.329 ± 0.182	0.046 ± 0.043	1.261 ± 0.182	0.221 ± 0.081	0.899 ± 0.181
	4	104	21	(0.202 ± 0.048)	0.009 ± 0.029	1.516 ± 0.180	0.053 ± 0.045	1.448 ± 0.180	0.263 ± 0.086	1.070 ± 0.179
	Total	260	45	(0.173 ± 0.035)	0.008 ± 0.025	1.395 ± 0.115	0.048 ± 0.032	1.327 ± 0.115	0.235 ± 0.055	0.959 ± 0.114
3	1	100	30	(0.30 ± 0.0820)	0.012 ± 0.031	1.874 ± 0.184	0.071 ± 0.051	1.799 ± 0.184	0.584 ± 0.128	0.947 ± 0.182
	2	101	38	(0.376 ± 0.076)	0.013 ± 0.031	2.113 ± 0.184	0.080 ± 0.053	2.038 ± 0.184	0.701 ± 0.139	1.138 ± 0.182
	4	101	45	(0.446 ± 0.111)	0.014 ± 0.032	2.310 ± 0.185	0.088 ± 0.055	2.234 ± 0.184	0.801 ± 0.149	1.300 ± 0.182
	5	105	45	(0.429 ± 0.065)	0.014 ± 0.031	2.264 ± 0.181	0.086 ± 0.053	2.188 ± 0.181	0.777 ± 0.144	1.261 ± 0.179
	Total	407	158	(0.388 ± 0.042)	0.013 ± 0.025	2.148 ± 0.096	0.082 ± 0.033	2.073 ± 0.096	0.719 ± 0.073	1.167 ± 0.092
4	1	48	15	(0.313 ± 0.099)	0.018 ± 0.042	1.908 ± 0.264	0.106 ± 0.082	1.797 ± 0.264	0.680 ± 0.198	0.789 ± 0.262
	2	102	53	(0.520 ± 0.062)	0.023 ± 0.035	2.497 ± 0.184	0.141 ± 0.066	2.384 ± 0.184	1.048 ± 0.169	1.216 ± 0.181
	3	103	32	(0.311 ± 0.116)	0.018 ± 0.033	1.902 ± 0.182	0.106 ± 0.058	1.791 ± 0.182	0.677 ± 0.136	0.785 ± 0.179
	Total	253	100	(0.395 ± 0.052)	0.020 ± 0.028	2.162 ± 0.119	0.121 ± 0.043	2.050 ± 0.119	0.833 ± 0.097	0.966 ± 0.116
5	1	106	47	(0.443 ± 0.083)	0.028 ± 0.037	2.290 ± 0.180	0.169 ± 0.070	2.142 ± 0.180	0.864 ± 0.151	1.175 ± 0.178
	4	101	35	(0.347 ± 0.084)	0.025 ± 0.036	2.009 ± 0.184	0.147 ± 0.068	1.862 ± 0.183	0.705 ± 0.140	0.959 ± 0.182
	5	102	18	(0.176 ± 0.043)	0.017 ± 0.033	1.394 ± 0.182	0.099 ± 0.057	1.254 ± 0.181	0.392 ± 0.105	0.533 ± 0.180
	Total	309	100	(0.324 ± 0.042)	0.024 ± 0.027	1.937 ± 0.108	0.141 ± 0.042	1.791 ± 0.108	0.665 ± 0.080	0.905 ± 0.105

Table 4.88. Estimated blood dose per treatment cycle. Doses estimated utilizing the physically derived ratios of dose by CTPV models. Standard Error of the mean included per dose.

For the ^{223}Ra absorbed blood dose at C2, the $CTPV_1$ and $CTPV_2$ were found to be 0.008 ± 0.025 and 0.048 ± 0.032, both lower than the M-$FISH_{LET}$ estimate of 0.150 ± 0.046 Gy. For C3 the ^{223}Ra absorbed blood dose estimated from CTPV methods was between 0.013 ± 0.025 and 0.082 ± 0.033 Gy ($CTPV_1$ and $CTPV_2$ respectively) with the M-$FISH_{LET}$ absorbed blood dose estimated at 0.719 ± 0.073 Gy. By the final sample point studied here (C5), the absorbed blood dose from ^{223}Ra was estimated as 0.024 ± 0.027 Gy by $CTPV_1$ and 0.141 ± 0.042 Gy for $CTPV_2$ with the M-$FISH_{LET}$ absorbed blood dose estimate at 0.665 ± 0.080 Gy (see Figure 4.5).

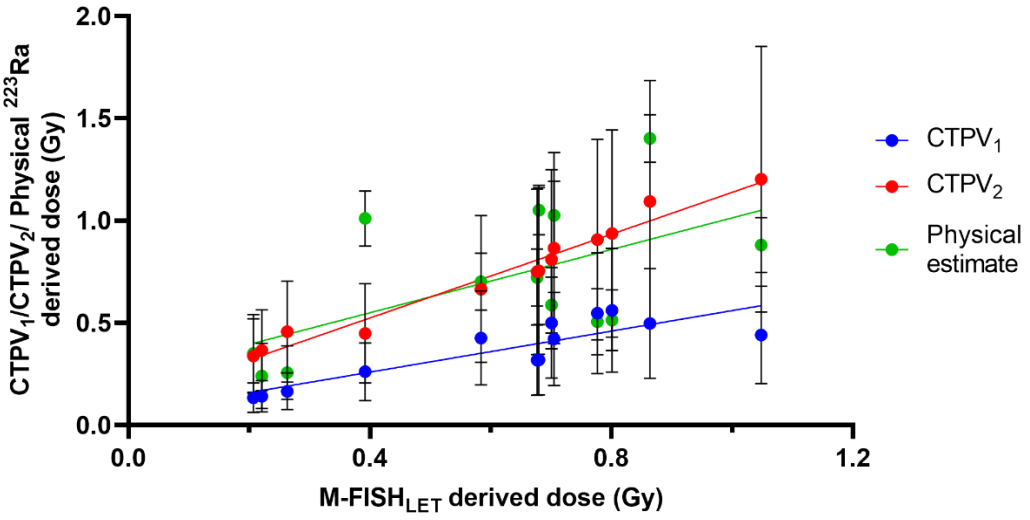

Figure 4.55. Comparison of ^{223}Ra absorbed blood dose models.

The M-$FISH_{LET}$ ratio was implemented in the dicentric assay estimates of blood dose for n = 5 patients (patients 1-5), the estimates for these patients were compared across all other models. $CTPV_1$ and $CTPV_2$ calculated from the dicentric assay utilizing the physical blood dose estimates by ^{223}Ra and respective IMRT models. Simple linear regression plotted for $CTPV_1$ Y = 0.019*X + 0.004, R^2 = 0.559 and for $CTPV_2$ Y = 0.115*X + 0.025, R^2 = 0.600. Physical ^{223}Ra dose estimated through clearance of ^{223}Ra from circulation 24 h post administration. Simple linear regression plotted for Y = 0.028*X + 0.012, R^2 = 0.301. The error associated with the physical ^{223}Ra was conservatively estimated to 50% and propagated to $CTPV^1$, $CTPV^2$. The error for M-$FISH_{LET}$ dose was propagated as 30% for C2 and 14% for C3-C5.

4.3 Discussion

The aim of this chapter was to assess whether ^{223}Ra alone could potentially expose circulating PBL to a significant dose. In the previous chapter it was found that complex chromosomal aberrations were present after mixed radiotherapy schedule was completed. This suggesting that the complex aberrations found within circulating PBLs were a result of ^{223}Ra exposure. Whether the PBLs were exposed in proximity to BM, in an organ tissue or in circulation it is currently unknown. Previous literature of both animal and human studies (78, 400-402) suggests ^{223}Ra to not accumulate in non-target soft tissue (386) and any initial uptake is cleared rapidly (152-154). As the retention in organs has been suggested to be low, the dose to PBLs in organ tissues was expected to be negligible in this scenario. The majority of complex aberrations were found to contain unstable dicentric chromosomes, therefore, it was thought unlikely for a large fraction of PBLs (during treatment cycles) to represent the progeny of exposed HSCs (giving rise to PBL containing stable transmissible aberrations). Therefore, the focus of this chapter was geared towards the exposure of PBLs in circulation that may have been exposed in transit to target bone metastatic sites.

To date, only one other study has estimated the potential absorbed blood during this localization period (363). The risk of circulatory system exposure by ^{223}Ra appears to have been overshadowed by the risk of BM exposure (315), which poses a major threat for both acute toxicity and genomic instability (potential for leukemogenesis). Indeed, the majority of dose appears to be delivered at target metastatic sites, surrounding endosteal cells and to the BM compartment (389). An emerging body of evidence has suggested low dose exposure to the circulatory system to increase the risk of many diseases including coronary heart disease (as here reviewed (403-405)). Therefore, estimating the absorbed blood dose may be important not only for evaluating the current dosing strategy but also assessing whether an increased risk following transit exposure may be plausible. In an effort to quantify the absorbed blood dose, a combination of approaches was taken. Firstly, existing clearance models were evaluated and grouped together to estimate the potential dose per cycle and by end of treatment. These ^{223}Ra physical models based on the unique pharmacokinetics of the [^{223}Ra]$RaCl_2$ whilst for the IMRT physical dose the treatment planned areas derived from CT scans.

The physically derived ^{223}Ra dose was estimated for each patient's treatment cycle as some variations between patient weight (up to 8% body weight loss by C6) were observed over the treatment course. The average absorbed blood dose was estimated as 0.012 ± 0.002 Gy per treatment cycle. This value found to be in similar range to that reported by Schumann *et al.* (2021 (363)) of 0.016 Gy within 24 h of a single intravenous administration, this estimated by Y-H2AX dose reconstruction. Another study with ^{224}Ra isotope by Stephan *et al.* (2005 (406) for the treatment of ankylosing spondylitis, reported an estimated absorbed blood dose of 0.047 Gy, this following ICRP 67 model. The patients received an administered activity of 1 MBq per fraction per week over 10 weeks. In this study the dicentric assay was used and the *in vitro* calibration curve implemented by Schmid *et al.* (1996 (407)) ^{241}Am α-particles. The main source of uncertainty when estimating the physically derived ^{223}Ra absorbed blood dose was the error associated with the clearance models used. These varied by up to 50% reflecting large errors associated with interindividual variation. Although all studies selected were in agreeance that ≤1% of ^{223}Ra activity remained in the blood after 24 h. The main limitation for Schumann *et al.* (2021 (363)) was the clearance kinetics of ^{223}Ra. Although Schumann *et al.* periodically sampled the remaining activity in the blood of each patient, the activity remaining in the blood was limited by the low number of sampling points and the low activity concentrations in the blood. No attempt was made by Schumann *et al.* to quantify the errors associated with this other than reporting interindividual variation as large. Both Schumann *et al.* (2021 (363)) and Stephan *et al.* (2005 (406)) also had a small sample size of nine and six patients respectively. As per this study, five patients were followed by M-FISH technique, a key limitation was indeed this small sample size. Increasing the analysis to more patients may increase the reliability of the ^{223}Ra dose estimations. As seen in the dicentric equivalent frequencies in C5, Patient-5 had a decreased frequency of dicentric equivalents compared to the other patients. In this study, the dose estimation was followed across five treatment cycles, this reflective of 20 weeks of treatment. Unlike the study by Schumann *et al.* (2021 (363)) whereby only one administration was followed, further uncertainties remain as to whether the clearance of ^{223}Ra was consistent across the treatment. With reduced clearance efficacy this could result in a higher absorbed blood dose in later treatment cycles. Nevertheless, these estimates of ^{223}Ra absorbed blood dose are comparable with both studies considering the high error associated of 50%.

The IMRT dose was estimated from the proposed models by Moquet *et al.* (2018 (325)) These models based on the CT plan area which, unlike ^{223}Ra, was tailored to the disease burden of each patient with the number of fractions, dose and area covered dependent upon patient specific information (Supplementary Table 3). The BF_1 model applied flow dynamics within the 95% high dose region and assumed volume of 6 L passing through this area in 1 minute of IMRT exposure. As patient data was available in our study, the blood volume was estimated from the measured patient weight. This model was found to fit well for the prostate area volume and as patient specific data was available, it was possible to estimate a blood volume for each patient reducing the 20% uncertainty reported by Moquet *et al.* (2018 (325)). The BF_1 model was however, found to not be suited for lymph node areas as the flow of lymph fluid differs from that of blood. Lymph nodes are in proximity of vascularized tissue, they do not circulate blood, instead they circulate lymph fluid. Approximately ~4 L shift through the lymph nodes per day (395), during IMRT the patient is not mobile therefore any fluid shift was assumed to be negligible during treatment. The lymph node absorbed blood dose per fraction was estimated to range between 0.004-0.015 Gy, this equivalent to 0.152-0.508 Gy by IMRT completion depending on patient. The combination of prostate dose from the BF_1 model and lymph node dose from BF_2, may together be a reasonable estimate of absorbed blood dose for high dose regions. Together the absorbed blood dose was estimated between 1.131-2.470 Gy following completion of personalised IMRT schedules. The uncertainty for the BF model for high dose volume was estimated to be 2-3% as reported by Moquet *et al.* 2018. To further this model, the beam on times during the IMRT administration could be used to reduce the uncertainty. However, the low dose region was not considered in either BF model variant, therefore, both will underestimate the total absorbed blood dose.

The CTPV model was thought to be the most representative, as not only prostate and lymph nodes are exposed during IMRT but also a large area received low dose exposed. The CTPV model enabled the estimation of absorbed blood dose from the whole CT planned area including the low dose region. For comparison to the BF mode,l a second variant of this model was made here termed $CTPV_2$ (also with high dose regions only). The average absorbed blood dose per fraction was estimated as 0.101 Gy for $CTPV_1$ and 0.016 Gy for $CTPV_2$. The estimated uncertainty from the CTPV were considered to be lower than BF

model at 6%. The uncertainty including minimal planned volume error between 1-1.5% variation and the error during dose delivery to mapped regions to be less than 3%. The 3% estimate based on the published estimates of the upper bound of inter-treatment dosimetric uncertainty (408) with larger variation detected by treatment QA triggering re-planning and re-validation. The whole body volume applied for the estimates was derived from the individual patients weight, it was assumed that 1.01 g of human body mass fits within 1 cm^3 and that the tissue density within the target volume was consistent with this for the scaling factor estimation. The error attributed to whole body volume estimates were considered within an error of 1%. The propagation of errors considered here resulted in the reported 6% total error.

The physically derived models were expressed as a dose ratio and applied to the IAEA model usually reserved for a criticality scenario. This model originally designed to separate and quantify neutron and gamma exposures following inadvertent exposure (236). In doing so, biodosymetric dose estimates were derived from the use of the dicentric assay. The dicentric equivalent frequencies were collected from simple dicentric exchanges and from the breakdown of complex chromosomal exchanges. Some doubts have been raised following dicentric chromosome detection by M-FISH, for our study no significant difference was observed between S.S. Giemsa and FISH probe painting. The reasoning being that DAPI channel was used for evaluating the number of centromeres present per chromosome rather than visualising the chromosome under fluorescent probe only. The calibration curve selected for IMRT absorbed blood dose estimation was that from Lloyd 1986 publication where whole blood was irradiated *in vitro* utilizing a ^{60}Co source with dose range of 0-5 Gy. The dicentric yield was entered into Dose Estimate V5.2 (329) with the following coefficients $\alpha = 0.0756 \pm 0.0031$, $\beta = 0.0149 \pm 0.0060$ and $C = 0.0004 \pm 0.0009$ (327). This being a well-established calibration curve utilized in many exposure scenarios for γ-ray and X-ray dose estimation by Public Heath England and was judged to be the most comparable curve in terms of type and energy of radiation exposure. As there is currently no ^{223}Ra calibration data, a calibration curve which emits α-particles of a similar energy to ^{223}Ra was selected. ^{239}Pu has a comparable energy of 5.16 MeV per α-particle. The curve coefficients were: $\beta = 0.3696 \pm 0.0322$, $C = 0.0019 \pm 0.0126$ (328) and was established by irradiating whole blood with ^{239}Pu in the range of 0-1.6 Gy.

In cases where an individual is exposed to an unknown source, the pattern of aberrations found in PBL could be indicative of whether the expose is of high or low LET. *In vitro* studies have shown the efficacy of M-FISH technique to discriminate between population of cells exposed to varying LET, this demonstrated by the concept of the C-ratio previously described. M-FISH technique enables the distinction between aberrations consistent with high LET exposure and those consistent with low LET exposure. Employing complex aberrations as a marker of high LET exposure, it is possible to subdivide the cells containing these aberrations as cells exposed to ^{223}Ra. While cells not containing simple aberrations were instead likely to have been exposed to IMRT. As simple aberrations are mainly a product of low LET exposure at doses ≤ 2Gy and the IMRT treatment was administered in 2 Gy fractions, all cells containing simple aberrations were assumed to be of IMRT origin. As per Chapter 3, the likelihood of a PBL cells being exposed to multiple fractions *in vivo* was considered to be low. These assumptions enabled the generation of an *in vivo* dose ratio (M-FISH$_{LET}$) for subsequential absorbed dose estimation.

The CTPV derived ratios assume that IMRT induced aberrations accumulated in the circulatory blood pool by C3 are not cleared from the peripheral pool in the following C4 and C5 treatment cycles and similarly for the ^{223}Ra, it was assumed the aberrations accumulate through treatment with no clearance. This results in a plateau of IMRT dose for CTPV$_1$ as the dose ratio was based on a large IMRT component with a small ^{223}Ra dose. For CTPV$_2$, as the model was based on high dose regions areas, the IMRT estimated dose was lower than CTPV$_1$, therefore when expressed as a ratio with ^{223}Ra, this assumes a higher proportion of absorbed blood dose to be attributed to ^{223}Ra, which decreases the estimated dose for C4 and C5. The dicentric assay was estimated from the ratio of physical ^{223}Ra and CTPV dose estimates with a conservative error of 50% being attributed to the ^{223}Ra dose, this was considered to be the largest uncertainty.

The M-FISH$_{LET}$ model was based on the chromosomal aberration spectrum in PBL sampled 4 weeks after each ^{223}Ra administration. Following IMRT completion, the dose was estimated at 1.167 ± 0.092 Gy. This was based on the assumption that all IMRT induced aberrations would be of simple type while ^{223}Ra aberrations were of complex type. As a larger proportion of cells containing complex aberrations than simple chromosomal aberrations was observed, this was reflected in the dose ratio. Accordingly, the dose attributed to ^{223}Ra

was proportionally larger than that attributed to IMRT. The resulting IMRT absorbed blood dose estimated by M-FISH$_{LET}$ was therefore lower than both CTPV dose estimates. The physically derived ^{223}Ra estimates were representative of the period taken for ^{223}Ra to clear from the blood within a 24 h period. Due to the sampling schedule being every 4 weeks, it cannot be excluded that absorbed dose from ^{223}Ra was also received by circulating PBLs in the vicinity of metastatic sites, especially as metastatic sites tend to be highly vascularized (409-411). The M-FISH$_{LET}$ absorbed blood dose estimates may better account for this as aberrations sampled directly from the blood are utilised for the ratio. The ^{223}Ra dose by C5 estimated by M-FISH$_{LET}$ to be 0.665 ± 0.080 Gy, this estimate significantly larger than CTPV$_1$ 0.024 ± 0.027 Gy and CTPV$_2$ 0.141 ± 0.042 Gy. The largest uncertainty in the M-FISH$_{LET}$ absorbed blood dose estimation was found to be also in C2 whereby the variation in the frequency of cells consistent with IMRT exposure (cells containing simple aberrations only) was up to 13% and for those consistent with ^{223}Ra exposure of up to 28%. This error also highlighted by Schumann *et al.* (2021 (363)) whereby low dose exposure resulted in low frequency of foci. This being a methodological limitation whereby the number of cells may need increasing in future studies. In our study, the error from the calibration curve used was estimated to be 12 and 23% for IMRT and ^{223}Ra absorbed blood dose estimates, respectively. The total propagated error on absorbed dose was within 30% for the M-FISH$_{LET}$ derived estimates.

For the dose ratio of M-FISH$_{LET}$, the complexity of chromosome exchange observed in PBLs was used as a biomarker of radiation quality as reviewed by Anderson (2019 (349)) this being a promising biomarker for unknown α-particle exposure. In Anderson *et al.* (2002 (348)), PBL were exposed *in vitro* to 0.5 Gy of α-particles (3.26 MeV equivalent to 1 mean α-particle traversal) resulting in 83% of total chromosomal events being of complex kind. This suggested damage following α-particle exposure results primarily in complex exchanges. Based on this principle, all cells which contained at least one complex chromosome exchange were categorised as having been traversed by high LET α-particles emitted from the ^{223}Ra, while cells containing only simple rearrangements were categorised as being exposed to low LET radiation from IMRT. The main drawback for the M-FISH$_{LET}$ model was that not all complex events will be solely attributed to ^{223}Ra only exposure and also not all simple events will be attributed to IMRT. Although *in vitro* studies do show the majority of

high-LET induced damage to result in complex chromosome aberrations largely independent of dose (237, 241, 412-414), it is also the case that the simple exchanges can be directly induced after α-particles of lower incident LET (368). Likewise, exposure by low-LET radiation will result in the formation of some complex exchanges following high dose exposure of >2 Gy (370, 415, 416). Anderson *et al.* (2002 (348)) identified 36% exchanges within aberrant PBL exposed *in vitro* to 3 Gy x-rays (250 kV) as having at least one complex. Although much lower that reported value of 83% following α-particle exposure, this is still a significant proportion of complex exchanges. Study by Pignalosa *et al.* (2013 (417)) and Hartel *et al.* (2009 (355)) of PC patients, identified an increasing fraction of complex exchanges of 20-40% following exposure of large target field by IMRT. Therefore, it is likely that IMRT absorbed blood dose may be underestimated when assuming all complex aberrations are only attributed to ^{223}Ra.

To further validate and develop this model, an *in vitro* ^{223}Ra calibration curve should be created. This enabling a quantification simple rearrangement induced by ^{223}Ra. The C-ratio has been found to significantly change dependent on the energy and LET of the α-particle. With increasing α-particle LET the likelihood of a complex aberration occurring also increases (368). Therefore, it becomes important to have a calibration curve that mimics the LET of ^{223}Ra α-particles in the blood. Following this, an *in vivo* calibration curve may also be of use as the quantity of ^{223}Ra administered varies based on patient weight, therefore the frequency of complex events may potentially vary between patients. At present, studies with patients receiving only ^{223}Ra are being carried out and blood samples from these patients may be of use for further quantification of ^{223}Ra circulatory exposure.

To consider why the expected blood dose differs between models, it may be plausible that the M-FISH dose estimates are representative of more than just transit blood dose exposure. As the sampling of PBL occurs 4 weeks after ^{223}Ra administration, we are unable to distinguish between the PBL exposed during the transit of ^{223}Ra and that from PBL circulating in vicinity of metastatic sites. This being as normal bone is highly vascularized by both nutrient and periosteal artery system and in CRPC patients, bone metastases result in an increased vascularization (25, 55, 418). With the new blood vessels induced by proangiogenic factors differing to normal blood vessels by having irregular structures with

leaky walls facilitating tumour spread (419, 420), this may also result in the increase of circulating PBL exposure.

Other sources of uncertainty include the changes *in vivo* following blood exposure. The dicentric quantification was based on cytogenetic observations of sampled PBL, the resulting doses estimated will be directly affected by haematopoietic cell death and repopulation dynamics. The IMRT dose estimates were found to plateau between C3-C5 suggesting cells containing unstable aberrations remain over the time course studied. However, IMRT has been shown to significantly decrease the number of PBLs in circulation, and therefore the clearance and repopulation dynamics should also be taken into consideration for the CTPV models (355, 421, 422). For the M-FISH model, although the dynamics of repopulation/ clearance of aberrant cells was unknown, the differences in dose assessments may also stem from changes in the peripheral blood pool. The repopulation dynamics will be discussed in later chapters with haematological data. It is also important to consider the killing effect differences between ^{223}Ra *in vivo* and an apoptotic assay should be considered as cytogenetic techniques will identify cells that may potentially have been exposed to ^{223}Ra and incorrectly rearranged. We are unable to quantify cells that have been exposed to ^{223}Ra and correctly repaired, although the frequency is likely to be very low, or able to quantify the cells that have been exposed to ^{223}Ra having directly induced apoptosis *in vivo* or unable to divide *in vitro* therefore undergoing programmed cell death.

The models suggest PBLs were exposed to a substantial dose by ^{223}Ra in transit and an attempt was made to estimate the absorbed blood dose. The key observations and limitations were discussed and although the limitations described here were significant there is scope to improve the models. The models presented provide an initial estimation of cumulative absorbed dose received to the blood during incremental IMRT fractions and ^{223}Ra injections. The estimates move towards assessing patient specific dose information for mixed field treatment to help optimise treatment outcomes and minimise patient risk in the future.

Chapter 5: Could bone marrow stem cells be exposed to ^{223}Ra?

5.1 Introduction

A long standing dilemma with radiotherapy treatment is the potential exposure of normal tissues, that may cause symptomatic injury increasing the side effects during and following radiotherapy (as reviewed (423)). As a result, many radiotherapy advances aim to maximise targeting to the tumour and minimise the exposure of surrounding tissues and cells (424, 425). Clinical and histological features of normal tissue exposure may not be apparent imminently and can be described as acute (within weeks), consequential (months), or late effects (years) depending on when they may present. The risk following these is dependent on the dose, size of area, treatment modality and organs exposed (425, 426). Toxicity may arise from cell death impacting tissue/ organ function or may arise from delayed effects in surviving cell fractions (and progeny) initially not presenting abnormalities. To prevent these, advances in traditional radiotherapy treatment, increasing dose while minimising non-target area exposure, and improvements of targeted radionuclide therapy delivery have been made (427, 428). Although recent advancements in dose delivery are promising, the push towards finding truly targeted therapies remains.

The novel pharmaceutical ^{223}Ra has generated a great deal of interest for its potential use in advanced stage bone disease, because ^{223}Ra has the potential to effectively target metastatic cells in the bone whilst greatly minimizing toxicity to the surrounding tissues. This was proven in the landmark ALSYMPCA clinical trial that demonstrated low initial toxicity in the majority of patients (79, 80, 429) with follow-up studies demonstrating low haematological toxicity up to three years post therapy (162, 163, 365, 430, 431). This could mean ^{223}Ra treatment of many different cancer types also metastasising to bone regions (432-434). There is also the potential to offering earlier treatment for patients with good prognosis, that would otherwise not be offered radiotherapy. With the emitted α-particle range being ≤100 μm, it is likely for only small areas of the BM to be directly exposed, hence, the resulting haematological toxicity is likely to be minimal and temporary (431, 435, 436). Although ^{223}Ra treatment is highly targeted, some risk of exposure remains for cells in

the vicinity of metastatic regions, including the haematopoietic stem cells residing in the BM. Furthermore, a great deal of uncertainty remains surrounding the estimated BM dose from ^{223}Ra, the heterogenous distribution of dose at metastatic sites and, the delayed implications, if any, for the patient (437, 438). Indeed, few studies have assessed nonclinical endpoints following *in vivo* exposure by ^{223}Ra. To date, only two case studies have reported leukaemia following ^{223}Ra although no causal link has been established as for both cases, the patients received varying forms of chemotherapy and radiotherapy in combination to ^{223}Ra (316, 317).

Genomic instability refers to alterations to a cell genome following changes in genome maintenance which leads to uncontrolled proliferation, cell death evasion and invasive properties all characteristic of cancer. Cancer cells will contain multiple genomic alterations such as base pair mutation, nucleotides insertions/deletions, copy number variant, microsatellites instability, chromosomal/ chromatid aberrations, or aneuploidy. In tumour development genomic instability is one of the main drivers which facilitates disease progression. Unstable chromosomal aberrations are classified as non-transmissible, as they lack the ability to correctly segregate for multiple rounds of cellular division. Conversely, stable chromosomal aberrations are able to segregate and be passed through indefinite rounds of cellular division. Previous cytogenetic studies have demonstrated the persistence and transmissibility of stable aberrations after α-particle exposure (237, 238, 439-441). Haematopoietic cells have the ability to transmit both simple and complex stable aberrations to daughter cells as demonstrated in *in vitro* and *in vivo* studies (283, 442, 443). Accordingly, an increase in the frequency of stable transmissible aberrations in PBLs may be an indicator of aberrant haematopoietic cell expansion following treatment exposure. If so, an increased frequency in stable transmissible complex aberrations may be indicative of BM exposure by ^{223}Ra.

The paradigm that only direct exposure of the cell to an exogenous factor results in genomic instability has long been challenged with many studies having identified what are broadly termed as delayed and bystander effects. These effects being associated with delayed genetic and phenotypic changes in daughter cells of those previously identified as apparently normal (269, 270, 274, 444, 445). Mouse studies have identified increased frequencies of unstable *de novo* aberrations after BM transplantation techniques following

high-LET neutron exposure (275, 276). Cytogenetic *in vitro* studies utilizing α-particle sources have also identified increased frequencies in chromatid aberrations of non-exposed lymphocytes and examples of this includes neighbours of cells traversed by α-particle (273, 446-448). Although the mechanisms are not yet fully understood, extracellular factors have been suggested as causative agents such as those present in blood plasma. Studies with plasma taken from exposed individuals and used as culture medium for normal leukocytes has resulted chromosomal breakage induction *in vitro* (449-453). A recent study by Leung *et al.* (2020 (454)) found evidence of induced antiproliferative/cytotoxic bystander effects in breast cancer xenografts in the BM of mice treated with ^{223}Ra. In humans this could suggest an increased risk for neighbouring BM cells following ^{223}Ra treatment.

Genomic instability from direct exposure or bystander effects may result in chromosomal loss or gain from mis-segregation errors during division (455). This mis-segregation is often derived from chromosomal damage, whereby the number of centromeres is impaired. This may include centromeric loss (acentric fragments) whereby kinetochore structures needed for microtubule attachment are dysfunctional and this results in random chromosomal segregation to a daughter cell. Chromosomes may present multiple centromeres which can result in an excessive number of microtubule attachments leading to forces in opposing directions, and this may lead to the formation of anaphase bridges which may eventually force the chromosome to break (456). Alternatively, the polycentric chromosomes may undergo whole chromosome mis-segregation to a daughter nucleus or form a micronucleus (456-460). Genomic instability may also present itself as chromosome numerical imbalances. These losses or gains are prevalent in tumours and tumour-derived cell lines and are associated with errors in mitotic segregation (461). The chromosomes involved are often termed lagging chromosomes as they lag at the mitotic spindle during anaphase stage. The pathway by which chromosome lagging occurs is not clear but recent studies have suggested this to be associated with errors in the activation of DNA damage responses (462, 463).

To date, no study has investigated markers of delayed genomic instability following ^{223}Ra treatment in humans. The aim of this chapter was to examine if there was any cytogenetic evidence of delayed genomic in circulating PBLs long after completion of treatment. As BM biopsies were not available for histological assessment after completion of treatment,

cytogenetic markers of induced damage and markers of genomic instability in PBL were quantified to assess whether the current treatment regime shows evidence of potential exposure to BM cells. Chromosomal aberrations were quantified during treatment by M-FISH and an increased frequency of aberrant stable transmissible cells was observed in later treatment cycles. This analysis was carried out as a pilot with a limited sampled size of two patients and further analysis with more patients and a larger sample size may be needed. Whole chromosomal aneuploidy levels showed no signs of non-random chromosomal loss, it may be possible that following treatment, changes in the BM niche and/or delayed effects may result in an elevated frequency of *de novo* chromosomal aberrations. For this, the frequency of unstable chromosomal aberrations was quantified in the last treatment cycle and compared with follow up blood samples of three patients with no significant change. Chromatid aberrations were also quantified, and an increased frequency was observed at the one year follow up time point. The increased frequency of chromatid aberrations may be a result of delayed or bystander effects potentially at BM sites.

5.2 Results

5.2.1 ^{223}Ra results in a substantial dose deposition to the red marrow

After intravenous administration, ^{223}Ra becomes carrier free in the blood and, due to its calcium mimetic properties will localize to areas of high bone remodelling (464). These areas are likely to be in vicinity of bone metastatic sites where an increased rate of bone resorption and formation results in an increased calcium uptake. At these sites, the ^{223}Ra will be incorporated into the growing hydroxyapatite layer of the bone endosteum before it decays, releasing high energy α-particles (464). The close proximity of the bone endosteum to the red BM may be associated with a risk of haematopoietic cell exposure within these actively dividing sites (465, 466). As prostate cancer patients exhibit ongoing bone fracture formation both during and after treatment (467), it may also be possible for the ^{223}Ra to localize even closer to the BM than modelled so far, potentially contributing towards a more substantial exposure than previously thought.

To determine whether a substantial dose may be deposited at these sites, dose estimation was carried out for the two regions anticipated to have the highest energy deposition. The osteogenic cell layer is the most outer layer of the bone where the ^{223}Ra is actively taken-up with the highest dose deposition. The neighbouring red BM, which is in vicinity of target metastatic cells, is expected to receive the second highest dose. A simple estimation of absorbed dose to these sites was made from the published data by the European Medicines Agency (324). Figure 5.1 illustrates the absorbed dose ranges for ten patients; these estimates are for each ^{223}Ra administration. A dose range of 4.963 ± 0.067 to 7.832 ± 0.062 Gy was estimated per injection to osteogenic cells, as this is the region with highest dose deposition where metastatic sites are targeted. The dose to the red marrow was estimated to range from 0.598 ± 0.008 to 0.944 ± 0.007 Gy per injection. Both these estimates suggest a substantial dose was delivered in proximity and to the marrow itself.

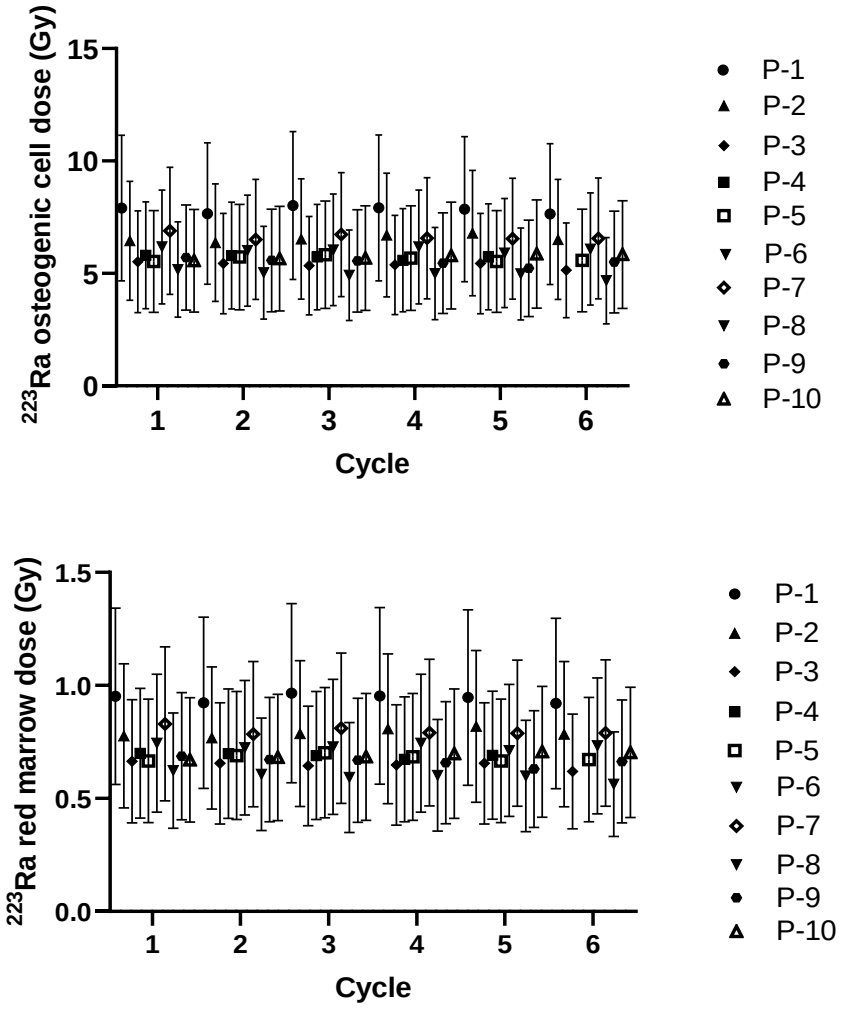

Figure 5.11 ^{223}Ra absorbed bone dose.

Dose estimated for ten patients (P1-P10) across six intravenous administrations with the exception of Patient-4 who received five injections. Panel a) dose received by osteogenic cells and panel b) dose received by the red marrow. Error bars represent coefficient of variation reported as 41% by the European Medicines Agency (324).

No significant difference was observed between the individual patient dose estimates, although patients of higher weight, and hence injected activities, were estimated to have been exposed to a higher dose. The current dose estimations assume equal and homogeneous uptake of the ^{223}Ra, although it is likely for patients with higher metastatic burdens to be exposed to higher doses. This due to larger metastatic sites potentially having a greater calcium intake during active growth. The risk associated with direct exposure of the BM, is the potential exposure of haematopoietic cells, including lymphocyte progenitor

cells that will then be released into circulation. The exposure may result in cell death of populations in the marrow and hence lead to the depletion of circulating blood cells leading to anaemia and lymphopenia as found in previous studies (163, 320-322, 401, 430). These effects are likely to be temporary, with surviving fractions of haematopoietic cells eventually boosting the peripheral blood pool (this will be discussed further in Chapter 6). To date the prospective delayed and bystander effects following potential ^{223}Ra exposure of haematopoietic cells, has not been investigated. As a substantial dose is expected in vicinity or, directly to haematopoietic cells residing in the BM, the following analysis aims to elucidate the cellular fate during and after treatment completion.

5.2.2 Markers of BM exposure in the peripheral blood pool

In the previous chapter, chapter 4, dose assessment was performed by the analysis of unstable chromosomal events present in circulating PBL sampled during treatment. The dicentric chromosome frequencies collected are a good indicator of recent exposure and therefore an ideal marker of blood dose estimates for the treatment periods of C1-C5. In the case of past exposure, stable aberrations are considered a more appropriate marker because these are retained within subsequent generations of the circulating PBL pool (236). *In vivo* studies have successful reconstructed whole body, partial body and BM dose, years after exposure following nuclear accidents or accidental exposures to nuclear workers (357, 359, 468-472), including low dose exposure scenarios (473). This is due to stable aberrations often being tolerated during normal cell function and hence, aberrant cells persist in circulation (474). Indeed, in many cases cells containing stable transmissible aberrations retain the ability to undergo proliferation and even differentiation, rendering these cells a marker for stem cell exposure (475). In the event of red marrow exposure, progenitor cells may be exposed, and the surviving fraction of cells, which may contain chromosomal aberrations, could then undergo further cell division and differentiation. At this point it is likely for cells containing unstable aberrations to eventually be unable to further proliferate and unlikely to then be translated into aberrations in the circulatory system. Instead, in the case of stable aberrations these will be likely transmitted to daughter cells and further differentiate in to mature circulating cells.

As the exposure of this patient cohort was recent, dose estimation was carried out with the dicentric assay (Chapter 4). In the above section, the expected dose to the BM was also quantified based on the expected absorbed dose as published by the European Medicines Agency safety assessment (Methods 2.7.2) (324). These estimates suggest a potential dose of 0.598 ± 0.008 to 0.944 ± 0.007 Gy to the BM per injection, resulting from direct exposure to α-particles. The treatment regime spans over 6 months and as circulating PBLs are exposed to ^{223}Ra, the drop in PBL counts is likely to stimulate cellular replenishment firstly from thymic and, later, haematopoietic pool (476). Therefore, an increased frequency of stable transmissible cells may be expected in the case of significant exposure of hematopoietic cells residing in the BM cavity (477-479).

5.2.2.1 A deviation from expected simple chromosomal ratio was observed

The induction of dicentric chromosomes and reciprocal translocations should follow a ratio of 1:1 as they both result from a single break in two chromosomes with the rearrangement to dicentric or translocation being random (480). A deviation from this ratio in the PBL could indicate replenishment of PBL by aberrant cells containing stable exchanges. The frequencies of simple translocations and dicentrics were previously analysed for samples C2-C5 and can be seen in Figure 5.2, comparing each patient sampled per cycle. No statistical difference in the frequency of pooled dicentric chromosomes and reciprocal translocations per cycle was found ($P \geq 0.654$ one-way ANOVA). Some deviations from the 1:1 ratio were observed between patients. This included Patient-1 with a C4 dicentric frequency of 0.104 ± 0.045 which is lower that the reciprocal translocation frequency of 0.250 ± 0.082 and Patient-4 who at C5 had respective frequencies of 0.168 ± 0.042 and 0.307 ± 0.674. However, these were not found to be statistically significantly different (two-tail unpaired t test Patient-1 C4 $P=0.120$, Patient-4 C5 $P=0.082$) and may instead be a reflection of uncertainty associated with the smaller sample size.

Similar analysis was not possible on many of the later cycle samples due to an increased frequency of 2nd division cells. The same analysis was therefore carried out as a pilot on two patients for which follow up samples were available, and which contained ≤5% 2nd division

cells. The first follow-up sample was collected 8 weeks after the final ^{223}Ra administration (F1) and second follow up was sampled 4 months after the last ^{223}Ra administration (F2).

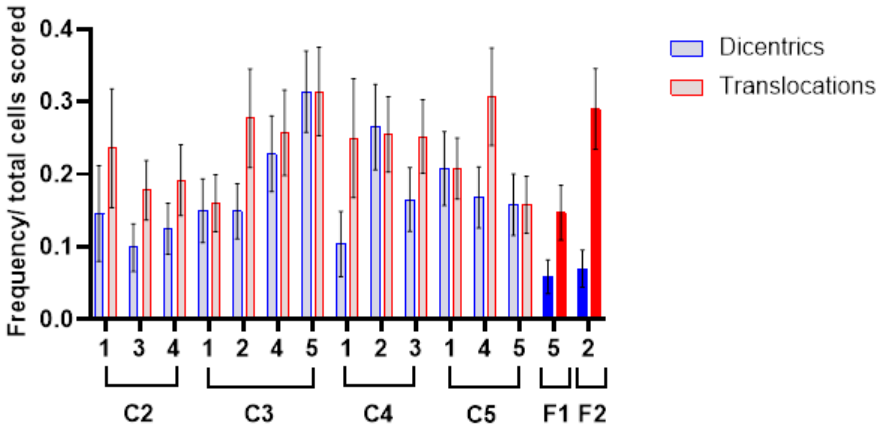

Figure 5.22 Changes in simple aberration population.

The frequency of simple dicentrics (blue) and reciprocal translocations (red) was gathered during treatment from Table 3.1 for five patients. The patient ID is listed on the X axis (1-5). The frequencies with standard error can be seen in the lighter bar colours from C2-C5. The frequencies of simple aberrations in follow up samples was collected for F1 (8 weeks) and F2 (4 months).

Over all timepoints, both patients displayed a lower frequency of dicentric chromosomes compared to reciprocal translocations. At the F1 timepoint, Patient-5, shows a decreasing trend for simple dicentric exchanges relative to that observed at C5. The frequency of translocations was instead, maintained, suggesting persistence of stable cells between C5 and F1. As the frequency of translocations should remain constant, this may represent a maintenance or gradual repopulation scenario with new PBL carrying stable transmissible exchanges. This scenario further reinforced by the data associated with the Patient-2 later follow up F2, whereby a statistically significant difference (One-way ANOVA $P<0.001$) was observed between dicentric and translocation events. The last sample collected during treatment for Patient-2 was C4 and at this point the ratio of dicentric to translocation events is near 1:1, this also suggesting a maintenance or repopulation resulting in a higher translocation frequency by the F2 timepoint.

5.2.2.2 Non-transmissible cells are cleared from the peripheral pool

To quantify the changes of transmissible cells during treatment and in the follow up samples, cells containing balanced stable rearrangements including reciprocal translocations and/or stable complex exchanges were grouped as transmissible. Those containing unstable, incomplete exchanges or missing chromosomes were classed as non-transmissible. To then assess whether these aberrations could have resulted from cell proliferation at BM sites, the stable exchanges were compared to identify potential clonal cells. The frequency of non-transmissible cells was seen to significantly increase between C2 and C4, from 0.265 ± 0.027 to 0.411 ± 0.031 (one-way ANOVA P=0.003). This appears to then decrease in C5 as there is no significant difference between earlier C2 and C3 (one-way ANOVA C2-C5 P=0.562 and C3-C5=0.517) as seen in Table 5.1. This potentially suggests a cellular repopulation resulting in the dilution of these aberrant cells and/or clearance by mitotic cell death of unstable cells.

Overall, an increasing trend for stable cells was observed between C2 (0.042 ± 0.013) and C5 (0.097 ± 0.017) of treatment cycles as per Table 5.1. The frequency of cells containing stable complex events also increases from 0% recorded in C2 to 20% of transmissible cells in C5 containing at least one complex exchange. Patient-5 F1 sample had a lower frequency 0.049 ± 0.022 than the previous sample at C5 of 0.088 ± 0.028, although this change was not found to be statistically significant (one-way ANOVA P=0.457). An increase for Patient-2 from C4 (0.118 ± 0.032) to an F2 sample frequency of 0.140 ± 0.035 was observed, but this was also found to not be statistically significant (one-way ANOVA P=0.879). The fraction of cells containing a transmissible complex increased for Patient-2, with the last treatment sample C4 containing 25%, and with this increasing to 29% in the later F2 sample. The mean frequency of non-transmissible cells declined in late treatment, i.e. at timepoint C5 and in the two follow up samples collected. The Patient-2 frequency of non-transmissible cells decreased from 0.392 ± 0.049 at C4 to 0.250 ± 0.044 in the F2 sample (Unpaired t test P=0.031). Patient-5 also displayed a decrease from C5 0.245 ± 0.043 from to 0.250 ± 0.044 in F1, however this was not found to be statistically significantly different (Unpaired t test P=0.620). A decreasing trend could potentially be observed in the later follow up sample from Patient-5 (not analysed here).

Cycle	ID	Cells scored	T Cells	T cell subtypes		NT cells
				Simple exchanges	Complex exchanges	
C2	1	55	2 (0.036 ± 0.025)	100% (0.036 ± 0.026)	-	13 (0.236 ± 0.058)
	3	101	6 (0.059 ± 0.024)	100% (0.059 ± 0.024)	-	23 (0.228 ± 0.042)
	4	104	3 (0.029 ± 0.017)	100% (0.029 ± 0.017)	-	33 (0.317 ± 0.046)
	Total	260	11 (0.042 ± 0.013)	100% (0.042 ± 0.013)	-	69 (0.265 ± 0.027)
C3	1	100	6 (0.060 ± 0.024)	100% (0.060 ± 0.024)	-	33 (0.330 ± 0.047)
	2	101	11 (0.109 ± 0.031)	82% (0.089 ± 0.029)	18% (0.020 ± 0.014)	35 (0.347 ± 0.048)
	4	101	8 (0.079 ± 0.027)	100% (0.079 ± 0.027)	-	37 (0.366 ± 0.048)
	5	105	4 (0.038 ± 0.019)	75% (0.029 ± 0.016)	25% (0.010 ± 0.010)	44 (0.419 ± 0.048)
	Total	407	29 (0.071 ± 0.013)	90% (0.064 ± 0.012)	10% (0.007 ± 0.004)	149 (0.366 ± 0.024)
C4	1	48	2 (0.042 ± 0.029)	50% (0.021 ± 0.021)	50% (0.021 ± 0.021)	18 (0.375 ± 0.071)
	2	102	12 (0.118 ± 0.032)	75% (0.088 ± 0.028)	25% (0.029 ± 0.017)	40 (0.392 ± 0.049)
	3	103	6 (0.058 ± 0.023)	83% (0.049 ± 0.021)	17% (0.010 ± 0.010)	46 (0.447 ± 0.049)
	Total	253	20 (0.079 ± 0.017)	75% (0.059 ± 0.015)	25% (0.020 ± 0.009)	104 (0.411 ± 0.031)
C5	1	106	9 (0.085 ± 0.028)	78% (0.066 ± 0.024)	22% (0.019 ± 0.013)	39 (0.368 ± 0.047)
	4	101	12 (0.119 ± 0.032)	83% (0.099 ± 0.030)	17% (0.020 ± 0.014)	34 (0.337 ± 0.047)
	5	102	9 (0.088 ± 0.028)	78% (0.069 ± 0.025)	22% (0.020 ± 0.014)	25 (0.245 ± 0.043)
	Total	309	30 (0.097 ± 0.017)	80% (0.078 ± 0.015)	20% (0.020 ± 0.008)	98 (0.317 ± 0.027)
F1	5	102	5 (0.049 ± 0.022)	80% (0.039 ± 0.019)	20% (0.010 ± 0.010)	22 (0.216 ± 0.041)
F2	2	100	14 (0.140 ± 0.035)	71% (0.100 ± 0.030)	29% (0.040 ± 0.020)	47 (0.250 ± 0.044)

Table 5.11 Transmissibility of aberrant cell population.

Patient ID (ID) recorded per cycle for five patients sampled. The number of cells recorded as transmissible (T) or non-transmissible (NT) following M-FISH analysis is reported as a frequency of total cells scored with standard error of the mean. The percentage of T cells containing

simple only exchanges or at least one complex event is reported as a frequency for total cells scored also with standard error of the mean reported. NT cells include unstable simple exchanges (dicentrics and rings), break only and unstable complex exchanges.

5.2.3 Clonal cell analysis

Stable clonal aberrations are the ideal markers to potentially identify the effect of treatment on the BM area. As aberrations are induced in actively dividing haematopoietic progenitor cells, a proportion of these will be stable and not inhibit cell proliferation. With ongoing haematopoiesis over treatment course, it may be possible to identify clonal cells in later cycles or follow up samples. In this study, although an increase was observed for stable transmissible aberrations, only one clonal aberration was identified in a the follow up sample. This sample was from the 4 month (F2) follow up sample for Patient-2 in which two cells were found to contain a translocation between chromosomes 1 and 8, as seen in Figure 5.3. Upon further inspection of previous treatment cycles and the control sample, the same translocation was identified in the pre-treatment control. Therefore, this translocation is unlikely to have been induced by the current treatment and may reflect age increased genomic instability or potentially pre-clinical trial exposure to an unknown radionuclide.

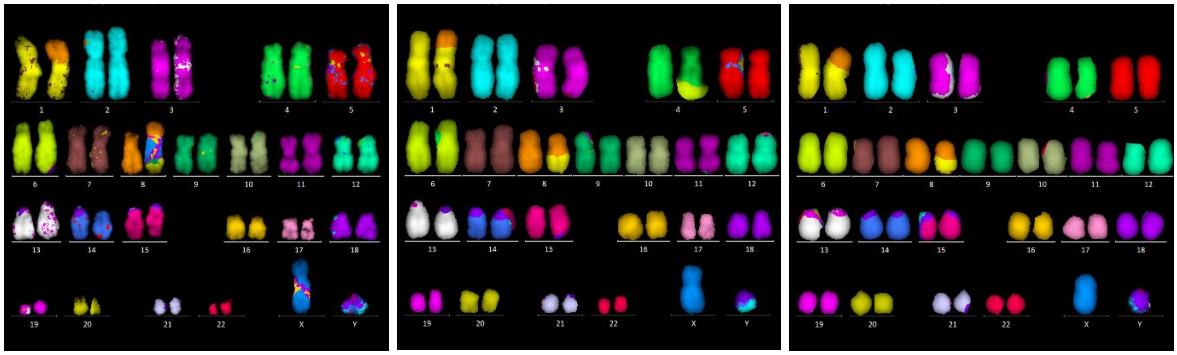

a) **b)** **c)**

Figure 5.33 Simple stable clonal cell.

Stable clonal cell containing a reciprocal translocation between chromosome 1 and 8. Clone identified in two cells of Patient-2 F2 samples a-b and in control sample c. 50 cells scored in C1 and 100 in F2.

5.2.4 Aneuploidy as a marker of genomic instability

Non-random whole chromosome aneuploidy could be an indicator of delayed effects of exposure in cells that are otherwise free of chromosomal damage. To assess whether the samples contained

non-random chromosomal loss or gain, the whole chromosome aneuploidy in apparently structurally normal cells was quantified. Cells with up to three missing chromosomes that appeared structurally normal during or after treatment were assessed, and the number of chromosomes involved was counted. Cells which appeared to be overspread were excluded as chromosomal loss was likely associated with drifting during the slide making process. An increase of non-random chromosomal aneuploidy was observed for three patients. Patient-2 displayed an increased loss of acrocentric chromosomes 13 and 22. Patient-5 was observed to have an elevated loss of chromosome 9 and, although this was higher than observed with other patients, this was in line with the frequency of involvement for other category C chromosomes (chromosomes 6-12). Lastly Patient-4 was found to have an elevated frequency of chromosome X, this being gained in 2 cells in early C2 and in 3 cells in C5.

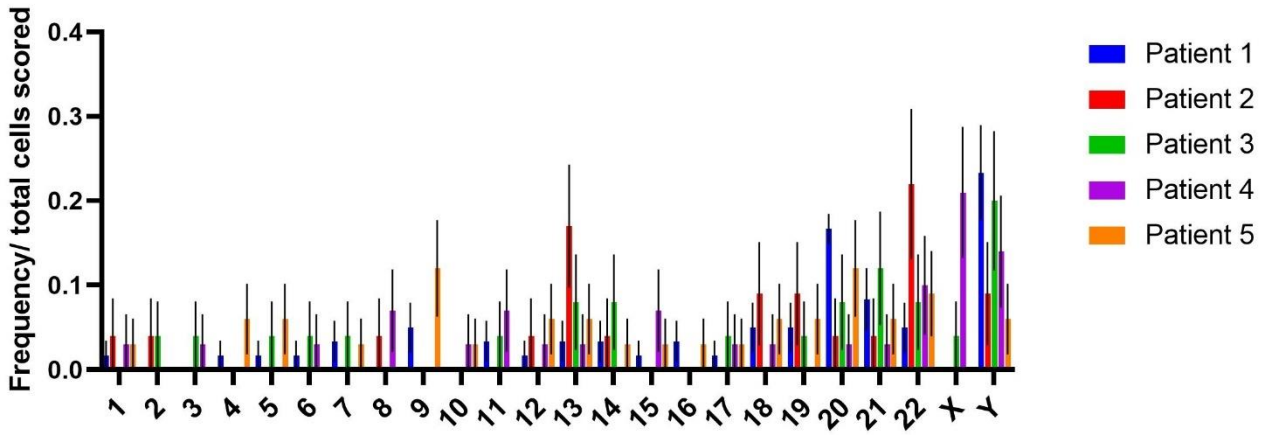

Figure 5.44 Chromosomal involvement in aneuploidy cells.

Structurally normal cells containing ≥43 chromosomes were analysed for five patients. The involvement of a chromosome (loss or gain) was expressed as a frequency per total aneuploidy cells scored. The frequency was collected across all treatment and follow up cycles. The chromosomal involvement was pooled for each patient cycle across all sampling times. The error bars report standard error of the mean.

Overall, a higher frequency of chromosomal loss was observed for chromosomes of smaller size, including those of category F, G and the sex chromosome Y (Figure 5.4). Gain of these small chromosomes was rare, the small size potentially being associated with drifting during the chromosome slide preparation therefore rendering these aneuploidy cells as artefacts.

In this study, this analysis was intended only for 1st *in vitro* division cells, therefore tetraploid cells were excluded. However, an increased numbers of tetraploid cells were observed with treatment progression, including cells that appear structurally normal and cells containing chromosomal rearrangements of spectrum consistent with the treatment (high and low LET). Figure 5.5 depicts an example of a cell containing complex chromosomal rearrangements of the unstable kind. The observed rearrangement includes a successful duplication of dicentric chromosomes (with involvement of chromosome 1 and 8 and chromosome 4 and 17) and acentric fragments. This cell was classified as non-transmissible, therefore unlikely to undertake further replication, and the cell would eventually undergo cell death as the chromosomes would be unable to correctly segregate into daughter cells.

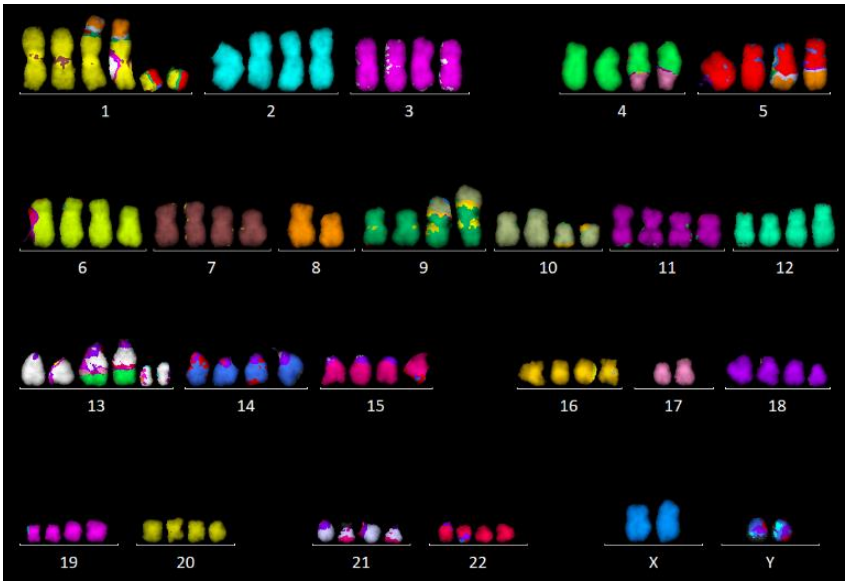

Figure 5.55 Aberrant tetraploid cell.

Abnormal tetraploid cell painted by M-FISH. The cell contains two unstable complex rearrangement between chromosomes 1,5,8 and chromosomes 4,9,10,13 and 17.

5.2.5 *De novo* aberrations as a marker of delayed effects

A cell may be exposed to ionizing radiation at various stages of its cell cycle. The cell cycle stage which it is exposed in will then dictate the pattern of aberration induced. In the event of a chromosome rearrangement induced during the initial G_0 stage, this will be visible in metaphase as both chromatids having been truncated with an acentric fragment. Instead, if a cell is exposed during G_2, it is possible for only one chromatid to be damaged (although isochromatid breaks also arise) as per Figure 5.6. This results in a normal chromatid and a truncated chromatid with an acentric chromatid fragment. The increased frequency of chromatid aberrations during G_2 is dependent on LET with high LET exposure inducing a higher frequency of chromatid aberrations (481). Maturing progenitor hematopoietic cells of PBLs will undergo differentiation and maturation in the BM, therefore exposure during cycling is more likely for hematopoietic cells than PBLs which mainly reside in G_0. However, as chromatid aberrations are unstable, it is unlikely for progenitor cells containing chromatid aberrations to successfully pass these aberrations on to their daughter cells (482). Delayed effects of exposure may result in *de novo* aberrations including both chromosomal and chromatid events, in progeny of apparently normal cells. Therefore, chromatid aberrations observed in the study samples could potentially be an indicator of delayed instability following direct and/or indirect exposure of haematopoietic cells.

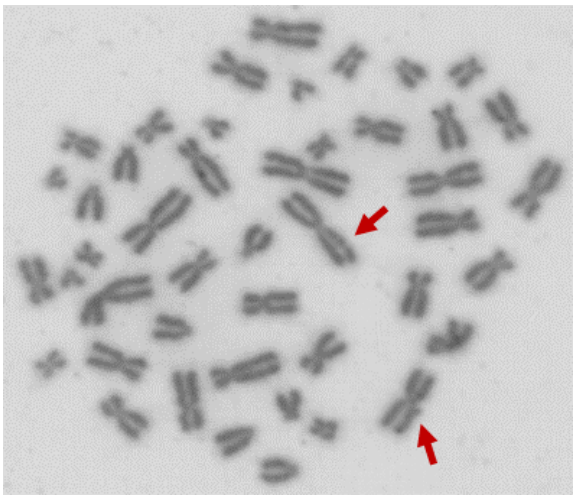

Figure 5.66 Cell containing chromatid aberrations.

Giemsa staining of 1st division metaphase spread analysed under brightfield x100 magnification (oil immersion). Upper red arrow pointing at a chromatid discontinuity and bottom arrow pointing at a chromatid fragment adjacent to the chromosome.

5.2.5.1 Delayed chromosomal events

To assess whether cytogenetic markers of delayed instability are present after treatment, the follow up samples (F1, F2 and/or F3) were assessed for the occurrence of *de novo* unstable aberrations in three patients, and the frequencies of these were compared with those in the last sample collected during treatment (C6). The follow up samples were selected instead of treatment cycles as they were thought to provide a longer break to maximise the potential to identify any PBL pool replenishment following radiotherapy. To quantify unstable chromosomal and chromatid aberrations, the Harlequin solid stain technique was used as per method section 2.3.4, which enabled the scoring of only 1st *in vitro* cell division cells. For all patients, a sample at C6 (last treatment cycle) and F3 (1 year follow up) was available for analysis, with two patients also having and earlier follow up sample of either F1 (8 weeks) or F2 (4 months after last treatment administration).

Unstable chromosomal aberrations including dicentric chromosomes, rings, acentric fragments and discontinuities were scored. The pooled frequencies of aberrations for all three patients highlighted a significant decrease in frequency from 1.261 ± 0.100 at C6 to 0.826 ± 0.071 by F3 (Two-tailed unpaired t test P=0.001). Some differences between patients were also observed. For example, patients 1 and 3 displayed significant decreases between C6 and F3, but Patient-2 instead had no change in unstable chromosomal aberrations of all categories between C6 and F3 (one-way ANOVA P≥0.844). This suggests loss of unstable aberrations with time for Patient-1 and 3, whereas for Patient-2, clearance may be delayed and displayed as maintenance of unstable cells in the peripheral pool.

Direct exposure by high-LET is likely to result in the formation of multiple chromosomal aberrations events due to clustered damage. Delayed direct and indirect effects of radiation exposure may result in a lower number of chromosomal events formed. Indirect effects are unlikely to result in the type of clustered damage which is observed following α-particle exposure, indeed, Hou and Little (2001 (268)) suggested that the induction of DSBs by delayed effects may result from different mechanisms to those induced by direct effects. The pattern of damage following delayed effects may therefore be simpler compared with fewer exchanges/events. When observing the distribution of cells with multiple chromosomal events, the frequency of cells containing 4 and ≥ 5 events reduced after C6 for both Patient-1 and Patient-3. This suggests clearance of cells with a high

damage burden from the circulatory pool. Cells with lower number of events were not found to increase in frequency. However, for Patient-2 the frequencies of cells containing 4 and ≥ 5 events remained constant suggesting delayed clearance of heavily damaged cells. A trend in increased frequency of cells containing 2 events in F2 and F3 was also observed, although this was not found to be statistically significant.

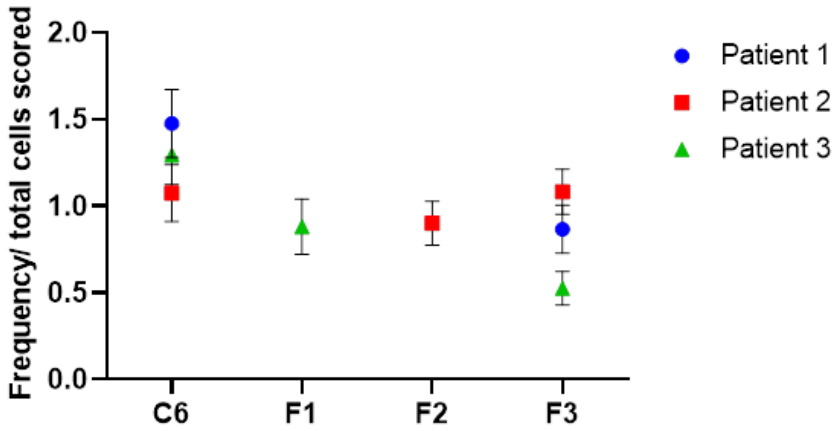

Figure 5.77 *De novo* unstable chromosomal aberrations.

Data presented for three patients. ≥200 metaphase spreads were scored by Harlequin solid stain. Unstable chromosomal aberrations including dicentric chromosomes, rings, acentric fragments, and discontinuities were scored at time points C6, last treatment cycle; F2, 4 months follow up; and F3, 1 year follow up from C1 collection. The frequency of unstable chromosomal events plotted for three patients. The error bars represent standard error of the mean.

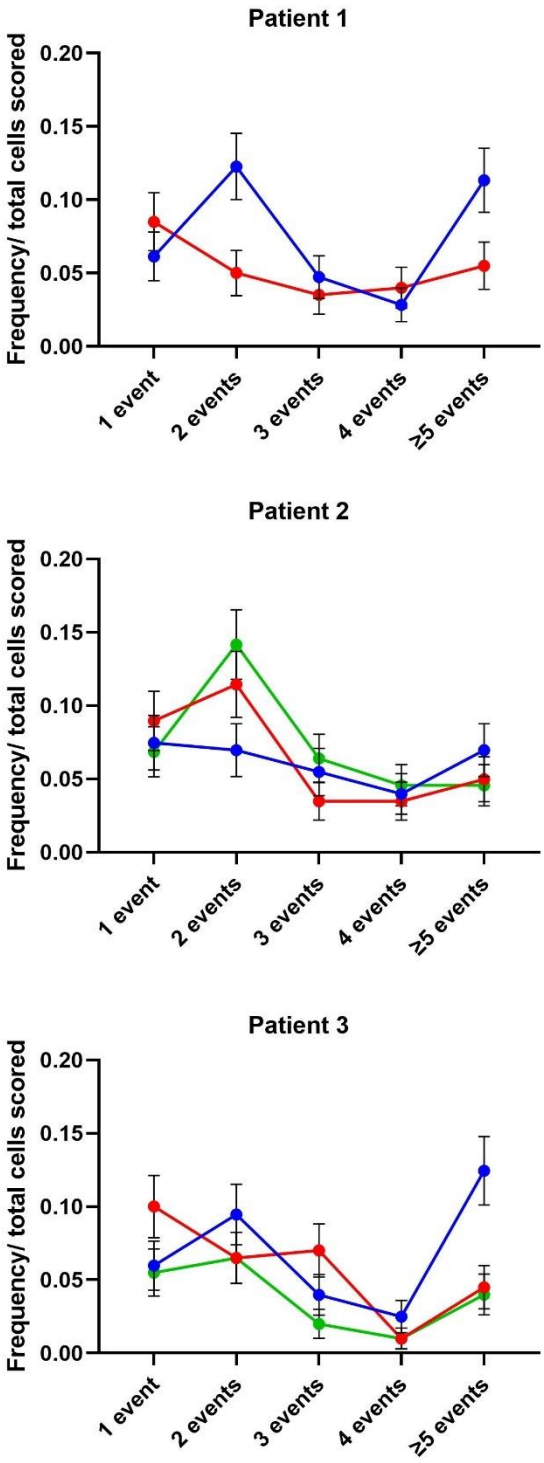

Figure 5.88 Changes in the chromosomal aberration distribution.

The frequency of cells containing one or more unstable chromosomal events (dicentric chromosomes, rings, acentric fragments, and discontinuities) presented for three patients. Sampling C6 (blue), F2 (green) and F3 (red). The frequency of unstable chromatid events plotted for three patients. The error bars represent standard error of the mean.

5.2.5.2 Delayed chromatid events

Previous *in vitro* studies following α-particle exposure have identified increased frequencies of *de novo* chromatid aberrations after culturing of mouse colonies that initially appeared to not present signs of DNA damage (260). This observation was confirmed in a study where human BM was exposed *ex vivo* (256). An earlier *in vivo* mouse study involving BM transplantation from irradiated mice to non-irradiated subjects, found an increase in chromatid aberrations following cell proliferation (443). Therefore, it may be possible for changes in chromatid aberration frequencies observed at later times to reflect *de novo* delayed and/or bystander effects.

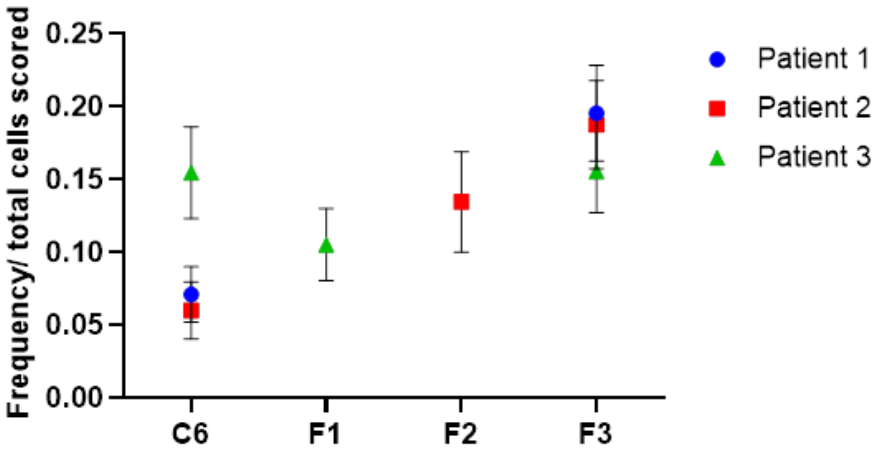

Figure 5.99 *De novo* unstable chromatid aberrations.

Chromatid frequencies (including fragments, discontinuities and sister unions) were collected for three patients (1-3). ≥200 metaphase spreads were scored per cycle. C6, last treatment cycle; F2, 4 months follow up; and F3, 1 year follow up from C1 collection. The error bars represent standard error of the mean.

The frequency of chromatid aberrations, including fragments, discontinuities and sister unions, was collected for the samples C6 and F1 to F3 (Figure 5.9). Unlike the chromosomal events, the pooled frequencies of observed unstable chromatid aberrations for the three patients suggested a significantly increasing trend from C6 of 0.094 ± 0.014 to F3 of 0.179 ± 0.018 (one-way ANOVA P=0.001). As shown in Figure 5.9, Patient-2 displayed an increasing trend through all samples. Patient-1 also had a substantial increased frequency between C6 and F3, but no sample was taken for the earlier F1 or F2 timepoints. For Patient-2, the frequency of chromatid events remained constant between C6 and F3 with a small but not statistically significant increase after F1 after a

previous decrease between C6-F1 (one-way ANOVA P>0.919). Although overall differences are evident between the patients, the frequencies in F3 are consistent between patients, potentially suggesting similar delayed responses to treatment in terms of chromatid aberrations for all three patients.

5.2.5.3 Changes in the PBL population

Circulating PBLs spend the majority of their life in G0/G1, therefore the damage induced will result in mainly chromosomal aberrations. Previous *in vitro* studies indicate relatively low frequencies of chromatid aberrations even with high LET exposure (483), although high LET exposure is potentially associated with a more complex spectrum of chromatid rearrangements (484). Other studies with *in vitro* G_1 cell exposure have suggested a shift in aberration spectrum following high LET exposure with an increased fraction of chromatid:chromosomal aberrations (485-487) compared to those observed following low LET exposure. Stephan *et al.* (2005 (406)) identified an increased frequency of cells containing chromatid only events after radiotherapy by ^{224}Ra, and this was suggested to be indicative of delayed instability via bystander effects.

In this study, assigning the abnormal cell populating into three separate groups, chromosomal only, chromatid only and chromosomal + chromatid cells, it was possible to assess whether any one of these specific fractions of cells was found to increase, i.e. to indicate either exposure of cycling cells and/or bystander effects from BM niche changes.

For all patients, the C6 samples were found to mainly contain chromosomal aberrations with some cells containing a mixture of both chromosomal and chromatid events, while the smallest fraction contained chromatid aberrations only (Figure 5.10). By F3, the frequencies of cells containing chromatid only aberrations were found to follow an increasing trend for all patients, with Patient-1 and 2 displaying a significant increase between C6 and F3 $P \leq 0.005$ (one-way ANOVA). This suggests a change in the peripheral cell population with a decreasing trend in cells containing chromosomal only exchanges after treatment completion for Patient-1 and 3. A small increase in total abnormal cells was observed in Patient-2 between C6 (0.309 ± 0.033) and F3 (0.3653 ± 0.033). This increase can be mainly attributed to increased number of cells containing chromatid only aberrations and a smaller increase in cells containing mixed aberrations.

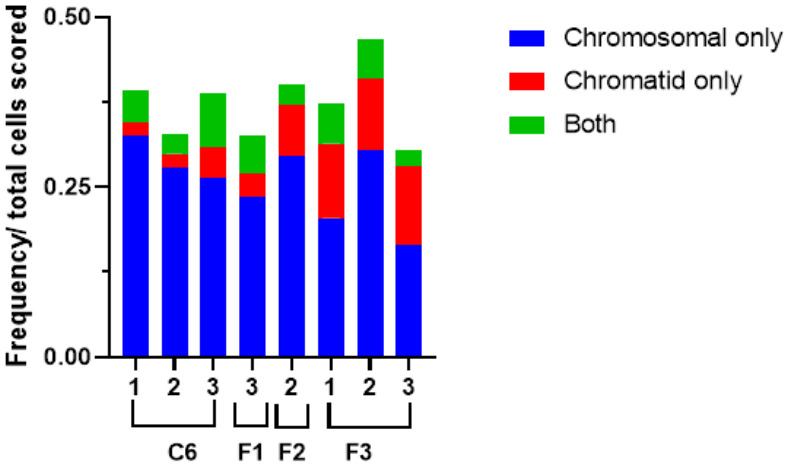

Figure 5.1010. Changes in aberrant PBL population distribution.

Cells were grouped in three categories including chromosomal only aberrations (dicentrics, rings, fragments and discontinuities), chromatid only (fragments, discontinuities and sister unions) and both types. The frequency for each category was recorded for three patients (Patient ID 1-3). C6, last treatment cycle; F2, 4 months follow up; and F3, 1 year follow up from C1 collection. The total column representative of the total frequency of abnormal cells scored.

5.3 Discussion

This chapter, along with previous Chapter 4 dose estimations, suggested haematopoietic stem cells residing in the BM may be at risk of direct exposure to ionizing radiation from internalised ^{223}Ra. During ^{223}Ra decay, the potential for red marrow exposure is dependent on the range of the emitted α-particles (≤ 100 µm in tissue) and the proximity and quantity of ^{223}Ra incorporated. The pharmacokinetics of ^{223}Ra incorporation and range of non-targeted exposure has not been estimated in this study, but as Sgouros *et al.* (466) discussed, distances of ≤ 100 µm between the BM and the incorporated ^{223}Ra could result in outer regions of the BM being exposed. This, coupled with clinical studies of advanced prostate cancer patients which indicate a significant number of skeletal features associated with disease progression (488, 489), indicates that it may be possible for ^{223}Ra to be incorporated into bone in very close proximity to the cells of the BM. Whether a substantial portion of haematopoietic cells are, in actuality, exposed, would depend on their cellular distribution within the red marrow. Previous studies have suggested BM cells are non-uniformly distributed and are likely to be within 100 µm of bone surfaces (490, 491). In terms of the amount of ^{223}Ra deposited, this would theoretically be dependent on the number and size of metastatic sites present in the individual, and the injected activity. The saturation point, whereby ^{223}Ra may no longer be incorporated and instead is cleared from the system, has also not yet been quantified. Recent clinical trials have focused on the dosing of ^{223}Ra as it is currently based on the weight of the patient and not on its metastatic bone load, with 55 kbq/kg of body weight remaining the recommended dose (153, 366, 492). This dosing strategy is potentially concerning, as the uptake of ^{223}Ra is assumed to have a positive relationship with high metastatic load due to the upregulated calcium intake of bone metastatic cells. This will be further explored in Chapter 6.

The estimated BM dose presented here suggests a significant dose of between 0.598 ± 0.008 and 0.944 ± 0.007 Gy per cycle administration. These estimates are based on the absorbed radiation doses expected per organ (324), including that of α-particle emission only, as α-particles were expected to be the main contributor of absorbed dose. The estimates represent a simplistic model suggesting that compartments containing haematopoietic cells may be directly exposure to ^{223}Ra. This being said, a study on bone microarchitecture of prostate cancer patients presenting bone metastases, observed an increase in bone connectivity and surface irregularity (60), which itself may attenuate exposure of the marrow by increasing the distance between ^{223}Ra localization sites

and red marrow. Uncertainties remain as to whether the ^{223}Ra distribution is indeed homogeneous and hence whether the dose to red BM could potentially be heterogenous (315). To date, the current literature is yet to assess the true effect of ^{223}Ra on bone regions. Further studies are needed to quantify the distribution of ^{223}Ra in patients, including changes with metastatic burden, differences in bone remodelling due to skeletal related events, patient differences including body weight, and the resulting red marrow dose delivered. In Chapter 4, the dose to circulating PBL was estimated from both biokinetic and cytogenetic assessment during treatment. The estimates presented in this chapter, although simplistic, suggest a substantial dose may also be delivered to PBL progenitor cells residing in the BM. In this scenario, markers of exposure would be expected to be apparent in the circulating progeny of surviving cells of the BM, particularly in later follow up cycles. Stable aberrations induced in precursor haematopoietic cells capable of undergoing cellular proliferation and differentiation may, through further growth, differentiation and maturation, eventually reach the peripheral blood pool and then have the potential to be sampled. In the case of long-lived stable rearrangements directly induced in circulating cells, these would most likely remain in circulation for the lifetime of the cell, as these rearrangements may not provide a disadvantage to the cell. In fact, the reciprocal translocation assay is routinely used for retrospective dosimetry following exposure months or years prior (236). The frequencies of reciprocal translocations sampled in this study in the two pilot follow up samples from two patients (Patient-2 and Patient-5), remained constant. This suggests a maintenance of stable aberrant cells with aberrations induced during treatment. However, the frequency of simple dicentric events was not found to remain constant. Patient-5 had a loss of over 60% by the F1 timepoint (C5 0.158 ± 0.042 vs F1 0.059 ± 0.023) and Patient-2 a loss of over 70% (C4 0.265 ± 0.059 vs F2 0.070 ± 0.026). Although this cannot be directly measured from our samples, there may be a loss of unstable aberrations either by cell death and/or dilution from cellular replenishment where the frequency of stable aberrant cells will also be diluted by normal cells. Retrospective dosimetry studies following accidental human exposure and *in vivo* animal studies, support the preferential maintenance and persistence of cells containing translocations over dicentrics (472, 493). A similar trend was observed in prostate cancer patients follow up samples following IMRT by Hartel *et al.* (2018 (369)). As reported, the frequency of translocations remained in a similar range after treatment completion (6.6 ± 0.6 per 100 cells of 14 patients) as in the 1 year (8.0 ± 0.7 per 100 cells of 13 patients) and 2.5 year follow up (7.3 ± 0.8 per 100 cells of 6 patients) samples.

A large decrease in dicentric frequency of approximately 35% was observed after the first year (from 6.3 ± 0.6 to 4.1 ± 0.5 per 100 cells) and this decreased by a further 18% (to 3.0 ± 0.5 per 100 cells) by the time the last 2.5 year follow up sample was taken. With cellular replenishment from normal BM cells, aberrant cells should decrease over time as the aberrant pool is effectively diluted. Lindholm *et al.* (2002 (494)) observed a decrease in the dicentric and translocation frequencies in the two years follow up samples of accidentally exposed individuals. Dicentric chromosomes have a shorter half-life than reciprocal translocations, although up to 70% loss of reciprocal translocations was observed. In this study, the reduction of dicentric frequency is most likely attributed to cell death, as cells containing dicentric chromosomes are unstable and unable to successfully divide long term in the periphery. In our study, the patient aberration frequency did not reduce equally across aberration types. As expected, persistence of reciprocal translocation and loss of dicentric chromosomes suggests a changing aberration spectrum with time. As the samples were collected from the patients at varying timepoints, it was not possible to compare the rate of unstable aberration loss, but it appears that both of the pilot sample patients used for this part of the study (Patients 2 and 5) exhibited a similar rate of change. In the case of repopulation by normal healthy cells, the frequency of reciprocal translocations should also be found to decrease over time. Instead, for both patients, the expected 1:1 ratio of simple dicentrics:simple translocations was found to increase. The previously study mentioned by Hartel *et al.* (2018 (369)) also reported a similar trend where the ratio of dicentrics:translocations changed from almost 1:1 at treatment completion to 0.51 in the first year follow up and 0.41 by the 2.5 year follow up time point. The ratios of frequencies in the samples in this study followed a similar change in ratio, with Patient-5 early F1 follow up having a ratio of 0.40 and the Patient-2 later follow up F2 ratio decreasing to 0.29. Therefore, the change seen in the observed aberration ratio could be a marker of haematopoietic stem cell exposure, as was also reported by Hartel *et al.* (2018 (369)).

Following the standard definition of a clone that it contains the same structural rearrangement in at least 2 cells, no clonal cells containing stable rearrangements were identified in the two patient pilot. Note, though, that to avoid an *in vitro* artifact resulting from some cells entering a 2nd mitosis during the culture period, three cells are often needed for confirmation of clonal status (495). So, a direct relation between BM exposure and an increase in frequency of transmissible cells in this study could not be drawn. However, this may be due to the sample number being too small and/or the sampling points being too early for a high yielding expansion of the aberrant hematopoietic

pool. In previous studies following accidental radiation exposure, the rate of clonal cells was found to be low. Lucas *et al.* (1992 (496)), which was a Hiroshima A-bomb follow up study, detected just two individual with clones out of 20 (100 metaphase cells scored per individual) by G banding. Salassidis *et al.* (1995 (359)) detected one individual in 12 Chernobyl victims. Multiple follow-up samples presented similar frequencies over a two years period, of 0.33-0.39 ± 0.03 clones out of 328-400 cells scored by FISH. The study by Hartel *et al.* (2018 (369)) identified a handful of patients only with clonal cells (two out of fourteen patients), this was based on large samples of $>$ 1000 cells (rate of 1.5-5.0 clonal cells per 1000 cells) (369). It may also be possible for heavily damaged cells containing more complex damage to have been cleared more rapidly from the circulatory pool, as a high frequency of complex chromosomal events was observed in Chapter 3. The potential for early peripheral pool expansion potentially trigged by low PBL counts cell due to combined IMRT and ^{223}Ra treatment was not considered. In the case of cellular expansion following combined treatment, a higher frequency of translocations may be initially observed compared to dicentric chromosomes which would be cleared from the PBL population by reproductive cell death. Following normal cellular repopulation, the resulting frequencies would then evenly be diluted over time. The transmissibility analysis of this study, although limited in sample size and number of patients, suggests persistence of transmissible cells for both patients. The frequency of non-transmissible aberrant cells was found to decrease for Patient-2 (as seen in Table 5.1) and persist for Patient-5. As highlighted by previous *in vitro* studies, the ratio of dicentric:translocations alone cannot be used to identify whether clearance or repopulation is taking place (497, 498) as cells containing translocations may also be made unstable by presence of further rearrangements or incompletion repair. Further work will be needed with a larger cell sample size and more patients to detect whether the changing ratios of dicentrics:translocations observed in this study may be associated with persistence or stable abnormal cell expansion.

Ionizing radiation exposure is associated with delayed segregation errors *in vivo* (457, 460) and *in vitro* (458, 459) that may result in increased aneuploidy following both high and low dose exposure (455, 499). A study by Rowley *et al.* 2017 on non-random chromosomal abnormalities in secondary cancers of previously radiotherapy treated patients identified non-random aneuploidy in cells containing other chromosomal rearrangements, as well as cells otherwise structurally normal. To assess whether non-random chromosomal loss was evident during and after treatment, structurally normal cells with aneuploidy were assessed and the frequency of aneuploidy for each involved

chromosome was collected. The scoring of cells with aneuploidy for this analysis was based on the analysis of cells with a minimum number of 43 chromosomes and the inclusion of metaphases cells that were not overspread. Chromosome categories F and G, characterized by their smaller size, were found to have an increased frequency of involvement. A positive trend was observed towards aneuploidy of smaller chromosome (categories F, G and Y chromosome), with few exceptions. All five patients included in this study commonly showed losses for chromosomes 20-22, which could potentially be non-random and could be used as an early indicator for cancer relapse. Chromosomal loss may be associated with size, as smaller chromosomes are more likely lost. However, other studies that have considered non-disjunction (whereby lagging chromosomes are mis-segregated) have suggested chromosome size to not be the main factor in aneuploidy cell formation. In fact, recent studies using chemicals to disrupt normal chromosomal segregation identified the larger chromosomes, 1 and 2, as more prone to lagging due to cohesion fatigue and hence mis-segregation (500). Although for our patient cohort, no significant elevation of non-random chromosome aneuploidy was observed in autosomal pairs, the sex chromosomes X and Y had a high level of loss/gains for all patients. This may be a result of age-related instability as previous studies have identified the gain of chromosome X and loss/gain of chromosome Y to be associated with aging (501). This has also been confirmed by other studies utilising techniques such as *in situ* hybridization of interphase cells (502) and micronuclei studies with Y positive staining (503). Aneuploidy involving chromosome gain is rare and the majority of cells identified with aneuploidy had missing chromosomes, with the exception of chromosome X. This was also observed in previous studies where men were more likely to the gain an X than lose it, and this potentially suggests an increased likelihood of chromosome X non-disjunction in older men (502, 504). Chromosome Y was found mainly to be lost, with the occasional gain, and this is also consistent with previous publications (501, 502, 504). In this study, the patient median age was 63, as reported in the trial first publication (322), so these sex chromosome aneuploidies are likely to be a normal reflection of age and not ionizing radiation. Another point to consider is that M-FISH analysis for the detection of aneuploidy is often accompanied by a high rate of artefacts due to overspreading of chromosomes and chromosomal drifting (505). The rate of true aneuploidy is therefore hard to quantify as individual scorers may differ in their inclusion criteria.

Non-clonal aberrations thought to result from delayed genomic instability, have been observed in many studies of *in vivo* mouse exposure (276, 283, 443, 506), *in vitro* human haematopoietic cell

exposure to both high and low LET radiation (256, 258, 260) and many more (As reviewed here (507)). In this study, the frequency of unstable chromosomal events, scored by Harlequin solid stain, was not found to increase in follow up samples, suggesting no *de novo* chromosomal aberrations induced within the one year follow up period. This was also observed by M-FISH analysis as the frequency of non-transmissible cells was reduced by the end of treatment compared to following the first treatment rounds. The frequency of chromatid type aberrations was instead found to increase with time, particularly cells containing exclusively chromatid aberrations. The explanation for this is unknown but the observation is consistent with delayed expression of instability. The increase in chromatid aberrations by the F3 timepoint is unlikely to represent delayed spontaneous damage by ROS in circulating PBLs but could be related to enhanced respiratory burst capabilities by ROS (508) which could link to haematopoietic differentiation. A previous study of ankylosing spondylitis patients that had received Radium-224 (^{224}Ra) treatment (a weekly dose of 1 MBq for 10 weeks), found an elevated frequency of both chromosomal and chromatid aberrations in PBLs during treatment (406). In this study the frequency of cells containing chromatid only events increased after 4 months (F2) for Patient-2 and for all other two patients by 6 months (F3), and the half-life of ^{223}Ra is 11.3 days, these chromatid events cannot be solely attributed to direct cell exposure. Therefore, delayed and/or bystander effects may be at play, although the mechanisms currently unknown. A substantial dose of 4.963 ± 0.067 to 7.832 ± 0.062 Gy was estimated to the neighbouring osteogenic cells this reinforcing the possibility of delayed/bystander effects detected in follow up samples. As haematopoietic cells are tightly regulated by the bone niche, which is directly linked to osteogenic cell activities and cascade signalling (52), cellular communications between the two may invoke genomic instability phenotypes in haematopoietic cells that have not been exposed to radiation. Delayed phenotypic expression of an unstable genome has been demonstrated *in vitro* using many end points, including reduced proliferation rates (252, 253, 271, 509) and delayed apoptotic death (510, 511). Therefore, the proliferative rates may have also be affected in the present study *in vitro* cultured PBLs as the stimulation of lymphocytes was found to be challenging (Chapter 3). Kadhim *et al.* studies found haematopoietic expansion of exposed colonies resulted in an increased frequency of chromatid events following *in vitro* division (256, 260), and suggested that some chromatid aberrations induced in the marrow may be converted to reciprocal translocations following division (255).

It is also important to note that chromatid aberrations could also be a marker of an unknown exogenous exposure. The patient cohort studied did not received further treatment following trial completion. Although no increases in chromosomal aberration frequencies were shown in this study, chromatid aberrations in the follow up samples may still constitute initial evidence of *de novo* aberration formation and/or bystander effects. Further analysis with large patient sample size, increased number of cells scored and later follow up sample analysis by M-FISH may elucidate where changes in PBL aberration spectrum could indeed be derivative of BM exposure.

Chapter 6: Risks of haematological toxicity and leukemogenesis

6.1 Introduction

Radiotherapy is often recommended in combination to surgery and/or chemotherapy however, some individuals may be more susceptible to adverse effects. Clinical studies have suggested functional impairment including fatigue (512), increased risk of infection (513) and even cognitive defects (514) to be increased in older individuals following radiotherapy, therefore, extra considerations are often made (515). As reviewed by Chang *et al.* (2017 (516)), older adults may have diminished organ functions with stress responses being affected (517) and, other metabolic function alterations associated with ageing (as reviewed by Barzilai 2012 (518)); all of which may in turn increase radiosensitivity. Whether these are truly age related changes remains debated as some *in vitro* studies have found no increased radiosensitivity in primary human cancer cells (519, 520) of older individuals. Chromosomal study by Baeyens *et al.* 2005 (521) identified no difference in age of onset and chromosomal radiosensitivity in PBL of breast cancer patients so ultimately, the risk of toxicity following treatment could be simply based on individual genetic differences (522).

Toxicity may be divided into two categories. The first being early/acute toxicity usually induced during treatment (within 90 days of start) and, delayed/late toxicity either after treatment completion or, in the months following. Acute toxicity results from cell death in highly proliferating tissues, this includes haematopoietic system, the gastrointestinal tract and skin (167). Acute toxicity may be temporary and reversible, with younger individuals recovering more rapidly. To assess for acute haematological toxicity such as anaemia, neutropenia, thrombocytopenia and leukopenia, haematological parameters can be monitored as this results in poor health affecting the quality of life of the patient. The risk of infection is may also be increased following large changes in normal haematological parameters and in some cases, can impact treatment outcome by increasing the tumour hypoxic environment (As reviewed by Shesha 2001 (523)). Although these symptoms may also be temporary, the impact may be greater in older individuals (As reviewed by O'Donnovan *et al.* 2017 (524)).

The risk of haematological toxicity is dependent on dose, with increased dose linearly associated with a decrease in blood cell counts (525-527). Fractionated treatment overcomes this dose limiting

factor by spreading the delivered dose over multiple fractions while increasing the overall cumulative final dose. Although fractionated treatment reduces toxicity, this may still be associated with haematological toxicity either due to patient sensitivity to ionizing radiation, exposure of surrounding normal tissue and/or, direct exposure of the red BM (94, 95, 422, 528, 529). The latter potentially results in a significant risk of delayed toxicity, which may manifest towards the end of treatment and/or following completion.

The red BM is an active site of haematopoiesis whereby HSC are stimulated to proliferate, and daughter cells differentiate into varying blood precursor cells. The risk associated with bone marrow exposure is high due to the potential for long lasting blood component depletion as a consequence haematopoietic stem cells and, other progenitors, undergo cell death (530, 531). Exposure of the bone marrow may also affect the bone, bone marrow niche and, microarchitecture which can in turn result in delayed bone marrow disorders (532). The exposure of haematopoietic progenitor cells may also result in the survival of exposed fractions of damaged cells, potentially resulting in cells carrying mutations and or chromosomal aberrations (497). Certain rearrangements may result in abnormal cell proliferation and trigger oncogenic growth associated with leukemogenesis, the most notable example being the Philadelphia chromosome in chronic myeloid leukaemia (288, 533, 534). Secondary cancers are also a risk following radiotherapy treatments; with increased patient survival and remission times (535) an excess risk for leukaemia and solid tumours may occur (281, 536-539). The potential rollout of ^{223}Ra treatment to younger cohorts and other cancer types, including those in paediatric patients, thus poses a long term risk that has yet to be quantified.

In previous chapters, elevated frequencies of chromosomal aberrations in cells of the blood were associated with the treatment. This includes aberrations consistent with both IMRT and ^{223}Ra exposure. The dose estimation following treatment may suggest a significant dose is delivered to the BM region by ^{223}Ra (Chapter 5). Although there was no evidence of chromosomal aberrations of clonal descent attributed to the treatment, the risk of leukemogenesis in the following months/years remains unknown. During this study, the haematological parameters were closely monitored for acute haematological toxicity by the collection of blood cell counts. In this chapter, this data will be discussed together with the chromosomal aberrations detected to assess acute treatment related toxicities. For this, patient deviations from the planned treatment schedule will also be discussed. As the current dosing strategy is based only on weight, the prognostic markers

(PSA and ALP) will also be used to discuss whether patients receiving a lower/higher dose of ^{223}Ra appear to have a greater clinical benefit. The results may present a potential stepping stone towards optimizing individual patient dosing.

6.2 Results

6.2.1 Individualised patient treatment schedule

In our study, the treatment regime entails 7.5 weeks of combined IMRT and ^{223}Ra followed by 4 months of ^{223}Ra administration only. The dose delivered by IMRT was split in to 37 individual 2 Gy fractions aimed at the prostate with concomitant boost to surrounding lymph nodes. The total cumulative delivered dose by IMRT was planned to be in the region of 74 Gy. The ^{223}Ra was administered cyclically at six individual intravenous administrations, with a dose of 55 kbq/kg of body weight. In the event of toxicity or changes to the patients' overall health, the regime was either paused or terminated. For the thirteen patients enrolled in the trial, the planned treatment regime can be seen in Table 6.11 with deviations from treatment plans highlighted.

Five patients had changes to their treatment plan. For Patient-4, IMRT resulted in early toxicity and the number of fractions was reduced from 37 to 30. Following this, Patient-4 was not eligible for the last administration of ^{223}Ra, due to haematological toxicity. Patient-12 did not receive the last ^{223}Ra administration for unknown reasons. The IMRT treatment plans were adjusted for three patients with Patient-5 and Patient-13 having a lower prescribed dose from the onset, Patient-9 received a lower concomitant dose to lymph nodes due to proximity to the bowel.

Patient ID	IMRT			^{223}Ra		Deviations from treatment plan
	Planned Fractions	Prostate Dose (Gy)	LN Dose (Gy)	Injections	Injected activity (kb/kg)	
1	37	74.3	61.5	6	56.9	
2	37	74.1	61.5	6	55.8	
3	37	74.5	61.4	6	56.6	
4	30	74.1	61.0	5	57.7	-5 IMRT fractions, -1 ^{223}Ra injection
5	35	69.6	55.9	6	56.9	Lower prescribed dose IMRT
6	37	74.4	61.3	6	56.9	
7	37	74.2	61.2	6	56.9	
8	37	73.9	61.3	6	57.7	
9	37	74.3	53.0	6	57.0	Reduced dose to LN
10	37	74.2	60.9	6	56.3	
11	37	74.0	60.5	6	55.6	
12	37	74.2	60.6	5	56.6	Unknow reason for ^{223}Ra reduction
13	35	70.6	50.6	6	55.6	Lower prescribed dose IMRT

Table 6.11 Delivered treatment plan.

^{223}Ra Injected activity calculated as a mean injected activity across all patient administered doses. IMRT dose delivered to prostate and lymph nodes (LN) are described with deviations from the planned 37 fractions. The ADRRAD treatment plan was supplied by Queens University Belfast with administered doses reported by clinical team.

6.2.2 Haematological response as a function of dose.

Haematological monitoring is important during radiotherapy and/or chemotherapy treatment as these agents may result in myelosuppression during or following treatment. Significant reduction in blood cell components may result in many moderate or more severe symptoms depending on the type of blood cell drop and numbers. In the case of white blood cell loss this may increase the risk of infection, low red blood cell counts may result in anaemia and low platelets can causes excessive bleeding. During radiotherapy treatment, these haematological parameters were monitored with lower threshold values set prior to therapy. In the case of patients falling under this threshold, treatment was paused or terminated.

Lymphocytes are widespread circulating cells that are sensitive to ionizing radiation exposure. The normal PBL range for a healthy adult male is 1.5-4.5x10^9 cells/L (540), varying slightly depending on health status, age and lifestyle. For the study there was no lower threshold set for lymphopenia and instead the haematological counts were closely monitored throughout the ADRADD trial. Following the first administration of ^{223}Ra in conjunction to the 20 IMRT planned fractions (C1-C2), the lymphocyte cell population was found to decrease for all patients (one-way ANOVA $P<0.001$) from a mean value of 1.460 ± 0.136 to 0.550 ± 0.058x10^9 cells/L. A further decrease was then also observed after the 37 IMRT fractions and a further ^{223}Ra administration (C3) to 0.460 ± 0.040 x10^9 cells/L, although no statistically significant difference was observed between C2 and C3 (one-way ANOVA $P=0.994$). Following IMRT, the number of circulating PBL remained below normal ranges with some increase being observed towards the final sample (C6). The mean frequency for C6 remained statistically lower 0.570 ± 0.078x10^9 cells/L than the control sample (one-way ANOVA $P<0.001$). The number of circulating PBL appears to slowly increase following the end of treatment with only two patients returning to near control values during their F3 follow up. However, the mean for all patients studied remains below normal range suggesting a slow cellular repopulation.

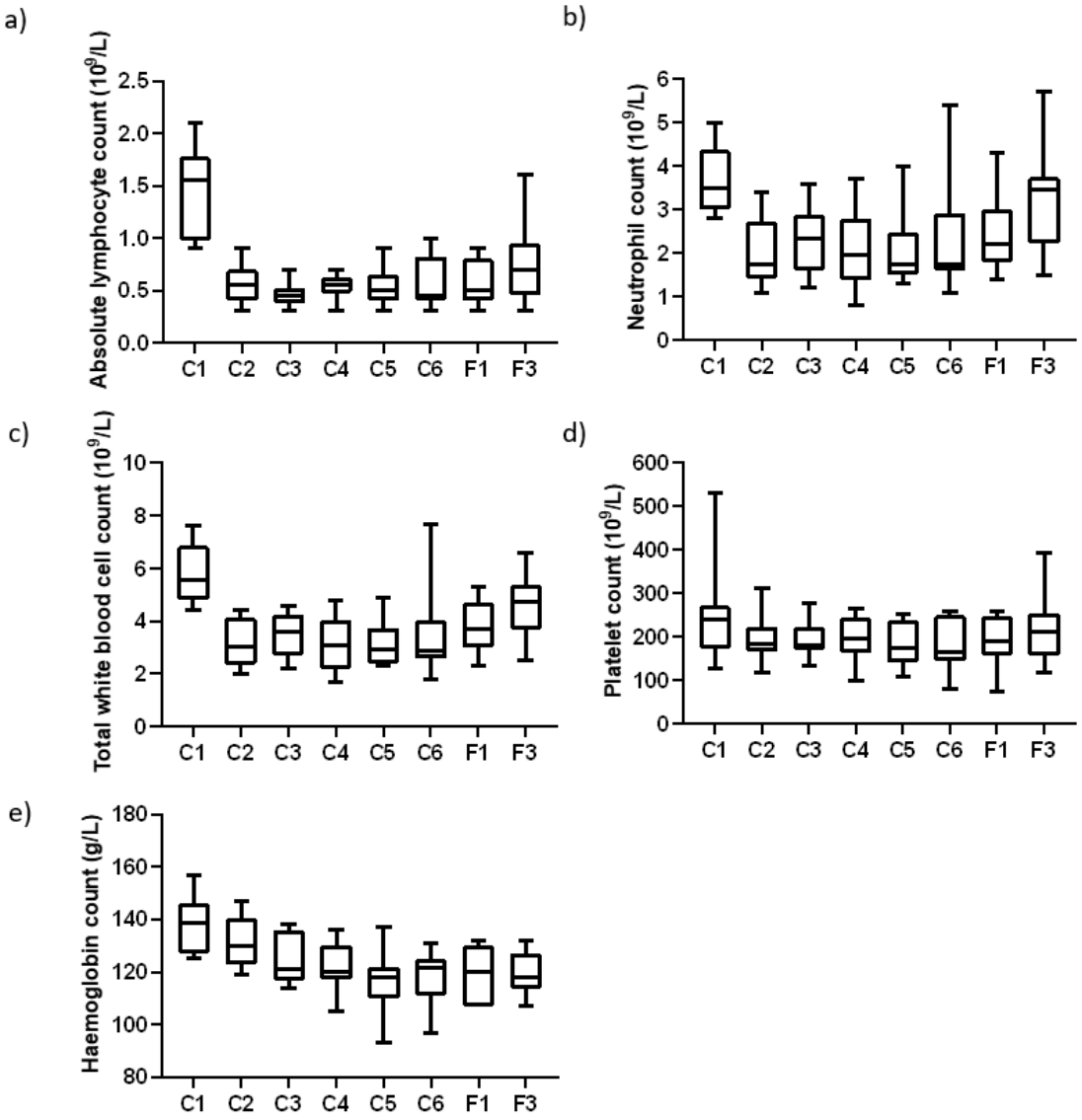

Figure 6.11 Monitored haematological parameters.

Blood samples were monitored for ten patients by the ADRRAD clinical trial team. Data was supplied for each sample collected for BUL. The mean counts with upper and lower limits were reported. a) absolute lymphocytes counts (cells x10^9/L), b) neutrophil counts (cells x10^9/L), c) Total white blood cell counts (cells x10^9/L), platelet count (cells x10^9/L) and haemoglobin (g/l). Samples were collected timepoints C1 - F3 as defined in methods 2.1.

The neutrophil counts were also monitored during treatment. The normal adult male range is in the region of 2.0-7.5x10^9 cells/L (540) and for this study the lower threshold was defined as ≥ 1.5x10^9 cells/L (Method section 2.2.1) with lower values requiring intervention. As per the lymphocyte

counts, the number of neutrophils was found to decrease following trial commencement from 3.700 ± 0.247 to 1.990 ± 0.238x10^9 cells/L (C1-C2). The rate of decrease was observed to be lower than that of lymphocytes and maintained in similar range between C2 and C6. Three patients were observed to drop below the threshold value of ≥ 1.5x10^9 cells/L. Patients 6 and 8 both dropped temporarily in C2 (Patient-6, 1.2 x10^9 cells/L and Patient-8, 1.1 x10^9 cells/L), recovered by C3 with values above threshold (Patient-6 1.6 x10^9 cells/L and Patient-8 2.5 x10^9 cells/L) before dropping further by C4 below threshold (Patient-6 0.8 x10^9 cells/L and Patient-8 1.4 x10^9 cells/L). Patient-5 was instead found to maintain a value below threshold from C3 to C6. The mean neutrophil value in F3 of 3.220 ± 0.384 x10^9 cells/L returned towards the C1 pre-treatment range of 3.700 ± 0.247x10^9 cells/L. By F1, the mean neutrophil counts were found to increase to 2.557 ± 0.365x10^9 cells/L, although not statistically different from C1 (one-way ANOVA P=0.237).

The mean absolute white blood cell counts were also found to significantly decrease between C1, 5.770 ± 0.350 x10^9 cells/L and C2, 3.130 ± 0.270 x10^9 cells/L (P>0.001 one-way ANOVA) with counts remaining lower than initial baseline throughout treatment. Following treatment (F3), the mean white blood cell count remained below control value 4.630 ± 0.399 x10^9 cells/L with only three patients returning to pre-treatment values or above. The mean white blood cell count for F3 was found to not be significantly statistically different to C1 suggesting a slow repopulation for all patients (one-way ANOVA P=0.315).

Other blood components such as the platelet and haemoglobin counts were also closely monitored. The normal range for platelet counts for a healthy adult male is 150-450x10^9 units/L with normal study baseline set at ≥100x10^9 units/L. The normal haemoglobin range is 130-180 g/L with study baseline set to 100 g/L (540). The mean platelet and haemoglobin values were consistent throughout treatment with Patient-4 dropping below threshold platelet value at C4, 99x10^9 units/L, and although recouping in C5, dropping further below the threshold at C6, 79x10^9 units/L. Patient-10 dropped below the threshold value for haemoglobin, and this was in the last two treatment cycles, with 93 g/L at C5 and 97 g/L at C6. Following treatment, the mean values for both platelets and haemoglobin were found to remain above study thresholds. The mean platelet count for two patients remained below C1 normal range at F3 follow up, with Patient-2, 131x10^9 units/L and Patient-4, 117x10^9 units/L. The haemoglobin values at F3 were also all above the defined study threshold but only two patients were within normal range, Patient-2, 131 g/L and Patient-3, 132 g/L, both borderline on the 130-180 g/L normal range and still below initial pre-treatment values.

6.2.3 Prognostic markers

To monitor the efficacy of treatment, the PSA and ALP levels were also collected. The rise in PSA level has been associated with the occurrence of prostate cancer and during treatment, as the primary tumour site is targeted, the PSA levels were expected to eventually decrease. PSA values below 0.5 ng/ml are usually associated with a favourable outcome (541). ALP changes have instead been linked with bone turnover (542-544), with elevated ALP at diagnosis associated with the occurrence of bone metastatic disease (545, 546). In our study, ^{223}Ra uptake to areas of increased bone turnover would result in a decreased activity following effective metastatic site targeting. Therefore, ALP level was hypothesised to decrease over the course of treatment following successful metastatic load targeting. Inversely, increasing levels of PSA and ALP during or after treatment completion may be markers of poor prognosis as they are an indicator of disease relapse (547-549). Both PSA and ALP levels were monitored in the control samples and during treatment with changes in baseline dependent on patient specific initial values.

The PSA and ALP levels were found to either decrease or remain in similar range for all patients, across the treatment. For a total of five patients, the PSA levels reduced by ≥50% between C1-F1 (Patient-3,4,7, 8 and 11). For three patients (Patient-1,2,13), smaller decreases were observed of ≤35%. The remaining two patients (6 and 12) reported increased values of PSA. Specifically, for Patient-6 there was an increase between C1, 0.76 ng/mL and C6, 0.88 ng/mL (No F1 available) representing a 16% increase. For Patient-12, a large increase was observed from C1, 0.49 ng/mL to F1, 53.55 ng/ml. For ALP a similar trend to PSA was observed, with 9 patients reporting a decreased value between 44-11% of the original. Whilst Patient-12 also displayed a marked increase in ALP from C1, 100 to F1, 760. The ALP levels decreased for the majority of patients through treatment.

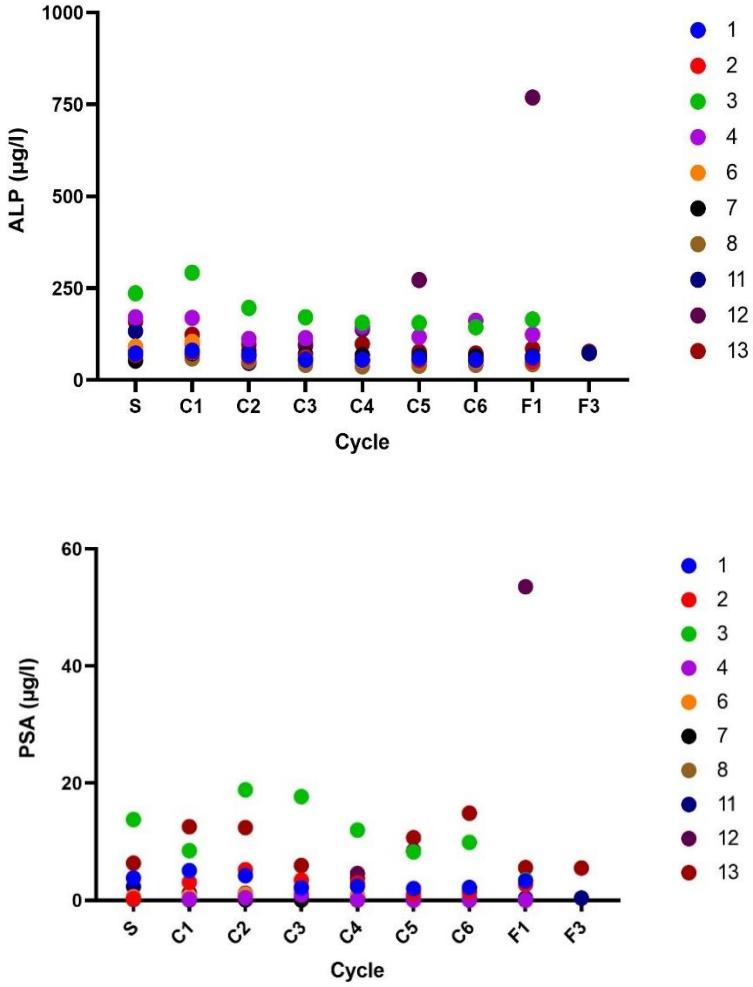

Figure 6.22 Changes in prognostic markers.

Data presented for ten patients. Upper panel ALP levels, lower panel PSA level. Values collected from screening date (S) and C1 pre-treatment to F3 by the ADRRAD clinical trial team.

6.2.4 The current dosing strategy and patient outcome

In chapter 4 the blood dose was estimated for both IMRT and ^{223}Ra, after IMRT completion the blood dose was estimated in the region of 1.167 ± 0.092 - 2.148 ± 0.096 Gy for IMRT and, 0.013 ± 0.025 - 0.719 ± 0.073 Gy for ^{223}Ra. This represented the largest dose delivered to PBL during treatment, reflected by a large number of aberrant cells 0.437 ± 0.025 and as described above 68% mean PBL cell death (C1 1.460 ± 0.136 to C3 0.460 ± 0.040). As might be expected, this suggests increased aberrant cell frequency is associated with PBL cell death. Following mixed radiotherapy, the mean PBL count increased in C4 by approximately 5% (to 0.540 ± 0.040) and remained at a similar level by C6 (to 0.570 ± 0.078). This suggested that for most patients there was a plateau in PBL counts in ^{223}Ra only cycles, whereby damaged cells were retained in circulation or alternatively, a balanced death/repopulation scenario. The administered ^{223}Ra dose does not appear to significantly increase the number of aberrant cells (P=0.086), or aberration events (P=0.079), between C2 and C5 as seen in Figure 6.33. This suggests the non-targeted exposure to PBL during treatment to not be significantly different in mixed therapy and ^{223}Ra only cycles.

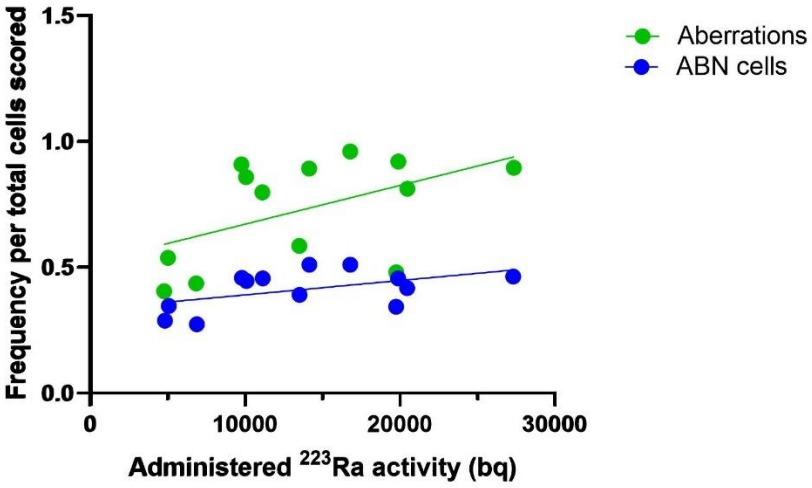

Figure 6.33. Abberation induction following ^{223}Ra dose.

Data presented for five patients (Patient-1-5) whereby samples were assessed by M-FISH. The frequency of individual aberrations and abnormal cells (ABN) per cycle was plotted against administered dose per cycle (bq).

The aim of the ADRADD clinical trial was to test the safety and efficacy of the treatment regime. This was achieved by monitoring haematological parameters as a measure of toxicity and, efficacy prognostic markers such as PSA and ALP. As the treatment is designed for palliative care, one of the desired outcomes was the reduction of skeletal metastatic burden to increase the quality of life. With ALP being a surrogate marker of bone turnover, positive response to ^{223}Ra would have resulted in reduced levels of ALP. With IMRT delivered to the primary tumour site, a decline in PSA was also hypothesized as a marker for positive response. The outcome from the patients including PSA and ALP changes from screening to F1 were plotted against the injected ^{223}Ra dose with the assumption that a higher administered dose may result in larger reduction of bone turnover marker ALP due to decreased metastatic burden.

The ALP levels were found to have a larger decrease between doses of 4000-5300 bq of injected activity (Figure 6.44). However, the linear relationship was not found to not be significantly different from zero (P=0.158). The data for Patient-12 was not included in this analysis as the deviation was abnormally large (however, this data also supported the direction of the trend). A larger decrease in PSA level was also observed between lower doses of ^{223}Ra between 4000-5000 bq. Like ALP, the linear relationship was not found to not be significantly different from zero (P=0.108). Although no significant difference was observed, there is an indication that lower administration of ^{223}Ra may be just as effective in managing bone metastatic sites. The reduction in administered dose may also have a preventative effect reducing the risk of toxicity and secondary cancers potentially associated with higher ^{223}Ra dose administration.

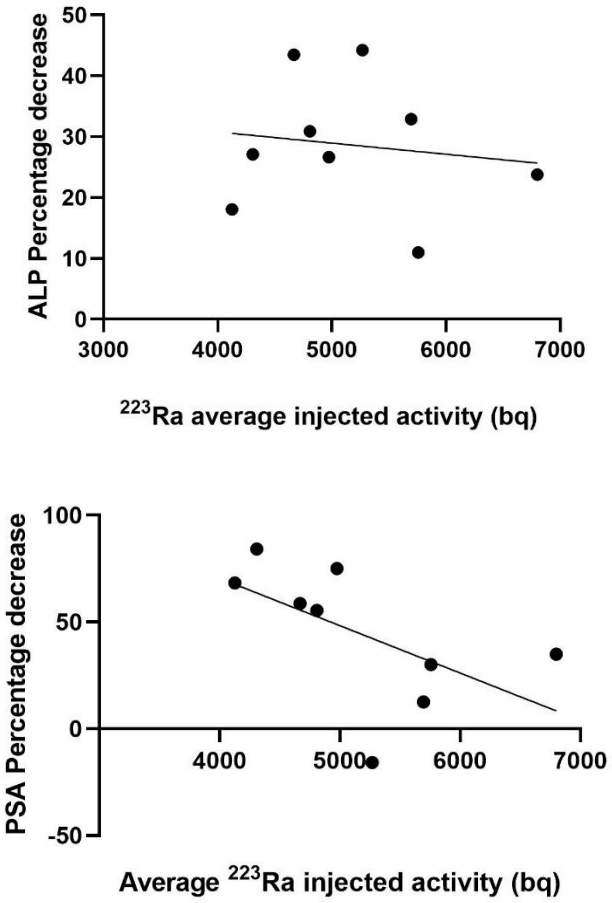

Figure 6.44 Prognostic markers.

Upper panel, the percentage change is described in terms of decrease for ALP. Lower panel percentage decrease of PSA. Negative values are reflective of patient value increase associated with poor response. Data included for 12 patients with the exclusion of Patient-12 due to extreme changes above 100%. ALP and PSA data was supplied for each sample collected by the ADRRAD clinical trial team

6.3 Discussion

The risk of toxicity in this study was primarily associated with acute toxicity following PBL depletion. This was thought to result from the period of mixed treatment whereby blood was exposed to both IMRT and ^{223}Ra. Any indication of this toxicity was considered to be a temporary effect and with IMRT completion, PBLs were expected to return rapidly to normal value range. Indeed, IMRT studies have shown to significantly decrease the number of PBLs in circulation (421, 422, 550). Lymphocytes radiation exposure and even low doses can significantly reduce the number of circulating PBL and sub-populations such as B-lymphocytes are more radiosensitive than T-lymphocytes (551). Lymphopenia induced during radiotherapy is associated with poor prognosis for varying cancer types including glioblastoma, small cell lung cancer and Cervical Cancer (552-556). It is thought that preventing drastic PBL loss may be associated with positive treatment outcome (As reviewed by Wang *et al.* 2020 (557)). This may relate to the central role of the immune system in cancer suppression as PBL mediate immunological mechanisms are critical for ongoing tumour suppression.

The 50% lethal dose for PBL is considered to be in the region of 1-2 Gy by radiotherapy administration (167). This consistent with the estimated dose delivered in the first two treatment cycles C1-C3 by IMRT exposure. In this study there was a drop of 68% for PBL counts by C3 as described in Figure 6.11. The larger decrease may be associated with the treatment fractionation over 7.5 weeks or alternatively from the additive effect of IMRT and ^{223}Ra combined treatment. Following IMRT completion the lymphocyte, neutrophil and total white blood cell count were found to remain low. It was originally thought that the 4 week break period between IMRT completion C3 and C4 sampling may provide a sufficient break for PBL repopulation from the BM. Indeed, radiotherapy studies have suggested white blood cell counts to increase within 6-8 weeks of therapy completion with a significant increase in lymphocyte population after 3 months (529, 558). In chapter 5, no significant increase in stable aberrant cells was observed along with no clonal cells. This suggesting no large immediate repopulation from the BM and/or slow repopulation with apparently normal cells assessed by M-FISH. In follow up samples there appears to be a larger cell population increase, therefore it may be that the cellular repopulation was slow or that ^{223}Ra resulted in a significant depletion of PBL in the circulatory pool between C4 and C6. The latter could result in a balanced death and repopulation scenario. In the case of slow repopulation this may also

be indicative of significant PBL exposure, although it cannot be solely attributed to ^{223}Ra, it could mean the treatment regime may result in long lasting toxicity to the bone marrow. Since this analysis was carried out, the full haematological counts have been published for the clinical trial. The haematological toxicities were reported as low with three patients out of thirty enrolled experienced grade 3 leucopenia, a single patient experienced grade 3 neutropenia and one other thrombocytopenia. The grade 3 haematological events described were reported as asymptomatic with no infections. The reported values compared the control sample collected to the first follow up sample (F1) and during the end of study follow up (F3).

Successful metastatic disease management was a key goal of the trial following ^{223}Ra treatment. The clinical trial team monitored bone scans during the treatment to monitor metastatic burden reduction (clinical data not collected as part of this study). The use of prognostic biomarkers has boomed over the years with several being proposed from readily available blood samples (as reviewed by Li *et al.* 2018 (547)). Most notably for prostate cancer patients, PSA has been recognised as a tumour marker for diagnostic and prognostic evaluation. Elevated levels of PSA followed by early biopsy collection have resulted in early prostate cancer detection even in asymptomatic patients (As reviewed by Constantinou and Feneley 2005 (559)). The increased detection of prostate cancer has also meant increased incidents but also improved the survival rates. Following radiotherapy treatment, the PSA levels usually drop with successful treatment outcome associated with maintained reduction in follow ups (As reviewed by Rukstalis 2002 (560)). The current cut off for initial diagnostic purposes is PSA is of 4 µg/l. It should be noted that the patients enrolled in this study had previously received chemotherapy docetaxel treatment and hormonal therapy for disease management, therefore, the cut off value of 4 µg/l is therefore not necessarily relevant, instead changes from the C1 sample were used for a simplistic assessment of treatment efficacy. By the last treatment cycle sampled, C6, the PSA values were observed to decrease for six patients. Of the patients that did not report decreased PSA values, Patient-6 reported a small increase with a similar value to C1 potentially indicating no PSA progression. In the treatment follow up samples, only two patients reported PSA increase with values higher than screening. Patient-2 PSA values increased from 0.31 µg/l at screening point to 2.70 µg/l in F1 follow up, however, this was a reported decrease from the sampled pre-treatment control C1 of 3.09 µg/l. The second patient experiencing elevated levels of PSA being Patient-12, whereby PSA levels increased from screening value of 0.22 µg/l to 53.55 µg/l sampled at F1. The high value in F1

sample suggesting PSA relapse for this patient. The reported changes occurred over time therefore the decreasing trends may be indicative of treatment accuracy, but caution should still be taken when assessing these. Although in this study PSA was discussed in terms of disease relapse, it cannot be excluded that changes in PSA may also be attributed to benign conditions induced from other medication or temporary inflammation.

Huggins and Hodges (1941 (561)) were the first to identify increased levels of ALP to be associated with bone metastatic disease. ALP is a bone specific marker associated with bone turnover (542-544), increased levels of ALP are associated with elevated bone formation by osteoblast activity during bone formation as well as bone resorption from osteoclasts. More recently elevated ALP at PC diagnosis has been associated with the presence of metastatic bone disease (545, 546). In our study ^{223}Ra administration was targeted for bone metastatic disease management, with decreasing metastatic disease burden ALP levels were thought to also decrease. For nine of ten patients, the ALP levels were found to decrease from pre-screening or pre-treatment control (C1) to later F1. Patient-12 was the only individual that did not display a decrease in ALP. The pre- treatment value of Patient-12 was of 100 µg/l increasing to 756 µg/l by F1 sampling. Patient-12 appears to be the only individual not responding to the treatment with both PSA and ALP results suggesting disease progression with no effect. It was found that the ^{223}Ra injected activity does not appear to significantly increase the number of aberrant cells (P=0.086) or aberration events (P=0.079) between C2 and C5. The aberration yield is associated with absorbed dose; therefore, a lower yield may indicate lower exposure. ALP levels were also not found to decrease further with increased injected activity, this suggesting lower administered doses to potentially be as effective. As no significant effect from higher ^{223}Ra activity was observed, it may suggest bone metastatic sites reaching a saturation point. Initial clinical trial for ^{223}Ra tested varying dose administrations of ^{223}Ra from 50 kBq/kg to 200 kBq/kg with lower dose of 50 kBq/kg resulting in similar decline in bone turn over markers (152-154). The dose of 55 kBq/kg being adopted after implementation of NIST update and this administered cyclically every 4 weeks for a total of 6 injections. The studies mentioned did not test lower doses and involved one single administration of ^{223}Ra. Therefore, a lower administered dose may have the similar effects while reducing the exposure of PBL during intravenous administration and reducing bowel exposure during excretion. This will need further evaluations potentially aided by bone scans able to detect changes to the bone metastatic load. This could indicate whether patients receiving higher injected activities indeed benefitted from the

higher dose. The dosing strategy currently does not take into account the metastatic burden and until this has been evaluated the dosing strategy can only be speculated upon.

Chapter 7: Discussion

CRPC is associated with poor prognosis and is currently uncurable. Upwards of 90% of patients with advanced disease present bone metastasis, these associated with acute symptoms such as severe pain, spinal fracture and spinal cord compression potentially resulting in paralysis (45). The treatment options available are tailored towards palliative care focusing on enhancing the quality of life and limiting suffering from disease progression. Current treatment options include chemotherapy, novel anti-hormonals and recently approved ^{223}Ra. The approval of ^{223}Ra was a big milestone as clinical trial ALSYMPCA determined significant improvement in the quality of life by delaying the onset of symptomatic skeletal related events, improving the quality of life and for the first time demonstrating an overall survival advantage with the use of ^{223}Ra. Although currently limited to CRPC use, ^{233}Ra has generated a great deal of interest for the potential application earlier in disease, for different cancer types and in paediatrics. Radiotherapies with α-particle emitters have the potential to be highly targeted treatments with high normal tissue sparing and hence minimal toxicity. However, uncertainties remain regarding the dose deposition at metastatic sites and whether BM cells in vicinity of target cells may be at risk of exposure. There are also further concerns as to the risks of combining ^{223}Ra with other treatments. The aim of this project was to resolve these uncertainties by assessing changes in the genomic structure of PBLs. PBLs may be in direct contact with ^{223}Ra in circulation as mature cells or as progenitor cell from exposed HSCs residing in BM sites, rendering these ideal cell models for cytogenetic analysis.

In this study, increased chromosomal aberration complexity was observed with ^{223}Ra treatment progression. The spectrum of chromosomal aberrations was used as a marker to distinguish cells exposed by ^{223}Ra from those exposed to IMRT. To do so, complex chromosomal aberrations associated with high LET exposure were used as a marker for ^{223}Ra exposure. Instead for IMRT, simple chromosomal aberrations were used as a marker, these consistent with low LET exposure. The frequency of complex chromosomal aberrations was observed to increase past the IMRT completion, suggesting ^{223}Ra as an inductor of complex chromosomal aberrations. This validating complex chromosomal aberrations as a potential marker for high LET exposure, particularly in cases where the exposure is unknown. To test this, a novel biodosymetric model based on the spectrum of aberration was proposed to measure the absorbed blood dose (here termed M-FISH$_{LET}$). This model was based on differentiating the populations of cells exposed to IMRT from those exposed to

^{223}Ra by the presence of complex chromosomal aberrations. The existing criticality model, usually applied to separate and quantify neutron and gamma exposures following a nuclear accident or incident, was then applied. The resulting dose estimates were compared to physically derived dose estimates also fed into the criticality model. The M-FISH$_{LET}$ dose estimates for ^{223}Ra were found to be larger than the physically derived models. One explanation for this may be that the M-FISH$_{LET}$ model may better account for the exposure of the circulatory pool (during the first 24 h transit period) and the exposure in vicinity of metastatic sites once ^{223}Ra is incorporated. Although this will need further verification, it may be possible for the spectrum of aberrations detected by M-FISH to provide an estimate of dose in the case of an unknown exposure.

The doses estimated here are themselves uncertain and as described, further work is needed to assess the proportion of complex aberrations following ^{223}Ra exposure and those potentially resulting from IMRT. To do so, samples may be needed from patients enrolled on ^{223}Ra only treatment to quantify the frequency of cells containing complex chromosomal aberrations. There are also limited cytogenetic studies following PC patients receiving IMRT treatment, for comparison it would be of use to evaluate aberration frequencies in patients with smaller field of exposure (prostate only) and larger including lymph nodes. In doing so it could be ascertained whether a proportion of complex aberrations in our study could be attributed to IMRT exposure, and if so, this could be accounted for in further analysis. Some other confounding effects were also not explored in our study, including the effect of hormone therapy which has been associated with increased level of spontaneous chromosomal aberrations in PBLs (562, 563). Although this remains debated (564), the frequency of aberrations may be increased and if repair pathways were also compromised, this may affect the spectrum of aberrations detected. The effect of chemotherapy on circulating PBLs also remains unknown. In our study, the initial PBL collected from C1-C3 resulted in poor metaphase yield and required extended culturing time and stimulation. This potentially being a delayed effect of chemotherapy whereby tubulin inhibitors such as docetaxel prevent cells from dividing *in vivo*, this may result in delayed PBL stimulation *in vitro*. In the case of delayed mitosis, this could result in preferential sampling of cells with less damage able to replicate. *In vitro* work should therefore be carried out to assess the combination of radiotherapy and chemical exposure. In doing so, changes in the mitotic rates could be assessed and the effect on chromosomal aberration frequency and spectrum quantified. Where possible, further studies

should also be carried out *in vivo* with patient cohorts not treated for hormonal therapy and/or chemotherapy.

The physical estimates presented for ^{223}Ra and IMRT are also themselves uncertain. The physical ^{223}Ra absorbed blood dose was estimated from existing pharmacokinetic clearance models (152-154) within the first 24 h of administration. However, these estimations were limited by a high uncertainty due to the median values selected from three publications, these presenting a high degree of interindividual variation. In future studies estimating ^{223}Ra absorbed blood dose, patient specific clearance data could be collected over the initial 24 h period. This establishing interindividual variations on a larger sample size and also enabling the use of patient specific clearance to model the absorbed blood dose. The values from the three publications used were limited by the low number of sampling times and a low patient number. As a result, a high uncertainty within the first 4 h of treatment in all publications was reported. By sampling at smaller intervals, a more accurate pharmacokinetic clearance model could be drawn. Lastly, all pharmacokinetic clearance model data was collected from a single ^{223}Ra administration; with disease progression it is unknown whether the normal clearance of the radionuclide from the blood is affected. If so, as the metastatic load decreases, there may be a reduced uptake in some patients, this resulting in a higher absorbed blood dose. The physical absorbed blood dose for IMRT was estimated by two models proposed by Moquet *et al.* (2018 (325)). As reported in Chapter 2, the uncertainties for these estimates remained high even following input from individual patient data. The models proposed by Moquet *et al.* did not consider lymph node dynamics and in future work this should be considered. Exposure to the lymph nodes poses uncertainties not just for dose estimation but also whether static PBLs may be exposed for a longer period of time during fractionated treatment, if so, this may increase the frequency of complex chromosomal aberrations. Indeed, previous study by Hartel *et al.* (2018 (369)) suggested PC patients with a larger field of exposure to have a higher frequency of complex chromosomal aberrations. There are few studies reporting chromosomal aberrations following IMRT treatment of PC patients and, to our knowledge, this is the first study assessing chromosomal aberrations as a result of ^{223}Ra treatment. To optimise the dose estimation model presented, data collected from patients received solely ^{223}Ra would be beneficial. Further studies on IMRT alone could also be used to expand on the LN dose estimates and gather C-Ratios for each independent treatment type.

M-FISH assay enabled the identification of chromosomal aberrations of stable and unstable kind. Unstable dicentric chromosomes were used in the criticality model to estimate IMRT/^{223}Ra dose. Due to their instability (hence inability to replicate successfully for multiple rounds) it was assumed that these dicentric chromosomes were present in PBLs exposed in the peripheral blood pool. This principle forming the basis of the gold standard dicentric assay (236). The formation of DSBs in two chromosomes usually has a 50% chance of resulting in a dicentric chromosome or a reciprocal translocation. A 1:1 ratio was therefore expected, and found, during the treatment cycles. In the later follow up samples of two patients, a deviation from the expected 1:1 was observed. Although the reason for this could not be confirmed it could suggest a faster clearance of unstable cells. Cells containing reciprocal translocations may instead persist in circulation as they are stable. The lymphocyte counts provided by the clinical team in Belfast suggest no further cell loss by the follow up sample collection. Instead, a small increase in counts was reported. On the contrary, the frequency of abnormal cells falls for both patients and this could also suggest dilution from new healthy cell repopulation. In this study, there was no indication of clonal cell expansion however, this does not suggest BM sparing. Existing BM models suggest a considerable proportion may be exposed in vicinity of metastatic sites (389, 431) to ^{223}Ra. The resulting BM cell death may cause a slower cellular repopulation, this potentially seen for some patients that did not recover to normal cell counts in F3 sample. Later timepoint past F3 will be needed to assess the risk of leukaemia following treatment. This analysis will be essential before rollout of treatment to patients with better prognosis or younger cohort of paediatric patients for other cancer treatment.

An increased rate of genomic instability may also be used to assess potential risk of secondary cancers. Chromatid aberrations are indicators of genomic instability which may be a result of direct exposure of precursor cells, delayed effects, or bystander effects. In this study, samples from three patients were assessed by solid stain analysis for the last treatment cycle C6, early follow up F1 and one year follow up F3. An increased frequency of chromatid aberrations was identified by F3. This potentially suggesting delayed effects or bystander effects at BM sites. Study by Lassmann and Nosske (2012 (389)) suggested a dose to the marrow in the region of 1.5 Gy based on ICRP Publication 67 (565), this consistent to the estimation in this study of 0.598 ± 0.008 to 0.944 ± 0.007 Gy per injection. In this study the dose to osteogenic cells was also estimated to be substantial at 4.963 ± 0.067 to 7.832 ± 0.062 Gy per administration. As the bone and BM niche are in tight communications, there may be a risk for bystander effects. Indeed *in vivo* study by Stephan *et al.*

(2005 (406)) following ^{224}Ra treatment use, reported an increased frequency of chromatid aberrations that were attributed to bystander effects. Another *in vivo* study of ^{224}Ra for radiotherapy, suggested a possible risk of leukaemia and solid tumours following exposure to ^{224}Ra (309). To date, only a handful of cases of secondary leukaemia have been identified following ^{223}Ra therapy administered as per ADRRAD clinical trial (432, 433, 566). Although no causative link has currently been found between ^{223}Ra treatment and secondary leukaemia, further investigation should be carried out where samples may be collected at a later date to assess the potential for delayed late effects which could occur many years after treatment (93, 95, 374-377, 422, 529).

Exposure of non-cancerous cells and tissues surrounding the tumours is of concern in all radiotherapeutic treatments due to the risk of acute toxicity. In this study, the haematological toxicity risk was deemed low with most patients recovering by end of treatment and ADRRAD clinical trial team have reported low risk across the thirty patients studied. The risk for BM toxicity remains as symptoms could be delayed. Further risks such as those following blood vessel and bowel exposure remain unknown. Although the dose to these could potentially be low, prolonged inflammatory responses could result in increased risks of other diseases. To limit the toxicity risks, the dosing strategy may need re-evaluating. Initial data following ALP and PSA assessment, although limited, suggests lower administer activity of ^{223}Ra to be as effective as higher activities. The current dosing strategy is based on the patients weight and not metastatic burden; therefore, further analysis is needed to assess whether patients of larger weight had a similar metastatic burden to those of lower weight. The metastatic burden may be estimated from patient bone scans throughout treatment, this enabling true comparison between patients and also monitoring of metastatic bone reduction. Although PSA and ALP markers are useful for a simplistic assessment, they may not truly represent markers for treatment outcome. Indeed, PSA levels may be elevated following previous medication use or as a response to inflammatory prostate disease, which may be triggered from radiotherapy treatment. Although in the control samples there were no indications of elevated unstable chromosomal aberrations consistent with previous radiotherapy, PSA and ALP are not reliable markers alone. Further markers to evaluate treatment outcome were not available for analysis. The collection of other serum markers for bone disease progression such as prostatic acid phosphatase, hK2 (same family as PSA), Insulin-like growth factor-1, transforming growth factor-β1 and many more could be collected/ monitored through the treatment to further assess the outcome. Bone scans will also be of interest to monitor changes in size and number of

metastatic sites further elucidating the individual response to varying ^{223}Ra administered. In the ADRRAD clinical trial toxicity to ^{223}Ra (with subsequent discontinuation of treatment) was indicated by larger drops of normal blood cell counts. The blood cell counts, and ALP changes were collected by the ADDRAD clinical team and have since been published by Turner *et al.* (2021 (567)) finding low toxicity across the 30 patients recruited.

In conclusion, this patient group presented a unique opportunity to address important radiobiological research questions pertaining to the cellular and tissue level damage associated with ^{223}Ra. This study is the first to demonstrate non-target exposure of the blood by cytogenetic assessment. Increased frequencies of chromatid aberrations associated with delayed effects suggests potential concerns for delayed toxicity or malignancies. Although initial trial outputs indicate low haematological toxicity, further work will be essential to ensure safe rollout of the treatment to other patient groups. Preliminary data suggests the dosing strategy may need re-evaluating, as patients administered a lower activity responded just as well as those administered a higher activity. A reduced administered activity has the potential to reduce common radiotherapy side effects and the risk of delayed toxicities, therefore the dosing strategy will need exploring further. As the ADRRAD patient cohort was exposed in a unique mixed exposure scenario, it enabled the application of existing blood dosimetry models and the testing of the novel M-FISH$_{LET}$ model for an initial dose assessment of both ^{223}Ra and IMRT. Although limitations were present for all models described, the novel M-FISH$_{LET}$ model may provide a way of estimating dose following an unknown exposure. This having applicability in radiation protection following nuclear accident or incident. Quantifying the absorbed dose to non-target tissues was also an important step in evaluating the potential short and longer-term secondary radiation risks for patients. With further considerations, these estimates will ultimately contribute towards maximising clinical efficacy.

References

1. Prostate cancer incidence statistics [Internet].; 2017 [cited Dec 18, 2020]. Available from: https://www.cancerresearchuk.org/health-professional/cancer-statistics/statistics-by-cancer-type/prostate-cancer/incidence.

2. Sung H, Ferlay J, Siegel RL, Laversanne M, Soerjomataram I, Jemal A, et al. Global Cancer Statistics 2020: GLOBOCAN Estimates of Incidence and Mortality Worldwide for 36 Cancers in 185 Countries. CA: a cancer journal for clinicians. 2021 May;71(3):209-49.

3. Bray F, Ferlay J, Soerjomataram I, Siegel RL, Torre LA, Jemal A. Global cancer statistics 2018: GLOBOCAN estimates of incidence and mortality worldwide for 36 cancers in 185 countries. CA Cancer J Clin. 2018 -11;68(6):394-424.

4. NICE Guideline Updates Team (UK). Prostate cancer: diagnosis and management. 131st ed. London: National Institute for Health and Care Excellence (UK); 2019.

5. Rawla P. Epidemiology of Prostate Cancer. World journal of oncology. 2019;10(2):63-89.

6. Giri VN, Knudsen KE, Kelly WK, Abida W, Andriole GL, Bangma CH, et al. Role of Genetic Testing for Inherited Prostate Cancer Risk: Philadelphia Prostate Cancer Consensus Conference 2017. J Clin Oncol. 2018 -2-1;36(4):414-24.

7. Hjelmborg JB, Scheike T, Holst K, Skytthe A, Penney KL, Graff RE, et al. The Heritability of Prostate Cancer in the Nordic Twin Study of Cancer. Cancer Epidemiol Biomarkers Prev. 2014 -11-01 00:00:00;23(11):2303-10.

8. Damber J, Aus G. Prostate cancer. The Lancet. 2008 /05/17;371(9625):1710-21.

9. Grönberg H. Prostate cancer epidemiology. Lancet. 2003 -03-08;361(9360):859-64.

10. Thompson IM, Tangen CM, Tolcher A, Crawford ED, Eisenberger M, Moinpour CM. Association of African-American Ethnic Background With Survival in Men With Metastatic Prostate Cancer. JNCI: Journal of the National Cancer Institute. 2001 February 7,;93(3):219-25.

11. Damber JE. Prostate cancer: epidemiology and risk factors. Curr Opin Urol. 1998 -09;8(5):375-80.

12. Cancer incidence for common cancers [Internet].; 2018 [updated 23 Jan; cited 10/04/2018]. Available from: http://www.cancerresearchuk.org/health-professional/cancer-statistics/incidence/common-cancers-compared#heading-One.

13. About prostate cancer [Internet].; 2017 [updated July;]. Available from: https://prostatecanceruk.org/prostate-information/about-prostate-cancer.

14. Riihimäki M, Thomsen H, Brandt A, Sundquist J, Hemminki K. What Do Prostate Cancer Patients Die Of? Oncologist. 2011 -2;16(2):175-81.

15. Barry MJ. Screening for Prostate Cancer -- The Controversy That Refuses to Die. The New England Journal of Medicine. 2009 Mar 26,;360(13):1351-4.

16. Dandapani SV, PhD, Sanda MG, MD. Measuring Health-Related Quality of Life Consequences From Primary Treatment for Early-Stage Prostate Cancer. Seminars in radiation oncology. 2008;18(1):67-72.

17. Jani AB, Hellman S. Early prostate cancer: clinical decision-making. The Lancet. 2003 March 22,;361(9362):1045-53.

18. Conran CA, Brendler CB, Xu J. Personalized prostate cancer care: from screening to treatment. Asian journal of andrology. 2016 Jul;18(4):505-8.

19. Phillips JM, Crawford ED. Prostate-specific antigen (PSA) screening: has the pendulum swung too far? Asian Journal of Andrology. 2011 Sep;13(5):655-6.

20. Sim HG, Cheng C. What is the optimum PSA screening interval after an initial negative test? Nature Clinical Practice Urology. 2008 Mar;5(3):134-5.

21. Peres J. New PSA Guidelines Discourage Overscreening. Journal of the National Cancer Institute. 2012;104(1):8-9.

22. Cooper GM. The Development and Causes of Cancer. In: The Cell: A Molecular Approach. 2nd edition. Sinauer Associates; 2000.

23. Feitelson MA, Arzumanyan A, Kulathinal RJ, Blain SW, Holcombe RF, Mahajna J, et al. Sustained proliferation in cancer: mechanisms and novel therapeutic targets. Semin Cancer Biol. 2015 -12;35(Suppl):S25-54.

24. Witsch E, Sela M, Yarden Y. Roles for growth factors in cancer progression. Physiology (Bethesda). 2010 -04;25(2):85-101.

25. Hanahan D, Weinberg R. Hallmarks of Cancer: The Next Generation. Cell. 2011;144(5):646-74.

26. Coussens LM, Werb Z. Inflammation and cancer. Nature. 2002 -12-19;420(6917):860-7.

27. Hanahan D, Weinberg RA. The hallmarks of cancer. Cell. 2000 Jan 7,;100(1):57.

28. Yao Y, Dai W. Genomic Instability and Cancer. J Carcinog Mutagen. 2014;5.

29. Abbas T, Keaton MA, Dutta A. Genomic Instability in Cancer. Cold Spring Harbor perspectives in biology. 2013 Mar 1,;5(3):a012914.

30. Negrini S, Gorgoulis VG, Halazonetis TD. Genomic instability - an evolving hallmark of cancer. Nature reviews. Molecular cell biology. 2010 Mar;11(3):220-8.

31. Shah RB, Zhou M. Prostate Biopsy Interpretation. Cham: Springer International Publishing AG; 2019.

32. Baig FA, Hamid A, Mirza T, Syed S. Ductal and Acinar Adenocarcinoma of Prostate: Morphological and Immunohistochemical Characterization. Oman Med J. 2015 -5;30(3):162-6.

33. Jing Li Zhe Wang. The pathology of unusual subtypes of prostate cancer. Chinese journal of cancer research. 2016;28(1):130-43.

34. Ito K, Yamamoto T, Ohi M, Takechi H, Kurokawa K, Suzuki K, et al. Cumulative probability of PSA increase above 4.0 NG/ML in population-based screening for prostate cancer. Int J Cancer. 2004 -04-10;109(3):455-60.

35. Adhyam M, Gupta AK. A Review on the Clinical Utility of PSA in Cancer Prostate. Indian journal of surgical oncology. 2012 Mar 3,;3(2):120-9.

36. Diamandis EP, Yu H. NONPROSTATIC SOURCES OF PROSTATE-SPECIFIC ANTIGEN. Urologic Clinics of North America. 1997 May 1,;24(2):275-82.

37. Pezaro C, Woo HH, Davis ID. Prostate cancer: measuring PSA. Internal Medicine Journal. 2014;44(5):433-40.

38. Croswell JM, Kramer BS, Crawford ED. Screening for prostate cancer with PSA testing: current status and future directions. Oncology (Williston Park, N.Y.). 2011 May;25(6):452-63.

39. Ni Chen Qiao Zhou. The evolving Gleason grading system. 中国癌症研究：英文版. 2016;28(1):58-64.

40. Ahmed HU, Arya M, Freeman A, Emberton M. Do low-grade and low-volume prostate cancers bear the hallmarks of malignancy? The Lancet Oncology. 2012 /11/01;13(11):e509-17.

41. Schröder FH, Hermanek P, Denis L, Fair WR, Gospodarowicz MK, Pavone-Macaluso M. The TNM classification of prostate cancer. The Prostate. 1992;21(S4):129-38.

42. Frederick L, Greene, David L. Page, Irvin D. Fleming, April G. Fritz, Charles M. Balch, Daniel G. Haller, Monica Morrow. AJCC Cancer Staging Manual . 7th ed. Chicago: AMERICAN JOINT COMMITTEE ON CANCER; 2010.

43. Nørgaard M, Jensen AØ, Jacobsen JB, Cetin K, Fryzek JP, Sørensen HT. Skeletal Related Events, Bone Metastasis and Survival of Prostate Cancer: A Population Based Cohort Study in Denmark (1999 to 2007). Journal of Urology, The. 2010;184(1):162-7.

44. Howard LE, De Hoedt AM, Aronson WJ, Kane CJ, Amling CL, Cooperberg MR, et al. Do skeletal-related events predict overall survival in men with metastatic castration-resistant prostate cancer? Prostate Cancer and Prostatic Diseases. 2016 Dec;19(4):380-4.

45. Saad F, Ivanescu C, Phung D, Loriot Y, Abhyankar S, Beer TM, et al. Skeletal-related events significantly impact health-related quality of life in metastatic castration-resistant prostate cancer: data from PREVAIL and AFFIRM trials. Prostate Cancer and Prostatic Diseases. 2017 Mar;20(1):110-6.

46. Carmona Echeverria LM, Drudge-Coates L, Wilkins CJ, Muir GH. Bone Scan Is of Doubtful Value as a First Staging Test in the Primary Presentation of Prostate Cancer. ISRN Oncology. 2012 /11/05;2012:e585017.

47. Cecchini MG, Wetterwald A, Pluijm Gvd, Thalmann GN. Molecular and Biological Mechanisms of Bone Metastasis. EAU Update Series. 2005 December 1,;3(4):214-26.

48. Wong SK, Mohamad N, Giaze TR, Chin K, Mohamed N, Ima-Nirwana S. Prostate Cancer and Bone Metastases: The Underlying Mechanisms. Int J Mol Sci. 2019 -5-27;20(10).

49. Bussard KM, Gay CV, Mastro AM. The bone microenvironment in metastasis; what is special about bone? Cancer Metastasis Rev. 2008 -03;27(1):41-55.

50. Macedo F, Ladeira K, Pinho F, Saraiva N, Bonito N, Pinto L, et al. Bone metastases: an overview. Oncology reviews. 2017 May 9,;11(1):321.

51. Paget S. THE DISTRIBUTION OF SECONDARY GROWTHS IN CANCER OF THE BREAST. The Lancet. 1889 March 23,;133(3421):571-3.

52. Roberto Tamma, Tiziana Annese, Domenico Ribatti. The Role of Bone Stem Cell Niches in Bone Metastasis. Applied sciences. 2020 Oct 1,;10(7713):7713.

53. Saki N, Abroun S, Farshdousti Hagh M, Asgharei F. Neoplastic bone marrow niche: hematopoietic and mesenchymal stem cells. Cell journal (Yakhteh). 2011;13(3):131-6.

54. Bagi CM. Skeletal implications of prostate cancer. J Musculoskelet Neuronal Interact. 2003 -06;3(2):112-7.

55. Tamma R, Ribatti D. Bone Niches, Hematopoietic Stem Cells, and Vessel Formation. Int J Mol Sci. 2017 -1-13;18(1).

56. Roodman GD. Mechanisms of Bone Metastasis. The New England Journal of Medicine. 2004 Apr 15,;350(16):1655-64.

57. Clarke B. Normal Bone Anatomy and Physiology. Clin J Am Soc Nephrol. 2008 -11;3(Suppl 3):S131-9.

58. Morris MJ, Scher HI. Clinical approaches to osseous metastases in prostate cancer. Oncologist. 2003;8(2):161-73.

59. Westendorf JJ, Kahler RA, Schroeder TM. Wnt signaling in osteoblasts and bone diseases. Gene. 2004 -10-27;341:19-39.

60. Sone T, Tamada T, Jo Y, Miyoshi H, Fukunaga M. Analysis of three-dimensional microarchitecture and degree of mineralization in bone metastases from prostate cancer using synchrotron microcomputed tomography. Bone. 2004 August 1,;35(2):432-8.

61. Tamada T, Sone T, Jo Y, Imai S, Kajihara Y, Fukunaga M. Three-dimensional trabecular bone architecture of the lumbar spine in bone metastasis from prostate cancer: comparison with degenerative sclerosis. Skeletal Radiol. 2005 Mar;34(3):149-55.

62. Clarke NW, Hart CA, Brown MD. Molecular mechanisms of metastasis in prostate cancer. Asian journal of andrology. 2009 Jan;11(1):57-67.

63. Carpenter RS, Marbourg JM, Brennan FH, Mifflin KA, Hall JCE, Jiang RR, et al. Spinal cord injury causes chronic bone marrow failure. Nat Commun. 2020 -07-24;11(1):1-13.

64. Kimura T. Multidisciplinary Approach for Bone Metastasis: A Review. Cancers (Basel). 2018 -5-24;10(6).

65. Huang J, Shen J, Li X, Rengan R, Silvestris N, Wang M, et al. Incidence of patients with bone metastases at diagnosis of solid tumors in adults: a large population-based study. Ann Transl Med. 2020 -4;8(7).

66. Seyfried TN, Huysentruyt LC. On the Origin of Cancer Metastasis. Crit Rev Oncog. 2013;18(1-2):43-73.

67. OGAWA M. Differentiation and proliferation of hematopoietic stem cells. Blood. 1993;81(11):2844-53.

68. Ogawa M, Porter PN, Nakahata T. Renewal and commitment to differentiation of hemopoietic stem cells (an interpretive review). Blood. 1983 -05;61(5):823-9.

69. Samuel H. Cheshier, Sean J. Morrison, Xinsheng Liao, Irving L. Weissman. In vivo Proliferation and Cell Cycle Kinetics of Long-Term Self-Renewing Hematopoietic Stem Cells. Proceedings of the National Academy of Sciences of the United States of America. 1999 Mar 16,;96(6):3120-5.

70. Catlin SN, Busque L, Gale RE, Guttorp P, Abkowitz JL. The replication rate of human hematopoietic stem cells in vivo. Blood. 2011 -4-28;117(17):4460-6.

71. Tao Cheng, Neil Rodrigues, Hongmei Shen, Yong-guang Yang, David Dombkowski, Megan Sykes, et al. Hematopoietic Stem Cell Quiescence Maintained by p21cip1/waf1. Science. 2000 Mar 10,;287(5459):1804-8.

72. Arai F, Hirao A, Ohmura M, Sato H, Matsuoka S, Takubo K, et al. Tie2/Angiopoietin-1 Signaling Regulates Hematopoietic Stem Cell Quiescence in the Bone Marrow Niche. Cell. 2004;118(2):149-61.

73. Seshadri M, Qu C. Microenvironmental Regulation of Hematopoietic Stem Cells and Its Implications in Leukemogenesis. Curr Opin Hematol. 2016 -7;23(4):339-45.

74. Janeway C. Immunobiology: The Immune System in Health and Disease.
. In: Immunobiology. 6. ed. ed. New York, NY [u.a.]: Garland Science; 2005.

75. Stirewalt DL, Radich JP. The role of FLT3 in haematopoietic malignancies. Nature reviews. Cancer. 2003 Sep;3(9):650-65.

76. Pido-Lopez J, Imami N, Aspinall R. Both age and gender affect thymic output: more recent thymic migrants in females than males as they age. Clinical & Experimental Immunology. 2001 Sep;125(3):409-13.

77. Wilson J, Alberts B. Lymphocytes and the Cellular Basis of Adaptive Immunity. In: Molecular Biology of the Cell. 5th ed. New York, NY [u.a.]: Taylor and Francis, Garland; 2008.

78. Parker C, Finkelstein SE, Michalski JM, O'Sullivan JM, Bruland Ø, Vogelzang NJ, et al. Efficacy and Safety of Radium-223 Dichloride in Symptomatic Castration-resistant Prostate Cancer Patients With or Without Baseline Opioid Use From the Phase 3 ALSYMPCA Trial. European Urology. 2016;70(5):875-83.

79. Parker C, Nilsson S, Heinrich D, Helle SI, O'Sullivan JM, Fosså SD, et al. Alpha emitter radium-223 and survival in metastatic prostate cancer. The New England journal of medicine. 2013 Jul 18,;369(3):213.

80. Parker C, Heinrich D, O'Sullivan JM, Fossa SD, Chodacki A, Demkow T, et al. Overall survival benefit and safety profile of radium-223 chloride, a first-in-class alpha-pharmaceutical: Results from a phase III randomized trial (ALSYMPCA) in patients with castration-resistant prostate cancer (CRPC) with bone metastases. Journal of Clinical Oncology. 2012 Feb 10,;30(5_suppl):8.

81. Becker A, Tennstedt P, Hansen J, Trinh Q, Kluth L, Atassi N, et al. Functional and oncological outcomes of patients aged

82. Twiss C, Slova D, Lepor H. Outcomes for men younger than 50 years undergoing radical prostatectomy. Urology (Ridgewood, N.J.). 2005;66(1):141-6.

83. Freedland SJ, Presti JC, Kane CJ, Aronson WJ, Terris MK, Dorey F, et al. Do younger men have better biochemical outcomes after radical prostatectomy? Urology. 2004 March 1,;63(3):518-22.

84. Zincke H, Oesterling JE, Blute ML, Bergstralh EJ, Myers RP, Barrett DM. Long-Term (15 Years) Results After Radical Prostatectomy For Clinically Localized (Stage T2c Or Lower) Prostate Cancer. The Journal of Urology. 1994 November 1,;152(5, Part 2):1850-7.

85. Long-Term Oncological Outcomes for Young Men Undergoing Radical Prostatectomy for Localized Prostate Cancer [Internet].: Hindawi; 2017 [updated /02/19; cited Nov 27, 2020]. Available from: https://www.hindawi.com/journals/bmri/2017/9858923/.

86. Stish BJ, Davis BJ, Mynderse LA, McLaren RH, Deufel CL, Choo R. Low dose rate prostate brachytherapy. Translational andrology and urology. 2018 Jun;7(3):341-56.

87. Brachytherapy for Cancer - National Cancer Institute [Internet].; 2018 [updated 05/01/ - 08:00; cited Jul 19, 2021]. Available from: https://www.cancer.gov/about-cancer/treatment/types/radiation-therapy/brachytherapy.

88. Arthur T. Porter, John C. Blasko, Peter D. Grimm, Sarada M. Reddy, Haakon Ragde. Brachytherapy for Prostate Cancer. CA Cancer. 1995 May-June;45(3):165-78.

89. Peschel RE, Colberg JW, Chen Z, Nath R, Wilson LD. Iodine 125 versus palladium 103 implants for prostate cancer: clinical outcomes and complications. Cancer J. 2004 May-Jun;10(3):170-4.

90. Buron C, Ph.D, Le Vu B, M.D, Cosset J, M.D, Pommier, Pascal, M.D., Ph.D, Peiffert D, M.D, Delannes M, M.D, et al. Brachytherapy versus prostatectomy in localized prostate cancer: Results of a French multicenter prospective medico-economic study. International journal of radiation oncology, biology, physics. 2007;67(3):812-22.

91. Sharkey J, Cantor A, Solc Z, Huff W, Chovnick S, Behar R, et al. Brachytherapy versus radical prostatectomy in patients with clinically localized prostate cancer. Curr Urol Rep. 2002 May;3(3):250-7.

92. Hurwitz M. Combined External Beam Radiotherapy and Brachytherapy for the Management of Prostate Cancer. Oncology & Hematology Review (US). 2006:29.

93. Vlachaki MT, Teslow TN, Amosson C, Uy NW, Ahmad S. IMRT versus conventional 3DCRT on prostate and normal tissue dosimetry using an endorectal balloon for prostate immobilization. Med Dosim. 2005;30(2):69-75.

94. Guckenberger M, Ok S, Polat B, Sweeney R, Flentje M. Toxicity after Intensity-Modulated, Image-Guided Radiotherapy for Prostate Cancer. Strahlenther Onkol. 2010 Oct;186(10):535-43.

95. Doležel M-, Odrážka K-, Vaňásek J, Štuk J, Hlávka A, Vítková M, et al. Long-Term Clinical Results of IGRT in Prostate Cancer Treatment. Klin Onkol. 2020;33(1):49-54.

96. Shearer RJ, Davies JH, Gelister JSK, Dearnaley DP. Hormonal Cytoreduction and Radiotherapy for Carcinoma of the Prostate. British Journal of Urology. 1992;69(5):521-4.

97. Padhani AR, MacVicar AD, Gapinski CJ, Dearnaley DP, Parker GJM, Suckling J, et al. Effects of Androgen Deprivation on Prostatic Morphology and Vascular Permeability Evaluated with MR Imaging. Radiology. 2001 February 1,;218(2):365-74.

98. Yang FE, Chen GTY, Ray P, Vaida F, Chiru P, Hamilton RJ, et al. The potential for normal tissue dose reduction with neoadjuvant hormonal therapy in conformal treatment planning for stage C prostate cancer. International journal of radiation oncology, biology, physics. 1995;33(5):1009-17.

99. Forman JD, Kumar R, Haas G, Montie J, Porter AT, Mesina CF. Neoadjuvant Hormonal Downsizing of Localized Carcinoma of the Prostate: Effects on the Volume of Normal Tissue Irradiation. null. 1995 January 1,;13(1):8-15.

100. Zelefsky MJ, Leibel SA, Burman CM, Kutcher GJ, Harrison A, Happersett L, et al. Neoadjuvant hormonal therapy improves the therapeutic ratio in patients with bulky prostatic cancer treated with three-dimensional conformal radiation therapy. International Journal of Radiation Oncology*Biology*Physics. 1994 July 1,;29(4):755-61.

101. Gandaglia G, Karakiewicz PI, Briganti A, Passoni NM, Schiffmann J, Trudeau V, et al. Impact of the Site of Metastases on Survival in Patients with Metastatic Prostate Cancer. Eur Urol. 2015 -08;68(2):325-34.

102. James ND, Spears MR, Clarke NW, Dearnaley DP, De Bono JS, Gale J, et al. Survival with Newly Diagnosed Metastatic Prostate Cancer in the "Docetaxel Era": Data from 917 Patients in the Control Arm of the STAMPEDE Trial (MRC PR08, CRUK/06/019). Eur Urol. 2015 -06;67(6):1028-38.

103. Sneller ZW, Hop WCJ, Carpentier PJ, Schröder FH. Prognosis and Prostatic Volume Changes During Endocrine Management of Prostate Cancer: A Longitudinal Study. The Journal of Urology. 1992 March 1,;147(3, Part 2):962-6.

104. Saad F, Hotte SJ. Guidelines for the management of castrate-resistant prostate cancer. Canadian Urological Association journal = Journal de l'Association des urologues du Canada. 2010 Dec;4(6):380-4.

105. James ND, Sydes MR, Clarke NW, Mason MD, Dearnaley DP, Spears MR, et al. Addition of docetaxel, zoledronic acid, or both to first-line long-term hormone therapy in prostate cancer (STAMPEDE): survival results from an adaptive, multiarm, multistage, platform randomised controlled trial. Lancet. 2016 -03-19;387(10024):1163-77.

106. Sweeney CJ, Chen Y, Carducci M, Liu G, Jarrard DF, Eisenberger M, et al. Chemohormonal Therapy in Metastatic Hormone-Sensitive Prostate Cancer. N Engl J Med. 2015 -08-20;373(8):737-46.

107. Sandler HM, Hu C, Rosenthal SA, Sartor O, Gomella LG, Amin M, et al. A phase III protocol of androgen suppression (AS) and 3DCRT/IMRT versus AS and 3DCRT/IMRT followed by chemotherapy (CT) with docetaxel and prednisone for localized, high-risk prostate cancer (RTOG 0521). JCO. 2015 June 20,;33(18_suppl):LBA5002-.

108. Fizazi K, Faivre L, Lesaunier F, Delva R, Gravis G, Rolland F, et al. Androgen deprivation therapy plus docetaxel and estramustine versus androgen deprivation therapy alone for high-risk localised prostate cancer (GETUG 12): a phase 3 randomised controlled trial. Lancet Oncol. 2015 -07;16(7):787-94.

109. James ND, Sydes MR, Mason MD, Clarke NW, Dearnaley DP, Spears MR, et al. Docetaxel and/or zoledronic acid for hormone-naïve prostate cancer: first overall survival results from STAMPEDE (NCT00268476). Journal of clinical oncology. 2015 May 20,;33(15_suppl):5001.

110. Tannock IF, de Wit R, Berry WR, Horti J, Pluzanska A, Chi KN, et al. Docetaxel plus Prednisone or Mitoxantrone plus Prednisone for Advanced Prostate Cancer. The New England Journal of Medicine. 2004 Oct 7,;351(15):1502-12.

111. Hwang C. Overcoming docetaxel resistance in prostate cancer: a perspective review. Ther Adv Med Oncol. 2012 -11;4(6):329-40.

112. Seruga B, Ocana A, Tannock IF. Drug resistance in metastatic castration-resistant prostate cancer. Nat Rev Clin Oncol. 2011 -01;8(1):12-23.

113. Galletti E, Magnani M, Renzulli ML, Botta M. Paclitaxel and docetaxel resistance: molecular mechanisms and development of new generation taxanes. ChemMedChem. 2007 -07;2(7):920-42.

114. Sgouros G, Bodei L, McDevitt MR, Nedrow JR. Radiopharmaceutical therapy in cancer: clinical advances and challenges. Nature reviews. Drug discovery. 2020 Sep;19(9):589-608.

115. De Vincentis G, Gerritsen W, Gschwend JE, Hacker M, Lewington V, O'Sullivan JM, et al. Advances in targeted alpha therapy for prostate cancer. Ann Oncol. 2019 -11-01;30(11):1728-39.

116. Parker C, Lewington V, Shore N, Kratochwil C, Levy M, Lindén O, et al. Targeted Alpha Therapy, an Emerging Class of Cancer Agents: A Review. JAMA Oncol. 2018 -12-01;4(12):1765-72.

117. Elgqvist J, Frost S, Pouget J, Albertsson P. The Potential and Hurdles of Targeted Alpha Therapy – Clinical Trials and Beyond. Front Oncol. 2014;0.

118. 68Ga-DOTA-FAPI and 177Lu-DOTA-FAPI Theranostic Pair in Patients With Various Types of Cancer (Locally Advanced or Metastatic Cancer). 2021 April 15,.

119. Ph.D JLS. First-in-human Study of the Theranostic Pair [68Ga]Ga DOTA-5G and [177Lu]Lu DOTA-ABM-5G in Pancreatic Cancer. 2021 March 22,.

120. 177Lu-PSMA-I&T PSMA Radioligand Therapy in Metastatic Castration-Resistant Prostate Cancer. 2019 December 4,.

121. MS, Pashtoon Murtaza Kasi, MD. Immunotherapy Combined With Yttrium-90 RadioEmbolization in the Treatment of Colorectal Cancer With Liver Metastases [iRE-C - Clinical Trial]. 2021 June 7,.

122. Radioembolization for HCC Patients With Personalized Yttrium-90 Dosimetry for Curative Intent (RAPY90D). 2020 March 28,.

123. MD PMH. Yttrium-90 Radiation Segmentectomy Versus Stereotactic Body Radiation Therapy (SBRT) for the Treatment of Early Stage Hepatocellular Carcinoma (HCC): A Pilot Study. 2020 July 28,.

124. A Phase 1, Open-label, First-in-human, Multi-center, Study to Evaluate the Safety, Tolerability, Pharmacokinetics, and Anti-tumor Activity of a Thorium-227 Labeled Antibody-chelator Conjugate, BAY 2315497 Injection Alone, and in Combination With Darolutamide (BAY 1841788), in Patients With Metastatic Castration Resistant Prostate Cancer. NIH U.S. National Library of Medicine: ClinicalTrials.gov; 2021 June 18,.

125. An Open-label, First-in-human, Multi-center Study to Evaluate the Safety, Tolerability, Pharmacokinetics and Anti-tumor Activity of a Thorium-227 Labeled Antibody-chelator Conjugate, BAY2287411 Injection, in Patients With Solid Tumors Known to Express Mesothelin. 2021 July 16,.

126. Open-label, Non-randomized Phase 1, Multicenter Study to Assess Radium- 223 Biodistribution in Participants With Bone Metastatic Castration Resistant Prostate Cancer (CRPC) Receiving Radium-223 Dichloride Treatment. 2021 June 14,.

127. Phase II Trial of Radium-223 Dichloride in Combination With Paclitaxel in Patients With Bone Metastatic Breast Cancer. 2021 July 2,.

128. Radium-223 Combined With Dexamethasone as First-line Therapy in Patients With Metastatic Castrate Resistant Prostate Cancer. 2021 April 16,.

129. A Phase I/II Study Evaluating Escalating Doses of 211At-Labeled Anti-CD45 MAb BC8-B10 (211At-BC8-B10) Followed by Related Haplo-Identical Allogeneic Hematopoietic Cell Transplantation for High-Risk Acute Leukemia or Myelodysplastic Syndrome (MDS). 2021 June 7,.

130. Navalkissoor S, Grossman A. Targeted Alpha Particle Therapy for Neuroendocrine Tumours: The Next Generation of Peptide Receptor Radionuclide Therapy. NEN. 2019;108(3):256-64.

131. Kunikowska J, Królicki L. Targeted α-Emitter Therapy of Neuroendocrine Tumors. Seminars in nuclear medicine. 2020 Mar;50(2):171-6.

132. Delpassand E, Tworowska I, Esfandiari R, Torgue J, Hurt JD, Nunez R. Phase I dose-escalation study of AlphaMedix for targeted-alpha-emitter therapy of PRRT-naive neuroendocrine patients. JCO. 2021 May 20,;39(15_suppl):4117-.

133. Petersen LJ, Lund L, Jønler M, Jakobsen M, Abrahamsen J. Samarium-153 treatment of bone pain in patients with metastatic prostate cancer. Dan Med Bull. 2010 -06;57(6):A4154.

134. Palmedo H, Manka-Waluch A, Albers P, Schmidt-Wolf IGH, Reinhardt M, Ezziddin S, et al. Repeated bone-targeted therapy for hormone-refractory prostate carcinoma: tandomized phase II trial with the new, high-energy radiopharmaceutical rhenium-188 hydroxyethylidenediphosphonate. J Clin Oncol. 2003 -08-01;21(15):2869-75.

135. Quirijnen JM, Han SH, Zonnenberg BA, de Klerk JM, van het Schip, A. D., van Dijk A, et al. Efficacy of rhenium-186-etidronate in prostate cancer patients with metastatic bone pain. J Nucl Med. 1996 -09;37(9):1511-5.

136. Porter AT. Strontium-89 (Metastron) in the treatment of prostate cancer metastatic to bone. Eur Urol. 1994;26 Suppl 1:20-5.

137. FURUBAYASHI N, NEGISHI T, URA S, HIRAI Y, NAKAMURA M. Palliative effects and adverse events of strontium-89 for prostate cancer patients with bone metastasis. Molecular and Clinical Oncology. 2015 Jan;3(1):257-63.

138. Kossman SE, Weiss MA. Acute myelogenous leukemia after exposure to strontium-89 for the treatment of adenocarcinoma of the prostate. Cancer. 2000;88(3):620-4.

139. Prestwich R, Bottomley D. Acute Myeloid Leukaemia following Strontium-89. Clinical Oncology. 2003 /10/01;15(7):441.

140. Dolezal J, Vizda J, Odrazka K. Prospective Evaluation of Samarium-153-EDTMP Radionuclide Treatment for Bone Metastases in Patients with Hormone-Refractory Prostate Cancer. UIN. 2007;78(1):50-7.

141. Anderson PM, Wiseman GA, Dispenzieri A, Arndt CAS, Hartmann LC, Smithson WA, et al. High-Dose Samarium-153 Ethylene Diamine Tetramethylene Phosphonate: Low Toxicity of Skeletal Irradiation in Patients With Osteosarcoma and Bone Metastases. JCO. 2002 January 1,;20(1):189-96.

142. Je B, Dj M, Lp K, Fv F. Dosimetry and toxicity of samarium-153-EDTMP administered for bone pain due to skeletal metastases. J Nucl Med. 1994 /01/01;35(1):63-9.

143. Denis-Bacelar A, Denis-Bacelar A, Chittenden S, Chittenden S, Dearnaley D, Dearnaley D, et al. Phase I/II trials of 186Re-HEDP in metastatic castration-resistant prostate cancer: post-hoc analysis of the impact of administered activity and dosimetry on survival. Eur J Nucl Med Mol Imaging. 2017 Apr;44(4):620-9.

144. Kolesnikov-Gauthier H, Carpentier P, Depreux P, Vennin P, Caty A, Sulman C. Evaluation of Toxicity and Efficacy of 186Re-Hydroxyethylidene Diphosphonate in Patients with Painful Bone Metastases of Prostate or Breast Cancer. J Nucl Med. 2000 10/01/;41(10):1689-94.

145. Liepe K, Kropp J, Runge R, Kotzerke J. Therapeutic efficiency of rhenium-188-HEDP in human prostate cancer skeletal metastases. British journal of cancer. 2003 Aug 18,;89(4):625-9.

146. Tagawa ST, Osborne J, Niaz MJ, Vallabhajosula S, Vlachostergios PJ, Thomas C, et al. Dose-escalation results of a phase I study of 225Ac-J591 for progressive metastatic castration resistant prostate cancer (mCRPC). JCO. 2020 February 19,;38(6_suppl):114-.

147. Hagemann UB, Wickstroem K, Hammer S, Bjerke RM, Zitzmann-Kolbe S, Ryan OB, et al. Advances in Precision Oncology: Targeted Thorium-227 Conjugates As a New Modality in Targeted Alpha Therapy. Cancer Biother Radiopharm. 2020 -9-01;35(7):497-510.

148. Morris MJ, De Wit R, Vogelzang NJ, Tagawa ST, Higano CS. A phase III trial of docetaxel versus docetaxel and radium-223 (Ra-223) in patients with metastatic castration-resistant prostate cancer (mCRPC): DORA. JCO. 2019 February 26,;37(7_suppl):TPS348-.

149. Mokhodoeva O, Vlk M, Málková E, Kukleva E, Mičolová P, Štamberg K, et al. Study of 223Ra uptake mechanism by Fe3O4 nanoparticles: towards new prospective theranostic SPIONs. J Nanopart Res. 2016 Oct 10,;18(10):1-12.

150. Geva R, Lopez J, Danson S, Joensuu H, Peer A, Harris SJ, et al. Radium-223 in combination with paclitaxel in cancer patients with bone metastases: safety results from an open-label, multicenter phase Ib study. Eur J Nucl Med Mol Imaging. 2018 Dec 13,;46(5):1092-101.

151. Jonasdottir TJ, Fisher DR, Borrebaek J, Bruland OS, Larsen RH. First in vivo evaluation of liposome-encapsulated 223Ra as a potential alpha-particle-emitting cancer therapeutic agent. Anticancer Res. 2006 Jul-Aug;26(4B):2841-8.

152. Yoshida K, Kaneta T, Takano S, Sugiura M, Kawano T, Hino A, et al. Pharmacokinetics of single dose radium-223 dichloride (BAY 88-8223) in Japanese patients with castration-resistant prostate cancer and bone metastases. Ann Nucl Med. 2016 Aug;30(7):453-60.

153. Chittenden SJ, Hindorf C, Parker CC, Lewington VJ, Pratt BE, Johnson B, et al. A Phase 1, Open-Label Study of the Biodistribution, Pharmacokinetics, and Dosimetry of 223Ra-Dichloride in Patients with Hormone-Refractory Prostate Cancer and Skeletal Metastases. Journal of nuclear medicine : official publication, Society of Nuclear Medicine. 2015 Sep;56(9):1304-9.

154. Carrasquillo J, O'Donoghue J, Pandit-Taskar N, Humm J, Rathkopf D, Slovin S, et al. Phase I pharmacokinetic and biodistribution study with escalating doses of 223Ra-dichloride in men with castration-resistant metastatic prostate cancer. Eur J Nucl Med Mol Imaging. 2013 Sep;40(9):1384-93.

155. Nilsson S, Strang P, Aksnes AK, Franzèn L, Olivier P, Pecking A, et al. A randomized, dose–response, multicenter phase II study of radium-223 chloride for the palliation of painful bone metastases in patients with castration-resistant prostate cancer. European Journal of Cancer. 2012 March 1,;48(5):678-86.

156. Diane S Abou, David Ulmert, Michele Doucet, Robert F Hobbs, Ryan C Riddle, Daniel LJ Thorek. Whole-Body and Microenvironmental Localization of Radium-223 in Naïve and Mouse Models of Prostate Cancer Metastasis. Journal of the National Cancer Institute. 2016 May 1,;108(5):1.

157. Nilsson S, Prof, Franzén L, MD, Parker C, Dr, Tyrrell C, FRCR, Blom R, MD, Tennvall J, Prof, et al. Bone-targeted radium-223 in symptomatic, hormone-refractory prostate cancer: a randomised, multicentre, placebo-controlled phase II study. Lancet Oncology, The. 2007;8(7):587-94.

158. Gjermund Henriksen, Knut Breistøl, Øyvind S Bruland, Øystein Fodstad, Roy H Larsen. Significant antitumor effect from bone-seeking, alpha-particle-emitting (223)Ra demonstrated in an experimental skeletal metastases model. Cancer research. 2002 Jun 1,;62(11):3120-5.

159. Pandit-Taskar N, Larson SM, Carrasquillo JA. Bone-Seeking Radiopharmaceuticals for Treatment of Osseous Metastases, Part 1: Therapy with 223Ra-Dichloride. Journal of Nuclear Medicine. 2013 December 16,.

160. Daniel Heinrich, Jasmin Bektic, Andries M. Bergman, Orazio Caffo, Richard Cathomas, Kim N. Chi, Gedske Daugaard, Daniel Keizman, Jon Kindblom, Gero Kramer, David Olmos,, Aurelius Omlin,, Srikala S. Sridhar, Marcello Tucci, Inge van Oort, Sten Nilsson. The Contemporary Use of Radium-223 in Metastatic Castration-resistant Prostate Cancer. Clinical Genitourinary Cancer. 2017;16(1):223-31.

161. Cathel Kerr. (223)Ra targets skeletal metastases and spares normal tissue. The Lancet. Oncology. 2002 Aug 1,;Sect. 3 (453).

162. Parker CC, Coleman RE, Sartor O. Three-year Safety of Radium-223 Dichloride in Patients with Castration-resistant Prostate Cancer and Symptomatic Bone Metastases from Phase 3 Randomized Alpharadin in Symptomatic Prostate Cancer Trial. . 2018 March;73(3):427-35.

163. Vogelzang NJ, Coleman RE, Michalski JM, Nilsson S, O'Sullivan JM, Parker C, et al. Hematologic Safety of Radium-223 Dichloride: Baseline Prognostic Factors Associated With Myelosuppression in the ALSYMPCA Trial. Clin Genitourin Cancer. 2017 -02;15(1):42,52.e8.

164. Vogelzang NJ, Parker C, Nilsson S, Coleman RE, O'Bryan-Tear CG, Shan M, et al. Updated analysis of radium-223 dichloride (Ra-223) impact on skeletal-related events (SRE) in patients with castration-resistant prostate cancer (CRPC) and bone metastases from the phase III randomized trial (ALSYMPCA). JCO. 2013 February 20,;31(6_suppl):11-.

165. Hoskin P, Sartor O, O'Sullivan JM, Johannessen DC, Helle SI, Logue J, et al. Efficacy and safety of radium-223 dichloride in patients with castration-resistant prostate cancer and symptomatic bone metastases, with or without previous docetaxel use: a prespecified subgroup analysis from the randomised, double-blind, phase 3 ALSYMPCA trial. The Lancet Oncology. 2014 November 1,;15(12):1397-406.

166. Sartor O, Coleman R, Nilsson S, Heinrich D, Helle SI, O'Sullivan JM, et al. Effect of radium-223 dichloride on symptomatic skeletal events in patients with castration-resistant prostate cancer and bone metastases: results from a phase 3, double-blind, randomised trial. The Lancet Oncology. 2014 June 1,;15(7):738-46.

167. Hall EJ, Giaccia AJ. Radiobiology for the Radiologist. In: Philadelphia: Wolters Kluwer Health; 2011. p. 104-6.

168. International Commission on Radiological Protection. Annals of the ICRP Radiological Protection in Medicine. Elsevier; 2007.

169. Lombardini ED, Pacheco-Thompson ME, Melanson MA. Chapter 44 - Radiation and Other Physical Agents. In: Haschek WM, Rousseaux CG, Wallig MA, editors. Haschek and Rousseaux's Handbook of Toxicologic Pathology (Third Edition). Boston: Academic Press; 2013. p. 1421-503.

170. Nickoloff JA, Sharma N, Taylor L. Clustered DNA Double-Strand Breaks: Biological Effects and Relevance to Cancer Radiotherapy. Genes. 2020 Jan 15,;11(1):99.

171. Choi WH, Cho J. Evolving clinical cancer radiotherapy: concerns regarding normal tissue protection and quality assurance. Journal of Korean medical science. 2016 Feb;31 Suppl 1(Suppl 1):S75-87.

172. Zeman EM. Chapter 1 - The Biological Basis of Radiation Oncology. In: Gunderson LL, Tepper JE, editors. Clinical Radiation Oncology (Fourth Edition). Philadelphia: Elsevier; 2016. p. 2,40.e5.

173. Wang W, Li C, Qiu R, Chen Y, Wu Z, Zhang H, et al. Modelling of Cellular Survival Following Radiation-Induced DNA Double-Strand Breaks. Scientific reports. 2018 Nov 1,;8(1):16202-12.

174. Wagner LK, Eifel PJ, Geise RA. Potential Biological Effects Following High X-ray Dose Interventional Procedures. Journal of Vascular and Interventional Radiology. 1994 January 1,;5(1):71-84.

175. Hill MA. Radiation Track Structure: How the Spatial Distribution of Energy Deposition Drives Biological Response. Clinical oncology (Royal College of Radiologists (Great Britain)). 2020 Feb;32(2):75-83.

176. Ward JF. DNA Damage Produced by Ionizing Radiation in Mammalian Cells: Identities, Mechanisms of Formation, and Reparability. In: Cohn WE, Moldave K, editors. Progress in Nucleic Acid Research and Molecular Biology. Academic Press; 1988. p. 95-125.

177. Davalli P, Marverti G, Lauriola A, D'Arca D. Targeting Oxidatively Induced DNA Damage Response in Cancer: Opportunities for Novel Cancer Therapies. Oxidative Medicine and Cellular Longevity. 2018 /03/27;2018:e2389523.

178. The role of oxidative damage to nucleic acids in the pathogenesis of neurological disease [Internet].: Landes Bioscience; 2007 []. Available from: http://hdl.handle.net/10355/17506.

179. Stewart RD. Induction of DNA Damage by Light Ions Relative to 60Co γ-rays. International journal of particle therapy. 2018 Aug;5(1):25-39.

180. Georgakilas AG, O'Neill P, Stewart RD. Induction and repair of clustered DNA lesions: what do we know so far? Radiat Res. 2013 Jul;180(1):100-9.

181. Semenenko VA, Stewart RD. A fast Monte Carlo algorithm to simulate the spectrum of DNA damages formed by ionizing radiation. Radiat Res. 2004 Apr;161(4):451-7.

182. Schipler A, Iliakis G. DNA double-strand–break complexity levels and their possible contributions to the probability for error-prone processing and repair pathway choice. Nucleic Acids Res. 2013 /09/01;41(16):7589-605.

183. Goodhead DT. Molecular and cell models of biological effects of heavy ion radiation. Radiation and environmental biophysics. 1995 Jun;34(2):67-72.

184. Nikitaki Z, Nikolov V, Mavragani IV, Mladenov E, Mangelis A, Laskaratou DA, et al. Measurement of complex DNA damage induction and repair in human cellular systems after exposure to ionizing radiations of varying linear energy transfer (LET). Free Radical Research. 2016 November 1,;50(sup1):S64-78.

185. Hada M, Georgakilas AG. Formation of clustered DNA damage after high-LET irradiation: a review. J Radiat Res. 2008 -05;49(3):203-10.

186. E. Hoglund, B. Stenerlow, E. Blomquist, J. Carlsson. DNA damage induced by radiation of different linear energy transfer: initial fragmentation. International Journal of Radiation Biology. 2000 January 1,;76(4):539-47.

187. Jones GDD, Milligan JR, Ward JF, Calabro-Jones PM, Aguilera JA. Yield of Strand Breaks as a Function of Scavenger Concentration and LET for SV40 Irradiated with4 He Ions. Radiation Research. 1993 November 1,;136(2):190-6.

188. Nikjoo H, O'Neill P, Terrissol M, Goodhead DT. Quantitative modelling of DNA damage using Monte Carlo track structure method. Radiat Environ Biophys. 1999 May 12,;38(1):31-8.

189. Nikjoo H, Uehara S, Wilson WE, Hoshi M, Goodhead DT. Track structure in radiation biology: theory and applications. Int J Radiat Biol. 1998 -04;73(4):355-64.

190. Nikjoo H, O'Neill P, Goodhead DT, Terrissol M. Computational modelling of low-energy electron-induced DNA damage by early physical and chemical events. Int J Radiat Biol. 1997 -05;71(5):467-83.

191. Anderson RM, Stevens DL, Goodhead DT. M-FISH analysis shows that complex chromosome aberrations induced by alpha -particle tracks are cumulative products of localized rearrangements. Proc Natl Acad Sci U S A. 2002 Sep 17,;99(19):12167-72.

192. Tracy BL, Stevens DL, Goodhead DT, Hill MA. Variation in RBE for Survival of V79-4 Cells as a Function of Alpha-Particle (Helium Ion) Energy. Radiation research. 2015 Jul;184(1):33-45.

193. Goodhead DT. Mechanisms for the Biological Effectiveness of High-LET Radiations. Journal of radiation research. 1999;40(suppl):1-13.

194. Sally A. Amundson, Khanh T. Do, Albert J. Fornace. Induction of Stress Genes by Low Doses of Gamma Rays. Radiation Research. 1999 Sep 1,;152(3):225-31.

195. Bradbury JM, Jackson SP. The complex matter of DNA double-strand break detection. Biochemical Society Transactions. 2003 February 1,;31(1):40-4.

196. Pandita TK, Richardson C. Chromatin remodeling finds its place in the DNA double-strand break response. Nucleic Acids Research. 2009 April 1,;37(5):1363-77.

197. Longhese MP, Bonetti D, Manfrini N, Clerici M. Mechanisms and regulation of DNA end resection. The EMBO Journal. 2010 September 1,;29(17):2864-74.

198. Mendez-Dorantes C, Bhargava R, Stark JM. Repeat-mediated deletions can be induced by a chromosomal break far from a repeat, but multiple pathways suppress such rearrangements. Genes Dev. 2018 04/01/;32(7-8):524-36.

199. Ferguson DO, Alt FW. DNA double strand break repair and chromosomal translocation: Lessons from animal models. Oncogene. 2001 Sep 10,;20(40):5572-9.

200. Maier P, Hartmann L, Wenz F, Herskind C. Cellular Pathways in Response to Ionizing Radiation and Their Targetability for Tumor Radiosensitization. Int J Mol Sci. 2016 -1-14;17(1).

201. Gudkov AV, Komarova EA. The role of p53 in determining sensitivity to radiotherapy. Nat Rev Cancer. 2003 -02;3(2):117-29.

202. Takasawa R, Nakamura H, Mori T, Tanuma S. Differential apoptotic pathways in human keratinocyte HaCaT cells exposed to UVB and UVC. Apoptosis. 2005 -10;10(5):1121-30.

203. Breckenridge DG, Germain M, Mathai JP, Nguyen M, Shore GC. Regulation of apoptosis by endoplasmic reticulum pathways. Oncogene. 2003 Nov 24,;22(53):8608-18.

204. Castedo M, Perfettini J, Roumier T, Andreau K, Medema R, Kroemer G. Cell death by mitotic catastrophe: a molecular definition. Oncogene. 2004 -04-12;23(16):2825-37.

205. Degterev A, Yuan J. Expansion and evolution of cell death programmes. Nat Rev Mol Cell Biol. 2008 -05;9(5):378-90.

206. Jonathan EC, Bernhard EJ, McKenna WG. How does radiation kill cells? Curr Opin Chem Biol. 1999 -02;3(1):77-83.

207. Erenpreisa J, Cragg MS. Mitotic death: a mechanism of survival? A review. Cancer cell international. 2001 Nov 23,;1(1):1.

208. Imreh G, Norberg HV, Imreh S, Zhivotovsky B. Chromosomal breaks during mitotic catastrophe trigger γH2AX-ATM-p53-mediated apoptosis. J Cell Sci. 2011 -09-01;124(Pt 17):2951-63.

209. Watson JD, Crick FHC. Molecular Structure of Nucleic Acids: A Structure for Deoxyribose Nucleic Acid. Nature. 1953 -04;171(4356):737-8.

210. Thompson J, Braun G, Tierney D, Wessels L, Schmitzer H, Rossa B, et al. Rosalind Franklin's X-ray photo of DNA as an undergraduate optical diffraction experiment. American Journal of Physics. 2018 February 1,;86(2):95-104.

211. Arnott S, Kibble TWB, Shallice T. Maurice Hugh Frederick Wilkins CBE: 15 December 1916 - 5 October 2004. Biogr Mem Fellows R Soc. 2006;52:455-78.

212. Alberts B, Johnson A, Lewis J, Raff M, Roberts K, Walter P. Chromosomal DNA and Its Packaging in the Chromatin Fiber. In: Molecular Biology of the Cell. 4th edition. New York: Garland Science; 2002.

213. Oleinick NL, Balasubramaniam U, Xue L, Chiu S. Nuclear Structure and the Microdistribution of Radiation Damage in DNA. International Journal of Radiation Biology. 1994 January 1,;66(5):523-9.

214. Borland L, Harauz G, Bahr G, van Heel M. Packing of the 30 nm chromatin fiber in the human metaphase chromosome. Chromosoma. 1988;97(2):159-63.

215. Sax K. TYPES AND FREQUENCIES OF CHROMOSOMAL ABERRATIONS INDUCED BY X-RAYS. Cold Spring Harb Symp Quant Biol. 1941 01/01/;9:93-103.

216. Sax K. An Analysis of X-Ray Induced Chromosomal Aberrations in Tradescantia. Genetics (Austin). 1940 Jan;25(1):41-68.

217. Sax K. Chromosome Aberrations Induced by X-Rays. Genetics. 1938 -9;23(5):494-516.

218. Lea DE. Action of radiations on living cells. 2. ed., repr. ed. Cambridge: Univ. Press; 1956.

219. Savage JR. Classification and relationships of induced chromosomal structual changes. J Med Genet. 1976 Apr;13(2):103-22.

220. Revell SH. The breakage-and-reunion theory and the exchange theory for chromosomal aberrations induced by ionizing radiations: a short history. Adv. Radiat. Biol., v. 4, pp. 367-416. 1974 Jan 1,.

221. Revell SH. The accurate estimation of chromatid breakage, and its relevance to a new interpretation of chromatid aberrations induced by ionizing radiations. Proc R Soc Lond B Biol Sci. 1959 -09-01;150:563-89.

222. Pfeiffer P, Goedecke W, Obe G. Mechanisms of DNA double-strand break repair and their potential to induce chromosomal aberrations. Mutagenesis. 2000 Jul;15(4):289-302.

223. Savage JRK. A brief survey of aberration origin theories. Mutation research. 1998;404(1):139-47.

224. Savage JR. Insight into sites. 366th ed. Mutat Res; 1996.

225. Chadwick KH, Leenhouts HP. The molecular theory of radiation biology. Berlin [u.a.]: Springer; 1981.

226. Chadwick KH, Leenhouts HP. The Rejoining of DNA Double-strand Breaks and a Model for the Formation of Chromosomal Rearrangements. International Journal of Radiation Biology and Related Studies in Physics, Chemistry and Medicine. 1978 January 1,;33(6):517-29.

227. Cornforth MN. Radiation-Induced Damage and the Formation of Chromosomal Aberrations. In: DNA Damage and Repair. Totowa, NJ: Humana Press; 1998. p. 559-85.

228. Greinert R, Detzler E, Volkmer B, Harder D. Kinetics of the Formation of Chromosome Aberrations in X-Irradiated Human Lymphocytes: Analysis by Premature Chromosome Condensation with Delayed Fusion. Radiation Research. 1995;144(2):190-7.

229. Loucas BD, Geard CR. Kinetics of Chromosome Rejoining in Normal Human Fibroblasts after Exposure to Low- and High-LET Radiations. Radiation Research. 1994;138(3):352-60.

230. Savage JR. Classification and relationships of induced chromosomal structual changes. Journal of medical genetics. 1976 Apr;13(2):103-22.

231. Yip M. Autosomal ring chromosomes in human genetic disorders. Transl Pediatr. 2015 -4;4(2):164-74.

232. Savage JR, Simpson PJ. FISH "painting" patterns resulting from complex exchanges. Mutat Res. 1994 -02;312(1):51-60.

233. Arlt MF, Rajendran S, Birkeland SR, Wilson TE, Glover TW. Copy number variants are produced in response to low-dose ionizing radiation in cultured cells. Environ Mol Mutagen. 2014 Mar;55(2):103-13.

234. Bakhoum SF, Kabeche L, Wood MD, Laucius CD, Qu D, Laughney AM, et al. Numerical chromosomal instability mediates susceptibility to radiation treatment. Nat Commun. 2015 -1-21;6:5990.

235. Crasta K, Ganem NJ, Dagher R, Lantermann AB, Ivanova EV, Pan Y, et al. DNA breaks and chromosome pulverization from errors in mitosis. Nature. 2012 Jan 18,;482(7383):53-8.

236. INTERNATIONAL ATOMIC ENERGY AGENCY. Cytogenetic Dosimetry: Applications in Preparedness for and Response to Radiation Emergencies. Vienna: IAEA; 2011.

237. Anderson RM, Marsden SJ, Wright EG, Kadhim MA, Goodhead DT, Griffin CS. Complex chromosome aberrations in peripheral blood lymphocytes as a potential biomarker of exposure to high-LET alpha-particles. Int J Radiat Biol. 2000 -01;76(1):31-42.

238. Boei, J. J. W. A., Vermeulen S, Mullenders LHF, Natarajan AT. Impact of radiation quality on the spectrum of induced chromosome exchange aberrations. International Journal of Radiation Biology. 2001 January 1,;77(8):847-57.

239. Gillian B. Curwen, E. Janet Tawn, Kevin K. Cadwell, Laura Guyatt, James Thompson, Mark A. Hill. mFISH Analysis of Chromosome Aberrations Induced In Vitro by α-Particle Radiation: Examination of Dose-Response Relationships. Radiation Research. 2012;178(5):414-24.

240. Blakely WF, Carr Z, Chu MC, Dayal-Drager R, Fujimoto K, Hopmeir M, et al. WHO 1st Consultation on the Development of a Global Biodosimetry Laboratories Network for Radiation Emergencies (BioDoseNet). Radiation Research. 2009 January 1,;171(1):127-39.

241. Griffin CS, Marsden SJ, Stevens DL, Simpson P, Savage JRK. Frequencies of Complex Chromosome Exchange Aberrations Induced by 238Pu α-particles and Detected by Fluorescence in Situ Hybridization Using Single Chromosome-specific Probes. International Journal of Radiation Biology. 1995 January 1,;67(4):431-9.

242. Behjati S, Gundem G, Wedge DC, Roberts ND, Tarpey PS, Cooke SL, et al. Mutational signatures of ionizing radiation in second malignancies. Nature communications. 2016 Sep 12,;7(1):12605.

243. Schwartz JL, Jordan R, Sun J, Ma H, Hsie AW. Dose-Dependent Changes in the Spectrum of Mutations Induced by Ionizing Radiation. Radiation Research. 2000;153(3):312-7.

244. Hsie AW, Porter RC, Xu Z, Yu Y, Sun J, Meltz ML, et al. Molecular markers of ionizing radiation-induced gene mutations in mammalian cells. Environ Health Perspect. 1996 May;104 Suppl 3:675-8.

245. Simpson PJ, Savage JR. Detecting 'hidden' exchange events within X-ray-induced aberrations using multicolour chromosome paints. Chromosome Res. 1995 -01;3(1):69-72.

246. Goodhead DT. Initial events in the cellular effects of ionizing radiations: clustered damage in DNA. Int J Radiat Biol. 1994 -01;65(1):7-17.

247. Hill MA, Griffin CS, Pyke EL, Stevens DL. Chromosome aberration induction is dependent on the spatial distribution of energy deposition through a cell nucleus. Radiat Prot Dosimetry. 2011 -02;143(2-4):172-6.

248. Bochtler T, Fröhling S, Krämer A. Role of chromosomal aberrations in clonal diversity and progression of acute myeloid leukemia. Leukemia. 2015 Jun;29(6):1243-52.

249. Trott K-, Hug O. Intraclonal Recovery of Division Probability in Pedigrees of Single X-irradiated Mammalian Cells. International Journal of Radiation Biology and Related Studies in Physics, Chemistry and Medicine. 1970 January 1,;17(5):483-6.

250. Elkind MM, Sutton H. X-Ray Damage and Recovery in Mammalian Cells in Culture. Nature. 1959 -10;184(4695):1293-5.

251. Puck TT, Marcus PI. Action of x-rays on mammalian cells. J Exp Med. 1956 -05-01;103(5):653-66.

252. Seymour CB, Mothersill C, Alper T. High yields of lethal mutations in somatic mammalian cells that survive ionizing radiation. Int J Radiat Biol Relat Stud Phys Chem Med. 1986 -07;50(1):167-79.

253. Gorgojo L, Little JB. Expression of lethal mutations in progeny of irradiated mammalian cells. Int J Radiat Biol. 1989 -04;55(4):619-30.

254. Thompson LH, Suit HD. Proliferation Kinetics of X-irradiated Mouse L Cells Studied with Time-lapse Photography. II. International Journal of Radiation Biology and Related Studies in Physics, Chemistry and Medicine. 1969 January 1,;15(4):347-62.

255. Kadhim MA, Lorimore SA, Townsend KMS, Goodhead DT, Buckle VJ, Wright EG. Radiation-induced Genomic Instability: Delayed Cytogenetic Aberrations and Apoptosis in Primary Human Bone Marrow Cells. International Journal of Radiation Biology. 1995 January 1,;67(3):287-93.

256. Kadhim MA, Lorimore SA, Goodhead DT, Wright EG, Hepburn MD, Buckle VJ. α-particle-induced chromosomal instability in human bone marrow cells. The Lancet. 1994 /10/08;344(8928):987-8.

257. Marder BA, Morgan WF. Delayed chromosomal instability induced by DNA damage. Mol Cell Biol. 1993 -11;13(11):6667-77.

258. Holmberg K, Fält S, Johansson A, Lambert B. Clonal chromosome aberrations and genomic instability in X-irradiated human T-lymphocyte cultures. Mutation Research/Fundamental and Molecular Mechanisms of Mutagenesis. 1993 April 1,;286(2):321-30.

259. Martins MB, Sabatier L, Ricoul M, Pinton A, Dutrillaux B. Specific chromosome instability induced by heavy ions: a step towards transformation of human fibroblasts? Mutat Res. 1993 -02;285(2):229-37.

260. Kadhim MA, Macdonald DA, Goodhead DT, Lorimore SA, Marsden SJ, Wright EG. Transmission of chromosomal instability after plutonium alpha-particle irradiation. Nature. 1992 -02-20;355(6362):738-40.

261. Sabatier L, Dutrillaux B, Martin MB. Chromosomal instability. Nature. 1992 -06-18;357(6379):548.

262. Roy K, Kodama S, Suzuki K, Fukase K, Watanabe M. Hypoxia relieves X-ray-induced delayed effects in normal human embryo cells. Radiat Res. 2000 -12;154(6):659-66.

263. Li J, O W, Li W, Jiang Z, Ghanbari HA. Oxidative stress and neurodegenerative disorders. International journal of molecular sciences. 2013 Dec 16,;14(12):24438-75.

264. J.Kim G, Chandrasekaran K, F.Morgan W. Mitochondrial dysfunction, persistently elevated levels of reactive oxygen species and radiation-induced genomic instability: a review. Mutagenesis. 2006 November 1,;21(6):361-7.

265. MOTHERSILL C, STAMATO TD, PEREZ ML, CUMMINS R, MOONEY R, SEYMOUR CB. Involvement of energy metabolism in the production of 'bystander effects' by radiation. British journal of cancer. 2000 May;82(10):1740-6.

266. Bowler DA, Moore SR, Macdonald DA, Smyth SH, Clapham P, Kadhim MA. Bystander-mediated genomic instability after high LET radiation in murine primary haemopoietic stem cells. Mutat Res. 2006 -05-11;597(1-2):50-61.

267. Suzuki M, Zhou H, Geard CR, Hei TK. Effect of Medium on Chromatin Damage in Bystander Mammalian Cells. Radiation Research. 2004;162(3):264-9.

268. Huo L, Nagasawa H, Little JB. HPRT Mutants Induced in Bystander Cells by Very Low Fluences of Alpha Particles Result Primarily from Point Mutations. Radiation Research. 2001 November 1,;156(5):521-5.

269. Zhou H, Randers-Pehrson G, Waldren CA, Vannais D, Hall EJ, Hei TK. Induction of a bystander mutagenic effect of alpha particles in mammalian cells. PNAS. 2000 -02-29 00:00:00;97(5):2099-104.

270. PRISE KM. Studies of bystander effects in human fibroblasts using a charged particle microbeam. International Journal of Radiation Biology. 1998 January 1,;74(6):793-8.

271. Seymour CB, Mothersill C. Delayed expression of lethal mutations and genomic instability in the progeny of human epithelial cells that survived in a bystander-killing environment. Radiation oncology investigations. 1997;5(3):106-10.

272. Butterworth KT, McMahon SJ, Hounsell AR, O'Sullivan JM, Prise KM. Bystander signalling: exploring clinical relevance through new approaches and new models. Clin Oncol (R Coll Radiol). 2013 -10;25(10):586-92.

273. Schmid E, Roos H. Influence of the bystander phenomenon on the chromosome aberration pattern in human lymphocytes induced by in vitro α-particle exposure. Radiat Environ Biophys. 2009 Apr;48(2):181-7.

274. Ponnaiya B, Jenkins-Baker G, Bigelow A, Marino S, Geard CR. Detection of chromosomal instability in alpha-irradiated and bystander human fibroblasts. Mutat Res. 2004 -12-02;568(1):41-8.

275. Lorimore SA, McIlrath JM, Coates PJ, Wright EG. Chromosomal instability in unirradiated hemopoietic cells resulting from a delayed in vivo bystander effect of gamma radiation. Cancer Res. 2005 -07-01;65(13):5668-73.

276. Watson GE, Lorimore SA, Macdonald DA, Wright EG. Chromosomal Instability in Unirradiated Cells Induced in Vivo by a Bystander Effect of Ionizing Radiation. Cancer Research. 2000 Oct 1,;60(20):5608-11.

277. Valentin J. Radiation and your patient: A guide for medical practitioners: ICRP Supporting Guidance 2 Approved by ICRP Committee 3 in September 2001. Annals of the ICRP. 2001;31(4):1-52.

278. Demoor-Goldschmidt C, de Vathaire F. Review of risk factors of secondary cancers among cancer survivors. British journal of radiology. 2019 Jan;92(1093):20180390.

279. Sountoulides P, Koletsas N, Kikidakis D, Paschalidis K, Sofikitis N. Secondary malignancies following radiotherapy for prostate cancer. Ther Adv Urol. 2010 -6;2(3):119-25.

280. Hijiya N, Hudson MM, Lensing S, Zacher M, Onciu M, Behm FG, et al. Cumulative incidence of secondary neoplasms as a first event after childhood acute lymphoblastic leukemia. JAMA. 2007 Mar 21,;297(11):1207-15.

281. Tward JD, Wendland MMM, Shrieve DC, Szabo A, Gaffney DK. The risk of secondary malignancies over 30 years after the treatment of non-Hodgkin lymphoma. Cancer. 2006 Jul 1,;107(1):108-15.

282. Walter AW, Hancock ML, Pui CH, Hudson MM, Ochs JS, Rivera GK, et al. Secondary brain tumors in children treated for acute lymphoblastic leukemia at St Jude Children's Research Hospital. J Clin Oncol. 1998 Dec;16(12):3761-7.

283. Watson GE, Pocock DA, Papworth D, Lorimore SA, Wright EG. In vivo chromosomal instability and transmissible aberrations in the progeny of haemopoietic stem cells induced by high- and low-LET radiations. Int J Radiat Biol. 2001 Apr;77(4):409-17.

284. Stimpson K, Matheny J, Sullivan B. Dicentric chromosomes: unique models to study centromere function and inactivation. Chromosome Res. 2012 Jul;20(5):595-605.

285. Nowell PC. The minute chromosome (Phl) in chronic granulocytic leukemia. Blut. 1962 -04;8:65-6.

286. Rowley JD. A New Consistent Chromosomal Abnormality in Chronic Myelogenous Leukaemia identified by Quinacrine Fluorescence and Giemsa Staining. Nature. 1973 -06;243(5405):290-3.

287. Asif M, Hussain A, Malik A, Rasool M. Three-way complex variant translocation involving short arm chromosome (1;9;22)(p36;q34;q11) in a chronic myeloid leukemia patient. Oncol Lett. 2015 -09;10(3):1728-30.

288. Kang Z, Liu Y, Xu L, Long Z, Huang D, Yang Y, et al. The Philadelphia chromosome in leukemogenesis. Chin J Cancer. 2016 -5-27;35.

289. Braunstein S, Nakamura JL. Radiotherapy-Induced Malignancies: Review of Clinical Features, Pathobiology, and Evolving Approaches for Mitigating Risk. Front Oncol. 2013;0.

290. Aguiar RCT. Therapy-Related Chronic Myeloid Leukemia: An Epidemiological, Clinical and Pathogenetic Appraisal. Leukemia & lymphoma. 1998;29(1-2):17-26.

291. Shimon I, Kneller A, Olchovsky D. Chronic myeloid leukaemia following 131I treatment for thyroid carcinoma: a report of two cases and review of the literature. Clin Endocrinol (Oxf). 1995 -11;43(5):651-4.

292. Bauduer F, Ducout L, Dastugue N, Marolleau J. Chronic myeloid leukemia as a secondary neoplasm after anti-cancer radiotherapy: a report of three cases and a brief review of the literature. Leuk Lymphoma. 2002 -05;43(5):1057-60.

293. Au WY, Ooi GC, Ma SK, Wan TSK, Kwong YL. Chronic myeloid leukemia in an adolescent with Ollier's disease after intensive X-ray exposure. Leuk Lymphoma. 2004 -03;45(3):613-6.

294. Ron E, Modan B, Boice JD. Mortality after radiotherapy for ringworm of the scalp. Am J Epidemiol. 1988 -04;127(4):713-25.

295. Hagmar L, Brøgger A, Hansteen IL, Heim S, Högstedt B, Knudsen L, et al. Cancer risk in humans predicted by increased levels of chromosomal aberrations in lymphocytes: Nordic study group on the health risk of chromosome damage. Cancer Res. 1994 -06-01;54(11):2919-22.

296. Bonassi S, Abbondandolo A, Camurri L, Dal Prá L, De Ferrari M, Degrassi F, et al. Are chromosome aberrations in circulating lymphocytes predictive of future cancer onset in humans? Preliminary results of an Italian cohort study. Cancer Genet Cytogenet. 1995 -02;79(2):133-5.

297. Bonassi S, Hagmar L, Strömberg U, Montagud AH, Tinnerberg H, Forni A, et al. Chromosomal Aberrations in Lymphocytes Predict Human Cancer Independently of Exposure to Carcinogens. Cancer Res. 2000 -03-15 00:00:00;60(6):1619-25.

298. Smerhovsky Z, Landa K, Rössner P, Brabec M, Zudova Z, Hola N, et al. Risk of cancer in an occupationally exposed cohort with increased level of chromosomal aberrations. Environ Health Perspect. 2001 -01;109(1):41-5.

299. Leenhouts HP, Brugmans MJP. An analysis of bone and head sinus cancers in radium dial painters using a two-mutation carcinogenesis model. Journal of Radiological Protection. 2000 Jun 1,;20(2):169-88.

300. Fry SA. Studies of U.S. Radium Dial Workers: An Epidemiological Classic. Radiat Res. 1998 /11/01;150(5s):S21-9.

301. Stebbings JH, Lucas HF, Stehney AF. Mortality from cancers of major sites in female radium dial workers. American Journal of Industrial Medicine. 1984;5(6):435-59.

302. R. E. Rowland, A. F. Stehney, H. F. Lucas. Dose-Response Relationships for Female Radium Dial Workers. Radiation Research. 1978 Nov 1,;76(2):368-83.

303. Spiers FW, Lucas HF, Rundo J, Anast GA. Leukaemia incidence in the U.S. dial workers. Health Phys. 1983;44 Suppl 1:65-72.

304. Rowland RE, Stehney AF, Lucas HF. Dose-response relationships for radium-induced bone sarcomas. Health Phys. 1983;44 Suppl 1:15-31.

305. Adams EE, Brues AM. Breast cancer in female radium dial workers first employed before 1930. J Occup Med. 1980 -09;22(9):583-7.

306. Hall P, Granath F, Lundell M, Olsson K, Holm L. Lenticular Opacities in Individuals Exposed to Ionizing Radiation in Infancy. Radiation Research. 1999;152(2):190-5.

307. Hayes BP, Fisher RF. Influence of a prolonged period of low-dosage x-rays on the optic and ultrastructural appearances of cataract of the human lens. British Journal of Ophthalmology. 1979 /07/01;63(7):457-64.

308. Wick RR, Nekolla EA, Gaubitz M, Schulte TL. Increased risk of myeloid leukaemia in patients with ankylosing spondylitis following treatment with radium-224. Rheumatology. 2008 Jun;47(6):855-9.

309. Wick RR, Nekolla EA, Gössner W, Kellerer AM. Late effects in ankylosing spondylitis patients treated with 224Ra. Radiat Res. 1999 Dec;152(6 Suppl):S8-S11.

310. Smith PG, Doll R. Mortality among patients with ankylosing spondylitis after a single treatment course with x rays. Br Med J (Clin Res Ed). 1982 -02-13;284(6314):449-60.

311. TIEPOLT C, GRÜNING T, FRANKE W-. Renaissance of 224Ra for the treatment of ankylosing spondylitis: clinical experiences. Nuclear Medicine Communications. 2002 Jan;23(1):61-6.

312. Priest ND, Dauer LT, Hoel DG. Administration of lower doses of radium-224 to ankylosing spondylitis patients results in no evidence of significant overall detriment. PLOS ONE. 2020 Apr 30,;15(4):e0232597.

313. Tiepolt C, Grüning T, Franke W-. Renaissance of 224 Ra for the treatment of ankylosing spondylitis: clinical experiences. Nucl Med Commun. 2002 Jan;23(1):61-6.

314. N D Priest. The prediction of the relative toxicities of radium 224 and of radium 226 in the bones of mice using Monte Carlo techniques. The British journal of radiology. 1987 Jul 1,;60(715):677-80.

315. Hobbs RF, Song H, Watchman CJ, Bolch WE, Aksnes A-, Ramdahl T, et al. A bone marrow toxicity model for 223Ra alpha-emitter radiopharmaceutical therapy. Physics in Medicine and Biology. 2012;57(10):3207-22.

316. Varkaris A, Gunturu K, Kewalramani T, Tretter C. Acute Myeloid Leukemia After Radium-223 Therapy: Case Report. Clinical Genitourinary Cancer. 2017 /08/01;15(4):e723-6.

317. Odo U, Vasudevamurthy AK, Sartor O. Acute Promyelocytic Leukemia After Treatment of Metastatic Castration-Resistant Prostate Cancer With Radium-223. Clinical Genitourinary Cancer. 2017 /06/01;15(3):e501-2.

318. Elke A. Nekolla, Albrecht M. Kellerer, Martin Kuse-Isingschulte, Erwin Eder, Heinz Spiess. Malignancies in Patients Treated with High Doses of Radium-224. Radiation Research. 1999 Dec 1,;152(6):S3-7.

319. Wick RR, Gössner W. Follow-up study of late effects in 224Ra treated ankylosing spondylitis patients. Health Phys. 1983;44 Suppl 1:187-95.

320. Turner PG, Jain S, Mitchell DM, Hounsell A, Biggart S, O'Sullivan JM. First Results from the ADRRAD Trial – Combination Androgen Deprivation Therapy (ADT), Whole Pelvis Radiotherapy (WPRT) and Radium 223 in Recently Diagnosed Metastatic Hormone Sensitive Prostate Cancer (MHSPCa). Clinical Oncology. 2018 -03-01;30(3):196.

321. Turner P, Jain S, Cole A, Biggart S, Hounsell A, O'Sullivan J. First Survival Data from the ADRRAD Clinical Trial; Pelvic Radiotherapy and Concurrent Radium-223 in Metastatic Hormone Sensitive Prostate Cancer (mHSPC). Clinical Oncology. 2020 /05/01;32(5):e130-1.

322. O'Sullivan J, Turner PG, Jain S, Grey A, Biggart S, Hounsell AR, et al. Results of the ADRRAD Trial of pelvic IMRT plus radium-223 in men with mHSPC metastatic to bone. JCO. 2020 February 19,;38(6_suppl):136-.

323. Speicher MR, Ballard SG, Ward DC. Karyotyping human chromosomes by combinatorial multi-fluor FISH. Nature genetics. 1996 Apr;12(4):368-75.

324. XOFIGO ANNEX I
SUMMARY OF PRODUCT CHARACTERISTICS [Internet].; 2018 [updated Oct 10,;]. Available from: https://www.ema.europa.eu/en/documents/product-information/xofigo-epar-product-information_en.pdf.

325. Moquet J, Higueras M, Donovan E, Boyle S, Barnard S, Bricknell C, et al. Dicentric Dose Estimates for Patients Undergoing Radiotherapy in the RTGene Study to Assess Blood Dosimetric Models and the New Bayesian Method for Gradient Exposure. Radiation research. 2018 Dec;190(6):596.

326. Human body weight to volume conversion [Internet]. [cited June 2020]. Available from: https://www.aqua-calc.com/calculate/weight-to-volume/substance/human-blank-body.

327. Lloyd DC, Edwards AA, Prosser JS. Chromosome Aberrations Induced in Human Lymphocytes by In Vitro Acute X and Gamma Radiation. Radiat Prot Dosimetry. 1986 /06/01;15(2):83-8.

328. Purrott RJ, Edwards AA, Lloyd DC, Stather JW. The Induction of Chromosome Aberrations in Human Lymphocytes by in Vitro Irradiation with α-particles from Plutonium-239. International Journal of Radiation Biology. 1980;38(3):277-84.

329. Ainsbury E, Lloyd D. DOSE ESTIMATION SOFTWARE FOR RADIATION BIODOSIMETRY. Health Physics. 2010 Feb;98(2):290-5.

330. International Atomic Energy Agency. cytogenetic analysis for radiation dose assessment . Vienna: IAEA; 2001. Report No.: 405.

331. Guerra Liberal, Francisco D. C., O'Sullivan JM, McMahon SJ, Prise KM. Targeted Alpha Therapy: Current Clinical Applications. Cancer Biotherapy and Radiopharmaceuticals. 2020 June 16,;35(6):404-17.

332. Edwards AA, Hone PA, Moquet JE, Lloyd DC. Simple chromosome exchanges are not linear with dose. Int J Radiat Biol. 1999 -09;75(9):1113-7.

333. Anderson RM. Cytogenetic Biomarkers of Radiation Exposure. Clin Oncol (R Coll Radiol). 2019 -05;31(5):311-8.

334. Cornforth MN, Durante M. Radiation quality and intra-chromosomal aberrations: Size matters. Mutat Res Genet Toxicol Environ Mutagen. 2018 Dec;836(Pt A):28-35.

335. Loucas BD, Cornforth MN. The LET Dependence of Unrepaired Chromosome Damage in Human Cells: A Break Too Far? Radiation Research. 2013;179(4):393-405.

336. Lloyd DC, Purrott RJ, Reeder EJ. The incidence of unstable chromosome aberrations in peripheral blood lymphocytes from unirradiated and occupationally exposed people. Mutation research. 1980;72(3):523-32.

337. Heath CW, Nadel MR, Zack MM, Chen ATL, Bender MA, Preston RJ. Cytogenetic Findings in Persons Living Near the Love Canal. JAMA : the journal of the American Medical Association. 1984 Mar 16,;251(11):1437-40.

338. Bender MA, Preston RJ, Leonard RC, Pyatt BE, Gooch PC, Shelby MD. Chromosomal aberration and sister-chromatid exchange frequencies in peripheral blood lymphocytes of a large human population sample. Mutation Research/Genetic Toxicology. 1988 March 1,;204(3):421-33.

339. Wojda A, Zietkiewicz E, Mossakowska M, Pawłowski W, Skrzypczak K, Witt M. Correlation Between the Level of Cytogenetic Aberrations in Cultured Human Lymphocytes and the Age and Gender of Donors. The journals of gerontology. Series A, Biological sciences and medical sciences. 2006 Aug;61(8):763-72.

340. Whitehouse C, Edwards A, Tawn E, Stephan G, Oestreicher U, Moquet J, et al. Translocation yields in peripheral blood lymphocytes from control populations. International Journal of Radiation Biology. 2005 Feb;81(2):139-45.

341. Tucker JD, Lee DA, Ramsey MJ, Briner J, Olsen L, Moore DH. On the frequency of chromosome exchanges in a control population measured by chromosome painting. Mutat Res. 1994 Oct-Dec;313(2-3):193-202.

342. Ramsey MJ, Moore DH, Briner JF, Lee DA, Olsen La, Senft JR, et al. The effects of age and lifestyle factors on the accumulation of cytogenetic damage as measured by chromosome painting. Mutat Res. 1995 Oct;338(1-6):95-106.

343. Janet Tawn E. The frequency of chromosome aberrations in a control population. Mutation Research/Environmental Mutagenesis and Related Subjects. 1987 December 1,;182(6):303-8.

344. Awa AA, Neel JV. Cytogenetic "rogue" cells: what is their frequency, origin, and evolutionary significance? Proc Natl Acad Sci U S A. 1986 -2;83(4):1021-5.

345. Tawn EJ, Cartmel CL, Pyta EMT. Cells with multiple chromosome aberrations in control individuals. Mutation Research Letters. 1985 December 1,;144(4):247-50.

346. Fox DP, Robertson FW, Brown T, Whitehead AR, Douglas JD. Chromosome aberrations in divers. Undersea Biomed Res. 1984 Jun;11(2):193-204.

347. Bloom AD, Neel JV, Tsuchimoto T, Meilinger K. Chromosomal breakage in leukocytes of South American Indians. CGR. 1973;12(3):175-86.

348. Anderson RM, Stevens DL, Goodhead DT. M-FISH Analysis Shows That Complex Chromosome Aberrations Induced by α-Particle Tracks Are Cumulative Products of Localized Rearrangements. Proceedings of the National Academy of Sciences - PNAS. 2002 Sep 17,;99(19):12167-72.

349. Anderson RM. Cytogenetic Biomarkers of Radiation Exposure. Clinical Oncology. 2019 May;31(5):311-8.

350. Berardinelli F, De Vitis M, Nieri D, Cherubini R, De Nadal V, Gerardi S, et al. mBAND and mFISH analysis of chromosomal aberrations and breakpoint distribution in chromosome 1 of AG01522 human fibroblasts that were exposed to radiation of different qualities. Mutation Research/Genetic Toxicology and Environmental Mutagenesis. 2015 November 1,;793:55-63.

351. Hill MA. Track to the future: historical perspective on the importance of radiation track structure and DNA as a radiobiological target. Int J Radiat Biol. 2017 -12-08;94(8):759-68.

352. Goodhead DT. Track Structure Considerations in Low Dose and Low Dose Rate Effects of Ionizing Radiation. In: Nygaard OF, Sinclair WK, Lett JT, editors. Advances in Radiation Biology. Elsevier; 1992. p. 7-44.

353. Sage E, Shikazono N. Radiation-induced clustered DNA lesions: Repair and mutagenesis. Free Radical Biology and Medicine. 2017 June 1,;107:125-35.

354. Lee R, Sommer S, Hartel C, Nasonova E, Durante M, Ritter S. Complex exchanges are responsible for the increased effectiveness of C-ions compared to X-rays at the first post-irradiation mitosis. Mutation research. Genetic toxicology and environmental mutagenesis. 2010;701(1):52-9.

355. Hartel C, Nikoghosyan A, Durante M, Sommer S, Nasonova E, Fournier C, et al. Chromosomal aberrations in peripheral blood lymphocytes of prostate cancer patients treated with IMRT and carbon ions. Radiotherapy and Oncology. 2009;95(1):73-8.

356. Livingston GK, Falk RB, Schmid E. Effect of Occupational Radiation Exposures on Chromosome Aberration Rates in Former Plutonium Workers. Radiat Res. 2006 /07/01;166(1):89-97.

357. Hande MP, Azizova TV, Burak LE, Khokhryakov VF, Geard CR, Brenner DJ. Complex chromosome aberrations persist in individuals many years after occupational exposure to densely ionizing radiation: An mFISH study. Genes, Chromosomes and Cancer. 2005;44(1):1-9.

358. Hande MP, Azizova TV, Geard CR, Burak LE, Mitchell CR, Khokhryakov VF, et al. Past Exposure to Densely Ionizing Radiation Leaves a Unique Permanent Signature in the Genome. The American Journal of Human Genetics. 2003 May 1,;72(5):1162-70.

359. Salassidis K, Georgiadou-Schumacher V, Braselmann H, Müller P, Peter RU, Bauchinger M. Chromosome Painting in Highly Irradiated Chernobyl Victims: A Follow-up Study to Evaluate the Stability of Symmetrical Translocations and the Influence of Clonal Aberrations for Retrospective Dose Estimation. International Journal of Radiation Biology. 1995 January 1,;68(3):257-62.

360. Roch-Lefèvre S, Pouzoulet F, Giraudet AL, Voisin P, Vaurijoux A, Gruel G, et al. Cytogenetic assessment of heterogeneous radiation doses in cancer patients treated with fractionated radiotherapy. The British journal of radiology. 2010 Sep;83(993):759-66.

361. Hartel C, Nasonova E, Fuss MC, Nikoghosyan AV, Debus J, Ritter S. Clinical and Translational Radiation Oncology. Clinical and translational radiation oncology. 2018 -10-10;13:57-63.

362. Tawn EJ, Whitehouse CA. Persistence of translocation frequencies in blood lymphocytes following radiotherapy: implications for retrospective radiation biodosimetry. J Radiol Prot. 2003 Dec;23(4):423-30.

363. Schumann S, Eberlein U, Lapa C, Müller J, Serfling S, Lassmann M, et al. α-Particle-induced DNA damage tracks in peripheral blood mononuclear cells of [223Ra]RaCl2-treated prostate cancer patients. European journal of nuclear medicine and molecular imaging. 2021 Feb 4,.

364. Schumann S, Eberlein U, Muhtadi R, Lassmann M, Scherthan H. DNA damage in leukocytes after internal ex-vivo irradiation of blood with the α-emitter Ra-223. Sci Rep. 2018 -02-02;8(1):2286.

365. Costa RP, Bordonaro S, Cappuccio F, Tripoli V, Murabito A, Licari M, et al. Hematologic toxicity of radium-223 in elderly patients with metastatic Castration Resistant Prostate Cancer: a real-life experience. Prostate international. 2019 Mar;7(1):25-9.

366. Subbiah V, Anderson PM, Kairemo K, Hess K, Huh WW, Ravi V, et al. Alpha Particle Radium 223 Dichloride in High-risk Osteosarcoma: A Phase I Dose Escalation Trial. Clin Cancer Res. 2019 -07-01 00:00:00;25(13):3802-10.

367. Livingston GK, Ryan TL, Smith TL, Escalona MB, Foster AE, Balajee AS. Detection of Simple, Complex, and Clonal Chromosome Translocations Induced by Internal Radioiodine Exposure: A Cytogenetic Follow-Up Case Study after 25 Years. CGR. 2019;159(4):169-81.

368. Rhona M. Anderson, David L. Stevens, Natalia D. Sumption, K. M Stuart Townsend, Dudley T. Goodhead, Mark A. Hill. Effect of Linear Energy Transfer (LET) on the Complexity of α-Particle-Induced Chromosome Aberrations in Human CD34+ Cells. Radiation Research. 2007;167(5):541-50.

369. Hartel C, Nasonova E, Fuss MC, Nikoghosyan AV, Debus J, Ritter S. Persistence of radiation-induced aberrations in patients after radiotherapy with C-ions and IMRT. Clinical and translational radiation oncology. 2018 Nov;13:57-63.

370. Loucas BD, Cornforth MN. Complex Chromosome Exchanges Induced by Gamma Rays in Human Lymphocytes: An mFISH Study. Radiat Res. 2001 /05/01;155(5):660-71.

371. Simpson PJ, Savage JR. Dose-response curves for simple and complex chromosome aberrations induced by X-rays and detected using fluorescence in situ hybridization. Int J Radiat Biol. 1996 -04;69(4):429-36.

372. Hei TK, Wu LJ, Liu SX, Vannais D, Waldren CA, Randers-Pehrson G. Mutagenic Effects of a Single and an Exact Number of α Particles in Mammalian Cells. Proceedings of the National Academy of Sciences - PNAS. 1997 Apr 15,;94(8):3765-70.

373. Raju MR, Eisen Y, Carpenter S, Inkret WC. Radiobiology of alpha particles. III. Cell inactivation by alpha-particle traversals of the cell nucleus. Radiat Res. 1991 -11;128(2):204-9.

374. Faghihi Moghaddam F, Bakhshandeh M, Ghorbani M, Mofid B. Assessing the out-of-field dose calculation accuracy by eclipse treatment planning system in sliding window IMRT of prostate cancer patients. Computers in biology and medicine. 2020 Dec;127:104052.

375. QUAN EM, LI X, LI Y, WANG X, KUDCHADKER RJ, JOHNSON JL, et al. A comprehensive comparison of IMRT and VMAT plan quality for prostate cancer treatment. Int J Radiat Oncol Biol Phys. 2012 -7-15;83(4):1169-78.

376. Teoh M, Clark CH, Wood K, Whitaker S, Nisbet A. Volumetric modulated arc therapy: a review of current literature and clinical use in practice. British journal of radiology. 2011;84(1007):967-96.

377. Gershkevitsh E, Clark C, Staffurth J, Dearnaley D, Trott K. Dose to Bone Marrow Using IMRT Techniques in Prostate Cancer Patients. Strahlenther Onkol. 2005 Mar;181(3):172-8.

378. Teh BS, Woo SY, Mai W, Mcgary JE, Carpenter LS, Lu HH, et al. Clinical experience with intensity-modulated radiation therapy (IMRT) for prostate cancer with the use of rectal balloon for prostate immobilization. Medical Dosimetry. 2002;27(2):105-13.

379. Xia P, Pickett B, Vigneault E, Verhey LJ, Roach M. Forward or inversely planned segmental multileaf collimator IMRT and sequential tomotherapy to treat multiple dominant intraprostatic lesions of prostate cancer to 90 Gy. International Journal of Radiation Oncology, Biology, Physics. 2001;51(1):244-54.

380. Ray K, Stick M. Chapter 32 - Radiation and Health Effects. In: Gupta RC, editor. Handbook of Toxicology of Chemical Warfare Agents (Second Edition). Boston: Academic Press; 2015. p. 431-46.

381. Mahadevan LS, Aliru ML, Yang X, Bodd MH, Singh PK, Yusuf SW, et al. Radiation-Induced Endothelial Vascular Injury. JACC Basic Transl Sci. 2019 Jan 1,;3(4):563-72.

382. Stewart FA, Hoving S, Russell NS. Vascular damage as an underlying mechanism of cardiac and cerebral toxicity in irradiated cancer patients. Radiat Res. 2010 -12;174(6):865-9.

383. Baselet B, Rombouts C, Benotmane AM, Baatout S, Aerts A. Cardiovascular diseases related to ionizing radiation: The risk of low-dose exposure (Review). International journal of molecular medicine. 2016 Dec;38(6):1623-41.

384. Hammi A, Paganetti H, Grassberger C. 4D blood flow model for dose calculation to circulating blood and lymphocytes. Phys Med Biol. 2020 03 02,;65(5):055008.

385. Yovino S, Kleinberg L, Grossman SA, Narayanan M, Ford E. The Etiology of Treatment-related Lymphopenia in Patients with Malignant Gliomas: Modeling Radiation Dose to Circulating Lymphocytes Explains Clinical Observations and Suggests Methods of Modifying the Impact of Radiation on Immune Cells. Cancer Invest. 2013 -2;31(2):140-4.

386. Flux GD. Imaging and dosimetry for radium-223: the potential for personalized treatment. British journal of radiology. 2017 Aug;90(1077):20160748.

387. Murray I, Chittenden SJ, Denis-Bacelar AM, Hindorf C, Parker CC, Chua S, et al. The potential of 223Ra and 18F-fluoride imaging to predict bone lesion response to treatment with 223Ra-dichloride in castration-resistant prostate cancer. Eur J Nucl Med Mol Imaging. 2017 Oct;44(11):1832-44.

388. Pacilio M, Ventroni G, De Vincentis G, Cassano B, Pellegrini R, Di Castro E, et al. Dosimetry of bone metastases in targeted radionuclide therapy with alpha-emitting (223)Ra-dichloride. Eur J Nucl Med Mol Imaging. 2016 Jan;43(1):21-33.

389. Lassmann M, Nosske D. Dosimetry of 223Ra-chloride: dose to normal organs and tissues. Eur J Nucl Med Mol Imaging. 2013 Jan;40(2):207-12.

390. Hilberath JN, Thomas ME, Smith T, Jara C, Fitzgerald DJ, Wilusz K, et al. Blood volume measurement by hemodilution: association with valve disease and re-evaluation of the Allen Formula. Perfusion. 2015 May 1,;30(4):305-11.

391. Inaba T. Quantitative measurements of prostatic blood flow and blood volume by positron emission tomography. J Urol. 1992 Nov;148(5):1457-60.

392. Zhang S, Qian H, Zhao Y, Sun K, Wang H, Liang G, et al. Relationship between age and prostate size. Asian J Androl. 2013 -01;15(1):116-20.

393. Leissner K-, Tisell L-. The Weight of the Human Prostate. Scandinavian Journal of Urology and Nephrology. 1979 January 1,;13(2):137-42.

394. Davidson DD, Koch MO, Lin H, Jones TD, Biermann K, Cheng L. Does the Size Matter?Prostate Weight Does Not Predict PSA Recurrence After Radical Prostatectomy. Am J Clin Pathol. 2010 /04/01;133(4):662-8.

395. Moore JE, Bertram CD. Lymphatic System Flows. Annu Rev Fluid Mech. 2018 -1;50:459-82.

396. Georgieva D, Staynova A, Hadjidekova V. Assessment of Cytogenetic Abnormalities by FISH in Lymphocytes from a Victim Accidentally Exposed to Cobalt-60. OBM Genetics. 2018 Aug 14,;2(4):1.

397. Straume T, Langlois RG, Lucas J, Jensen RH, Bigbee WL, Ramalho AT, et al. Novel Biodosimetry Methods Applied to Victims of the Goiania Accident. Health physics (1958). 1991;60(1):71-6.

398. Bao P, Lin C, Yang F, Guo Z, Guo T, Yang L, et al. Development of large-area quadrant silicon detector for charged particles. Chinese physics C. 2014 Dec;38(12):126001.

399. I.P E, WilliamE S, S.O E. Alpha-Particle Spectroscopy and Ranges in Air. ; 2014.

400. Jiang W, Ulmert D, Simons BW, Abou DS, Thorek DL. The impact of age on radium-223 distribution and an evaluation of molecular imaging surrogates. Nucl Med Biol. 2018;62-63:1-8.

401. Miederer M, Thomas C, Beck J, Hampel C, Krieger C, Baqué PE, et al. Haematopoietic toxicity of radium-223 in patients with high skeletal tumour burden. Nuclear medicine. 2015 May;54(5):197-203.

402. Nilsson S, Franzén L, Parker C, Tyrrell C, Blom R, Tennvall J, et al. Bone-targeted radium-223 in symptomatic, hormone-refractory prostate cancer: a randomised, multicentre, placebo-controlled phase II study. The Lancet Oncology. 2007 July 1,;8(7):587-94.

403. Wakeford R. Does Low-Level Exposure to Ionizing Radiation Increase the Risk of Cardiovascular Disease? Hypertension. 2019 June 1,;73(6):1170-1.

404. Little MP, Lipshultz SE. Low dose radiation and circulatory diseases: a brief narrative review. Cardio-oncology (London, England). 2015 Nov 26,;1(1):4.

405. Zielinski JM, Ashmore PJ, Band PR, Jiang H, Shilnikova NS, Tait VK, et al. Low dose ionizing radiation exposure and cardiovascular disease mortality: cohort study based on Canadian national dose registry of radiation workers. Int J Occup Med Environ Health. 2009;22(1):27-33.

406. Stephan G, Kampen W, Noßke D, Roos H. Chromosomal aberrations in peripheral lymphocytes of patients treated with radium-224 for ankylosing spondylitis. Radiat Environ Biophys. 2005 May;44(1):23-8.

407. Schmid E, Hieber L, Heinzmann U, Roos H, Kellerer AM. Analysis of chromosome aberrations in human peripheral lymphocytes induced by in vitro α-particle irradiation. Radiation and environmental biophysics. 1996 Aug;35(3):179-84.

408. Thwaites D. Accuracy required and achievable in radiotherapy dosimetry: have modern technology and techniques changed our views? J Phys : Conf Ser. 2013 June;444:012006.

409. Bielenberg DR, Zetter BR. The Contribution of Angiogenesis to the Process of Metastasis. Cancer J. 2015;21(4):267-73.

410. Chavez-MacGregor M, Aviles-Salas A, Green D, Fuentes-Alburo A, Gómez-Ruiz C, Aguayo A. Angiogenesis in the Bone Marrow of Patients with Breast Cancer. Clin Cancer Res. 2005 -08-01 00:00:00;11(15):5396-400.

411. Mundy GR. Metastasis to bone: Causes, consequences and therapeutic opportunities. Nature Reviews: Cancer. 2002 Aug 1,;2(8):584-93.

412. Barquinero JF, Stephan G, Schmid E. Effect of americium-241 α-particles on the dose–response of chromosome aberrations in human lymphocytes analysed by fluorescence in situ hybridization. International Journal of Radiation Biology. 2004 February 1,;80(2):155-64.

413. Moquet JE, Fernández JL, Edwards AA, Lloyd DC. Lymphocyte chromosomal aberrations and their complexity induced in vitro by plutonium-239 alpha-particles and detected by FISH. Cell Mol Biol (Noisy-le-grand). 2001 -05;47(3):549-56.

414. Testard I, Dutrillaux B, Sabatier L. Chromosomal aberrations induced in human lymphocytes by high-LET irradiation. Int J Radiat Biol. 1997 -10;72(4):423-33.

415. Loucas BD, Durante M, Bailey SM, Cornforth MN. Chromosome Damage in Human Cells by γ Rays, α Particles and Heavy Ions: Track Interactions in Basic Dose-Response Relationships. Radiat Res. 2013 -1;179(1):9-20.

416. Cornforth MN. Analyzing radiation-induced complex chromosome rearrangements by combinatorial painting. Radiat Res. 2001 -05;155(5):643-59.

417. Pignalosa D, Lee R, Hartel C, Sommer S, Nikoghosyan A, Debus J, et al. Chromosome inversions in lymphocytes of prostate cancer patients treated with X-rays and carbon ions. Radiotherapy and Oncology. 2013 /11/01;109(2):256-61.

418. Raymaekers K, Stegen S, van Gastel N, Carmeliet G. The vasculature: a vessel for bone metastasis. Bonekey Rep. 2015 -09-09;4.

419. McDonald DM, Baluk P. Significance of Blood Vessel Leakiness in Cancer. Cancer Res. 2002 -09-15 00:00:00;62(18):5381-5.

420. Duque JL, Loughlin KR, Adam RM, Kantoff PW, Zurakowski D, Freeman MR. Plasma levels of vascular endothelial growth factor are increased in patients with metastatic prostate cancer. Urology. 1999 -09;54(3):523-7.

421. Sanguineti G, Giannarelli D, Petrongari MG, Arcangeli S, Sangiovanni A, Saracino B, et al. Leukotoxicity after moderately Hypofractionated radiotherapy versus conventionally fractionated dose escalated radiotherapy for localized prostate Cancer: a secondary analysis from a randomized study. Radiat Oncol. 2019 -1-30;14.

422. Miszczyk M, Majewski W. Hematologic Toxicity of Conformal Radiotherapy and Intensity Modulated Radiotherapy in Prostate and Bladder Cancer Patients. Asian Pacific journal of cancer prevention : APJCP. 2018 Oct 26,;19(10):2803-6.

423. Bentzen SM. Preventing or reducing late side effects of radiation therapy: radiobiology meets molecular pathology. Nature reviews. Cancer. 2006 Sep;6(9):702-13.

424. Baskar R, Lee KA, Yeo R, Yeoh K. Cancer and Radiation Therapy: Current Advances and Future Directions. Int J Med Sci. 2012 -2-27;9(3):193-9.

425. Prasanna PGS, Stone HB, Wong RS, Capala J, Bernhard EJ, Vikram B, et al. Normal tissue protection for improving radiotherapy: Where are the Gaps? Transl Cancer Res. 2012 -6;1(1):35-48.

426. Dörr W, Hendry JH. Consequential late effects in normal tissues. Radiotherapy and Oncology. 2001 /12/01;61(3):223-31.

427. Glide-Hurst CK, Chetty IJ. Improving radiotherapy planning, delivery accuracy, and normal tissue sparing using cutting edge technologies. J Thorac Dis. 2014 -4;6(4):303-18.

428. Bhide SA, Nutting CM. Recent advances in radiotherapy. BMC medicine. 2010 Apr 28,;8(1):25.

429. Parker CC, Pascoe S, Chodacki A, O'Sullivan JM, Germá JR, O'Bryan-Tear CG, et al. A randomized, double-blind, dose-finding, multicenter, phase 2 study of radium chloride (Ra 223) in patients with bone metastases and castration-resistant prostate cancer. Eur Urol. 2013 -02;63(2):189-97.

430. Jacene H, Gomella L, Yu EY, Rohren EM. Hematologic Toxicity From Radium-223 Therapy for Bone Metastases in Castration-Resistant Prostate Cancer: Risk Factors and Practical Considerations. Clin Genitourin Cancer. 2018 -08;16(4):e919-26.

431. Hobbs RF, Song H, Watchman CJ, Bolch WE, Aksnes A, Ramdahl T, et al. A bone marrow toxicity model for ^{223}Ra alpha-emitter radiopharmaceutical therapy. Phys Med Biol. 2012 -05-21;57(10):3207-22.

432. Ueno NT, Tahara RK, Fujii T, Reuben JM, Gao H, Saigal B, et al. Phase II study of Radium-223 dichloride combined with hormonal therapy for hormone receptor-positive, bone-dominant metastatic breast cancer. Cancer Medicine. 2020;9(3):1025-32.

433. McKay RR, Bossé D, Gray KP, Michaelson MD, Krajewski K, Jacene HA, et al. Radium-223 Dichloride in Combination with Vascular Endothelial Growth Factor–Targeting Therapy in Advanced Renal Cell Carcinoma with Bone Metastases. Clin Cancer Res. 2018 -09-01 00:00:00;24(17):4081-8.

434. Subbiah V, Anderson P, Rohren E. Alpha Emitter Radium 223 in High-Risk Osteosarcoma: First Clinical Evidence of Response and Blood-Brain Barrier Penetration. JAMA Oncology. 2015 May 1,;1(2):253-5.

435. Bruland ØS, Nilsson S, Fisher DR, Larsen RH. High-Linear Energy Transfer Irradiation Targeted to Skeletal Metastases by the α-Emitter 223Ra: Adjuvant or Alternative to Conventional Modalities? Clin Cancer Res. 2006 -10-15 00:00:00;12(20):6250s-7s.

436. Henriksen G, Fisher DR, Roeske JC, Bruland ØS, Larsen RH. Targeting of osseous sites with alpha-emitting 223Ra: comparison with the beta-emitter 89Sr in mice. J Nucl Med. 2003 Feb;44(2):252-9.

437. Moreira HMR, Guerra Liberal, Francisco D. C., O'Sullivan JM, McMahon SJ, Prise KM. Mechanistic Modeling of Radium-223 Treatment of Bone Metastases. International Journal of Radiation Oncology*Biology*Physics. 2019 April 1,;103(5):1221-30.

438. Taprogge J, Murray I, Gear J, Chittenden SJ, Parker CC, Flux GD. Compartmental Model for 223Ra-Dichloride in Patients With Metastatic Bone Disease From Castration-Resistant Prostate Cancer. International journal of radiation oncology, biology, physics. 2019 Nov 15,;105(4):884-92.

439. Anderson RM, Marsden SJ, Paice SJ, Bristow AE, Kadhim MA, Griffin CS, et al. Transmissible and Nontransmissible Complex Chromosome Aberrations Characterized by Three-Color and mFISH Define a Biomarker of Exposure to High-LET α Particles. Radiation Research. 2003 January 1,;159(1):40-8.

440. Deng W, Morrison DP, Gale KL, Lucas JN. A comparative study on potential cytogenetic fingerprints for radiation LET in human lymphocytes. Int J Radiat Biol. 2000 -12;76(12):1589-98.

441. Griffin CS, Marsden SJ, Stevens DL, Simpson P, Savage JR. Frequencies of complex chromosome exchange aberrations induced by 238Pu alpha-particles and detected by fluorescence in situ hybridization using single chromosome-specific probes. Int J Radiat Biol. 1995 -04;67(4):431-9.

442. Sumption N, Goodhead DT, Anderson RM. Alpha-Particle-Induced Complex Chromosome Exchanges Transmitted through Extra-Thymic Lymphopoiesis In Vitro Show Evidence of Emerging Genomic Instability. PLoS ONE. 2015 August 7,;10(8):1-20.

443. Watson GE, Lorimore SA, Wright EG. Long-term in vivo transmission of alpha-particle-induced chromosomal instability in murine haemopoietic cells. Int J Radiat Biol. 1996 -02;69(2):175-82.

444. Sawant SG, Randers-Pehrson G, Geard CR, Brenner DJ, Hall EJ. The bystander effect in radiation oncogenesis: I. Transformation in C3H 10T1/2 cells in vitro can be initiated in the unirradiated neighbors of irradiated cells. Radiat Res. 2001 -03;155(3):397-401.

445. Zhou H, Suzuki M, Randers-Pehrson G, Vannais D, Chen G, Trosko JE, et al. Radiation risk to low fluences of alpha particles may be greater than we thought. Proc Natl Acad Sci U S A. 2001 -12-04;98(25):14410-5.

446. Lehnert BE, Goodwin EH, Deshpande A. Extracellular factor(s) following exposure to alpha particles can cause sister chromatid exchanges in normal human cells. Cancer Res. 1997 -06-01;57(11):2164-71.

447. Deshpande A, Goodwin EH, Bailey SM, Marrone BL, Lehnert BE. Alpha-particle-induced sister chromatid exchange in normal human lung fibroblasts: evidence for an extranuclear target. Radiat Res. 1996 -03;145(3):260-7.

448. Nagasawa H, Little JB. Induction of sister chromatid exchanges by extremely low doses of alpha-particles. Cancer Res. 1992 -11-15;52(22):6394-6.

449. Pant GS, Kamada N. Chromosome aberrations in normal leucocyte cultures induced by plasma irradiated in vitro. Indian Journal of Experimental Biology. 1978;16(5):605-6.

450. Pant GS, Kamada N. Chromosome aberrations in normal leukocytes induced by the plasma of exposed individuals. Hiroshima Journal of Medical Sciences. 1977;26(2-3):149-54.

451. Littlefield LG, Hollowell JG, Pool WH. Chromosomal Aberrations Induced by Plasma from Irradiated Patients: An Indirect Effect of X Radiation. Radiology. 1969 October 1,;93(4):879-86.

452. Hollowell JG, Littlefield LG. Chromosome Damage Induced by Plasma of X-Rayed Patients: An Indirect Effect of X-Ray∗. Proceedings of the Society for Experimental Biology and Medicine. 1968 October 1,;129(1):240-4.

453. Goh K, Sumner H. Breaks in Normal Human Chromosomes: Are They Induced by a Transferable Substance in the Plasma of Persons Exposed to Total-Body Irradiation? Radiation Research. 1968 July 1,;35(1):171-81.

454. Leung CN, Canter BS, Rajon D, Bäck TA, Fritton JC, Azzam EI, et al. Dose-Dependent Growth Delay of Breast Cancer Xenografts in the Bone Marrow of Mice Treated with 223Ra: The Role of Bystander Effects and Their Potential for Therapy. Journal of Nuclear Medicine. 2020 Jan;61(1):89-95.

455. Uchida IA, Lee CP, Byrnes EM. Chromosome aberrations induced in vitro by low doses of radiation: nondisjunction in lymphocytes of young adults. Am J Hum Genet. 1975 -5;27(3):419-29.

456. Pampalona J, Roscioli E, Silkworth WT, Bowden B, Genescà A, Tusell L, et al. Chromosome Bridges Maintain Kinetochore-Microtubule Attachment throughout Mitosis and Rarely Break during Anaphase. PLoS One. 2016 -1-19;11(1).

457. Natarajan AT, Darroudi F, Mullenders LHF, Farooqi Z, Balajee AS, Boei, J. J. W. A, et al. In vivo assays for detection and evaluation of aneugens. United States: Springer-Verlag, New York, NY (United States); Dec 31, 1993.

458. Darroudi F, Meijers CM, Hadjidekova V, Natarajan AT. Detection of aneugenic and clastogenic potential of X-rays, directly and indirectly acting chemicals in human hepatoma (Hep G2) and peripheral blood lymphocytes, using the micronucleus assay and fluorescent in situ hybridization with a DNA centromeric probe. Mutagenesis. 1996 September 1,;11(5):425-33.

459. Kirsch-Volders M, Tallon I, Tanzarella C, Sgura A, Hermine T, Parry EM, et al. Mitotic non-disjunction as a mechanism for in vitro aneuploidy induction by X-rays in primary human cells. Mutagenesis. 1996 July 1,;11(4):307-13.

460. Boei JJ, Natarajan AT. Detection of chromosome malsegregation to the daughter nuclei in cytokinesis-blocked transgenic mouse splenocytes. Chromosome Res. 1995 -01;3(1):45-53.

461. Parry EM, Ulucan H, Wyllie FS, Wynford-Thomas D, Parry JM. Segregational fidelity of chromosomes in human thyroid tumour cells. Chromosoma. 1998 Dec;107(6):491-7.

462. Wilhelm T, Olziersky A, Harry D, Sousa FD, Vassal H, Eskat A, et al. Mild replication stress causes chromosome mis-segregation via premature centriole disengagement. Nat Commun. 2019 -08-08;10(1):1-14.

463. Bakhoum SF, Kabeche L, Murnane JP, Zaki BI, Compton DA. DNA-Damage Response during Mitosis Induces Whole-Chromosome Missegregation. Cancer Discov. 2014 -11-01 00:00:00;4(11):1281-9.

464. Sten Nilsson, Roy H. Larsen, Sophie D. Fosså, Lise Balteskard, Kari W. Borch, Jan-Erik Westlin, et al. First Clinical Experience with α-Emitting Radium-223 in the Treatment of Skeletal Metastases. Clinical Cancer Research. 2005 Jun 15,;11(12):4451-9.

465. Turner PG, O'Sullivan JM. 223Ra and other bone-targeting radiopharmaceuticals—the translation of radiation biology into clinical practice. The British Journal of Radiology. 2015 Jun;88(1050):20140752.

466. Sgouros G, Hobbs RF, Song H. Modelling and Dosimetry for Alpha-Particle Therapy. Curr Radiopharm. 2011 -7;4(3):261-5.

467. Alonzi R, Parker CC, Tunariu N, Koh D, Staffurth J, Blackledge MD, et al. Fracture risk after radium-223 (Ra-223) in metastatic castration resistant prostate cancer (mCRPC). JCO. 2019 May 20,;37(15_suppl):e16513-.

468. Cho MS, Lee JK, Bae KS, Han E, Jang SJ, Ha W, et al. Retrospective biodosimetry using translocation frequency in a stable cell of occupationally exposed to ionizing radiation. Journal of Radiation Research. 2015 Jul;56(4):709-16.

469. Camparoto ML, Ramalho AT, Natarajan AT, Curado MP, Sakamoto-Hojo ET. Translocation analysis by the FISH-painting method for retrospective dose reconstruction in individuals exposed to ionizing radiation

10 years after exposure. Mutation Research/Fundamental and Molecular Mechanisms of Mutagenesis. 2003 September 29,;530(1):1-7.

470. Pressl S, Romm H, Ganguly BB, Stephan G. Experience with FISH-detected Translocations as an Indicator in Retrospective Dose Reconstructions. Radiation Protection Dosimetry. 2000 March 1,;88(1):45-9.

471. BAUCHINGER M, SALASSIDIS K, BRASELMANN H, VOZILOVA A, PRESSL S, STEPHAN G, et al. FISH-based analysis of stable translocations in a Techa River population. International Journal of Radiation Biology. 1998 January 1,;73(6):605-12.

472. LUCAS, D. C. LLOYD J. E. MOQUET S. ORAM A. A. EDWARDS J. N. Accidental intake of tritiated water: a cytogenetic follow-up case on translocation stability and dose reconstruction. International Journal of Radiation Biology. 1998 January 1,;73(5):543-7.

473. Little MP, Kwon D, Doi K, Simon SL, Preston DL, Doody MM, et al. Association of Chromosome Translocation Rate with Low Dose Occupational Radiation Exposures in U.S. Radiologic Technologists. Radiation Research. 2014;182(1):1-17.

474. Lindholm C, Edwards A. Long-term persistence of translocations in stable lymphocytes from victims of a radiological accident. International Journal of Radiation Biology. 2004 August 1,;80(8):559-66.

475. Spruill MD, Nelson DO, Ramsey MJ, Nath J, Tucker JD. Lifetime Persistence and Clonality of Chromosome Aberrations in the Peripheral Blood of Mice Acutely Exposed to Ionizing Radiation. Radiation Research. 2000;153(1):110-21.

476. Williams K, Hakim FT, Gress RE. T Cell Immune Reconstitution Following Lymphodepletion. Semin Immunol. 2007 -10;19(5):318-30.

477. Kraft D, Ritter S, Durante M, Seifried E, Fournier C, Tonn T. Transmission of clonal chromosomal abnormalities in human hematopoietic stem and progenitor cells surviving radiation exposure. Mutation research. 2015 Jul;777:43-51.

478. Greulich KM, Kreja L, Heinze B, Rhein AP, Weier H-G, Brückner M, et al. Rapid detection of radiation-induced chromosomal aberrations in lymphocytes and hematopoietic progenitor cells by mFISH. Mutation research. 2000;452(1):73-81.

479. AMENOMORI T, HONDA T, OTAKE M, TOMONAGA M, ICHIMARU M. Growth and differentiation of circulating hemopoietic stem cells with atomic bomb irradiation-induced chromosome abnormalities. Experimental hematology. 1988;16(10):849-54.

480. Evans HJ. Chromosome Aberrations Induced by Ionizing Radiations. In: Bourne GH, Danielli JF, editors. International Review of Cytology. Academic Press; 1962. p. 221-321.

481. Kawata T, Ito H, Uno T, Saito M, Yamamoto S, Furusawa Y, et al. G2 chromatid damage and repair kinetics in normal human fibroblast cells exposed to low- or high-LET radiation. Cytogenet Genome Res. 2004;104(1-4):211-5.

482. Ritter S, Nasonova E, Gudowska-Nowak E, Scholz M, Kraft G. High-LET-induced chromosome aberrations in V79 cells analysed in first and second post-irradiation metaphases. Int J Radiat Biol. 2000 -02;76(2):149-61.

483. Zhuanzi W, Wenjian L, Dejuan Z, Wei W, Xigang J, Qingxiang G. Chromatid-type aberrations following irradiation in G0 lymphocytes with heavy ions. Mutat Res. 2007 -04-01;617(1-2):98-103.

484. Loucas BD, Eberle RL, Durante M, Cornforth MN. Complex chromatid-isochromatid exchanges following irradiation with heavy ions? Cytogenet Genome Res. 2004;104(1-4):206-10.

485. Ritter S, Nasonova E, Scholz M, Kraft-Weyrather W, Kraft G. Comparison of chromosomal damage induced by X-rays and Ar ions with an LET of 1840 keV/micrometer in G1 V79 cells. Int J Radiat Biol. 1996 -02;69(2):155-66.

486. E. Nasonova, S. Ritter, T. Fomenlcova, G. K, t. INDUCTION OF CHROMOSOMAL DAMAGE IN CHO-Kl CELLS AND THJ3R REPAIR-DEFICIENT MUTANT XRSS BY X-RAY AND PARTICLE IRRADIATION. 1998 January 1,;22:569-78.

487. Sevan'kaev AV, Zherbin EA, Luchnik NV, Obaturov GM, Kozlov VM. Cytogenetic effects induced by neutrons in human peripheral blood lymphocytes in vitro. I. Dose-effect relationship for different types of chromosome aberrations when exposed to neutrons with different energies. Genetika. 1979 -06;15(6):1046-60.

488. Klaassen Z, Howard LE, Hoedt Ad, Amling CL, Aronson WJ, Cooperberg MR, et al. Factors predicting skeletal-related events in patients with bone metastatic castration-resistant prostate cancer. Cancer. 2017;123(9):1528-35.

489. Bubendorf L, Schöpfer A, Wagner U, Sauter G, Moch H, Willi N, et al. Metastatic patterns of prostate cancer: An autopsy study of 1,589 patients. Human pathology. 2000;31(5):578-83.

490. Bourke VA, Watchman CJ, Reith JD, Jorgensen ML, Dieudonne A, Bolch WE. Spatial gradients of blood vessels and hematopoietic stem and progenitor cells within the marrow cavities of the human skeleton. Blood. 2009;114(19):4077-80.

491. Watchman CJ, Bourke VA, Lyon JR, Knowlton AE, Butler SL, Grier DD, et al. Spatial Distribution of Blood Vessels and CD34+ Hematopoietic Stem and Progenitor Cells Within the Marrow Cavities of Human Cancellous Bone. The Journal of nuclear medicine (1978). 2007 Apr 1,;48(4):645-54.

492. Sternberg CN, Saad F, Graff JN, Peer A, Vaishampayan UN, Leung E, et al. A randomised phase II trial of three dosing regimens of radium-223 in patients with bone metastatic castration-resistant prostate cancer. Annals of oncology. 2020 Feb;31(2):257-65.

493. Jn L, Fs H, Ce B, Ab C, T S. Stability of the translocation frequency following whole-body irradiation measured in rhesus monkeys. Int J Radiat Biol. 1996 /09/01;70(3):309-18.

494. Lindholm C, Romm H, Stephan G, Schmid E, Moquet J, Edwards A. Intercomparison of translocation and dicentric frequencies between laboratories in a follow-up of the radiological accident in Estonia. Int J Radiat Biol. 2002 -10;78(10):883-90.

495. Nakamura N, Nakano M, Kodama Y, Ohtaki K, Cologne J, Awa AA. Prediction of Clonal Chromosome Aberration Frequency in Human Blood Lymphocytes. rare. 2004 /03;161(3):282-9.

496. Lucas JN, Awa A, Straume T, Poggensee M, Kodama Y, Nakano M, et al. Rapid Translocation Frequency Analysis in Humans Decades after Exposure to Ionizing Radiation. International Journal of Radiation Biology. 1992 January 1,;62(1):53-63.

497. Matsumoto K, Ramsey MJ, Nelson DO, Tucker JD. Persistence of Radiation-Induced Translocations in Human Peripheral Blood Determined by Chromosome Painting. Radiation Research. 1998;149(6):602-13.

498. Tucker JD, Breneman JW, Briner JF, Eveleth GG, Langlois RG, Moore II DH. Persistence of radiation-induced translocations in rat peripheral blood determined by chromosome painting. Environmental and molecular mutagenesis. 1997;30(3):264-72.

499. Natarajan AT, Vyas RC, Wiegant J, Curado MP. A cytogenetic follow-up study of the victims of a radiation accident in Goiania (Brazil). Mutation Research/Fundamental and Molecular Mechanisms of Mutagenesis. 1991 March 1,;247(1):103-11.

500. Worrall JT, Tamura N, Mazzagatti A, Shaikh N, van Lingen T, Bakker B, et al. Non-random Mis-segregation of Human Chromosomes. Cell reports (Cambridge). 2018 Jun 12,;23(11):3366-80.

501. Stone JF, Sandberg AA. Sex chromosome aneuploidy and aging. Mutat Res. 1995 -10;338(1-6):107-13.

502. Guttenbach M, Koschorz B, Bernthaler U. Sex chromosome loss and aging: In situ hybridization studies on human interphase nuclei. American Journal of Human Genetics. 1995 Nov 1,;57(5).

503. Nath J, Tucker JD, Hando JC. Y Chromosome aneuploidy, micronuclei, kinetochores and aging in men. Chromosoma. 1995 Aug 1,;103(10):725-31.

504. Fitzgerald PH, McEwan CM. Total aneuploidy and age-related sex chromosome aneuploidy in cultured lymphocytes of normal men and women. Human genetics. 1977 Dec 23,;39(3):329-37.

505. Brown T, Fox DP, Robertson FW, Bullock I. Non-random chromosome loss in PHA-stimulated lymphocytes from normal individuals. Mutation research. Mutation research letters. 1983;122(3):403-6.

506. Pampfer S, Streffer C. Increased chromosome aberration levels in cells from mouse fetuses after zygote X-irradiation. Int J Radiat Biol. 1989 -01;55(1):85-92.

507. Lorimore SA, Coates PJ, Wright EG. Radiation-induced genomic instability and bystander effects: inter-related nontargeted effects of exposure to ionizing radiation. Oncogene. 2003 Oct 13,;22(45):7058-69.

508. Clutton SM, Townsend KM, Walker C, Ansell JD, Wright EG. Radiation-induced genomic instability and persisting oxidative stress in primary bone marrow cultures. Carcinogenesis. 1996 -08;17(8):1633-9.

509. Mendonca MS, Kurohara W, Antoniono R, Redpath JL. Plating Efficiency as a Function of Time Postirradiation: Evidence for the Delayed Expression of Lethal Mutations. Radiation Research. 1989 August 1,;119(2):387-93.

510. Limoli CL, Hartmann A, Shephard L, Yang CR, Boothman DA, Bartholomew J, et al. Apoptosis, reproductive failure, and oxidative stress in Chinese hamster ovary cells with compromised genomic integrity. Cancer Res. 1998 -08-15;58(16):3712-8.

511. Jamali M. Persistent increase in the rates of apoptosis and dicentric chromosomes in surviving V79 cells after X-irradiation. International Journal of Radiation Biology. 1996 January 1,;70(6):705-9.

512. Denkinger MD, Hasch M, Gerstmayer A, Kreienberg R, Nikolaus T, Hancke K. Predicting fatigue in older breast cancer patients receiving radiotherapy. A head-to-head comparison of established assessments. Z Gerontol Geriatr. 2015 -02;48(2):128-34.

513. Gomez-Millan J. Radiation therapy in the elderly: more side effects and complications? Crit Rev Oncol Hematol. 2009 -07;71(1):70-8.

514. Stylopoulos LA, George AE, de Leon MJ, Miller JD, Foo SH, Hiesiger E, et al. Longitudinal CT study of parenchymal brain changes in glioma survivors. AJNR Am J Neuroradiol. 1988 May-Jun;9(3):517-22.

515. Keenan LG, O'Brien M, Ryan T, Dunne M, McArdle O. Assessment of older patients with cancer: Edmonton Frail Scale (EFS) as a predictor of adverse outcomes in older patients undergoing radiotherapy. Journal of Geriatric Oncology. 2017 May 1,;8(3):206-10.

516. Chang S, Goldstein NE, Dharmarajan KV. Managing an Older Adult with Cancer: Considerations for Radiation Oncologists. Biomed Res Int. 2017;2017.

517. Asthana S, Halter JB, High KP, Ouslander JG, Ritchie CS, Studenski S, et al. Hazzard's Geriatric Medicine and Gerontology. 7th ed. ed. New York, N.Y: McGraw-Hill Education LLC; 2017.

518. Barzilai N, Huffman DM, Muzumdar RH, Bartke A. The Critical Role of Metabolic Pathways in Aging. Diabetes. 2012 -6;61(6):1315-22.

519. Rudat V, Dietz A, Conradt C, Weber K, Flentje M. In vitro radiosensitivity of primary human fibroblasts. Lack of correlation with acute radiation toxicity in patients with head and neck cancer. Radiotherapy and Oncology. 1997 May 1,;43(2):181-8.

520. Rosen EM, Goldberg ID, Myrick KV, Levenson SE. Radiation Survival of Vascular Smooth Muscle Cells as a Function of Age. International Journal of Radiation Biology and Related Studies in Physics, Chemistry and Medicine. 1985 January 1,;48(1):71-9.

521. Baeyens A, Van den Broecke R, Makar A, Thierens H, De Ridder L, Vral A. Chromosomal radiosensitivity in breast cancer patients : influence of age of onset of the disease. . 2005.

522. Palumbo E, Piotto C, Calura E, Fasanaro E, Groff E, Busato F, et al. Individual Radiosensitivity in Oncological Patients: Linking Adverse Normal Tissue Reactions and Genetic Features. Frontiers in oncology. 2019 Oct 1,;9:987.

523. Shasha D. The negative impact of anemia on radiotherapy and chemoradiation outcomes. Semin Hematol. 2001 -07;38(3 Suppl 7):8-15.

524. O'Donovan A, Leech M, Gillham C. Assessment and management of radiotherapy induced toxicity in older patients. Journal of Geriatric Oncology. 2017 /11/01;8(6):421-7.

525. Kuncman Ł, Stawiski K, Masłowski M, Kucharz J, Fijuth J. Dose-volume parameters of MRI-based active bone marrow predict hematologic toxicity of chemoradiotherapy for rectal cancer. Strahlenther Onkol. 2020 -11;196(11):998-1005.

526. Lee J, Lin J, Sun F, Lu K, Lee C, Chen Y, et al. Dosimetric predictors of acute haematological toxicity in oesophageal cancer patients treated with neoadjuvant chemoradiotherapy. British journal of radiology. 2016 Oct;89(1066):20160350.

527. Wan J, Liu K, Li K, Li G, Zhang Z. Can dosimetric parameters predict acute hematologic toxicity in rectal cancer patients treated with intensity-modulated pelvic radiotherapy? Radiat Oncol. 2015 -08-04;10:162.

528. Jutzy J, Degnan M, Arya R, Peters P, Daily EW, Howard AR, et al. Hematological Toxicity in Cervix Cancer Patients Treated with Extended Field with IMRT or VMAT and Feasibility in Achieving Bone Marrow Planning Constraints. International journal of radiation oncology, biology, physics. 2018 Nov 1,;102(3):e626-7.

529. Sini C, Fiorino C, Perna L, Noris Chiorda B, Deantoni CL, Bianchi M, et al. Dose-volume effects for pelvic bone marrow in predicting hematological toxicity in prostate cancer radiotherapy with pelvic node irradiation. Radiother Oncol. 2016 Jan;118(1):79-84.

530. Fuks Z, Strober S, Bobrove AM, Sasazuki T, McMichael A, Kaplan HS. Long term effects of radiation of T and B lymphocytes in peripheral blood of patients with Hodgkin's disease. J Clin Invest. 1976 -10;58(4):803-14.

531. Till JE, McCULLOCH EA. A direct measurement of the radiation sensitivity of normal mouse bone marrow cells. Radiat Res. 1961 -02;14:213-22.

532. Green DE, Rubin CT. Consequences of irradiation on bone and marrow phenotypes, and its relation to disruption of hematopoietic precursors. Bone. 2014 -6;0:87-94.

533. Kolomietz E, Al-Maghrabi J, Brennan S, Karaskova J, Minkin S, Lipton J, et al. Primary chromosomal rearrangements of leukemia are frequently accompanied by extensive submicroscopic deletions and may lead to altered prognosis. Blood. 2001 -06-01;97(11):3581-8.

534. Nowell C. The minute chromosome (Ph1) in chronic granulocytic leukemia. Blut. 1962 Apr;8(2):65-6.

535. Arnold M, Rutherford MJ, Bardot A, Ferlay J, Andersson TM, Myklebust TA, et al. Progress in cancer survival, mortality, and incidence in seven high-income countries 1995–2014 (ICBP SURVMARK-2): a population-based study. The Lancet Oncology. 2019 Sep 11,;20(11):1493-505.

536. Feller A, Matthes KL, Bordoni A, Bouchardy C, Bulliard J, Herrmann C, et al. The relative risk of second primary cancers in Switzerland: a population-based retrospective cohort study. BMC cancer. 2020 Jan 21,;20(1):51.

537. He X, Wu W, Ding Y, Li Y, Si J, Sun L. Excessive risk of second primary cancers in young-onset colorectal cancer survivors. Cancer Med. 2018 -3-13;7(4):1201-10.

538. Schaapveld M, Aleman BMP, van Eggermond AM, Janus CPM, Krol ADG, van der Maazen, Richard W. M., et al. Second Cancer Risk Up to 40 Years after Treatment for Hodgkin's Lymphoma. New England Journal of Medicine. 2015 December 24,;373(26):2499-511.

539. Schaapveld M, Visser O, Louwman MJ, de Vries, Elisabeth G. E., Willemse PHB, Otter R, et al. Risk of New Primary Nonbreast Cancers After Breast Cancer Treatment: A Dutch Population-Based Study. JCO. 2008 March 10,;26(8):1239-46.

540. Haematology Normal Adult Reference Ranges [Internet].; 2017 [updated 19/05/; cited 20/07/2021]. Available from: https://www.royalwolverhampton.nhs.uk/services/service-directory-a-z/pathology-services/departments/haematology/haematology-normal-adult-reference-ranges/.

541. Zietman AL, Tibbs MK, Dallow KC, Smith CT, Althausen AF, Zlotecki RA, et al. Use of PSA nadir to predict subsequent biochemical outcome following external beam radiation therapy for T1-2 adenocarcinoma of the prostate. Radiother Oncol. 1996 -08;40(2):159-62.

542. King EJ, Delory GE. Acid and Alkaline Phosphatases in Their Relation to Malignant Disease. Postgrad Med J. 1948 -06;24(272):299-306.

543. Roberts WM. Variations in the Phosphatase Activity of the Blood in Disease. Br J Exp Pathol. 1930 -04;11(2):90-5.

544. Kay HD. Plasma Phosphatase in Osteitis Deformans and in other Diseases of Bone. Br J Exp Pathol. 1929 -08;10(4):253-6.

545. Karhade AV, Thio, Quirina C B S, Kuverji M, Ogink PT, Ferrone ML, Schwab JH. Prognostic value of serum alkaline phosphatase in spinal metastatic disease. British journal of cancer. 2019 Mar;120(6):640-6.

546. Lim SM, Kim YN, Park KH, Kang B, Chon HJ, Kim C, et al. Bone alkaline phosphatase as a surrogate marker of bone metastasis in gastric cancer patients. BMC Cancer. 2016 -7-4;16.

547. Li D, Lv H, Hao X, Hu B, Song Y. Prognostic value of serum alkaline phosphatase in the survival of prostate cancer: evidence from a meta-analysis. Cancer management and research. 2018;10:3125-39.

548. Kim SH, Shin K, Moon S, Jang J, Kim HS, Suh J, et al. Reassessment of alkaline phosphatase as serum tumor marker with high specificity in osteosarcoma. Cancer Med. 2017 -5-11;6(6):1311-22.

549. Crook JM, Choan E, Perry GA, Robertson S, Esche BA. Serum prostate-specific antigen profile following radiotherapy for prostate cancer: implications for patterns of failure and definition of cure. Urology. 1998 -04;51(4):566-72.

550. Landoni V, Fiorino C, Cozzarini C, Sanguineti G, Valdagni R, Rancati T. Predicting toxicity in radiotherapy for prostate cancer. Physica medica. 2016 Mar;32(3):521-32.

551. Lavin MF, Kidson C. Repair of ionizing radiation induced DNA damage in human lymphocytes. Nucleic Acids Res. 1977 -11;4(11):4015-22.

552. Rudra S, Hui C, Rao YJ, Samson P, Lin AJ, Chang X, et al. Effect of Radiation Treatment Volume Reduction on Lymphopenia in Patients Receiving Chemoradiotherapy for Glioblastoma. International Journal of Radiation Oncology*Biology*Physics. 2018 May 1,;101(1):217-25.

553. Davuluri R, Jiang W, Fang P, Xu C, Komaki R, Gomez DR, et al. Lymphocyte Nadir and Esophageal Cancer Survival Outcomes After Chemoradiation Therapy. International Journal of Radiation Oncology*Biology*Physics. 2017 September 1,;99(1):128-35.

554. Cho O, Oh Y, Chun M, Noh OK, Lee H. Radiation-related lymphopenia as a new prognostic factor in limited-stage small cell lung cancer. Tumor Biol. 2016 Jan;37(1):971-8.

555. Cho O, Chun M, Chang S, Oh Y, Noh OK. Prognostic Value of Severe Lymphopenia During Pelvic Concurrent Chemoradiotherapy in Cervical Cancer. Anticancer research. 2016 Jul;36(7):3541-7.

556. Wild AT, Ye X, Ellsworth SG, Smith JA, Narang AK, Garg T, et al. The Association Between Chemoradiation-related Lymphopenia and Clinical Outcomes in Patients With Locally Advanced Pancreatic Adenocarcinoma. Am J Clin Oncol. 2015 -6;38(3):259-65.

557. Wang X, Wang P, Zhao Z, Mao Q, Yu J, Li M. A review of radiation-induced lymphopenia in patients with esophageal cancer: an immunological perspective for radiotherapy. Ther Adv Med Oncol. 2020 January 1,;12:1758835920926822.

558. Pinkawa M, Djukic V, Klotz J, Petz D, Piroth MD, Holy R, et al. Hematologic changes during prostate cancer radiation therapy are dependent on the treatment volume. Future Oncology. 2014 April 1,;10(5):835-43.

559. Constantinou J, Feneley MR. PSA testing: an evolving relationship with prostate cancer screening. Prostate cancer and prostatic diseases. 2006 Mar;9(1):6-13.

560. Rukstalis DB. Treatment Options after Failure of Radiation Therapy—A Review. Rev Urol. 2002;4(Suppl 2):S12-7.

561. Huggins C, Hodges CV. Studies on prostatic cancer: I. The effect of castration, of estrogen and of androgen injection on serum phosphatases in metastatic carcinoma of the prostate. . Cancer Res. 1941;1(4):293-7.

562. Tedeschi B, Spadoni GL, Sanna ML, Vernole P, Caporossi D, Cianfarani S, et al. Increased chromosome fragility in lymphocytes of short normal children treated with recombinant human growth hormone. Hum Genet. 1993 -06;91(5):459-63.

563. Slyper AH, Shadley JD, Van Tuinen P, Richton SM, Hoffmann RG, Wyatt DT. A Study of Chromosomal Aberrations and Chromosomal Fragility after Recombinant Growth Hormone Treatment. Pediatric research. 2000;47(5):634-9.

564. Bozzola M, Tettoni K, Severi F, Capra E, Danesino C, Scappaticci S. Does growth hormone treatment increase chromosomal abnormalities? Clinical Endocrinology. 1997;47(3):363-6.

565. ICRP. Age-dependent Doses to Members of the Public from Intake of Radionuclides - Part 2 Ingestion Dose Coefficients. ICRP Publication 67. Ann. 1993;ICRP 23(3-4).

566. Perrone S, Ortu La Barbera E, Ottone T, Capriata M, Passucci M, Filippi L, et al. Acute Promyelocytic Leukemia After Radium-223 Exposure for Prostate Cancer in a Chemotherapy-Naïve Patient. Nucl Med Mol Imaging. 2020 -10;54(5):256-60.

567. Turner PG, Jain S, Cole A, Grey A, Mitchell D, Prise KM, et al. Toxicity and Efficacy of Concurrent Androgen Deprivation Therapy, Pelvic Radiotherapy, and Radium-223 in Patients with De Novo Metastatic Hormone-Sensitive Prostate Cancer. Clinical cancer research. 2021 Aug 15,;27(16):4549-56.